

Bangor University

DOCTOR OF PHILOSOPHY

Shell growth and repair in the common whelk *Buccinum undatum*

Colvin, Charlotte

Award date:
2023

Awarding institution:
Bangor University

[Link to publication](#)

General rights

Copyright and moral rights for the publications made accessible in the public portal are retained by the authors and/or other copyright owners and it is a condition of accessing publications that users recognise and abide by the legal requirements associated with these rights.

- Users may download and print one copy of any publication from the public portal for the purpose of private study or research.
- You may not further distribute the material or use it for any profit-making activity or commercial gain
- You may freely distribute the URL identifying the publication in the public portal ?

Take down policy

If you believe that this document breaches copyright please contact us providing details, and we will remove access to the work immediately and investigate your claim.



PRIFYSGOL
BANGOR
UNIVERSITY

Shell growth and repair in the common whelk

Buccinum undatum

Charlotte N. Colvin, MMBiol, PGCertHE

School of Ocean Sciences, Bangor University, Menai Bridge, Anglesey, LL59 5AB, UK

Submitted in accordance with the requirements for the degree of Doctor of Philosophy 2023

'I hereby declare that this thesis is the results of my own investigations, except where otherwise stated. All other sources are acknowledged by bibliographic references. This work has not previously been accepted in substance for any degree and is not being concurrently submitted in candidature for any degree unless, as agreed by the University, for approved dual awards.

I confirm that I am submitting this work with the agreement of my supervisor(s).'

'Yr wyf drwy hyn yn datgan mai canlyniad fy ymchwil fy hun yw'r thesis hwn, ac eithrio lle nodir yn wahanol. Caiff ffynonellau eraill eu cydnabod gan droednodiadau yn rhoi cyfeiriadau eglur. Nid yw sylwedd y gwaith hwn wedi cael ei dderbyn o'r blaen ar gyfer unrhyw radd, ac nid yw'n cael ei gyflwyno ar yr un pryd mewn ymgeisiaeth am unrhyw radd oni bai ei fod, fel y cytunwyd gan y Brifysgol, am gymwysterau deuol cymeradwy.

Rwy'n cadarnhau fy mod yn cyflwyno'r gwaith hwn gyda chytundeb fy Ngoruchwyliwr (Goruchwylwyr)

Summary

The common whelk, *Buccinum undatum* (Neogastropoda: Buccinidae), also known as 'buckie' or waved whelk, is a commercially important shellfish species distributed throughout the North Atlantic with over 22,000 tonnes landed in UK waters in 2020, at a value of approximately £27 million. Whelks have no planktonic larval stage, with larvae developing directly in egg cases laid annually by female whelks. Due to this and their limited mobility, whelk populations are often geographically isolated, with a heightened risk of stock depletion and increased concern for conservation and fishery management.

Whelks are vulnerable to damage from a variety of factors, including feeding, predation, burrowing, mechanical fishery gears and riddling, a process used in the whelk fishery to grade catch by size. Often these incidences of shell damage are recorded as scars on the shell surface following periods of re-growth. Understanding the process(es) involved in shell repair following damage and the consequent recovery mechanisms, is important for the continued sustainability of whelk fisheries. However, there is currently little work into the frequency and degree of shell damage in inshore fisheries, and the mechanisms of repair of the whelk's shell. This thesis focuses on exploring shell variation and the levels of shell damage seen in whelk populations, whilst identifying factors affecting shell growth and repair, and inspecting shell microstructure and trace element incorporation. Each chapter aims to build on the previous, to create an understanding of the natural variation seen and underlying processes affecting shell growth and repair in this species.

Initially, a sample of 4000 whelk shells from locations around the UK were assessed (Chapter 2), recording incidences of shell scarring and internal colour, followed by quantitative measurement through spectrophotometry and Raman analysis. The degree of shell damage and variation of internal shell colour were both significantly different between geographic locations, with most whelk shells seeing slight to moderate shell damage, and either a white or brown internal shell colour.

Having evidenced that damage and re-growth of the shell occurs, a series of experimental damages were carried out using live tank-reared and wild-caught whelk held in laboratory-controlled conditions (Chapter 3). In whelks with experimentally-damaged shells significant

differences in the rate of shell growth and repair were observed when investigating life stage, temperature, and season. For experiments of feeding regime, significant differences were only found for total shell growth, and for sex, significant differences were only found for shell repair rates. Nonetheless, for all experiments, shell damage did not significantly affect the rate of total shell growth. Through the characterisation of these biological and environmental factors, this chapter demonstrates that there are multiple factors controlling shell growth and repair rates.

Shells of these whelks were then prepared to assess the original and repaired sections using scanning electron microscopy (SEM) and X-ray diffraction (μ XRD) for structural assessment (Chapter 4) and X-ray fluorescence (μ XRF), laser ablation-inductively coupled plasma-mass spectrometry (LA-ICP-MS), and extended X-ray absorption fine structure (μ EXAFS) for trace element analysis (Chapter 5). These data confirmed whelk shells to be fully aragonitic and established they are formed of only two distinct microstructures; prismatic and crossed lamellar. Inert-element bond lengths and trace element incorporations were consistent within a shell layer, including into new growth, however for trace element incorporation higher concentrations of Mg, Sr and Ba were seen in the outer prismatic layers.

Through the combined findings of this thesis, insight has been gained into the variability in shell structure of the whelk, whilst establishing underlying causes for changes in rates of shell growth and repair. These findings will help feed into fisheries research, where current management plans require an increased understanding of this data-poor commercial species. Through improvements in the understanding of the controls on shell growth and shell damage and the frequency of shell repair, it will be easier to sustainably manage these stocks.

Acknowledgements

First and foremost, I would like to thank my family, in particular my mum and dad for funding my PhD and supporting me continuously throughout my research and career, without your continual backing this would not have been possible (special thank you to dad for reading through my thesis for me!). I would also like to thank my brother James for his support and my partner Nathaniel, who has bought me plenty of snacks whilst I have sat at my desk and is always there to encourage me to just sit still that little bit longer to finish writing each section.

I initially started my research into whelk back in 2015 alongside Prof. Chris Richardson and Dr Phil Hollyman during my MDegree at Bangor University, and thanks to their backing I was able to continue answering my many research questions into this PhD. I would like to say a massive thank you to all my supervisors, Dr Ian McCarthy, Dr Simon Chenery, Dr Phil Hollyman and Prof. Chris Richardson. Each of you have provided me with guidance, support, knowledge, and have always answered my questions, even when I have gone completely off track.

Thank you to my colleagues in Ocean Sciences. A massive thank you to Berwyn Roberts is needed. He has endured my many questions, whelk mess, and has been out in awful weather collecting samples with me over the years, but nevertheless has continued to help and support my research. Thank you also to Dr Natalie Hold and Dr James Waggitt, both of whom have helped guide me through the final stages of my thesis write up, through offering advice and providing further opportunities for me within my research career.

This research would also have not been possible without the kind support from the Department of Earth Sciences at Cambridge University, the British Geological Survey, where Simon and his team have not only taught me many new investigative skills but have allowed me access to use the facilities, including the LA-ICP-MS. Finally, thank you to Dr Konstantin Ignatyev, Dr Tina Geraki and Diamond Light Source for granting facility use of the i18 beamline.

Table of Contents

Summary.....	2
Acknowledgements	4
Table of Contents	5
Abbreviations.....	9
<i>Chapter 1 - General Introduction.....</i>	<i>10</i>
Figures.....	11
The ecology of <i>Buccinum undatum</i>	12
Reproduction	14
Growth.....	16
Fisheries and commercial importance.....	17
Shell Damage	20
Environmental damage to shells.....	21
Fishery-related shell damage	22
Gaps in literature and structure of thesis	24
<i>Chapter 2 – Assessment of the shells of Buccinum undatum</i>	<i>26</i>
Figures.....	27
Tables	29
Introduction.....	30
Morphometric variation	30
Shell colour differences and shell pigment presence.....	33
Materials and Methods	37
Assessment of shell damage	39
Assessment of shell colour	40
Results.....	43
Shell comparisons between <i>Buccinum undatum</i> populations	43
Distribution of shell damage in five <i>Buccinum undatum</i> populations.	44
Shell colour variation between <i>Buccinum undatum</i> populations	49
Quantification of internal shell colour	51
Spectrophotometry	51
Raman spectroscopy	56

Discussion	63
Shell variation and shell damage amongst <i>Buccinum undatum</i> populations	63
Colour variation and pigment presence	64
Summary.....	66
<i>Chapter 3 - Shell repair and growth in experimentally-damaged Buccinum undatum</i>	68
Figures.....	69
Tables	71
Introduction	72
Materials and Methods	75
Sample collection	76
Tank reared juvenile whelks.....	76
Wild caught whelks.....	78
Tank based experiments	79
Labelling of whelks.....	80
Shell damage and measurement of shell repair	82
Determination of sexual maturity.....	83
Statistical analysis.....	84
Results.....	87
Prior shell damage and Retractability of body.....	87
Life Stage	91
Sex and Maturity	93
Feeding Regime	97
Seawater Temperature	100
Seasonal Variation	102
Discussion	109
Further implications	114
<i>Chapter 4 - Shell structure of Buccinum undatum</i>	116
Figures.....	117
Introduction.....	119
Calcium Carbonate (CaCO ₃)	121
Mollusc shell formation.....	122
Materials and Methods	124

Sample preparation	124
Shell Embedding	124
Block preparation	126
Thin sections	127
Transmission synchrotron analysis (μ XRD)	128
Reflection and transmission microscopy	129
Calcein staining and fluorescence microscopy	130
Scanning Electron Microscopy (SEM)	131
Results	133
Micro X-ray Diffraction (μ XRD)	133
Reflection, transmission, and fluorescence microscopy	135
Scanning Electron Microscopy (SEM)	138
Discussion	144
Summary	145
<i>Chapter 5 - Trace element incorporation in Buccinum undatum shells</i>	147
Figures	148
Tables	150
Introduction	151
Bond length and crystal structure	151
Trace element incorporation	152
Strontium and Magnesium	154
Barium	155
Other trace elements	156
Vital effects	157
Materials and Methods	158
Temperature-controlled and manipulated seawater chemical composition experiments	159
Sample preparation	161
Diamond Light Source	161
μ EXAFS – Micro Extended X-Ray Absorption Fine Structure	162
μ XRF – Micro X-Ray Fluorescence	162
British Geological Survey	163

Laser Ablation-Inductively Coupled Plasma-Mass Spectrometry (LA-ICP-MS).....	163
Results.....	165
Crystal structure and bond length studies (μ EXAFS)	165
Trace element incorporation (μ XRF and LA-ICP-MS).....	168
μ XRF	168
LA-ICP-MS.....	169
Discussion	178
Conclusion	182
<i>Chapter 6 - General Discussion.....</i>	<i>183</i>
<i>Appendices.....</i>	<i>221</i>
Appendix 1 – Atlas of shell damage	222
Appendix 2 – FITYK data processing method notes.....	229
Appendix 3 – Peak height, area, and full width half maximum under the 5 prominent peak positions used to fit spectra	241
Appendix 4 – DISP056 Dispensation for the collection of undersized whelks	242
Appendix 5 – Grant SP20234 Diamond Light Source.....	245
Appendix 6 – Overview of analytical techniques	249
Raman Spectroscopy	250
Synchrotron Analysis	252
Micro-X-ray Diffraction μ XRD	254
XAS – X-Ray Absorption Spectroscopy	255
Extended X-ray Absorption Fine Structure EXAFS	257
Micro-X-ray Fluorescence μ XRF	258
Laser Ablation-Inductively Coupled Plasma-Mass Spectrometry LA-ICP-MS.....	260
Appendix 7 – Data processing; μ EXAFS - ATHENA.....	262
Appendix 8 – Methods used for processing μ XRF maps	263
Appendix 9 – Process for data analysis of laser output.....	266
Appendix 10 – Paper manuscript	268

Abbreviations

UK	United Kingdom
USA	United States of America
FAO	Food and Agriculture Association
MLS	Minimum landing size
MMO	Marine management organisation
SW	Seawater
TRJ	Tank reared juvenile whelk
JW	Juvenile wild caught whelk > UK SOM 45 mm
MW	Mature wild caught whelk > UK SOM 45 mm
SOM	Size at onset of maturity
LWST	Low water spring tide
TSL	Total shell length
TW	Total weight
ApL	Aperture length
SD	Standard deviation
SE	Standard error
XLAM	Crossed-lamellar
WSSR	Weighted sum of squared residuals
QC	Quality control
BGS	British Geological Survey
DLS	Diamond Light Source
KB	Kirkpatrick-Baez
LA-ICP-MS	Laser ablation - inductively coupled plasma - mass spectrometry
μ XRD	Micro X-ray diffraction
μ XRF	Micro X-ray fluorescence
μ EXAFS	Micro extended X-ray absorption fine structure
SEM	Scanning electron microscope

Chapter 1 – General Introduction

Figures

Figure 1.1: Global distribution of the neogastropod mollusc <i>Buccinum undatum</i> shown by red shading (Image adapted from FAO).	12
Figure 1.2: External morphology of <i>Buccinum undatum</i> indicating the shell whorls and waves. Shell width and total shell length is represented by the yellow arrows.	14
Figure 1.3: Visual observation of male and female <i>Buccinum undatum</i> . (A) shows a male with the penis marked with an X and (B) shows a female where the lack of a penis can clearly be seen.....	15
Figure 1.4: Female <i>Buccinum undatum</i> in the laboratory laying egg capsules on the tank surface.	16
Figure 1.5: Global capture production for live weight (tonnes) for <i>Buccinum undatum</i> landed between 1950-2020. (Data accessed from FAO FishStat, 2023).....	18
Figure 1.6: A) 'Inkwell' B) 'Laydown' whelk pots used for the capture and fisheries of <i>Buccinum undatum</i>	19
Figure 1.7: Commercial whelk riddle used to filter whelk samples to collect those above the minimum landing size (UK 45 mm).	20
Figure 1.8: Live <i>Buccinum undatum</i> , showing multiple scarring lines from shell damage.	21

In this general introduction, the broader context of the biology and ecology of the European common whelk, *Buccinum undatum* Linnaeus, 1758 will be reviewed, along with its importance as a commercial species. It will also examine the literature on environmental and anthropogenic shell damage and the potential impacts imposed on whelks, along with their life history and mechanisms of shell growth. Finally, this introduction will outline the research aims of this thesis by listing the aims of each subsequent chapter, along with their significance to current literature. Note. Where the term ‘whelk’ is used, this specifically refers to *Buccinum undatum*.

The ecology of *Buccinum undatum*

Buccinum undatum, the common or waved whelk, is a neogastropod mollusc. It is a boreal species found and caught most frequently between depths of 40 and 60 m; however, they also occur at depths of up to 1200 m (Nielsen, 1974; Valentinsson *et al.*, 1999; Valentinsson, 2002). Whelks are most found in coastal waters along the continental shelf, with a preference for sandy or stony substratum. Although primarily occurring within European waters of the Northeast Atlantic (Hayward and Ryland, 2011), they are also seen in Canada (Borsetti *et al.*, 2020), the Arctic Circle (76°N) (Woods and Joansson, 2017), Greenland (Golikov, 1968), and the seas off New Jersey, USA (38°N) (Borsetti *et al.*, 2018) (Figure 1.1).

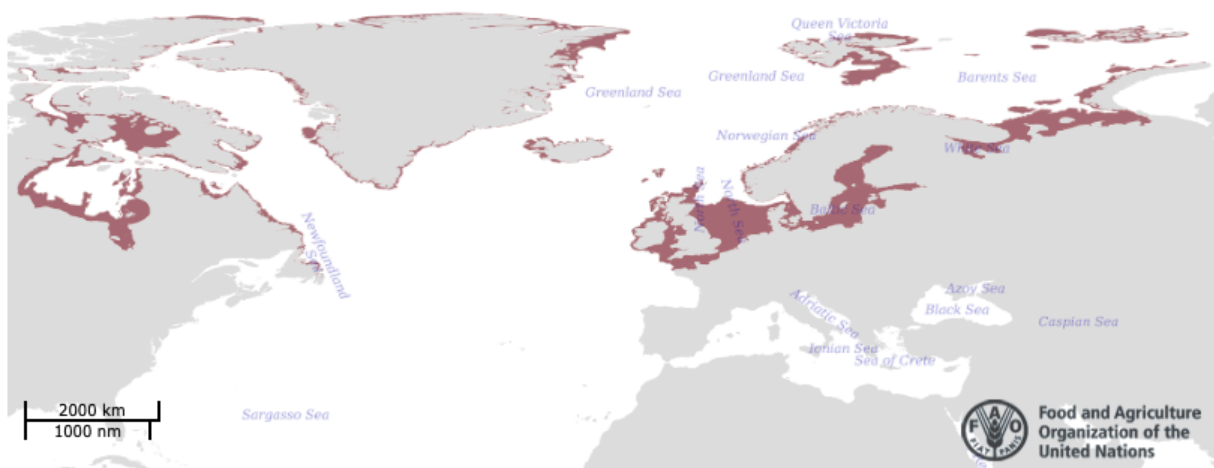


Figure 1.1: Global distribution of the neogastropod mollusc *Buccinum undatum* shown by red shading (Image adapted from FAO).

While they are a slow-moving species, covering a maximum range of approximately 50 m day⁻¹, whelks can move relatively fast when required over a shorter time scale at approximately 11 cm min⁻¹ (Hancock 1960; Himmelman, 1988). Population density is seen to vary from 0.2 to 4.5 individuals m⁻², with levels seen to change because of fishery pressure and the local environment (Himmelman, 1988; Jalbert *et al.*, 1989; Phillips, 2022; Colvin *et al.*, 2022a). Distribution is affected by a range of factors. It is mainly determined by their limited thermal tolerance. Whelks have a preference for colder sea water temperatures and are found down to -1°C, with temperatures exceeding 29°C proving lethal, due to the effect on metabolic capabilities (Hancock, 1960). Within UK waters, sudden temperature fluctuations above 18°C see increased mortality rates of adult whelks, with their normal range sitting between 4 to 18°C (Colvin pers. obs.; Smith *et al.*, 2013). Furthermore, northern France, and the coastlines of southern England, are thought to be close to their southernmost limit, due to warmer water temperatures, being a limiting factor in reproductive success, (McIntyre *et al.*, 2015).

Whelks are carnivorous scavengers, using chemoreception to locate prey, to an area of approximately 585 m² (Himmelman, 1988). Their diet is seen to be variable, dependant on the size of the whelk, and consists mainly of polychaetes, fish, crustaceans, bivalves, and echinoderms. Kleptoparasitic behaviour has also been recorded in populations, with exploitation of sea stars in the Mingan Islands (Rochette *et al.*, 2001; Brokordt *et al.*, 2003). Seasonal changes and their local environment see further effects, with those living in sandy sediments seeing the greatest food intake (Himmelman and Hamel, 1993).

The external morphology of a whelk's shell consists of approximately 7 to 8 whorls which can reach up to 15 cm in length and 6 cm in width. The shells form a conical undulating shape with shell waves present over the outer surface (Figure 1.2). Shell colour has been seen to vary, from yellow brown, to purple or white at some locations, with populations seeing a varied morphology both between geographic areas and within the same location (Hayward and Ryland, 2011).

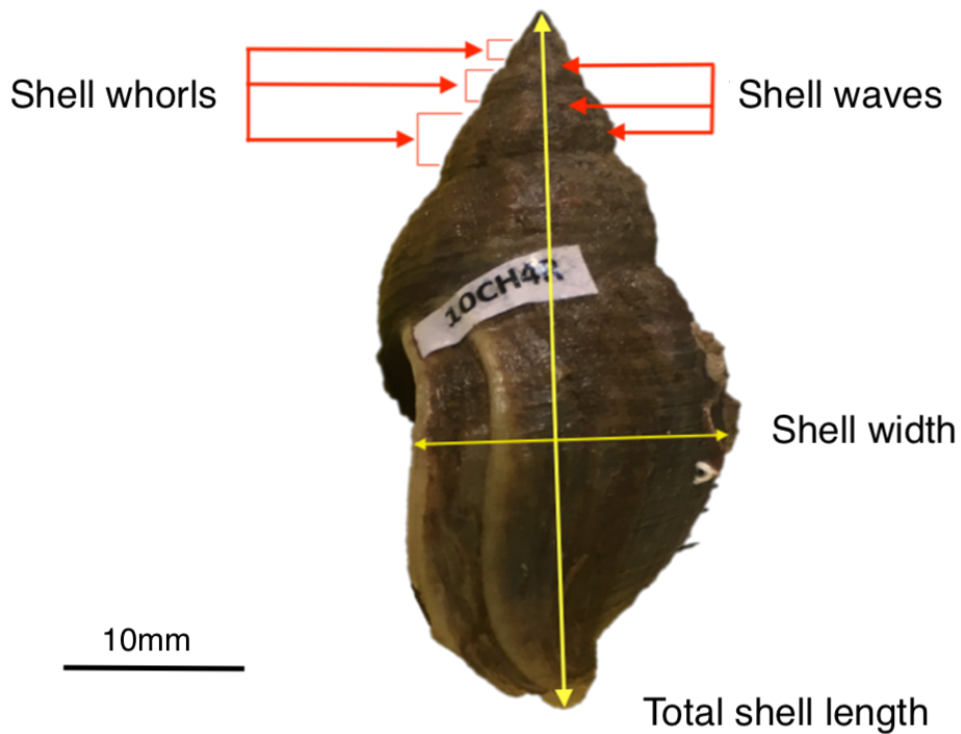


Figure 1.2: External morphology of *Buccinum undatum* indicating the shell whorls and waves. Shell width and total shell length is represented by the yellow arrows.

Reproduction

Previous research has found *B. undatum* to be gonochoric; differentiation of sex is clear, with males distinguished by a large muscular penis within the mantle cavity, along the right side of the head (Figure 1.3) (Fretter, 1953; Kideys *et al.*, 1993). Both the male and female gonads are similar in size and form, and located alongside the digestive gland (Kideys *et al.*, 1993). For marine gastropods, particularly species such as the whelk, the process of gamete production and storage, as well as copulation, holding of sperm and fertilisation leading to the formation and laying, are all fundamental steps in reproduction. Egg-laying has been reported at various times throughout the year, dependant on location. For populations in the Gulf of St Lawrence, Canada, the process of egg-laying occurs between late May to August (Martel *et al.*, 1986; Himmelman and Hamel, 1993), differing from that of European waters, where the laying process occurs from autumn to winter. More specifically, for example, within the Isle of Man, in the Irish Sea, and off the coasts of Wales the laying process occurs from late December to January (Kideys *et al.*, 1993). Nonetheless, although variation is seen, females generally begin egg laying once temperatures drop below 9°C and whelks have been reported to have a distinct annual breeding cycle (Martel *et al.*, 1986).

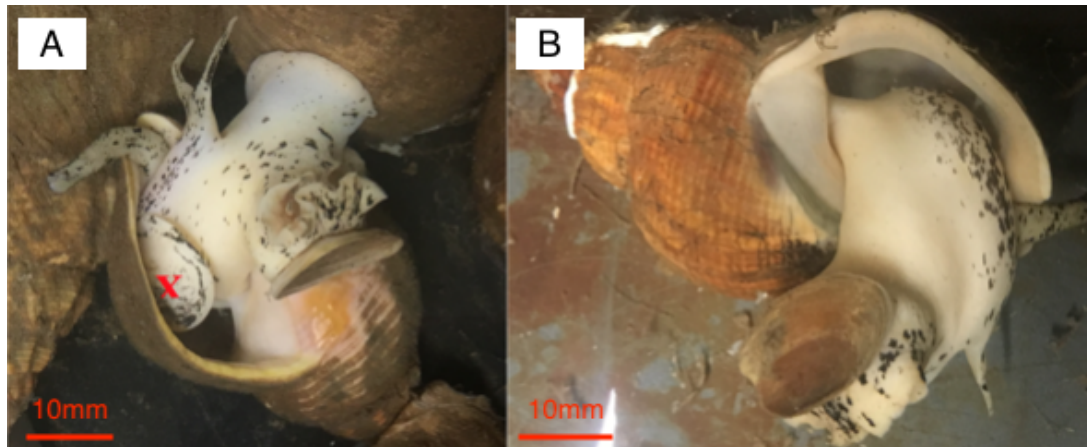


Figure 1.3: Visual observation of male and female *Buccinum undatum*. (A) shows a male with the penis marked with an X and (B) shows a female where the lack of a penis can clearly be seen.

During egg laying, the female whelks will deposit eggs within capsules onto hard substratum, including seaweeds, piers, and crustaceans such as crabs (pers. obs.) (Figure 1.4). It is at this stage that the highest mortality rates are found, chiefly because of predation (Fahy *et al.*, 2000; Fahy, 2001; Dumont *et al.*, 2008). Within a single location, multiple females may lay their eggs, with each producing up to 140 capsules (Martel *et al.*, 1986). Although each capsule presents the opportunity for over 3000 embryos to occur, approximately 1% are seen to develop, with juveniles feeding on the surrounding egg cases (Fretter and Graham, 1962; Martel *et al.*, 1986; Valentinsson, 2002; Magnúsdóttir, 2010). Development is direct and juvenile whelks emerge into the benthos after 3 to 8 months and can reach a maximum age of around 12 years. With no planktonic stage and a moderately sedentary life, populations are often geographically isolated (Hancock, 1963; Santareli, 1985; Vaneltinsson, 2002; Pálsson *et al.*, 2014).

Research by Brokordt *et al.* (2003), has found that maternal care in whelks, during and after egg laying, sees a reduction in the escape capability of adult females from predatory organisms, whereas for male whelks little or no change in capability was observed. It was assumed this was due to the increased energetic investment for mature females, whereby, processes such as encapsulation, as well as locating egg laying sites and egg laying itself, are highly energetically costly (Perron, 1981; Sullivan and Mangel, 1984). Furthermore, whelks have been seen to reduce feeding activities during breeding, with less than 10% of whelks, both male and female, having food within their stomachs during the breeding season (Himmelman

and Hamel, 1993). Female whelks can spend up to seven days without feeding during egg laying (Martel *et al.*, 1986; Brokordt *et al.*, 2003).



Figure 1.4: Female *Buccinum undatum* in the laboratory laying egg capsules on the tank surface.

Due to the whelk's life history traits, their limited movement and high site-fidelity, phenotypic and local adaptations occur, with disparities in growth and metabolic activity between region (Weetman *et al.*, 2006; Haig *et al.*, 2015). Further implications on recovery within depleted populations is seen because of restricted gene flow and limited population mixing (Valentinsson *et al.*, 1999; Weetman *et al.*, 2006; Borsetti *et al.*, 2018).

Growth

In any animal, growth is shown by the increase in size and weight, occurring due to the assimilation of food, conversion to energy, and consequent increase in biomass (Von Bertalanffy, 1938; Kideys and Hartnoll, 1991). Although for many organisms, this growth ceases with time, *B. undatum* exhibits continual growth throughout its life cycle (Kideys, 1996). Unlike with many bivalve molluscs, gastropod shells rarely show external surface rings, and for those where this is visible, they often do not correspond to a predictable growth metric (Schöne *et al.*, 2007). With the increasing damage to the shell surface, this further reduces the ability to use the shell as a reliable aging method (Mensink *et al.*, 2000; Hollyman, 2017; Colvin *et al.*, 2022b). As a result of this, alternative aging techniques are used for gastropod species through examining the ring structure of the dorsal surface of the operculum or using statoliths (Santarelli and Gros, 1985, Dorset, 1986; Chatzinikolaou and Richardson, 2007; Lawler, 2013; Hollyman *et al.*, 2018).

Molluscan shells are structurally complex, made up of intricate microstructures, and form to protect the internal soft tissues (Simkiss and Wilbur, 1989; Palmer, 1991). Typically, the shells of molluscan species, are composed of a solid calcium carbonate (CaCO_3) phase amongst an organic matrix. For most molluscs, the CaCO_3 present is either calcite or aragonite, both of which have a similar crystal structure, however, for some instances vaterite or a combination of different polymorphs can occur (Gong *et al.*, 2012; Checa, 2018; Clark *et al.*, 2020). The shell itself is formed through the process of biomineralization, and it is thought that deposition occurs at the mantle edge (Watabe, 1983; Clark *et al.*, 2020). This process, coupled with the incorporation and formation of the organic matrix is highly energetically costly (Ebert, 1968; Ruppert *et al.*, 2004; Melzner *et al.*, 2011; Thomsen *et al.*, 2013). Further incorporation into the shell can occur through the substitution of Ca^{2+} with trace elements, and it is processes such as this that enable molluscan shells to provide an archive of environmental changes (Höche *et al.*, 2022).

Fisheries and commercial importance

B. undatum is one of the most consumed shellfish within archaeological records, and is of great commercial interest in European waters, with the highest landings coming from within Northern Europe; the greatest of these landings coming from the UK (Heude-Berthelin *et al.*, 2011; Colvin *et al.*, 2022a). Within the UK fishery, whelk are the third most landed invertebrate species by total weight, at 20,000 tonnes and an economic value of over £20 million annually, whilst within Wales, whelks are the highest, at over 5,000 tonnes landed at over £2.2 million (MMO, 2020). Whelks have long been exploited, mainly as they are the largest edible marine gastropod within the North Atlantic (Fahy *et al.*, 1995; Shelmerdine *et al.*, 2007). A small global fishery for whelks began operating in the early 1900's, and by 1911, 4500 tonnes were reported for annual landings in England and Wales (Dakin, 1912). In response to the increase in demand from overseas markets, primarily East Asia (South Korea and Japan) landings have seen a dramatic increase since 1995 (Figure 1.5). As a result of the increased demand, the UK fishery increased effort with the increased price per tonne, from £230 in 1990 to £1177 in 2022 (MMO, 2018; MMO, 2022). For Wales 2018 saw the total value of whelk landings (£7.9 million) being greater than all other species combined for landings by UK vessels into Wales (MMO, 2018).

With the global rise in popularity of whelk consumption, a rapid expansion has occurred within the industry in European waters. This increase in demand has left fisheries, particularly within the British Isles, seeing a reduction in stock abundance and individual whelk quality, with progressive exploitation of the fishery itself (Fahy *et al.*, 1995, 2000). Throughout European waters, there are several large coastal fisheries operating, for example in waters around France, UK, Ireland, and Iceland (Fahy *et al.*, 1995, 2000, 2005; Nasution and Roberts, 2004; Shelmerdine *et al.*, 2007). These fisheries not only occur within Europe, but there are also active fisheries in Canada and North America, although initially starting as by-catch from lobster fisheries, in recent years’ purpose-designed whelk traps have been developed to increase yields (Jalbert *et al.*, 1989; Valentinsson *et al.*, 1999; Morel and Bossy, 2004; Shelmerdine *et al.*, 2007; maine.gov, 2016). The effects of the increase in industry pressures have been seen within many whelk populations, for example within the western Dutch Wadden Sea, where there has been a clear decline in numbers since the mid 1920’s, whereby landings saw a reduction from 500,000 kg in 1925 to almost 0 kg by 1970 along with further depletions seen in the southern North Sea. This was found to be a result of both overfishing, and lethal shell damage from mobile fishing gears (Cadée *et al.*, 1995; Nicholson and Evans, 1997; Valentinsson *et al.*, 1999).

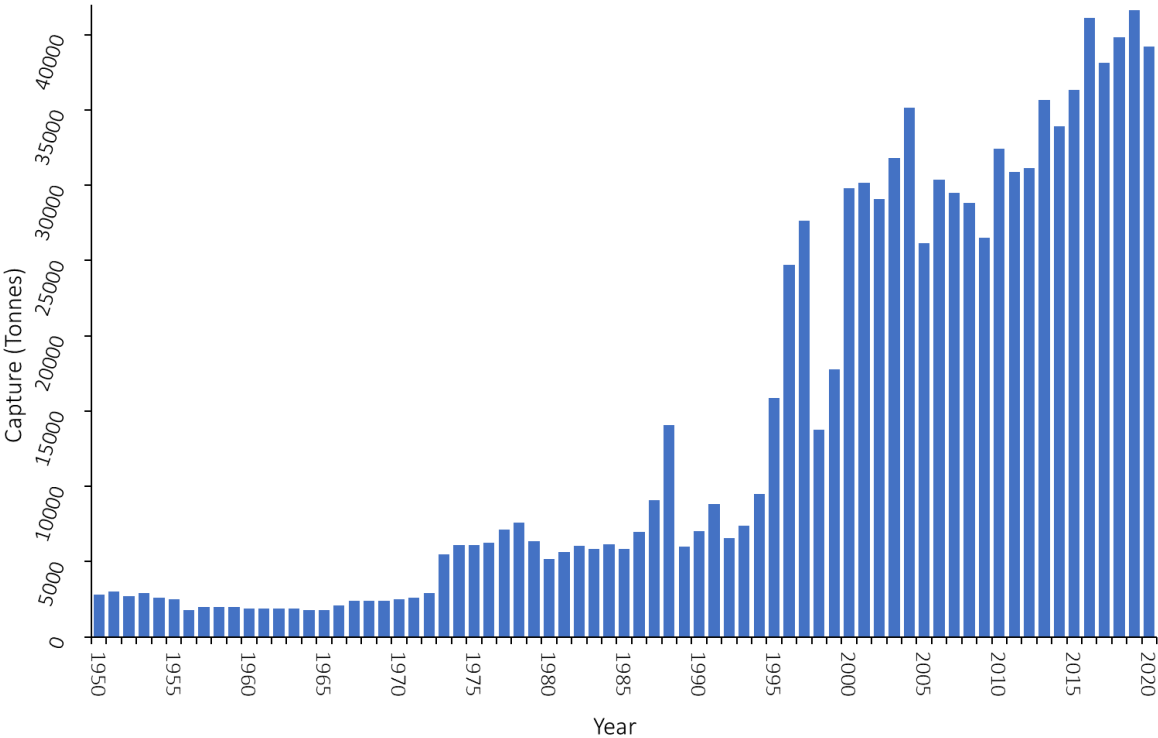


Figure 1.5: Global capture production for live weight (tonnes) for *Buccinum undatum* landed between 1950-2020. (Data accessed from FAO FishStat, 2023).

For many fisheries, static baited traps are used to catch whelks. These are either purpose built ‘inkwell’ pots, or ‘lay down’ pots, which are the cheaper alternative, made from recycled plastics and weighed down with a concrete block (Figure 1.6). Pots are laid down on the seabed, often in strings of hundreds at a time (dependant on boat deck-area), baited with a mixture of fish and crab and left on the sea-floor for up to 48 hours. This duration is known as the ‘soak-time’ and fishers aim for between 24 to 48 hours for maximum efficiency of the bait, after which point the catch rates are seen to drop (Bennet, 1974; Fahy, 2001; Jennings *et al.*, 2001). Some larger vessels within Welsh waters can work up to 1,000 pots in a day, though typically this value is between 300 to 400. Although by-catch is low, non-target species including crab and starfish are often caught (Moore and Howarth, 1996).



Figure 1.6: A) ‘Inkwell’ B) ‘Laydown’ whelk pots used for the capture and fisheries of *Buccinum undatum*.

Management strategies have been put in place to help maintain stocks, for example a standard European minimum landing size (MLS, also known as the minimum conservation reference size) of 45 mm shell height (Lawler, 2013). However, in recent years, publications have determined a decline in populations of the common whelk where they were once profuse (Mensink *et al.*, 2000). This has resulted in local governments and fishery administrations re-evaluating individual area-specific MLS values, and the implementation of the riddle; a device formed of a tray under a series of metal bars set at the minimum width of the shell, through which undersized whelk are passed (Figure 1.7). Within Welsh waters, through a consultation, the MLS for whelks has increased from 45 to 55 mm in 2019 and again to 65 mm in 2020 with the start of a stock assessment being developed for this data poor fishery (Hold *et al.*, 2021; Colvin *et al.*, 2022a, 2022b). Fisheries within the UK are also heavily restricted by weather and

storm impacts, meaning fishing activity is primarily within seven months per year, although it varies between location, catch-per-unit-effort, current markets, and demand of stock (Murray *et al.*, 2013). The fishery further depends on the ecology of the whelks, their feeding and behavioural traits, along with localised exploitation (Martel *et al.*, 1986; Fahy *et al.*, 1995; Fahy *et al.*, 2005). Nonetheless, whelk populations are particularly vulnerable to overexploitation because of their life history, with relatively fast early growth but slow adult growth and late maturation, as well as its direct development, and a lack of planktonic larval stage (Martel *et al.*, 1986; Strand and Jacobsen, 2002; Morel and Bossy, 2004; Nasution and Roberts, 2004).



Figure 1.7: Commercial whelk riddle used to filter whelk samples to collect those above the minimum landing size (UK 45 mm).

Shell Damage

There are a variety of factors that can result in damage to the shells of marine molluscs (see Appendix 1, atlas of shell damage). These include natural damage, for example storms with increased turbulence, as well as that of unsuccessful predatory attacks and boring (Checa, 1993; Mensink *et al.*, 2000; Ramsay *et al.*, 2001). Nevertheless, one of the key influencing factors is that of the fishing industry, both direct and indirect. The effects of overfishing,

bycatch and direct damage from mobile fishing gear are presenting serious hurdles to the development and sustainability of marine populations, with many experiencing long-term depletion at all trophic levels within the ecosystem (Cadée *et al.*, 1995; Fahy *et al.*, 1995; De Vooy and Van der Meer, 1998; Mensink *et al.*, 2000; Bergman *et al.*, 2001).

Environmental damage to shells

Whelks are subjected to predation by many marine organisms, for example starfish, crustaceans, and a variety of fish species including the Atlantic cod, *Gadus morhua* (Dakin, 1912; Feder, 1963; Mackie *et al.*, 1968; Harvey, 1990). Through crushing mechanisms or chipping at the aperture, crustacean predators gain access to the body. However, dependant on size and strength of the shell, this can be unsuccessful, leaving damage and consequent shell scarring on the whelks (Figure 1.8) (Ramsay *et al.*, 2001). Thinner-shelled whelks are often more vulnerable to predatory pressures than heavier-shelled ones from the same locations, as seen with whelks from Maces Bay in New Brunswick, Canada (Thomas and Himmelman, 1988).



Figure 1.8: Live *Buccinum undatum*, showing multiple scarring lines from shell damage.

It is not only the implication of predatory attacks that see damage to the shells of whelks. Their behavioural responses have been of note over the years, with violent escape mechanisms, often resulting in damage to the shell, particularly in response to starfish predation for example *Asterias rubens* (Ramsay and Kaiser, 1998; Laptikhovsky, 2014). This reaction has been seen as a result of steroid glycosides produced by the starfish, detected through chemosensory cells in the whelks resulting in a violent twisting of the foot, after which

escape is attempted (Feder, 1963; Mackie *et al.*, 1968; Mackie, 1970; Harvey *et al.*, 1987). The processes of feeding and attack by whelks on bivalve species further can result in damage to their shells (Scolding *et al.*, 2007). Whelks have been seen to use a technique to break into bivalve shells known as 'wedging'. This is a process by which the whelk inserts its shell lip into the valves of the bivalve, until the gap is wedged open and is large enough to insert the proboscis through the mantle cavity and feed using its radula once the pallial cavity and flesh has been accessed (Hancock, 1960; Nielsen, 1974). Additional methods have observed the whelks using their muscular foot to control the prey until in an adequate position to attack and feed when the bivalve opens its shell, as seen with the cockle *Cerastoderma edule* (Hancock, 1960; Nielsen, 1974, Scolding *et al.*, 2007). Due to the nature of the 'wedging' technique, shell thickness of the whelks is of key importance as thinner shells are less robust to this type of feeding strategy, resulting in greater damage to the shell lip (Scolding *et al.*, 2007).

Damage and shell fragmentation can also occur because of abiogenic factors, in particular with the effects of storms and consequent turbulence, rolling stones within the water column, as well as the effects of burrowing, although there has been little research into these implications (Checa, 1993; Kideys, 1994; Cadée, 1999). Understanding shell damage in benthic molluscs is perplexing as it is not only the implications of a single event causing destruction to the shell surface, but it also has many ecological and physiological consequences for the affected species (Mensink *et al.*, 2000; Ramsay *et al.*, 2001).

Fishery-related shell damage

Fishing, for both marine shellfish and fish species, has globally been a way of life for many people for a long time (Clark *et al.*, 2016), with commercial fishing designed to catch the maximum yield possible per unit effort (Bergmann *et al.*, 2001). Due to the overall procedure of mechanical fisheries, particularly mobile bottom fisheries, the methods used often cause disruptions to benthic infaunal and epifaunal communities (Van Beek *et al.*, 1990; Eleftheriou and Robertson, 1992; Currie and Parry, 1996; Kaiser and Spencer, 1996; Ramsay and Kaiser, 1998; Piet *et al.*, 2000). Fishery-related damage not only occurs directly through mobile fishing gears, but also as a result of handling, changes in water pressures and discarding of bycatch (Walker and Heessen, 1996; Nicholson and Evans, 1997; Phillipart, 1998; Kaiser *et al.*, 2000; Mensink *et al.*, 2000).

One of the most prominent impacts is that of direct damage to the shell, seen more frequently in recent years, with an increased mechanical advancement of mobile fishing gears (Jennings and Kaiser, 1998). Within the southern North Sea, an example of this is beam trawling for flatfish, with over 1000 trawlers currently operating; a huge increase in numbers from the 1970's (Riesen and Reise, 1982; Jennings and Kaiser, 1998; Kaiser, 1998; Mensink *et al.*, 2000; Bergmann *et al.*, 2001). A study from Mensink *et al.*, 2000, looking into shell damage in *B. undatum* showed that most of the damage observed was caused by beam trawls and tickler chains, with lighter shell damage caused as result of on deck handling. Similar effects have also been noted by Gaspar *et al.* (1994) for the razor clam *Ensis siliqua* in Portuguese waters. The clam also sees shell damage due to being subject to high levels of dredging within the Orkney Islands (UK), and in the *Nephrops* fishery within the Clyde Sea, where handling and discarding of by-catch see further shell damage implications (Robinson and Richardson, 1998; Bergmann *et al.*, 2001).

Studies from Fonds (1991, 1994), Fonds *et al.*, (1992), and Kaiser and Spencer (1995), report that whelks appear impervious to implications of trawling, with survival of up to 98-100%, over a short time scale of one week. However, Mensink *et al.*, (2000) found this decreased to 60% in a longer term six-week study post-damage with a 12 m beam trawl. The damage to the whelk populations not only occurs from direct impact with the trawl itself, but the distress from passing through nets on the seabed. In addition, an increased scavenger presence has been noted after trawl damage. For example, off the coast of Anglesey, this was seen with the starfish, *Asterias rubens*, and *Ophiura ophiura*, and crabs such as *Pagurus bernhardus* and *Liocarcinus depurator*, although different responses occurred between singular communities (Kaiser *et al.*, 1998; Ramsay and Kaiser 1998; Mensink *et al.*, 2000). Further damage is also seen through disruption to embryonic development, as capsules are removed from the substratum (Mensink *et al.*, 2000). Nonetheless, damage attained from fisheries is not only from beam trawls and discarding of by-catch, but also directly from the whelk fisheries themselves. This occurs through the process of riddling for size selection of whelks to land, whereby whelks are passed over a series of metal bars and tumbled allowing those below the MLS to be returned to sea (Cadée *et al.*, 1995; De Vooy and Van der Meer, 1998; Valentinsson *et al.*, 1999).

Gaps in literature and structure of thesis

With the increasing demand on *Buccinum undatum* fisheries, it is important to be able to understand and relate their recovery potential from damage incidents to the impact this has on the individual. Although some studies have investigated the direct influence of trawling damage on survival rates in *B. undatum* (Fonds, 1991; Fonds *et al.*, 1992; Fonds, 1994; Kaiser and Spencer, 1995; Mensink *et al.*, 2000), along with studies of growth in other species, for example, the Antarctic brachiopod *Liothyrella uva* (Cross *et al.*, 2015) and New Zealand brachiopod *Calloria inconspicua* (Cross *et al.*, 2016), there is still a paucity of information regarding environmental impacts along with the process and mechanisms of shell growth and repair and the factors affecting this within UK gastropod species, in particular that of *B. undatum*.

It is clear from this overview that as part of the protection of whelk fisheries a more detailed understanding of whelk's shell morphology and their ability to repair damage will be a valuable aid to fisheries management. In addition, understanding the impacts of shell damage to an individual will provide further information into their survival and growth capabilities. Throughout this thesis I investigate the variation and impact of shell damage on *B. undatum*. In addition, details of individual life history and development, along with key environmental factors, will be used to further assess impacts on shell growth and repair. I will also investigate the geochemistry of the shell and the elemental composition of both the original and repaired shell sections and compare individual structure through a variety of analytical techniques. The methods used will help provide a greater understanding into the variation and morphological differences found within *B. undatum* and allow us to build our knowledge on the impacts that both direct and indirect damage have on the growth and population structure of this commercially and ecologically important species.

Chapter 2 – Assessment of the shells of *Buccinum undatum*

This chapter will present data on the variation of shell repair within archived shells of *B. undatum*. Analysis of shell colour will build on work carried out by Magnúsdóttir *et al.* (2018 and 2019) where external shell colour of *B. undatum* was analysed off the coasts of Iceland. However, for this chapter the internal shell colour, and shell variations with respect to shell

damage will be examined in and around the UK, to assess variation within and between different locations.

Chapter 3 – *Shell repair and growth in experimentally-damaged *Buccinum undatum**

This chapter builds on work on shell damage and repair conducted by Colvin *et al.* (2022b). Mechanical shell damage will be carried out under laboratory conditions to assess rates of shell growth and re-growth in relation to different physiological and environmental conditions. This will add to the current gaps in literature surrounding the impacts of shell damage and mechanisms of recovery, to gain an insight into their recovery capability.

Chapter 4 – *Shell structure of *Buccinum undatum**

For this chapter the visible structure of the shell will be quantified, identifying the form of calcium carbonate, and looking at the distinct shell layers (microstructures) present. The imaging and analysis within this chapter will also be used as further validation into the underlying features of shell growth and structural re-growth.

Chapter 5 – *Trace element incorporation in *Buccinum undatum* shells*

Within this chapter I will build on the processes involved in shell repair. However, for this chapter I will look at an elemental scale. Through trace element analysis and mapping the periods of shell repair and original ‘normal’ shell growth, I can gain a further insight into how this rapid growth can occur and its physiological implications to *B. undatum*.

Chapter 6 – *General Discussion*

This discussion will draw together the findings throughout this thesis and highlight the relation to current literature and its importance for the population structure of *B. undatum* and their management.

Chapter 2 – Assessment of the shells of *Buccinum*
undatum

Figures

Figure 2.1: Morphological differences in the shells of *Buccinum undatum* (Taken from Dautzenberg and Fischer, 1912). Image 1-13, collection locations; 1) France, 2) Holy Island (Wales), 3) France, 4) Iceland, 5) France, 6) Sweden, 7) Unknown, 8) Shetland, 9) Iceland, 10) Norway, 11) Norway, 12) England, 13) England.32

Figure 2.2: Damage to the shell margin (lip) of the shell of *Buccinum undatum* (red arrows) with increased shell thickening resulting in a surface shell scar along margin of damage. Scale bar = 10mm. White label shows experiment and individual identifier of the whelk.33

Figure 2.3: Variations in shell colour of juvenile (A and B) and adult (C and D) *Buccinum undatum* from a single Menai Strait population. Clear differences in internal and external colour can be observed. Scale bars = 5mm.....34

Figure 2.4: Map of the United Kingdom (A) and North Wales (B) to show the main locations where *Buccinum undatum* were collected for the assessment of natural shell damage and shell colour. A) Sample sites J = Jersey, K = Kent and S = Saundersfoot and B) Purple circle denotes North Wales sampling, where A = Amlwch, B = Brynsciencyn, H = Holyhead, M = Menai Strait, N = Nefyn and R = Red Wharf Bay.....38

Figure 2.5: *Buccinum undatum*, in each of the 5 damage stages, A) No damage, B) slight damage, C) moderate damage, D) Heavy damage and E) severe damage. Examples of damage shown on C, D and E marked with red arrows. Yellow dashed line represents total shell length and black numbered arrows show whorl numbering from 1-6.40

Figure 2.6: Examples of internal shell colours of white, yellow, orange, brown and purple from *Buccinum undatum* shells, along with a Macbeth chart used for colour identification.41

Figure 2.7: Spectrophotometry equipment, showing the 400 µm halogen reflectance probe and white standard to indicate the set distance and angle used (arrow).....41

Figure 2.8: Fine polished blocks of *Buccinum undatum* shells embedded in resin. Cross sections allow internal shell layers to be visible under Raman microscopy.....42

Figure 2.9: Relationship between natural log (Ln) shell weight and Ln length in 500 *Buccinum undatum* caught between 2013 and 2019 from five locations around the UK $Y=2.63X-8.61$, $r^2 = 0.96$ (Saundersfoot), $Y=2.52X-7.97$, $r^2 = 0.98$ (Nefyn), $Y=2.92X-9.85$, $r^2 = 0.71$ (Holyhead), $Y=2.66X-8.78$, $r^2 = 0.97$ (Amlwch), $Y=2.70X-8.82$, $r^2 = 0.93$ (Kent).43

Figure 2.10: Plot of the total number of damage incidents/shell repairs per *Buccinum undatum* and total shell length (mm) (n = 500).....45

Figure 2.11: Plot of the total number of damage incidents/ shell repairs per *Buccinum undatum* and total shell weight (g) (n = 500).45

Figure 2.12: Total number of damage incidents/repairs in 100 *Buccinum undatum* shells from each location (bar). The red line shows data from shells displaying ≥ 1 damage incident/repair.47

Figure 2.13: Proportion of incidents/shell repairs on different parts of the shell from 100 *Buccinum undatum* from each of five locations.47

Figure 2.14: Number of shells from each of five locations displaying different levels of damage (from no damage to severe damage). 100 shells analysed from each location.48

Figure 2.15: Square shaped pieces cut from the internal shell of *Buccinum undatum* from Kent displaying a change in colour associated with shell damage.49

Figure 2.16: Pie chart showing the number of shells displaying one of the five internal colours - white, purple, brown, yellow, or orange of n = 4000 *Buccinum undatum* shells from all nine survey sites; Amlwch, Brynsiencyn, Holyhead, Jersey, Kent, Menai Strait, Nefyn, Red Wharf Bay and Saundersfoot.50

Figure 2.18: Variation in the five shell colours by location in 4000 *Buccinum undatum* shells. Proportion of colours present across the nine locations. Number of shells examined: Menai Strait (n = 308), Nefyn (n = 893), Brynsiencyn (n = 184), Jersey (n = 477), Saundersfoot (n = 302), Kent (n = 1171), Holyhead (n = 316), Amlwch (n = 302) and Red Wharf Bay (n = 47).50

Figure 2.18: Reflectance spectra from each internal shell colour from *Buccinum undatum*. From left to right yellow (A), brown (B), orange (C), white (D) and purple (E) coloured internal shell segments (\pm SD). The sixth and final figure (F) shows each spectrum plotted against the known colour wavelengths. Ribbons represent \pm SD.52

Figure 2.19: Peak centres from fitted spectra identifying the prominent (highest) peak positions of 520, 560, 620, 660 and 780 nm, identified with red arrows.....53

Figure 2.20: Voigt peaks fitted from prominent reflectance wavelengths (nm). a.u. on y-axis represents arbitrary units. Key peaks marked by dashed vertical lines (520, 560, 620, 660 and 780 nm). Coloured lines correspond to order of peak fitting $y = (\text{original spectra}), F[0](x) = \text{fit 1}$ through to $F[4](x) = \text{fit 5}$. $F(x)$ is final fitted spectra. Note not all colours have 5 peaks fitted. Figures show white, purple, brown, orange, and yellow from top to bottom.....55

Figure 2.21: Average peak height for each colour against highest (780 nm) lowest (520 nm) and mid (620 nm) prominent reflectance peaks for *Buccinum undatum* shell sections. Number of

shells within peak group for each colour varies depending on if a peak was fitted (See Appendix 2 and 3). Error bars $\pm 1SE$. a.u. represents arbitrary units.56

Figure 2.22: Screen shot image of Raman laser point (crossed hairs) for each shell layer measured, in the outer prismatic (A) and the crossed-lamellar B) and (C) shell microstructures. Final data comprised of multiple points per layer.58

Figure 2.23: Background corrected Raman spectra wavenumbers between 141 and 3200 cm^{-1} for shell microstructures indicated in Figure 2.22; outer prismatic, and two orientations of the crossed-lamellar structures in *Buccinum undatum* for each coloured shell, purple (P), orange (O), brown (B), white (W), and yellow (Y). Clear peaks marked with vertical dashed lines. Y-axis a.u. represents arbitrary units.....59

Figure 2.24: Scatter plot showing the relationship between the mean wavenumber (cm^{-1}) positions of the primary peaks.....60

Tables

Table 2.1: ANCOVA Multiple comparison matrix for the linear relationships of natural log (Ln) shell length and Ln shell weight of five geographical locations. (***) = significance, $p < 0.001$, N.S = non-significance, $p > 0.001$)44

Table 2.2: Chi squared test significance for (A) the variation in level of damage on the shells from five geographical locations and (B) variations in the degree of shell damage (no damage, to severe damage) by geographic location.....48

Table 2.3: Repeated Chi squared analyses for significant association of colour (W = white, P = purple, B = brown, Y = yellow, O = orange) amongst *Buccinum undatum* shells. The highest contributing colour to the test at each level was removed for each stage of the test.51

Table 2.4: Association of each of the nine locations against each visible colour for *Buccinum undatum* shells.....51

Table 2.5: A-C; Table of mean peak (P1 and P2) wavenumber values (cm^{-1}) with standard deviation (SD) calculated for each colour group of shells for crossed-lamellar 1 (XLAM1), crossed-lamellar 2 (XLAM2) and outer prismatic shell microstructures (Outer). Shells with no prominent peak 1 or peak 2 values were discounted and removed for these calculations (n=0).61

Introduction

Variations in phenotypic traits play an important role in evolutionary and ecological studies in the marine environment and are useful factors for understanding connectivity and delineating population boundaries (Levin, 1992; Woods and Jonasson, 2017; Magnúsdóttir, 2018; Benestan, 2020). Interspecific variation in marine gastropod shell morphology has been well studied in organisms from both intertidal and subtidal habitats (Vermeji, 1973; Palmer, 1985; Solas *et al.*, 2015). In contrast, intraspecifically, this level of understanding is still developing, particularly in relation to morphological variation within a single population, which is key for responding to the spatial management and conservation of exploited gastropod populations (Hollyman, 2017; Magnúsdóttir *et al.*, 2018; Magnúsdóttir *et al.*, 2019).

Morphometric variation

Morphological variations are often seen in response to local environmental factors and, in the long term, through the historical demography of a species. These variations can result from both abiotic and biotic factors such as wave exposure and predation pressure, for example shell shape variation in *Nucella lapillus* (Palmer, 1990; Pascoal *et al.*, 2012), and from anthropogenic effects, including damage arising from impacts with fishing gears (Cadée *et al.*, 1995; Nicholson and Evans, 1997; Ramsay and Kaiser, 1998; Valentinsson *et al.*, 1999; Mensink *et al.*, 2000). Due to the range of easily measurable morphological features (e.g., shell length, shell width and aperture shape), the shells of marine gastropods are an ideal candidate to explore shell shape variation. The common whelk, *Buccinum undatum*, has a highly variable shell morphology and its different life history traits are well recognised. These differences are often related to geographical location, for example external shell colour and shell morphometrics, including shell thickness and aperture shape (Thomas and Himmelman, 1988; Shelmerdine *et al.*, 2007; Magnúsdóttir, 2010; Haig *et al.*, 2015; Magnúsdóttir *et al.*, 2018; Emmerson *et al.*, 2020). However, differences in shell morphology are understudied within localised populations.

Sexual dimorphism has been observed within *B. undatum* populations (Ten Hallers-Tjabbes, 1979; Kenchington and Glass, 1996), where female whelks displayed taller (shell length) and heavier shells than male whelks. Nonetheless, although differences between sexes

have been noted in whelks from some areas, this has proved inconclusive in other populations, for example in Iceland, due to the inherent effect of location in addition to sex (Thomas and Himmelman, 1988; Magnúsdóttir, 2010; Hollyman, 2017). Differences in morphology not only occur over large geographic spatial scales, but also within a single area or population with changes in depth and hydrological conditions of the habitat and have been noted historically since the 1800's (Jeffries, 1867; Golijov, 1968).

Changes in gastropod shell shape and structure have been studied in *B. undatum* in response to predation and repeated shell damage from predators. Thomas and Himmelman (1988) and Gendron (1992) studied the variation in shell shape and structure of *B. undatum* exposed to a range of predators in the Gulf of St Lawrence, Canada. These authors showed that size selection of whelks as prey was based on whelk's shell thickness and aperture shape. For example, in areas with high starfish presence, shell apertures were smaller and rounder than in whelks from areas with low starfish numbers. In locations where there were high crustacean (crab and lobster) numbers, whelks shell thickness was greater, and the shell had a higher tensile strength to protect against crushing. Similar responses to predator presence and wave exposure have been documented for the dog whelk *Nucella lapillus* (Berry and Crothers, 1974; Crothers, 1983; Guerra-Varela, 2009). On sheltered rocky shore locations with high predator abundance, for example the common shore crab *Carcinus maenas*, dog whelk shells are thick, apertures are small and spire lengths long compared with dog whelk shells from wave-exposed rocky shores with low predator abundance where shells have small apertures and small spire lengths (Large and Smee, 2013). These morphological features have led to observable differences in the shell structure, strength, and shape over time, to allow the organism to adapt to its surroundings. The ecological adaptation of a species to their surrounding environment, and to local pressures is of key importance for survival and reproductive success (Linhart and Grant, 1996; Kawecki and Ebert, 2004; Sanford *et al.*, 2011; Peterson *et al.*, 2014).

Variation in whelks shell morphology arising from abiotic and biological factors has been documented for many years (Figure 2.1), with resultant effects described as being both environmentally and genetically controlled (Datzenberg and Fischer, 1912; Weetman *et al.*, 2006; Magnúsdóttir, 2010). Geographical variations and local adaptations in shell shape over both relatively small and large spatial scales are often explained as the result of evolution and limited genetic connectivity as well as a response to environmental heterogeneity

(Valentinsson *et al.*, 1999; Magnúsdóttir, 2019). This is particularly apparent in *B. undatum* which lay egg capsules, have direct larval development in the egg capsule, and where juveniles hatch directly from the egg capsules. Furthermore, offshore variations in morphology may be linked to migrations of localised sub-populations, and limited mobility (Weetman *et al.*, 2006).



Figure 2.1: Morphological differences in the shells of *Buccinum undatum* (Taken from Dautzenberg and Fischer, 1912). Image 1-13, collection locations; 1) France, 2) Holy Island (Wales), 3) France, 4) Iceland, 5) France, 6) Sweden, 7) Unknown, 8) Shetland, 9) Iceland, 10) Norway, 11) Norway, 12) England, 13) England.

Shell damage, and subsequent shell scarring can also arise from impacts with bottom towed fishing gears (e.g., beam trawls and scallop dredges), fished pots and size-selective riddling of the catch (Figure 2.2) (Mensink *et al.*, 2000; Ramsay *et al.*, 2000, 2001; Moschino *et al.*, 2003; Vasconcelos *et al.*, 2011). Such events can change the shell structure over time, with increased damage incidences often resulting in shell thickening (as demonstrated later in Chapter 4). The incidence of damage to the shell varies greatly between geographical location, chiefly because of fluctuations in predator presence and fishery demand. For example, in the coastal waters around the UK there is high demand for whelks and in 2020 >6000 tonnes were landed into UK ports (by UK vessels under 10 m), at a value of £7.7 million (MMO, 2020). The recent high demand for whelks has seen increased fishery effort and consequent disturbances to local populations, which in turn could lead to an increase in frequency of damage to the shells. Smaller shell size and lower reproductive output might result as whelks divert energy away from shell growth and reproduction to repair.

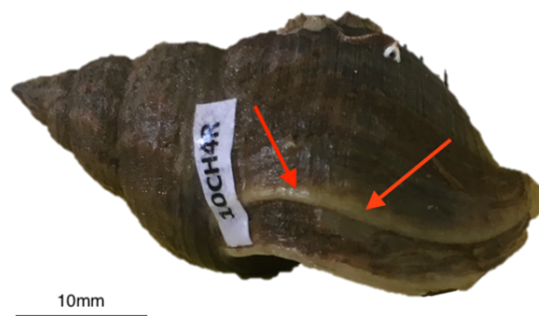


Figure 2.2: Damage to the shell margin (lip) of the shell of *Buccinum undatum* (red arrows) with increased shell thickening resulting in a surface shell scar along margin of damage. Scale bar = 10mm. White label shows experiment and individual identifier of the whelk.

Shell colour differences and shell pigment presence

The shells of molluscs frequently display differences in internal and external shell colour patterns (Hedegaard *et al.*, 2006; Williams, 2017; Saenko and Schilthuizen, 2021). For example, the inner layers of the clam *Mercenaria mercenaria* display patches of purple colour particularly around the umbo region (pers. obs.). The analysis of shell colour is no longer a purely subjective study, with practical methods allowing the elemental patterns to be measured within a colour spectrum (Endler, 1990). Colour in animals is most commonly used as a means of communication, thermoregulation and camouflage (Parker *et al.*, 1998; Fox and Moussalli,

2009) with variation in intensity and pattern occurring interspecifically (Sword and Simpson, 2000; McNaught and Owens, 2002; Hieber *et al.*, 2006). The natural appearance of a colour depends on three key processes, as explained by Endler (1990). Firstly, the physical process of light transmission and reflectance to reach the viewer, followed by the within-eye processes of refraction and photoreception. The final part is that of neural responses, giving an overall idea of colour and brightness.

Gastropods show a distinct variation in shell colour with different colour morphs seen between individuals, often because of geographic location and the surrounding environment (Sokolova and Berger, 2000; Sokolova *et al.*, 2000a). This has been seen in populations of flat periwinkle *Littorina obtusata*, whereby differences in colour are observed between individuals across temperature gradients. However, these differences are not significant enough to define a new species (Phifer-Rixey *et al.*, 2008). This has also been noted in the prosobranch *Austrocochlea constricta*, where banding patterns have been linked to diet availability and food presence (Underwood and Creese, 1976). *B. undatum* shows a similar response with differences in internal and external shell colouration with variations in pigmentation patterns on the shell (Figure 2.3) (pers. obs.; also, Magnúsdóttir, 2010; Magnúsdóttir *et al.*, 2018).

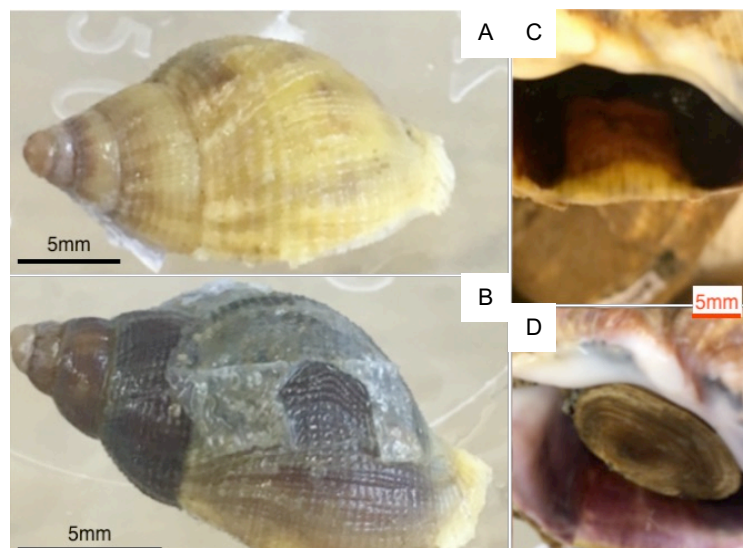


Figure 2.3: Variations in shell colour of juvenile (A and B) and adult (C and D) *Buccinum undatum* from a single Menai Strait population. Clear differences in internal and external colour can be observed. Scale bars = 5mm.

Little is currently known about why and how differences in shell colour arise, particularly on the inside of the shell. It is speculated that it maybe schemochromic, genetic, evolutionary,

or the result of biochromic pigment presence and differences in shell microstructure that cause variances in shell colour. It has also been suggested that molluscan shell colour may result from the disposal of metabolic by-products in the mineralising shell. Occasionally the variation may solely be the result of evolutionary processes although this is unlikely to be the only reason, with many factors influencing pattern and colour polymorphisms (Comfort, 1951; Wilbur and Owen, 1964; Nuttall, 1969; Currey and Taylor, 1974; Saleuddin and Wilbur, 1983; Kobluk and Mapes, 1989; Hedegaard *et al.*, 2006). Nonetheless, the importance of colour, which in some taxa maybe incidental, is often presented as short temporal scale adaptation as opposed to long-term change to enable them to blend in with their surroundings (Williams, 2017).

To understand the origin of molluscan shell colour it is important to first understand its formation and the nature of the pigments present (Williams, 2017). The perceived shell colour is a result of reflected or transmitted wavelengths of light. Pigmentation within the molluscan shell is highly varied in both the inner and outer shell layers, with crystal deposition producing patterning and differences in colour in the shell (Comfort, 1951). The visible colour produced can differ because of pigment type, but it is also as a response to its concentration, with higher concentrations often increasing the colour saturation (Hedegaard *et al.*, 2006). The presence of pigments in molluscan shells can be determined using Raman spectroscopy, although the identification of specific pigments and the location of colour within the shell matrix is still largely unknown (Burgio and Clark, 2000; Vandenabeele *et al.*, 2000; Hollyman, 2017; Williams, 2017). Williams (2017) noted that most chemical studies of the molluscan shell have taken place within the last 50 years and few of these have been fully comprehensive using the range of modern analytical techniques now available. Melanin, porphyrins, and bile pigments along with carotenoids that cause shell colouration have been detected within the shell and these pigments are generated by a common mechanism. However, there is a paucity of research investigating how and why they are incorporated into the shell and the energetic cost of this production within a single species. Within gastropod species, these pigments are generally produced from the shell secreting mantle and incorporated into the growing edge of the shell, with pigmentation usually found on the outer surface of the shell, although there are some exceptions to this such as deposition into the inner layers (Hollyman, 2017; Williams, 2017; Magnúsdóttir *et al.*, 2018).

In some instances, colour maybe incidental, as a result of pigment presence, but may prove relevant to shell construction itself. This is seen within other taxa, for example, melanin has been linked to carapace strength and helps reduce abrasion in insect cuticles and feathers in birds (Burrt, 1977; Bosner, 1996; True, 2003; Williams, 2017). Alongside the pigment melanin, one of the key enzymes used in the melanin pathway, tyrosine, has been noted as a fundamental amino acid used in biomineralization. There is also some evidence to support the theory of pigmentation and patterning being used by molluscs as a growth marker to control areas of growth within the shell (Sun *et al.*, 2015; Williams, 2017). However, shell colour has not only been seen as a result of pigment presence, but some molluscan species also display colour with the absence of pigments due to element incorporation within the shell calcium carbonate, for example with the incorporation of magnesium (Williams, 2017). Overall, there are many complex components involved within the internal structure of the shell that influence shell growth and colour of an organism, and it is both abiotic and biotic factors that drive the maintenance and diversity of the colour patterns seen. For marine gastropods that have evolved direct development of their young, for example *B. undatum*, a limited dispersal is seen which often results in a reduction in demographic variation, with reduced genetic connectivity (Magnúsdóttir *et al.*, 2018 and 2019). Within UK populations of *B. undatum* there is a striking difference in polymorphism between individuals, with variation occurring both in shell shape and structure, as well as marked differences in internal shell colour (Hollyman, 2017; pers. obs.).

This chapter will focus on addressing the differences in shell damage and internal shell colour of populations of *B. undatum* from UK waters and explore the natural incidences of shell damage and shell repair. It is hypothesised that there will be large variations in internal shell colour within a population of *B. undatum*, and significantly different levels of natural shell damage in shells from five geographically different locations as a result of different local environmental conditions. In shell-damaged populations it is hypothesised that there will be a notable increase in the shell weight to length ratio in whelks with higher levels of historic shell damage, due to an increased deposition leading to thickening of the shell.

Materials and Methods

Variations in the shells, within and between populations of *Buccinum undatum* was assessed using a series of visual and analytical techniques to ascertain differences in shell damage and shell colour. For these assessments dry shells were used from a large (>4000) whelk shell collection housed in the School of Ocean Sciences, Bangor University, with n = 500 used for analysis of previous damage, and 4000 used for assessment of colour. Shells had been collected between 2013 and 2019 by local fishermen from locations around the UK i.e., Jersey, Kent, Saundersfoot, Nefyn, Holyhead and Amlwch (Figure 2.4) and used in previous research on *B. undatum*. Additional live whelks were collected in 2018 and 2019 from the Menai Strait, Nefyn, and Brynsiencyn, North Wales, UK (Figure 2.4) and were also used in experiments reported later in Chapters 3 to 5. All shells had been air-dried and cleaned in fresh water after flesh removal and stored in airtight containers away from direct sunlight.

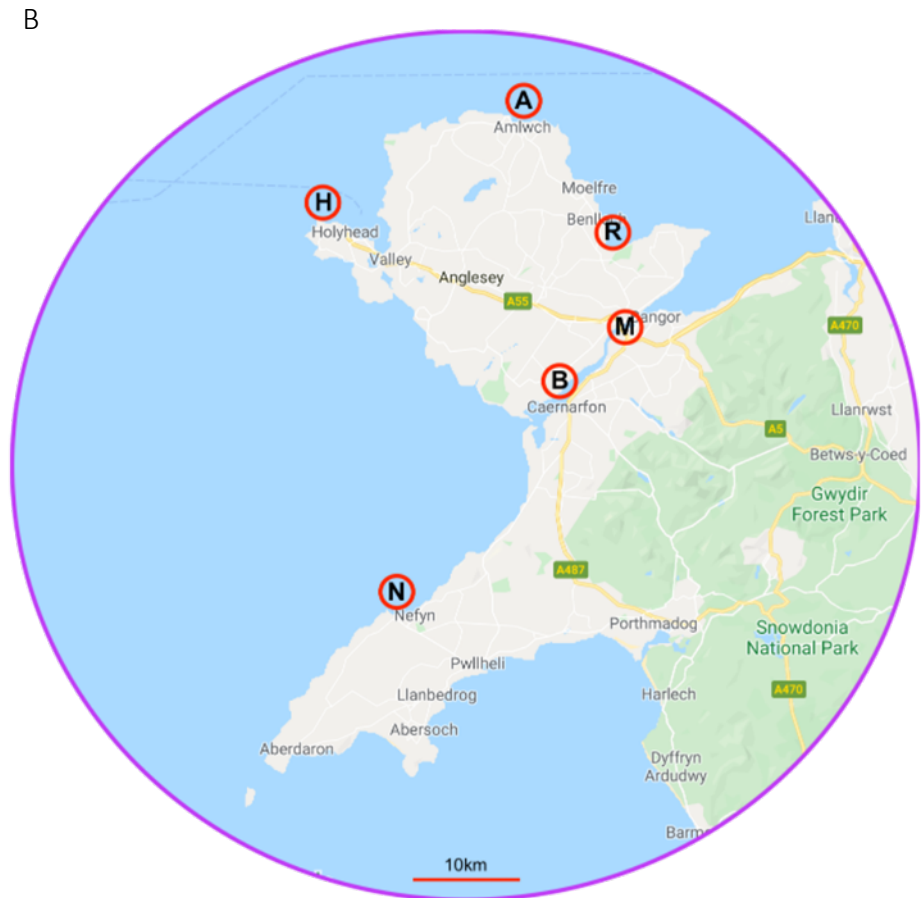
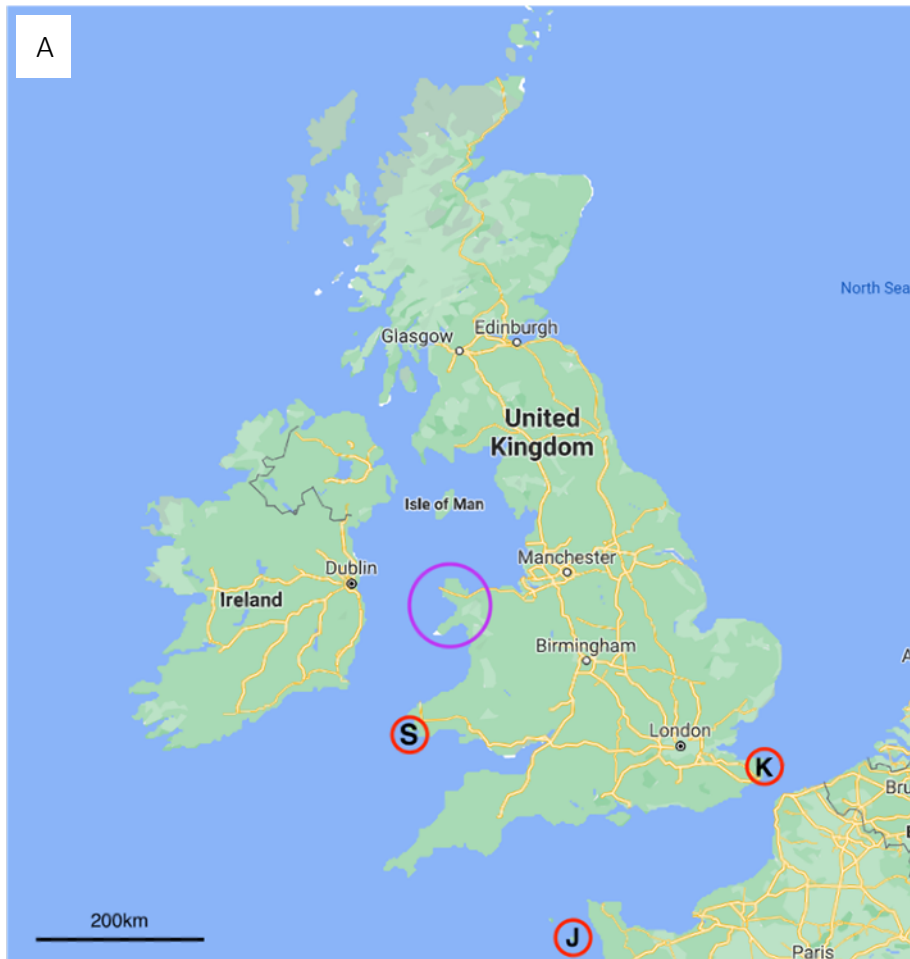


Figure 2.4: Map of the United Kingdom (A) and North Wales (B) to show the main locations where *Buccinum undatum* were collected for the assessment of natural shell damage and shell colour. A) Sample sites J = Jersey, K = Kent and S = Saundersfoot and B) Purple circle denotes North Wales sampling, where A = Amlwch, B = Brynsiencyn, H = Holyhead, M = Menai Strait, N = Nefyn and R = Red Wharf Bay.

Assessment of shell damage

The levels of shell damage previously received by whelks in their natural environment were assessed in 100 randomly selected shells of a range of sizes (20 to 109 mm total shell length) from each of five different geographical locations: Kent, Saundersfoot, Nefyn, Holyhead and Amlwch (total n = 100 per site) (Figure 2.4 and 2.5). Total shell length of each whelk was measured using Vernier callipers (to 0.1 mm) and weighed on a digital top-loading balance (to 0.01 g). These data were checked for normal distributions (Kolmogorov-Smirnov test) and homogeneity of variance (Levene's test), and log-transformed (Ln) shell weight plotted against Ln shell length for each whelk population. Length weight relationships in the five populations were investigated using a General Linear Model (GLM, using the *smatr* package in R; Warton *et al.*, 2012).

Each shell whorl was carefully inspected for damage/repair and the number of incidences recorded on each shell. The scale of damage/repair was assessed on a five-point scale i.e., (0) *undamaged* (no obvious repairs), (1) *slight damage* (one or two shell repairs) (2) *moderate damage* (two shell repairs but less than 4 repairs), (3) *heavy damage* (>4 shell repairs and usually the shell is badly damaged with numerous shell repairs) and (4) *severe damage* (entire shell is badly scarred and covered with major shell repairs) (see Figure 2.5). The number of shell repairs per shell was plotted against total shell length and then the number of shell repairs per shell at each of the five locations examined to investigate whether shell damage was related to individual whelk size and/or specific location. The location of shell damage on the different parts of the shell was recorded i.e., shell lip/margin, siphonal canal, shell spire and each whorl (whorl 1 at the spire through to the aperture whorl) (Figure 2.5).

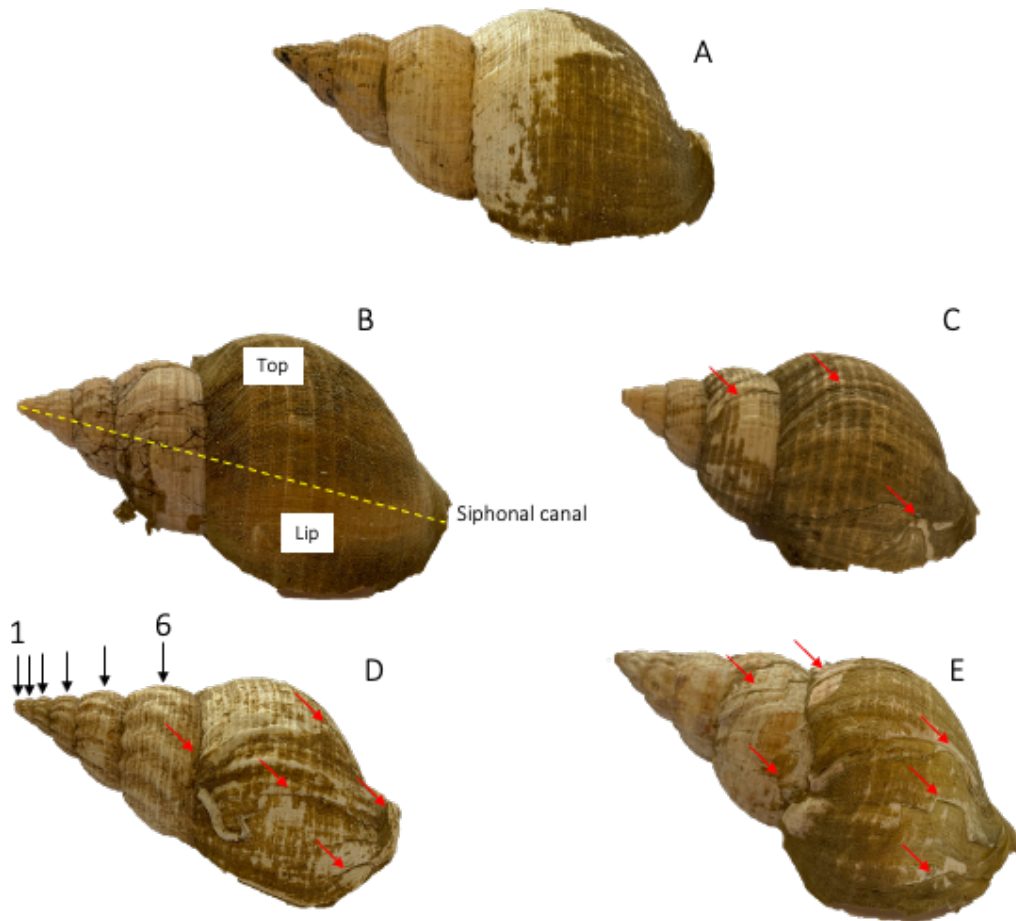


Figure 2.5: *Buccinum undatum*, in each of the 5 damage stages, A) No damage, B) slight damage, C) moderate damage, D) Heavy damage and E) severe damage. Examples of damage shown on C, D and E marked with red arrows. Yellow dashed line represents total shell length and black numbered arrows show whorl numbering from 1-6.

Assessment of shell colour

The internal shell colour of 4000 whelk shells from the School of Ocean Sciences collection that comprises nine locations around the UK: Amlwch, Brynsiencyn, Holyhead, Jersey, Kent, Menai Strait, Nefyn, Red Wharf Bay and Saundersfoot (Figure 2.4) was visually assessed and assigned a colour; either white, purple, brown, yellow, or orange (Figure 2.6). The total number of the whelks with the five different inner shell layer colours was determined and the proportion of each shell colour from each of the nine locations investigated. Visual colour assessment occurred alongside a Macbeth chart (Figure 2.6). Chi-Squared analysis was used to ascertain whether the frequency distributions of internal shell colour differed from the expected frequencies for each site. To quantify differences in inner shell colour between location, spectrophotometry was used (White *et al.*, 2015; Johnsen, 2016).

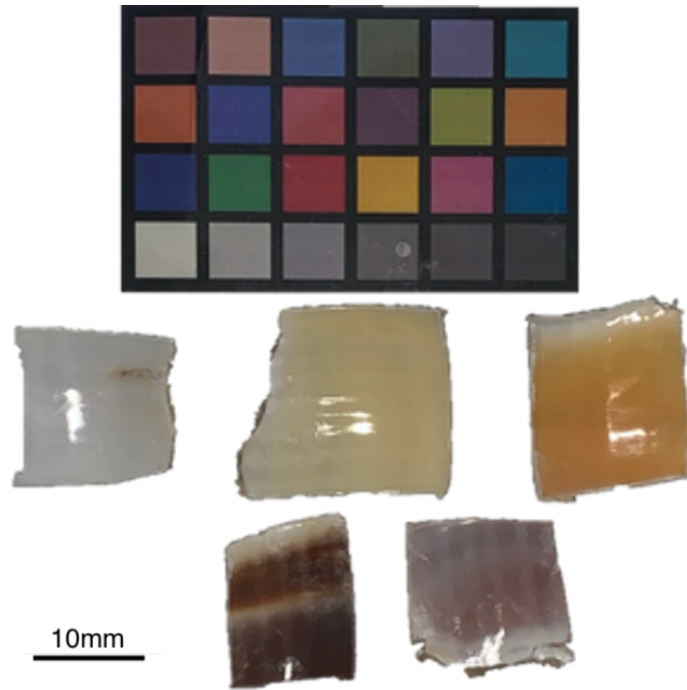


Figure 2.6: Examples of internal shell colours of white, yellow, orange, brown and purple from *Buccinum undatum* shells, along with a Macbeth chart used for colour identification.

Reflectance measurements were made in a darkened room using an Ocean Optics USB2000+ Spectrometer (200 – 1100 nm range), with a bifurcated 400 μm reflectance probe (Figure 2.7). After initial calibration of light and dark, using a white and black standard, twenty shells of each of the five colours were randomly selected from the 4000 shells and reflectance measurements made. Measurements were taken at three equidistant points on each inner shell surface, along the same axis at a 45° angle and set distance for standardisation.

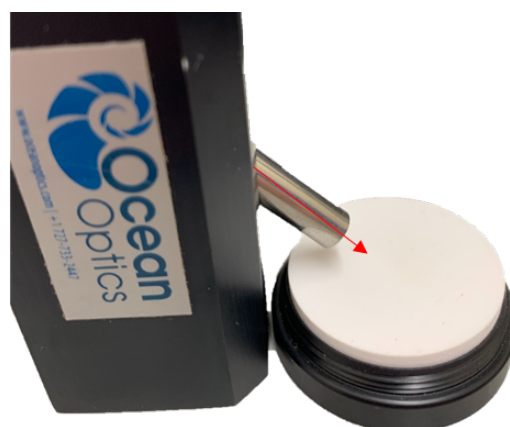


Figure 2.7: Spectrophotometry equipment, showing the 400 μm halogen reflectance probe and white standard to indicate the set distance and angle used (arrow).

Average measurements of reflectance were taken for each shell and plotted using the *Pavo* package in R-Studio (Maia *et al.*, 2013). Low wavelength data were removed before the spectral peaks were normalised and broken down into several Voigt peaks through deconvolution using Fityk 1.3.1 (Wojdyr, 2010). Individual positions of key wavelengths were ascertained and the differences in colour were determined through the difference in proportion of these peaks. Voigt peaks were used due to their precision in describing spectrographic data, as a convolution of Gaussian and Lorentz distributions (Gołabczak and Konstantynowicz, 2009; Schreier, 2018). Peak fitting varied between shells with some fitting four and others five to reduce the weighted sum of squared residuals (WSSR) value, often because of a lack of high wavelength data fitting higher wavelength peaks.

Having analysed the visual colour variations of the inner shell layers, Raman spectrometry was applied to further understand these variations by studying pigment colour presence. Sixty-four shells were selected with a range of the main five colours, and segments of shell were removed from the lip using a cutting wheel attached to a hand-held Dremel rotary tool. These pieces were embedded in resin and polished for analysis along the sectioned surfaces (Figure 2.8) (see Chapter 4 for details on the process of shell embedding and polishing). Raman analysis was carried out at the Oxford Diamond Light Source on the Reinshaw InVia Raman-Microscope, using a green laser at 473 nm (15 mW power and 20x magnification).

Two defined microstructures are present in the shells (see Chapter 4), the outer prismatic and crossed-lamellar (XLAM) layers and these were analysed. Two different crossed lamellar orientations were observed so both were analysed separately.



Figure 2.8: Fine polished blocks of *Buccinum undatum* shells embedded in resin. Cross sections allow internal shell layers to be visible under Raman microscopy.

Results

Shell comparisons between *Buccinum undatum* populations

The linear relationships between natural log (Ln-transformed) total weight and total shell length (Figure 2.9) appear similar between each location, with the steepest incline (slope) in the relationship in the Holyhead whelks and the greatest variation in the Ln weight to length relationship in the Amlwch whelks. Significant differences in these slopes were found, with Kent and Nefyn being different to all sites, $p < 0.001$ (Table 2.1).

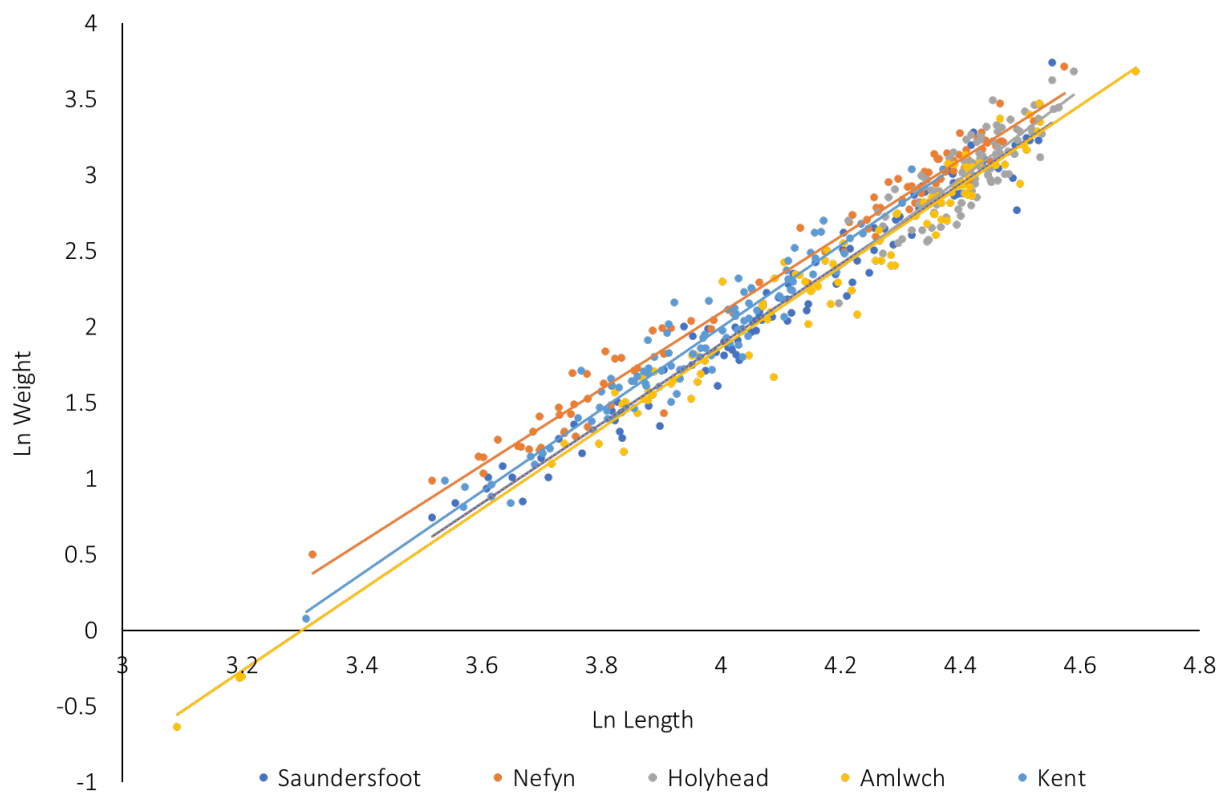


Figure 2.9: Relationship between natural log (Ln) shell weight and Ln length in 500 *Buccinum undatum* caught between 2013 and 2019 from five locations around the UK $Y=2.63X-8.61$, $r^2 = 0.96$ (Saundersfoot), $Y=2.52X-7.97$, $r^2 = 0.98$ (Nefyn), $Y=2.92X-9.85$, $r^2 = 0.71$ (Holyhead), $Y=2.66X-8.78$, $r^2 = 0.97$ (Amlwch), $Y=2.70X-8.82$, $r^2 = 0.93$ (Kent).

Table 2.1: ANCOVA Multiple comparison matrix for the linear relationships of natural log (Ln) shell length and Ln shell weight of five geographical locations. (***) = significance, $p < 0.001$, N.S = non-significance, $p > 0.001$)

Location	Amlwch	Kent	Holyhead	Nefyn	Saundersfoot
Amlwch	-				
Kent	***	-			
Holyhead	N.S	***	-		
Nefyn	***	***	***	-	
Saundersfoot	N.S	***	N.S	***	-

Distribution of shell damage in five *Buccinum undatum* populations.

The number of shell damage incidents/repairs with increasing total shell length generally shows that whelks between 20 and 110 mm frequently have up to 4 shell repairs and that the larger (older) whelk shells tend to have a greater number of damage incidents on their shell surfaces (Figure 2.10). Few shells had more than 6 repairs (4% total sample with 72% of these being from Holyhead). A Spearman's rank-order correlation showed the relationship between the total number of damage incidents/repairs and total shell length was statistically significant ($r_s = 0.371$, $n = 500$, $p < 0.01$), indicating that larger whelk shells have a greater number of damage incidents/repairs to their shell surface. The relationship between the total number of shell incidents and shell weight (Figure 2.11) showed a broadly similar pattern to the distribution of incidents with increasing total shell length. However, there was no clear indication that higher numbers of shell incidents/repairs resulted in heavier shells.

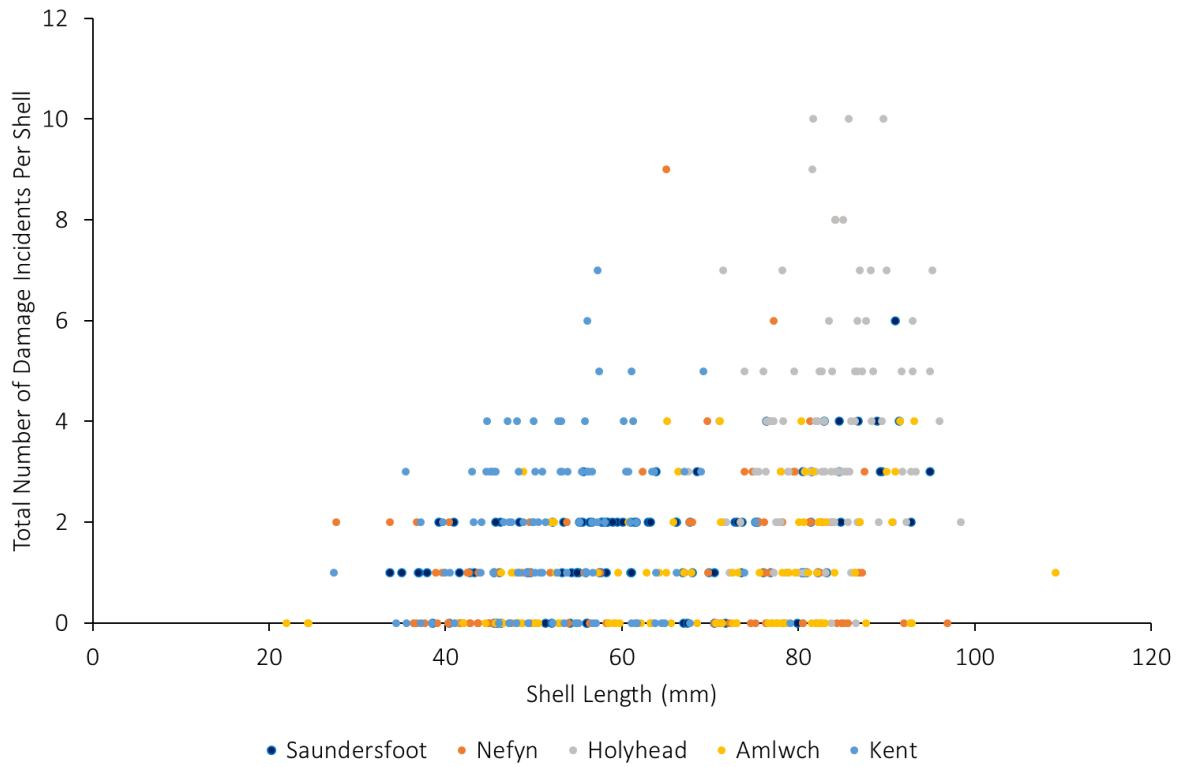


Figure 2.10: Plot of the total number of damage incidents/shell repairs per *Buccinum undatum* and total shell length (mm) (n = 500).

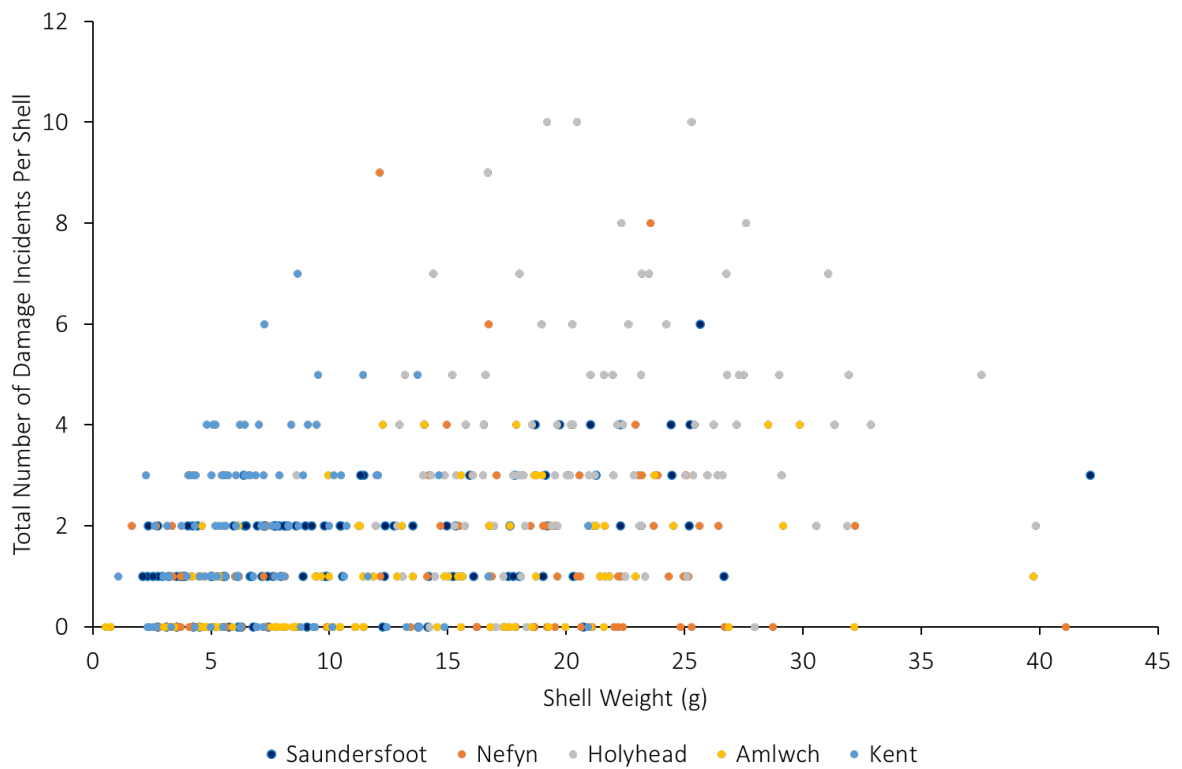


Figure 2.11: Plot of the total number of damage incidents/ shell repairs per *Buccinum undatum* and total shell weight (g) (n = 500).

The total number of damage incidents/repairs in 100 whelks from each location are shown in Figure 2.12. Holyhead whelks had the greatest overall damage with the most (369) shell incidents/repairs and over 95% of whelk shells displaying >1 damage incident. Whelk shells from Amlwch, by contrast, only had 93 incidents of damage with 51% of shells displaying >1 record of damage and no shells with heavy or severe damage. From these data, variations in shell damage were assessed, initially the position of damage on the shell (Figure 2.13) followed by the severity of damage (Figure 2.14).

Holyhead whelks, which had the greatest number of incidents of damage, displayed damage from the shell lip and siphonal canal around to whorl 3 (W3) of the shell. No shells appeared to have damage to whorls 1 or 2 (W1 or W2). The total number of damage incidents recorded on Holyhead whelks was 369, compared with an average of 140.5 incidents on shells from the 4 other locations. For the majority of whelks caught, damage was most commonly located on the lip of the shell ($n = 384$), with some individuals seeing repeated damage to this area, while the whorls appeared to receive the least collectively with whorls (W1-6) displaying a total of 117 repairs.

Of the 500 shells assessed, most had received 'slight shell damage' with only a few displaying severe or heavy damage. Severity of shell damage data from each location was investigated using a Chi-Squared test for association. Severity of shell damage varied significantly between location ($X^2 = 106.25$, d.f. = 16, $p < 0.001$). When the shell repair data were further broken down into individual geographical location using a goodness of fit model (Table 2.2), a consistent level of shell damage was observed (Table 2.2 A), with a variation in the level of damage seen on the shell between locations. However, when the makeup of different levels of shell damage within a single site was compared between geographical location no significant differences were found, i.e., the number of shells with no damage were proportional between locations (Table 2.2 B).

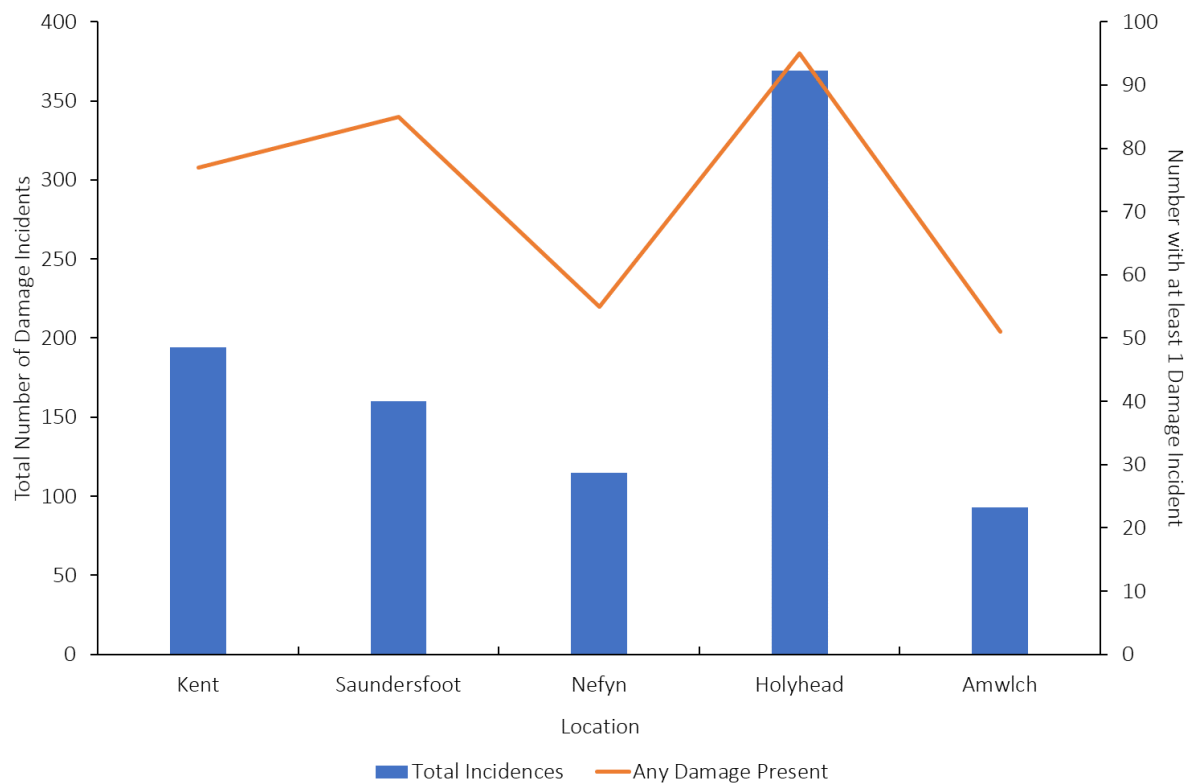


Figure 2.12: Total number of damage incidents/repairs in 100 *Buccinum undatum* shells from each location (bar). The red line shows data from shells displaying ≥ 1 damage incident/repair.

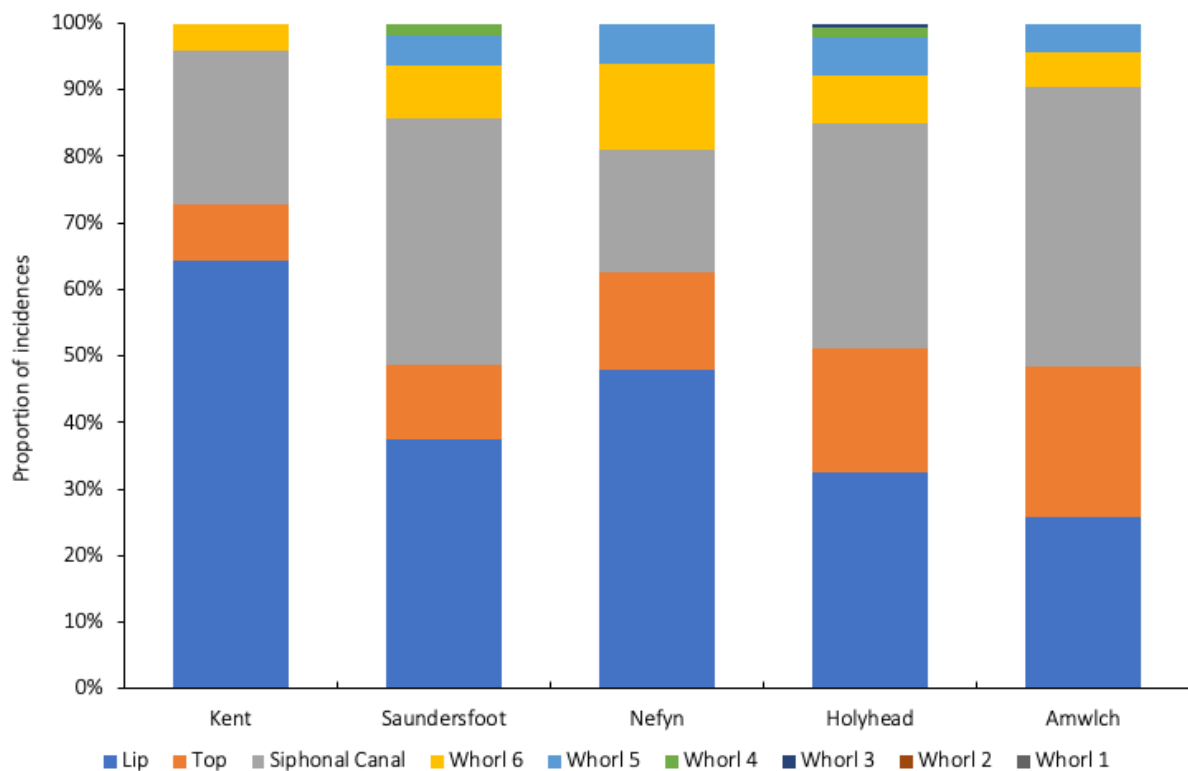


Figure 2.13: Proportion of incidents/shell repairs on different parts of the shell from 100 *Buccinum undatum* from each of five locations.

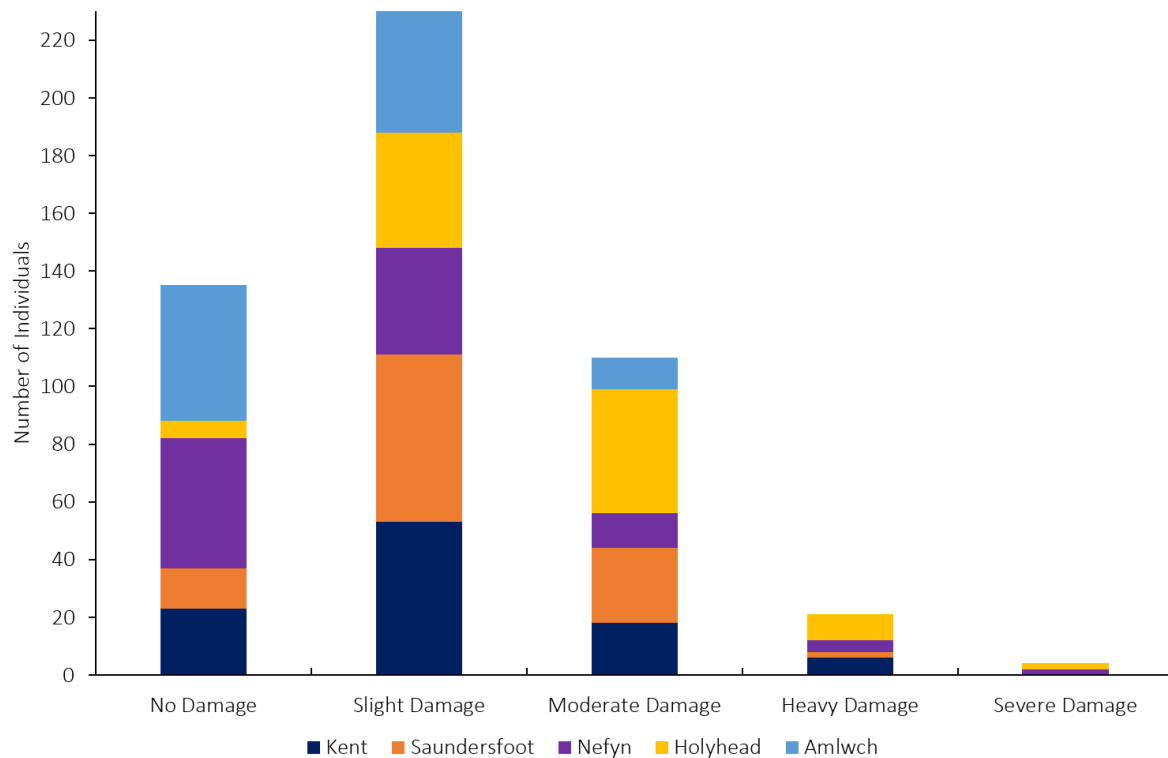


Figure 2.14: Number of shells from each of five locations displaying different levels of damage (from no damage to severe damage). 100 shells analysed from each location.

Table 2.2: Chi squared test significance for (A) the variation in level of damage on the shells from five geographical locations and (B) variations in the degree of shell damage (no damage, to severe damage) by geographic location.

	Test Variable	Against	Sig
A	Kent	Level of damage	0.001
	Saundersfoot		0.001
	Nefyn		0.001
	Holyhead		0.001
	Amlwch		0.001
B	No Damage	Location	0.737 N.S
	Slight Damage		0.327 N.S
	Moderate Damage		0.926 N.S
	Heavy Damage		0.805 N.S
	Severe Damage		0.679 N.S

Shell colour variation between *Buccinum undatum* populations

Differences in colour, and disruption to the internal shell colour in response to different levels of shell damage were observed amongst the different whelk populations studied (Figure 2.15). Five main internal shell colours were identified: white, purple, brown, yellow, and orange (Figure 2.6 and 2.16). A white internal shell was the most dominant colour amongst the 4000 shells examined comprising 39.9% (n = 1597) of all shells, compared with; 7.8% (n = 310) purple, 15.2% (n = 608) brown, 17.4% (n = 697) yellow and 19.7% (n = 788) orange respectively (Figure 2.16).

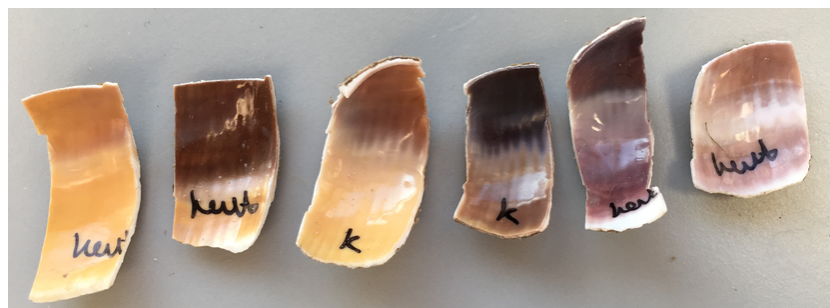


Figure 2.15: Square shaped pieces cut from the internal shell of *Buccinum undatum* from Kent displaying a change in colour associated with shell damage.

Internal shell colour was further investigated to assess whether location had any effect on shell colouration (Figures 2.16 and 2.17). With the exception of the Brynsiencyn shells, where a brown inner shell layer was the dominant colour, for all the other locations a white inner shell was significantly the most dominant shell colour, and an internal purple coloured shell was the least observed (Figure 2.16). There are widespread variations in the proportion of the different colours in the shells from the different locations. The cause of these variations is so far unknown. A Chi Squared Goodness of fit model showed significant deviation from the expected number of shells in the five colour categories ($X^2= 1153.66$, d.f. = 4, $p < 0.001$) amongst all the geographical locations combined. *Post hoc* analysis following the removal of the highest contributing colour (white), showed a significant difference between all shell colours (Table 2.3). Further analysis showed that shell colour varied significantly between each individual location ($X^2= 1054.26$, d.f. = 32, $p < 0.001$), and through further Chi Squared tests, investigating the contribution of other individual colours, and how they varied per location (Table 2.4), all shell colours with the exception of a purple internal shell colour were significantly different between the nine locations; the colour purple was not significantly different (Line 3, Table 2.4).

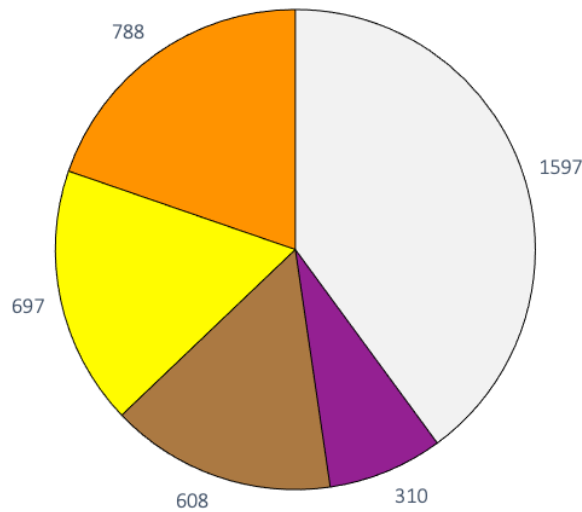


Figure 2.16: Pie chart showing the number of shells displaying one of the five internal colours - white, purple, brown, yellow, or orange of $n = 4000$ *Buccinum undatum* shells from all nine survey sites; Amlwch, Brynsiencyn, Holyhead, Jersey, Kent, Menai Strait, Nefyn, Red Wharf Bay and Saundersfoot.

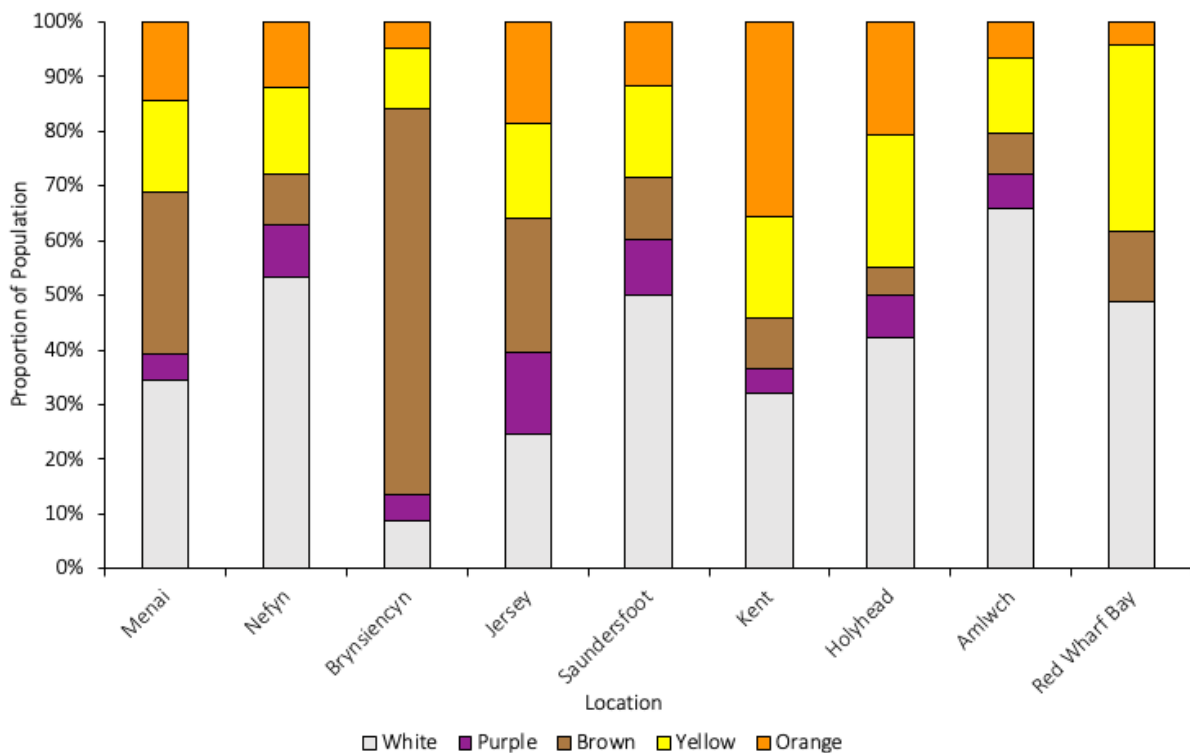


Figure 2.17: Variation in the five shell colours by location in 4000 *Buccinum undatum* shells. Proportion of colours present across the nine locations. Number of shells examined: Menai Strait ($n = 308$), Nefyn ($n = 893$), Brynsiencyn ($n = 184$), Jersey ($n = 477$), Saundersfoot ($n = 302$), Kent ($n = 1171$), Holyhead ($n = 316$), Amlwch ($n = 302$) and Red Wharf Bay ($n = 47$).

Table 2.3: Repeated Chi squared analyses for significant association of colour (W = white, P = purple, B = brown, Y = yellow, O = orange) amongst *Buccinum undatum* shells. The highest contributing colour to the test at each level was removed for each stage of the test.

Colours tested	DF	Chi Squared Statistic	Significance
WPBYO	4	9.45	<0.001
PBYO	3	161.14	<0.001
BYO	2	20.25	<0.001
YO	1	5.18	<0.05

Table 2.4: Association of each of the nine locations against each visible colour for *Buccinum undatum* shells.

Colour	DF	Chi Squared Statistic	Significance
White	8	237.36	<0.001
Purple	8	8.78	0.361 N.S.
Brown	8	22.91	<0.05
Yellow	8	41.61	<0.05
Orange	8	165.17	<0.001

Quantification of internal shell colour

Spectrophotometry

To test if the visual variation in shell colour is representative of a defined colour change, spectrophotometry was applied to the shells. Average peak intensity per colour was plotted against wavelength, with ribbons of error (\pm SD) (Figure 2.18). Brown and purple-coloured internal shell accounted for most of the variation around the mean whereas white, yellow, and orange had a much smaller deviation (Figure 2.18 A-E). Plots were then constructed against known colour spectra to examine each colour's peak position (Figure 2.18 F).

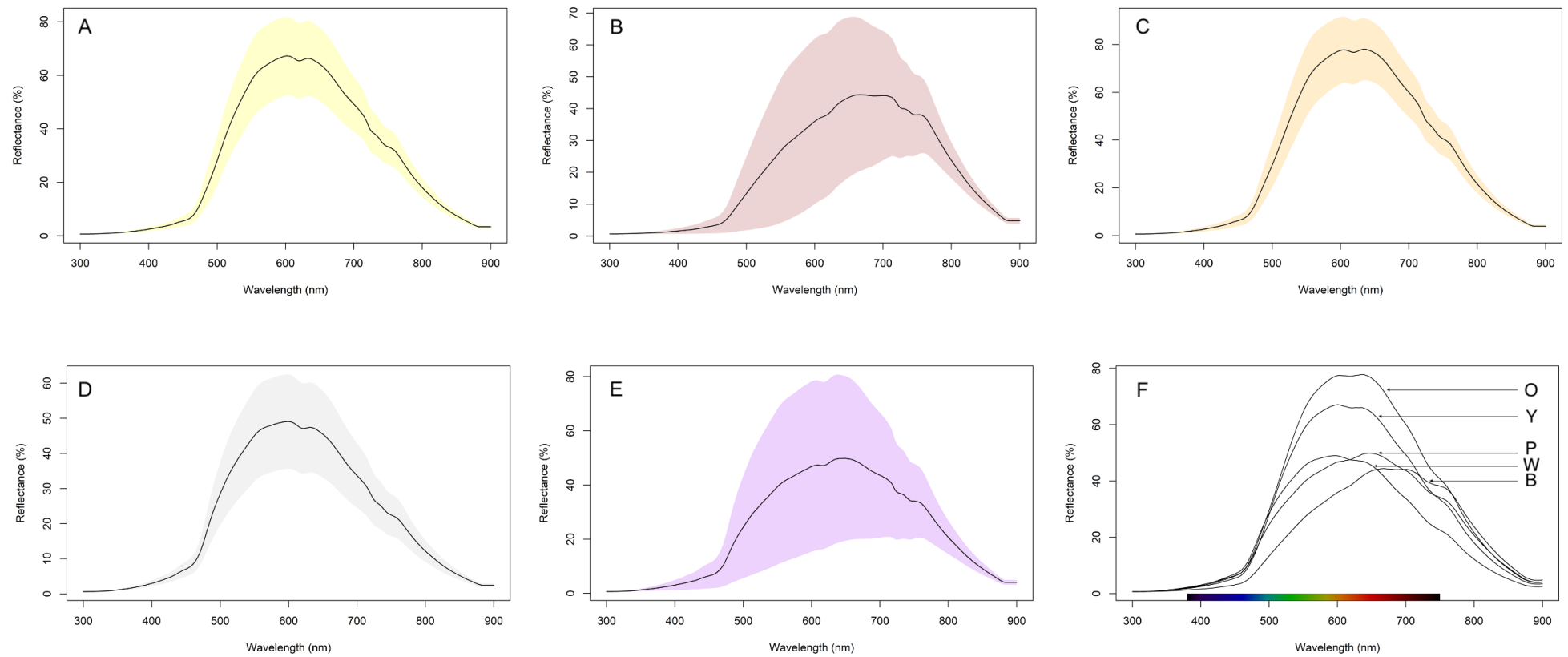


Figure 2.18: Reflectance spectra from each internal shell colour from *Buccinum undatum*. From left to right yellow (A), brown (B), orange (C), white (D) and purple (E) coloured internal shell segments (\pm SD). The sixth and final figure (F) shows each spectrum plotted against the known colour wavelengths. Ribbons represent \pm SD.

The differences in the spectra for each colour were considered likely to be the result of the mixing of different concentrations of several pigments. As each pigment would have their own spectra, the observed spectra would be the sum (composite) of those spectra. Therefore, to test this hypothesis the observed spectra were deconvoluted using the program Fityk.

Data were initially normalised to the peak maximum and to remove any uncertainty components, averages and standard deviations calculated for each shell. These data were not averaged for all shells of each colour, as spectrophotometry data showed they were significantly different. Initially, Fityk was allowed to identify its own peaks and a histogram of found peak centres from fitted spectra plotted (Figure 2.19). Five prominent peak positions of 520, 560, 620, 660 and 780 nm were identified (Figure 2.19), and these peak positions were then used to re-fit spectra to these values.

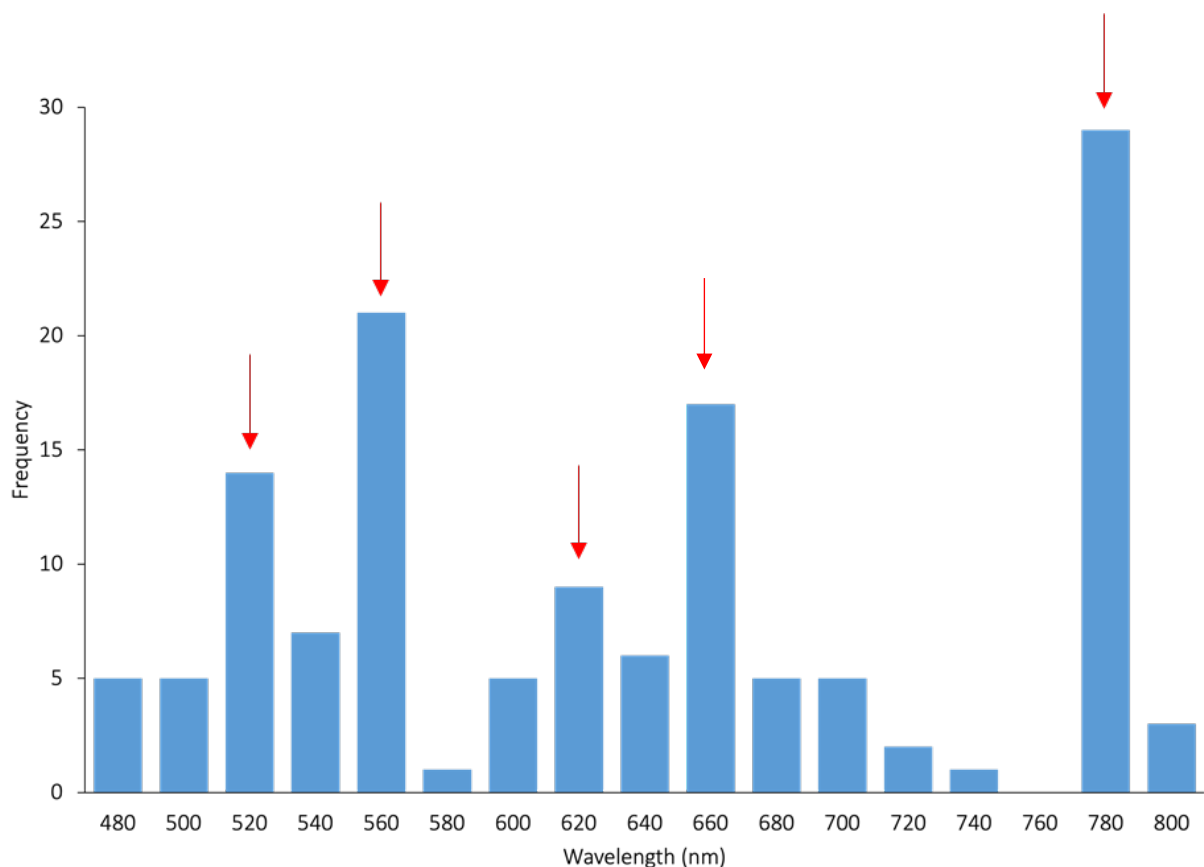


Figure 2.19: Peak centres from fitted spectra identifying the prominent (highest) peak positions of 520, 560, 620, 660 and 780 nm, identified with red arrows.

Plots were made as an example of each colour using spectra from the fitted prominent peaks, for an insight into the variation in potential pigment presence occurring, to detect any underlying causes of colour variation (Figure 2.20). The plots consist of the original spectrophotometry data, the final fitted spectra and its individual four or five component peaks. Variation in spectra composition was seen with changes in dominant peak height, with further changes seen in the order in which peaks were fitted and overall arrangement of key peaks. For each colour, plotted in Figure 2.20, this can clearly be seen by the change in composition of fitted peaks. Peaks were fitted dependant on WSSR value, with a lower value with a smaller change indicating a better fit.

The differences in spectra were quantified by plotting mean height against prominent maximum (780 nm), minimum (520 nm) and mid (620 nm) peaks to examine the variation seen with respect to colour (Figure 2.21). Peaks at 520 nm saw all colours to have very similar properties; at 780 nm, colours appear to have formed two distinct groups whereby purple and brown had a much higher peak height than white, orange, and yellow-coloured shells. For 620 nm all colours were more varied, with white being the most predominant change and with the greatest contribution at this wavelength, and purple and brown the least. From the combination of these analyses, from visual assessment to de-convolution of the spectra, differences in internal shell colour have been identified and the makeup of the individual spectra analysed.

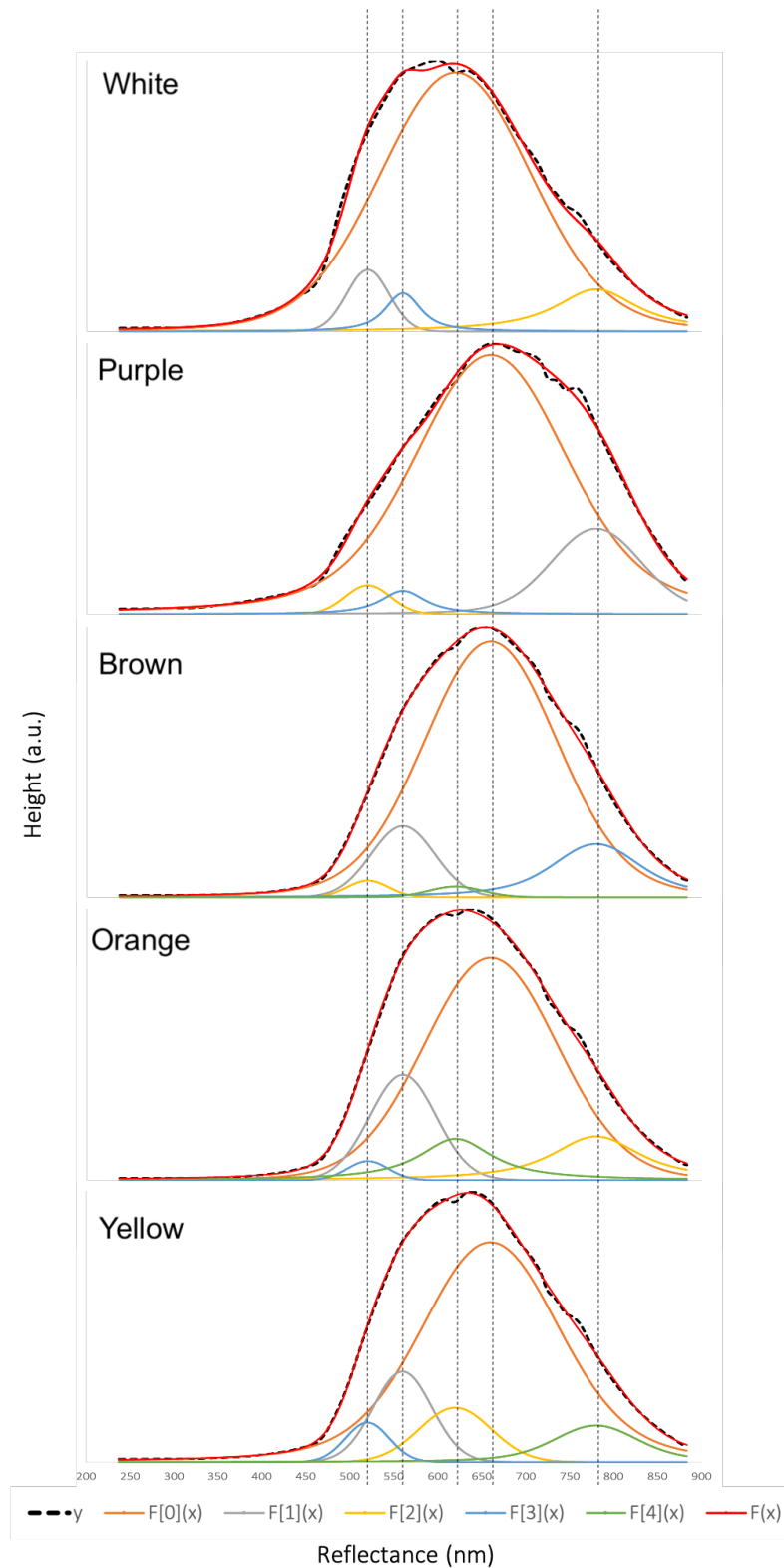


Figure 2.20: Voigt peaks fitted from prominent reflectance wavelengths (nm). a.u. on y-axis represents arbitrary units. Key peaks marked by dashed vertical lines (520, 560, 620, 660 and 780 nm). Coloured lines correspond to order of peak fitting $y =$ (original spectra), $F[0](x)$ = fit 1 through to $F[4](x)$ = fit 5. $F(x)$ is final fitted spectra. Note not all colours have 5 peaks fitted. Figures show white, purple, brown, orange, and yellow from top to bottom.

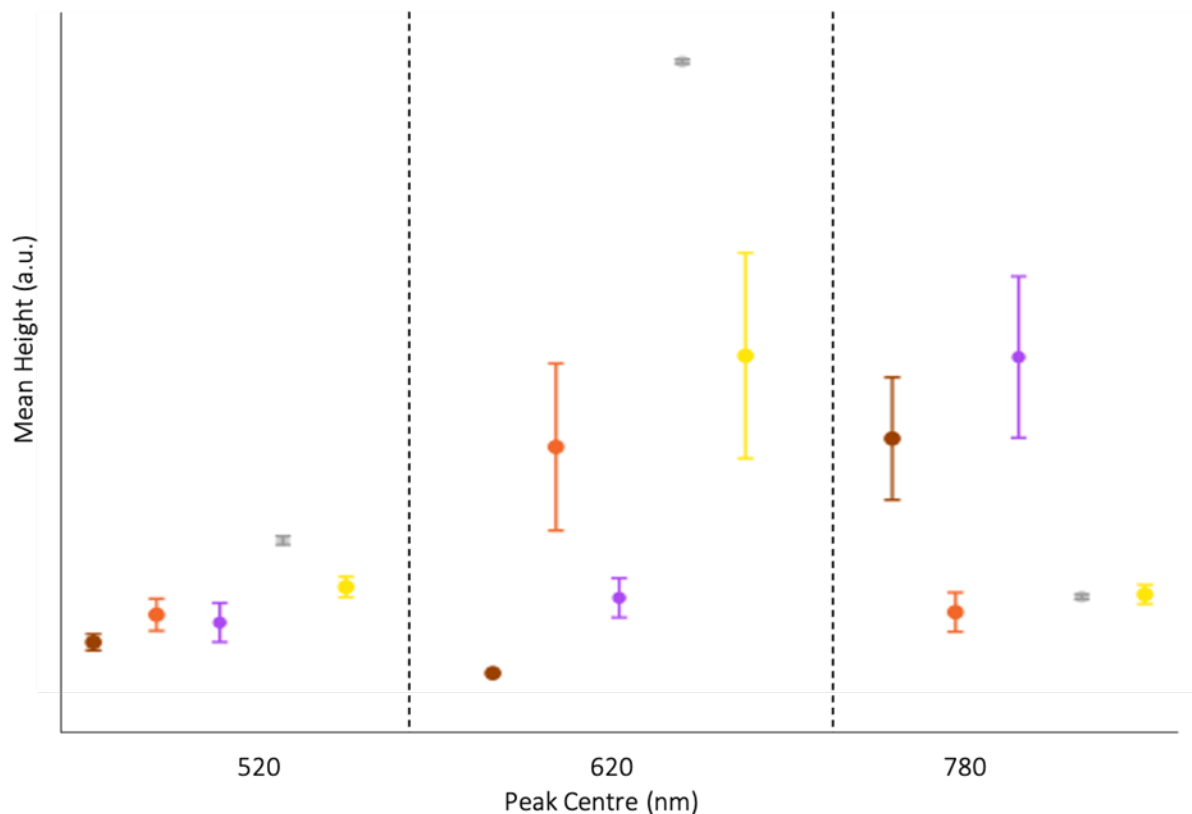


Figure 2.21: Average peak height for each colour against highest (780 nm) lowest (520 nm) and mid (620 nm) prominent reflectance peaks for *Buccinum undatum* shell sections. Number of shells within peak group for each colour varies depending on if a peak was fitted (See Appendix 2 and 3). Error bars $\pm 1SE$. a.u. represents arbitrary units.

Raman spectroscopy

Background on Raman spectroscopy can be found in Appendix 6.

Identification and comparison of the two highest spectral peaks were made. Spectroscopy data were sorted to examine the structure of the crossed-lamellar (XLAM) and the outer prismatic shell microstructures (Figure 2.22) (see Chapter 4 for further details about shell morphology and microstructures). Scatter plots were made to check data for consistency within a shell layer so average values could be used. Due to these being repeatable, for further measurements a single average value was taken from the 3 points per shell layer.

Colours were subdivided into additional groups of light and dark, and from initial analysis of peaks (highest peaks 1 and 2; P1 and P2), little to no variation was found between

colours across all shell layers (Table 2.5). In general, peak values showed little variation within XLAM1 with P1 between wavenumbers 1130-1140 cm^{-1} and P2 between 1531-1540 cm^{-1} . However, both XLAM 2 and the outer shell layers saw more variation in the wavenumbers i.e., (1129-1145 cm^{-1} , 1119-1145 cm^{-1} in XLAM2 and 1122-1154 cm^{-1} , 1503-1548 cm^{-1} in the outer prismatic layer). Although in tabulated mean values white shells saw an average peak value for both P1 and P2, only 2 of the overall 10 shells measured presented these peaks, compared with 14 out of 15 shells for brown samples (Table 2.5 A-C).

Spectra were then analysed with the removal of background data and plotted to compare against and within colour groups (Figure 2.23). The similarities in shell colour were further reflected through the spectra, and white shells again saw significant reduction in the presence of additional pigment peaks. For purple, orange and brown coloured shells, peaks appeared to be in similar positions, whereas yellow shells saw slightly lower wavenumber values for the prominent peaks. Overall, the spectra between 1600-3000 cm^{-1} saw clear similarities for crossed lamellar layers 1 and 2, however the outer prismatic shell layer appeared more varied with increased background interference post correction.

Values of the two highest peaks were used for comparison and pigment identification (Figure 2.24). The data obtained supported findings in Hollyman (2017) for carotenoid and polyene pigment presence however variation can be seen between shell layers for individual colours, with a spread of points within colour groups, and microstructure tested (Figure 2.24).

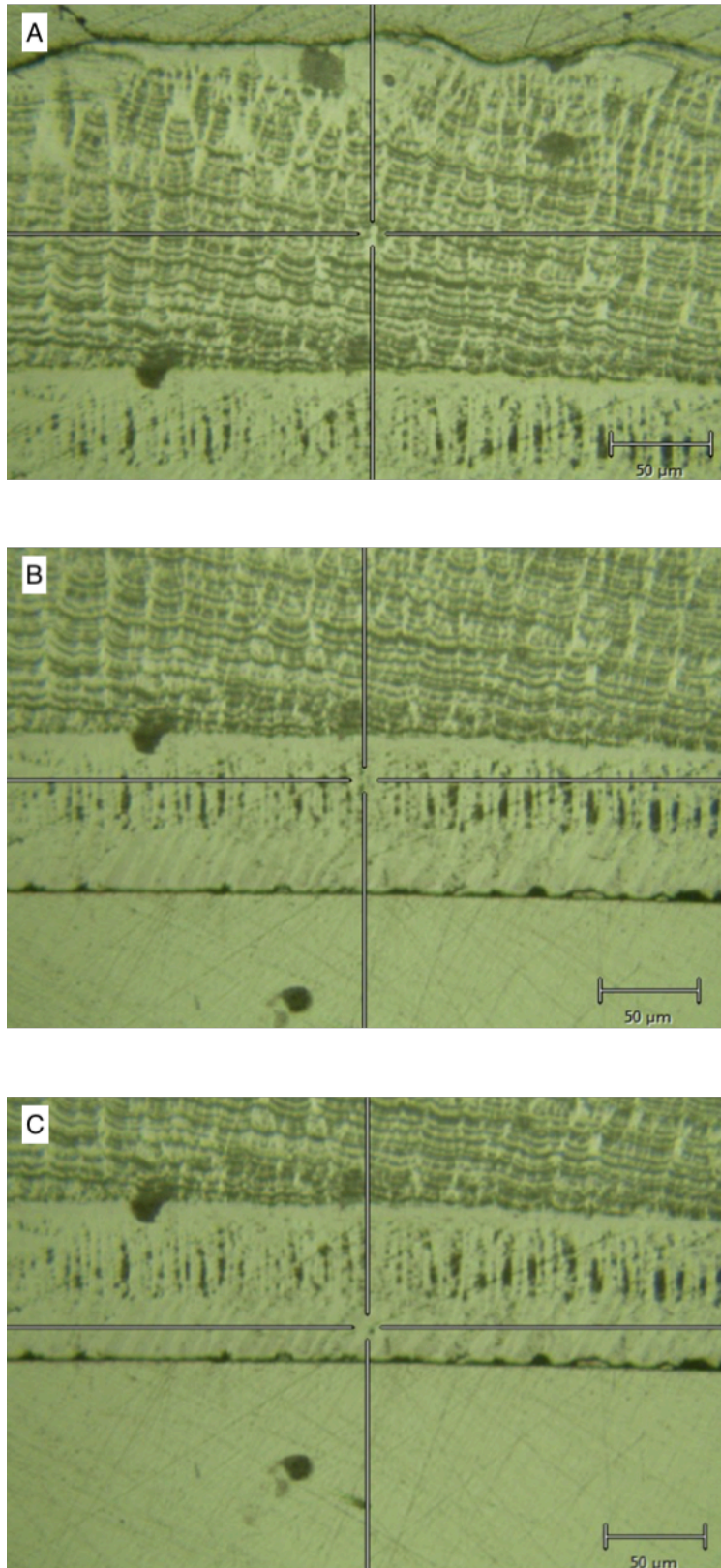


Figure 2.22: Screen shot image of Raman laser point (crossed hairs) for each shell layer measured, in the outer prismatic (A) and the crossed-lamellar B) and (C) shell microstructures. Final data comprised of multiple points per layer.

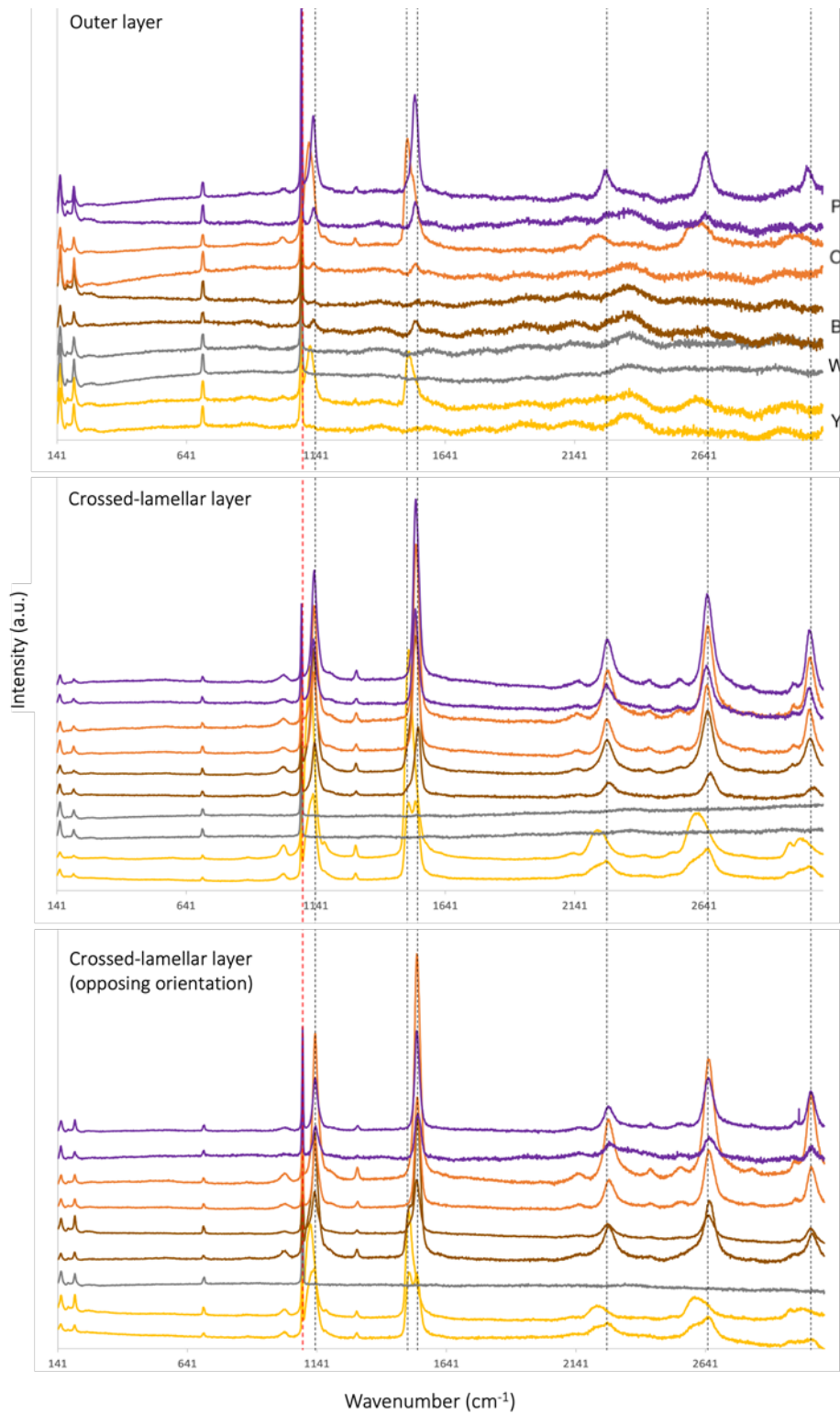


Figure 2.23: Background corrected Raman spectra wavenumbers between 141 and 3200 cm^{-1} for shell microstructures indicated in Figure 2.22; outer prismatic, and two orientations of the crossed-lamellar structures in *Buccinum undatum* for each coloured shell, purple (P), orange (O), brown (B), white (W), and yellow (Y). Clear peaks marked with vertical dashed lines. Y-axis a.u. represents arbitrary units.

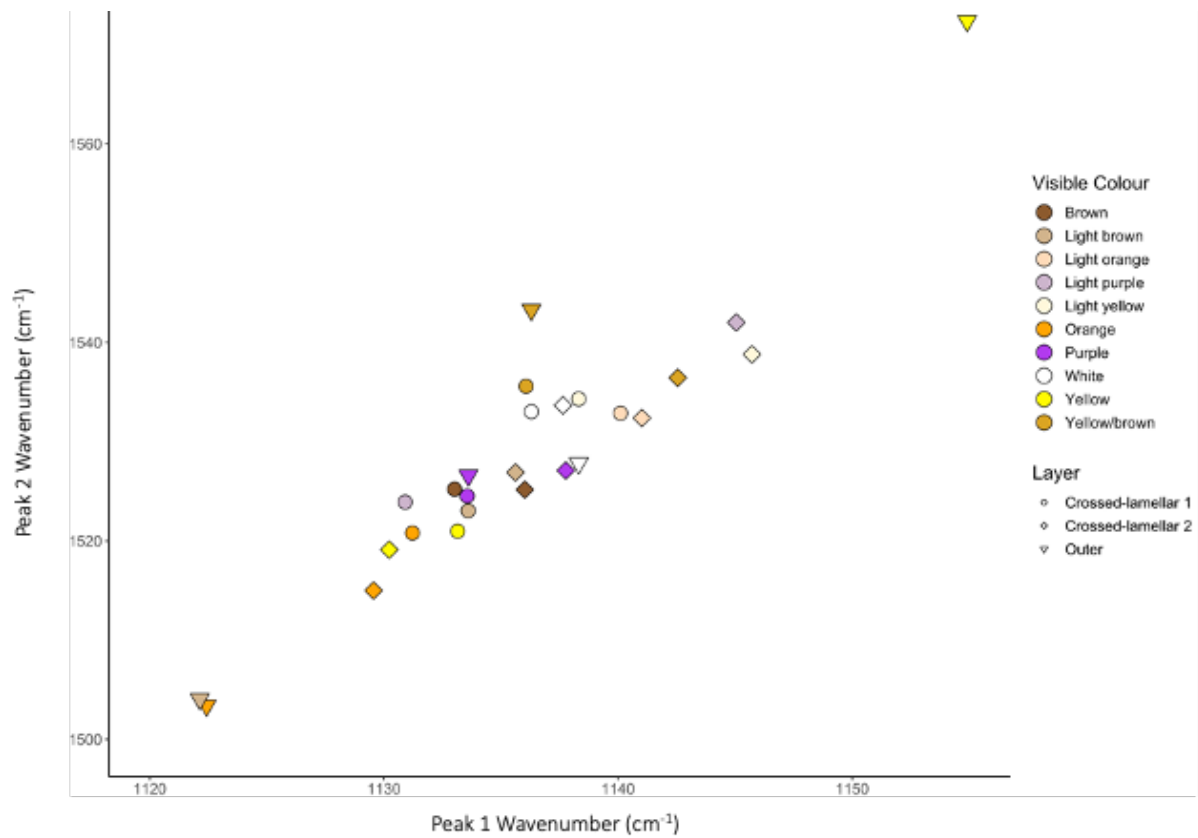


Figure 2.24: Scatter plot showing the relationship between the mean wavenumber (cm^{-1}) positions of the primary peaks.

Table 2.5: A-C; Table of mean peak (P1 and P2) wavenumber values (cm^{-1}) with standard deviation (SD) calculated for each colour group of shells for crossed-lamellar 1 (XLAM1), crossed-lamellar 2 (XLAM2) and outer prismatic shell microstructures (Outer). Shells with no prominent peak 1 or peak 2 values were discounted and removed for these calculations (n-0).

A			XLAM 1							
Colour	n	n - 0	Mean P1	SD	Mean P2	SD	Highest P1	Lowest P1	Highest P2	Lowest P2
brown	15	14	1133.02	6.99	1525.21	13.74	1141.01	1118.09	1539.44	1498.25
orange	5	4	1131.22	8.39	1520.79	13.81	1138.32	1119.34	1531.73	1500.83
purple	5	5	1133.56	10.96	1524.52	16.00	1139.67	1114.04	1538.16	1496.96
white	10	2	1136.30	0.95	1533.02	5.45	1136.97	1135.63	1536.87	1529.16
yellow	6	6	1133.15	8.01	1520.98	17.89	1145.05	1123.49	1540.72	1496.96
yellow/brown	3	3	1136.07	3.89	1535.58	6.80	1138.32	1131.58	1540.72	1527.87
light brown	6	4	1133.60	6.83	1523.04	17.06	1139.67	1124.84	1536.87	1499.54
light orange	3	3	1140.11	7.66	1532.87	5.51	1146.40	1131.58	1536.87	1526.59
light purple	3	2	1130.91	8.58	1523.91	16.24	1136.97	1124.84	1535.39	1512.43
light yellow	6	2	1138.32	1.91	1534.30	3.63	1139.67	1136.97	1536.87	1531.73

B XLAM 2										
Colour	n	n - 0	Mean P1	SD	Mean P2	SD	Highest P1	Lowest P1	Highest P2	Lowest P2
brown	15	10	1136.02	11.59	1525.16	14.53	1158.50	1119.44	1542.01	1496.96
orange	5	2	1129.56	8.58	1515.00	20.03	1135.63	1123.49	1529.16	1500.83
purple	5	5	1137.77	12.37	1527.09	15.30	1151.78	1119.44	1540.72	1500.83
white	10	2	1137.65	2.86	1533.66	6.36	1139.67	1135.63	1538.16	1529.16
yellow	6	5	1130.23	10.40	1519.11	19.63	1146.40	1119.44	1544.57	1496.96
yellow/brown	3	3	1142.55	7.45	1536.44	6.34	1151.01	1136.97	1540.72	1529.16
light brown	6	4	1135.62	8.16	1526.90	14.11	1146.40	1127.54	1539.44	1511.14
light orange	3	2	1141.02	3.81	1532.38	4.55	1143.71	1138.32	1535.59	1529.16
light purple	3	1	1145.05	-	1542.01	-	1145.05	1145.05	1542.01	1542.01
light yellow	6	2	1145.72	12.37	1538.80	6.36	1154.47	1136.97	1543.29	1534.30

C OUTER										
Colour	n	n - 0	Mean P1	SD	Mean P2	SD	Highest P1	Lowest P1	Highest P2	Lowest P2
brown	15	0	-	-	-	-	-	-	-	-
orange	5	1	1122.43	-	1503.41	-	1122.43	1122.43	1503.41	1503.41
purple	5	2	1133.61	4.76	1526.59	5.46	1136.97	1130.24	1530.45	1522.73
white	10	1	1138.32	-	1527.82	-	1138.32	1138.32	1527.82	1527.82
yellow	6	3	1154.91	17.86	1572.39	75.68	1165.22	1134.28	1652.52	1502.12
yellow/brown	3	2	1136.30	2.86	1543.29	7.25	1138.32	1134.28	1548.42	1538.16
light brown	6	2	1122.14	3.82	1504.05	6.38	1124.84	1119.44	1508.56	1499.54
light orange	3	0	-	-	-	-	-	-	-	-
light purple	3	0	-	-	-	-	-	-	-	-
light yellow	6	0	-	-	-	-	-	-	-	-

Discussion

Shell variation and shell damage amongst *Buccinum undatum* populations

Significant differences in the shell weight to total shell length relationships for whelks from the different locations were identified, however these differences were not consistent between all the sites. For example, non-significant relationships were apparent when Amlwch whelks were compared with both Holyhead, and Saundersfoot whelks and further between Holyhead directly with Saundersfoot. The significant differences in shell weight and total shell length in some populations is likely the interaction of environmental factors such as water flow, temperature, water depth and food availability. In this study, however, it was not possible to relate these differences to any specific factor(s).

Detailed inspection of whelk shells demonstrated variation in the number of damage incidents and severity of damage. Generally, the larger, older, whelks had more damage incidences on their shell surfaces. However, increased damage incidences did not significantly result in the production of a heavier shell. Originally it had been hypothesised that an increase in shell damage would likely be accompanied by an increase in shell deposition and shell thickening with a resultant increase in shell weight. Although this was not observed it has been reported elsewhere that following shell damage thickening of the shell occurs because of scars on the shell surface (Mensink *et al.*, 2000). Shell scarring has been recorded in a range of marine molluscs including the bivalves *Ensis siliqua* (Gaspar *et al.*, 1994) *Glycymeris glycymeris* (Ramsay *et al.*, 2000; Ramsay *et al.*, 2001) and the gastropod *Calliostoma zizyphinum* (Preston and Roberts, 2007) and for all occurrences, differing levels of damage were observed depending on the initial damage inflicted and the number of damage incidents encountered. With repeated damage to the mollusc shell, repeated thickening may occur, for example with shell layers being built up and receding back through the shell whorls (see Chapter 4 for more details).

Variation in the number of damage and repair incidences varied between sites, with Holyhead whelks displaying the greatest number and the greatest distribution of shell damage to the shell surface. Nevertheless, across all sites, no whelks showed damage to the earliest deposited shell whorls (W1 and 2) whilst the shell lip and the siphonal canal were the most frequently damaged. The damage to the shells and the variations between location could be

due to several factors including fishing pressures within a given area, intra-species variation and exposure to differences in tidal currents. Although these variations are seen, it would be necessary for future study to focus on identifying patterns of shell damage, associating a cause, and examining habitat structure and the local environment. These data would build on the work carried out within Appendix 1 (atlas of shell damage) to classify the different mechanisms of damage with shell fracture patterns .

The patterns seen in shell dimension results presented in this chapter are similar to those from previous studies where they have been investigated for fishery management purposes (Colvin *et al.*, 2022a). Relationships between shell weight and shell length are dependent on several factors, including the occurrence of previous shell damage incidents, variable environmental factors, including temperature and food availability, along with individual life history parameters. A possible further explanation for the differences seen could be because of dissimilarity of whelk fishing grounds and habitat type. For example, depth zones or sediment type have been seen to influence both the shell size and abundance of whelks on certain fishing grounds (Palmer, 1992; Valentinsson *et al.*, 1999; Haig *et al.*, 2015; Borsetti *et al.*, 2018; Emmerson *et al.*, 2020). Overall differences in growth rates, and the factors affecting this, will be investigated further in Chapter 3.

Colour variation and pigment presence

This study identified five main internal shell colour groups across all whelks sampled, with a white colour being the most prominent. Variations in internal shell colour between the source locations was seen for most of the colours. However, the proportion of purple-coloured shells remained consistently low and least dominant. The brown internal shell colouration was unusually predominant in Brynsiencyn shells. Having initially qualitatively identified internal shell colour by eye, individual shell pieces were quantitatively assessed using spectrophotometry. Although differences in spectral shape were seen, there were few differences in the peak wavelengths between groups. Internal coloured brown and purple shells continually displayed the widest variation in spectra however, these colours presented a more mottled and variable colour intensity on the inner surface.

Identifying a single cause for the visual variation in internal shell colour in *B. undatum* through spectrophotometry and qualitative observations, both between and within a geographic location proved difficult, with patterns of colour appearing different due to numerous factors in the natural environment (Williams, 2017). There is very little understanding of the evolution of molluscan shell colour except that it is likely a result of light interactions, structural colour, or pigment presence (Williams, 2017). Furthermore, the reasons behind the development of different colour morphs are often linked with ecological interactions. However, for many taxa, the necessity and importance of a coloured shell has yet to be identified (Williams, 2017; Magnúsdóttir *et al.*, 2018 and 2019).

Shelled mollusc species are not known to see in colour (Williams, 2017), though cryptic colouring often occurs (Cook, 1986; Parsonage and Hughes, 2002). As such, the use of coloured shells would be unlikely to be used for communication within the species. Nonetheless, the colours presented could be a result of camouflage to blend in with their local surroundings, with differences in sediment types and substrata often resulting in different colour morphs presenting, depending on suitability and predation pressures. Although these effects would typically be driven by predation pressures, whether this is the case for *B. undatum* is currently unknown. Similar to results from Magnúsdóttir *et al.*, (2018), where localised populations of whelks within Breidafjörður Bay, Western Iceland saw variations in external shell patterning and colour, results from this chapter found different internal shell colouring in localised populations of whelks in UK waters. These colour differences could further be a result of genetic variation or local environmental factors such as seawater (SW) temperature, food availability, pigment incorporation and algae presence on the shell surface (Williams, 2017; Magnúsdóttir *et al.*, 2018 and 2019). The effects of SW temperature on shell colour have been noted in some species to be linked to thermoregulation and UV protection. For example, Mitton (1977) and Lalli and Gilmer (1989) showed that a lighter coloured external shell on *Mytilis edulis*, heated up less than darker colour morphs. This has also been seen in the scallop *Argopecten purpuratus* where lighter yellow shelled individuals have lower survival and growth rates in colder SW temperatures than darker purple or brown morphs (Wolff and Garrido, 1991).

Shell colour, and the formation of pigments is a highly energetic process, and the development of which in marine molluscs are still largely unknown (Williams, 2017). In many cases, for example melanin in bird feathers and insect cuticles, colour is incidental, as a function

of strength (Burt, 1977; Bosner, 1996; Williams, 2017), which may be similar with that of the whelks, with pigment incorporation in the organic portion of the shell playing a part in shell construction itself. Strength and colour have also been noted in *Littoraria pallescens* (Cook and Kenyon, 1993), whereby darker shells were 22% stronger than lighter individuals of the same species, however in this instance shell strength appeared un-related to pigment presence.

Within molluscan shells, melanins, tetrapyrroles, polyenes and carotenoids are the main classes of pigments that have been identified (Comfort, 1951; Williams *et al.*, 2016; Saenko and Schilthuizen, 2021), all of which are responsible for the different colour properties within the organism. These pigments are either synthesised, produced as a by-product, or taken up from the diet (Moore, 1936; Comfort 1951; Saenko and Schilthuizen, 2021). From an analysis of the Raman spectra from molluscan shell, an expected peak of 1085 cm^{-1} was found for aragonite (Hedegaard *et al.*, 2006; Hollyman, 2017) along with further peaks at a higher wavenumber associated with the presence of pigments. These additional peaks proved most dominant in the crossed lamellar layers of the shell as opposed to the outer layers and were not present in any layer in the white shells, where little or no pigment presence was expected. The relationship between primary peak 1 and peak 2 has been shown to be due to the presence of polyene pigments (Hedegaard *et al.*, 2006) which could explain why they were only present within the coloured shell sections. Although the peak wavenumbers for many colours appeared similar, Hedegaard *et al.* (2006), reported that the differences in visual colour seen could also be as a result of the pigment interactions with the organic matrix or differing functional groups on the pigment itself.

Summary

This chapter has examined variation in the shell and natural shell damage in *Buccinum undatum* populations using both visual and analytical techniques. Whelk shells frequently experience damage in the wild and show periods of shell repair and scarring on the surface, with differences in severity of damage occurring between geographic locations. Overall, there were no clear differences in shell colour within the internal shell layers determined using both spectrometry and Raman spectral analysis, although differences were observed visually with the naked eye. Shells of *B. undatum* showed differences in their internal shell colour and pigment composition, and although it seems as though there are a lot of different pigment

components in different proportions in different colours, to take this research further with a more detailed analysis is outside the scope of this current PhD thesis. However, this would be an interesting area for future research. In addition, further understanding the importance of colour in *B. undatum* shells and why the distribution of light and dark or various colours on the internal shell layers occurs, in relation to predatory pressures and the surrounding habitat would provide further explanation into the morphological variation in the species. This primary chapter was undertaken to gain an initial understanding into the levels of shell damage in whelks, an overview of the weight – length variations observed from their shell and possible causes of internal shell colouration.

Chapter 3 – Shell repair and growth in experimentally-damaged *Buccinum undatum*

Work from this chapter has been published in the Journal of Experimental Marine Biology and Ecology
(June 2022) <https://doi.org/10.1016/j.jembe.2022.151720>

See Appendix 10

Figures

Figure 3.1: Collected <i>Buccinum undatum</i> egg masses, and juveniles hatching in the laboratory.	77
Figure 3.2: Seawater table with experimental 8 L tanks with mesh bases held in 15 L tanks supplied with flowing ambient temperature seawater.	77
Figure 3.3: Mesh lids on tanks with direct overhead flow of ambient seawater.....	77
Figure 3.4: Inkwell pots used for whelk collection.....	78
Figure 3.5: Experimental tank set up for those whelks placed in temperature-controlled conditions. The 175 L tank was either connected to a heater or chiller, depending on the seawater temperature required and time of year.....	80
Figure 3.6: Representation of a <i>Buccinum undatum</i> shell (Left) with total shell length (TSL) (red dashed line) aperture length (ApL) (solid red line) and minimum width (W) (blue dashed lines). <i>B. undatum</i> , number 38 (Right) with TSL (yellow dashed line) and an approximate square area of shell removed with a Dremel cutting wheel (black dotted line) (Day 0) and repair (Day 6). In this whelk complete repair took 21 days.	81
Figure 3.7: Diagrammatic representation of how retraction of the whelk body into the shell was scored from 1-4; left to right. The further the whelk retracted into the shell, the lower the score.	81
Figure 3.8: Dissected body of <i>Buccinum undatum</i> . A and B) juvenile male with small penis (A), mature male with large penis (B), C and D) females with gonad and digestive gland visible. ..	83
Figure 3.9: A and B) Average cumulative % repair (± 1 SE ribbon) and C and D) average cumulative growth (± 1 SE ribbon) with time for > and < SOM <i>Buccinum undatum</i> that had received minimal (blue) and substantial (orange) natural damage to their shells prior to their inclusion in the experiments and before the whelks were experimentally-damaged. Each line represents a level of previous natural shell damage that had been assessed on a scale of 0-4 (0 = no damage, 4 = > 4 events of shell damage), with 0-1 as minimal damage and >2 substantial previous damage.	88
Figure 3.10: A and B) average cumulative % repair (± 1 SE ribbon) C and D) average cumulative growth (± 1 SE ribbon) with time for > and < SOM <i>Buccinum undatum</i> . Each line corresponds to a measure of retractability into the shell of the individual whelk prior to experimental shell damage, <50 retraction into the shell or >50%.	89

Figure 3.11: A) average cumulative % repair (± 1 SE ribbon) and B) average cumulative growth (± 1 SE ribbon) with time for three different age groups of *Buccinum undatum*.92

Figure 3.12 A) average cumulative % shell repair (± 1 SE ribbon) and B) average cumulative shell growth (± 1 SE ribbon) with time for wild caught *Buccinum undatum*. Binary maturity assessed during winter months as yes (1) or no (0). Maturity groups: <SOM juvenile (JW), >SOM but juvenile and >SOM mature.....94

Figure 3.13: Average cumulative % shell repair rates (A and C) (± 1 SE ribbon) and average cumulative shell growth (B and D) (± 1 SE ribbon) in experimentally-damaged *Buccinum undatum* during the winter (A and C) and summer (B and D). Whelk sex determined through the presence or absence of a penis. JW refers to a wild caught juvenile whelk and MW a wild caught mature whelk.....95

Figure 3.14: A) Average cumulative % repair (± 1 SE ribbon) and B) average cumulative growth (± 1 SE ribbon) for *Buccinum undatum* presented with different feeding regimes (daily, once weekly, unfed). Two groups of whelks were used, tank-reared juvenile (TRJ) and wild-caught >SOM (MW). The TRJ and MW experiments continued for 15 days and 21 days respectively.98

Figure 3.15: A) Average cumulative % repair (± 1 SE ribbon) and B) average cumulative growth (± 1 SE ribbon) with time for *Buccinum undatum*. Two groups of whelks were used, tank-reared juvenile (TRJ) and wild caught >SOM (MW). TRJ experiments ran for 15 days at 5, 10 and 15°C and MW for 21 days at 5 and 10°C. No survival of MW whelks occurred at 15°C in both control groups and under experimental conditions.....101

Figure 3.16: A and B average (± 1 SE ribbon) cumulative % repair and C and D average (± 1 SE ribbon) cumulative growth for mature wild-caught *Buccinum undatum* maintained under temperature-controlled regimes (A and C) and under ambient conditions (B and D) during four seasons of the year (spring, summer, autumn, and winter). Each line represents a different season when the experiment was undertaken.....104

Figure 3.17: A and B Average (± 1 SE ribbon) cumulative % repair and C and D average (± 1 SE ribbon) cumulative shell growth for juvenile wild-caught *Buccinum undatum* maintained under temperature-controlled regimes (A and C) and under ambient conditions (B and D) during four seasons of the year (spring, summer, autumn, and winter). Each line represents a different season when the experiment was undertaken.....105

Figure 3.18: A and B Average (± 1 SE ribbon) cumulative % shell repair and C and D average cumulative shell growth for tank-reared juvenile *Buccinum undatum* maintained under

temperature-controlled regimes (A and C) and under ambient conditions (B and D) (during four seasons of the year (spring, summer, autumn, and winter). Each line represents a different season when the experiment was undertaken.....106

Tables

Table 3.1: Summary of the experimental design and set up for the <i>Buccinum undatum</i> laboratory-controlled shell damage experiments.	85
Table 3.2: Summary table listing the additional measures taken.	86
Table 3.3: Summary table of repair rates ($\text{mm}^2.\text{day}^{-1}$) and growth rates ($\text{mm}.\text{day}^{-1}$) of experimentally-damaged <i>Buccinum undatum</i> . Damaged vs control individuals were non-significant for all growth (TSL increase) experiments.....	90
Table 3.4: Summary of repair rates ($\text{mm}^2.\text{day}^{-1}$) and growth rates ($\text{mm}.\text{day}^{-1}$) of experimentally-damaged <i>Buccinum undatum</i> . Damaged vs control individuals were non-significant for all growth (TSL increase) experiments.....	96
Table 3.5: Summary of repair rates ($\text{mm}^2.\text{day}^{-1}$) and growth rates ($\text{mm}.\text{day}^{-1}$) of experimentally-damaged <i>Buccinum undatum</i> . Damaged vs control individuals were non-significant for all growth (TSL increase) experiments.....	99
Table 3.6: Summary of repair rates ($\text{mm}^2.\text{day}^{-1}$) and growth rates ($\text{mm}.\text{day}^{-1}$) of experimentally-damaged <i>Buccinum undatum</i> . Damaged vs control individuals were non-significant for all growth (TSL increase) experiments.....	107

Introduction

Understanding rates of individual growth and the factors which impact them are of key importance for the population management of marine organisms for both their conservation and fisheries. Growth and repair are fundamental processes within all organisms that are necessary for their survival, resilience, and population success (Sebens, 1987; Crawford and Whitney, 2010; Avanzi *et al.*, 2020). For most molluscs somatic and shell growth are seasonal and for some species growth occurs solely during embryonic and juvenile stages, but for the common whelk *Buccinum undatum*, growth is continual throughout its entire life (Kideys *et al.*, 1993).

In the marine environment there are a number of factors which result in damage to organisms and see changes to their growth rate (Dyke *et al.*, 1996; Harwood, 2001), particularly in some marine gastropod species. These changes occur both naturally, through environmental change and feeding behaviors (Connell, 1974; Kideys and Hartnoll, 1991; Goodwin *et al.*, 2001), as well as through anthropogenic disturbance including mechanical fishing gears (Cadée *et al.*, 1995; Fahy *et al.*, 1995; De Vooy and Van der Meer, 1998; Mensink *et al.*, 2000; Bergman *et al.*, 2001). For molluscs, biological shell damage can also occur because of the activities of boring organisms invading the shell surfaces, for example, sponges *Cliona* spp. and boring polychaete worms including *Polydora ciliata* (Martinelli, *et al.*, 2020).

Shell damage to the whelk *B. undatum* can arise from multiple factors. Their subsequent shell growth, recovery, and repair from such incidences can be further affected by their local environment and life history (Checa, 1993; Mensink *et al.*, 2000; Ramsay *et al.*, 2001; Colvin *et al.*, 2022b). The processes of shell growth and repair in molluscs is very intricate, the mechanisms and fundamentals of which will be covered further in Chapters 4 and 5. The growth of the shell is reliant upon the assimilation of specific elements from the surrounding environment (Ramsay *et al.*, 2001; Findlay *et al.*, 2011; Hollyman, 2017). Mollusc shells are generally composed of several layers of different mineralogical structure (Saleuddin and Wilbur, 1983; Watabe, 1983; Ruppert *et al.*, 2004; Harper *et al.*, 2009; Clark *et al.*, 2020). Currently little is known about the process of shell growth and repair in gastropods, and specifically *B. undatum*, with the deposition of different shell layers, and what implications the shell repair recovery process has on their life history (e.g., Colvin *et al.*, 2022b). Although

intraspecific variation within the shells of whelks appears adaptive, with shell thickness and speed of growth being correlated, it is unknown to what extent the morphological variation is genetic or ecophenotypic (Palmer, 1990).

Shell damage can affect the normal shell deposition processes until the damaged shell is repaired. Shell repair in molluscs is an energy-intensive process, especially during the formation of the organic matrix (Ebert, 1968; Palmer, 1990; Ruppert *et al.*, 2004; Thomsen *et al.*, 2013), and as a result, during shell repair molluscs may cease, or greatly reduce their metabolic expenses to successfully repair the damaged shell area. Seasonal fluctuations in food supply or a sudden change in food availability can result in depleted energy reserves (Melzner *et al.*, 2011). During prolonged periods of low food supply many metabolic activities will be affected and slowed down, including linear increases in growth to preserve energy reserves for fundamental life processes such as respiration. However, there is evidence (Palmer, 1983; Colvin *et al.*, 2022b) that linear shell growth and repair in gastropods, *Nucella lapillus* and *B. undatum* respectively, continue through periods of starvation, with protein catabolism serving as the main source of energy to the gastropod with the increased demand on amino acids for the organic framework of the shell.

Environmental perturbations, for example fluctuations in seawater temperature, both seasonally and because of abrupt changes, including the impact of storms, have further implications on the rates of shell growth and repair (Lammens, 1967; Ebert, 1968; Ramón *et al.*, 1995; Tomanek and Somero, 1999; Stillman, 2003; Thomsen *et al.*, 2013; Weiss *et al.*, 2014; Colvin *et al.*, 2022b). Seawater temperature is a key environmental factor, with significant biological and physical importance to bivalves (Almada-Villela *et al.*, 1982; Goodwin *et al.*, 2001) and to marine ecosystems (Harley *et al.*, 2006). For marine ectotherms, metabolic processes, including respiration, growth, feeding and reproduction all fluctuate with changing seawater temperatures (e.g., Connell, 1974 and specifically whelks e.g., Kideys and Hartnoll, 1991); with seawater (SW) temperature being noted as one of the key factors determining the maximum size a mollusc can attain (Goodwin *et al.*, 2001). Extreme changes in seawater temperature frequently results in the cessation of somatic and shell growth until conditions become more favourable, for example in *Mytilus edulis* (Page and Hubbard, 1987). An increase in SW temperature, generally results in increased rates of shell growth and repair and, as a result, metabolic changes and protein synthesis rates also change (Tomanek and Somero, 1999;

Stillman, 2003). Seasonal changes in SW temperature gives rise to seasonal shell growth that is evident as annual growth checks or rings on the shell surface (Page and Hubbard, 1987; Richardson, 2001; Soldati *et al.*, 2009). As seen on the shells of soft-shelled clams (*Mya arenaria*), common cockles (*Cerastoderma edule*), and mussels (*Mytilus edulis*) (Seed, 1968; Lutz, 1976; MacDonald and Thomas, 1980; Richardson *et al.*, 1980; Almada-Viella *et al.*, 1982). Annual rings are typified by steadily narrowing growth increments, to virtually no growth causing a clear line in shell section and a surface ring, often allowing an age estimate to be made. However, for *B. undatum* these are not reliable (Lammens, 1967; Arthur *et al.*, 1983; Krantz *et al.*, 1984; Ramon *et al.*, 1995; Thompson *et al.*, 2000; Hollyman, 2017).

Heightened SW temperature can increase the rate of many biological reactions, though only up to the thermal limit, at which point an organism is put under thermal stress (Davies, 1966; Foster, 1971; Clark *et al.*, 2008; Dong *et al.*, 2022; Molina *et al.*, 2022). In addition to implications on biological processes within the organism, a change in SW temperature also induces changes in the shell calcification process, with direct effects on the uptake of Ca^{2+} ions (Bevelander and Nakahara, 1969; Nakahara, 1983; Pons *et al.*, 2002; Thomsen *et al.*, 2010). The rate of uptake and active transport of Ca^{2+} ions into the extrapallial space increases with rising water temperatures (the process of calcification will be discussed further in Chapter 4). However, this response can also show a negative effect, with deformations occurring in the surface membranes, thus affecting enzyme activity and pump functioning (Bevelander and Nakahara, 1969; Pons *et al.*, 2002; Thomsen *et al.*, 2010; Lervik *et al.*, 2013). Moreover, variations in the incorporation of the ratios of isotopes of oxygen ($\text{O}^{16}/\text{O}^{18}$) and carbon ($\text{C}^{13}/\text{C}^{14}$) and trace elements, into the newly mineralising shell are temperature dependant (Helgeson *et al.*, 1978; Owen *et al.*, 2002; Richardson *et al.*, 2004; Ropp, 2013; Hollyman *et al.*, 2020).

Differences have also been observed in taxa of different size and ages (Tanabe, 1988; Palmer, 1990; Kideys, 1996; Richardson, 2001; Ruppert *et al.*, 2004), with implications being seen to enhance or impair the growth rates of the shell, through metabolic changes. Previous research has found these rates of growth to be increased within both smaller and younger individuals within molluscan species, including *B. undatum* (Richardson, 2001). In gastropods any increase in body mass requires an appropriate increase in shell size to accommodate the increase in flesh and to allow the retraction of the body and foot into the shell. Size increases are rapid during the early years of ontogenetic growth (Palmer, 1990), to ensure that small

individuals, that are usually preferentially attacked and consumed by predators, attain a size beyond which they cannot be eaten (Tanabe, 1988; Palmer, 1990; Seed and Hughes, 1995; Kideys, 1996). Furthermore, with increased age there is a decline in linear shell growth depicting a trade-off between the availability of energy reserves and shell formation (Tanabe, 1988; Palmer, 1990). In older (larger) gastropods the decline or temporary cessation in linear growth is seen when sexual maturity is reached, which is likely a result of the energetic implications of reproduction, which sees the switch from somatic to reproductive growth (Santarelli-Chaurand, 1985; Jalbert *et al.*, 1989; Kideys, 1996).

Chapter 3 examines if there are differences in the rates of shell growth and shell repair in *B. undatum* exposed to different environmental conditions, specifically seawater temperature and food supply, as well as studying their general biology and behavior and how these may further affect these rates. It is hypothesized that there will be significant difference in rates of shell growth and shell repair between whelks of different ages and stages of maturity. Furthermore, seawater temperature and food availability will have significant effects on shell growth and repair rates with whelks growing under more favorable conditions achieving the highest rates of both shell growth and shell repair.

Materials and Methods

To investigate the effect of environmental factors for example seawater (SW) temperature, food availability and seasonal effects on shell growth and shell repair in *Buccinum undatum*, a series of controlled laboratory experiments and seasonal collections in which shells were experimentally-damaged, were undertaken. Juvenile whelks (<1 mm) were hatched and reared from egg capsules in the laboratory (TRJ), and for comparison, juvenile (JW) and sexually mature whelks (MW) (classified as less than (<) the UK average size at onset of maturity (SOM) or greater than (>) average UK SOM of 45 mm) were collected from the natural environment at different times of the year (i.e., different seasonal seawater temperatures) and their shells experimentally-damaged and shell repair investigated.

Sample collection

Tank reared juvenile whelks

Newly laid egg cases of *B. undatum* were collected (November 2014, 2016, and 2017) at low water of spring tides (LWST) from Tal-y-Foel, Brynsiencyn, North Wales. Egg capsules begin to appear at this location around November (pers. obs.). Daily visits to the site were made at LWST, and when egg masses appeared on the pier pilings, they were gently removed so that the approximate date of laying was known (egg capsules in the egg mass usually mature and juvenile whelks hatch after about 1 month (pers. obs.)). Egg masses were transferred to the laboratory in seawater and immediately placed in multiple plastic 8 L tanks, whose bases had been removed and replaced with nylon mesh (Figure 3.1). These were suspended in 15 L tanks (Figure 3.2) and placed on a 2 m x 1 m seawater flow-through table (Figure 3.2). Fine mesh was placed over the outflow of each 15 L tank to retain any escaping juveniles.

Tanks were checked daily to ensure adequate water flow, and weekly each tank was removed, gently washed in seawater to remove any accumulating detritus, and the egg masses turned over. After one month, the first tank-reared juveniles (TRJ) were observed emerging from the egg capsules. These juveniles were carefully transferred daily (for a period of 2 weeks) to other 8 L tanks whose bases were similarly covered with fine mesh (Figure 3.2). These tanks were submerged in 15 L tanks (as above) with the addition of mesh lids (to prevent whelks escaping) and supplied with ambient temperature seawater (Figure 3.3). The position of the tanks in the seawater table was rotated daily, with new positions being determined using a randomly generated number, to ensure that there was no effect of tank position on shell growth rate. Every two days a freshly shucked mussel, *Mytilus edulis* (40 to 60 mm) in half shell was placed in each tank as a food source for the growing juvenile whelks, as this has been shown to be a suitable food source for juveniles of this species (Nasution and Roberts 2004; Hollyman 2017). When the juvenile whelks had reached a shell length of between 11 and 21 mm the first growth and shell repair experiments were undertaken.

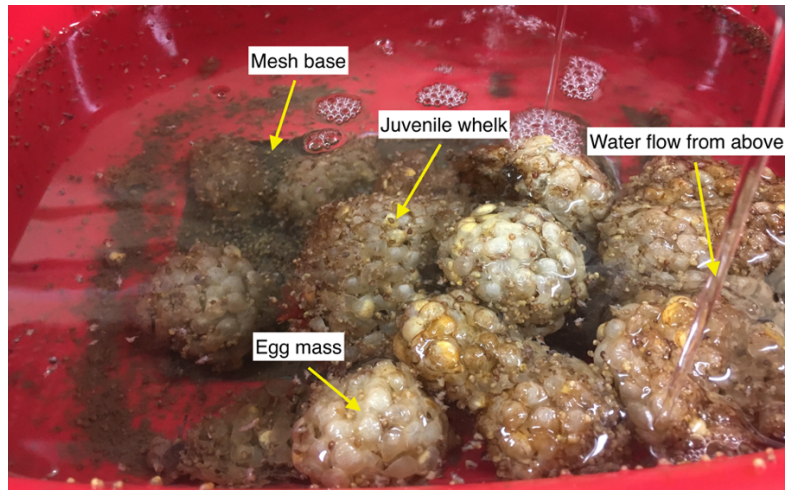


Figure 3.1: Collected *Buccinum undatum* egg masses, and juveniles hatching in the laboratory.

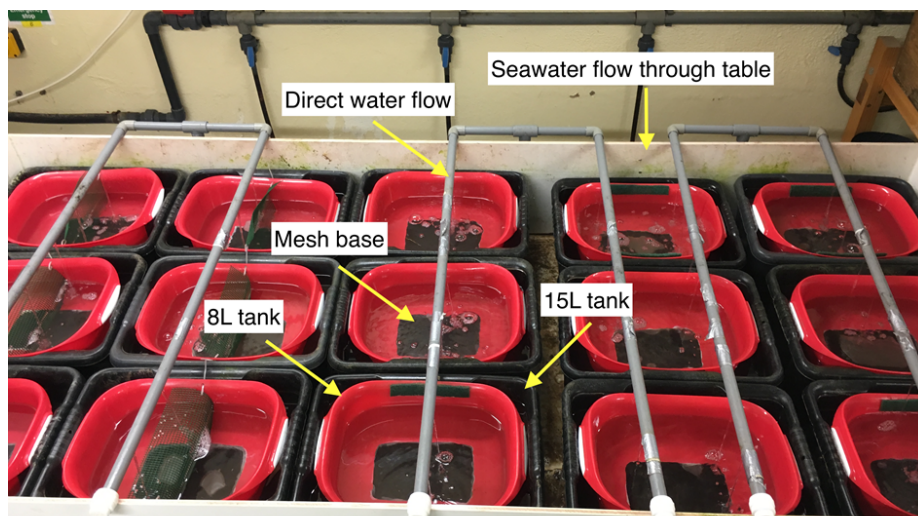


Figure 3.2: Seawater table with experimental 8 L tanks with mesh bases held in 15 L tanks supplied with flowing ambient temperature seawater.



Figure 3.3: Mesh lids on tanks with direct overhead flow of ambient seawater.

Wild caught whelks

Two size classes of whelks (Above UK and below UK average SOM of 45 mm) were collected using baited inkwell pots (Figure 3.4) deployed at Brynsiencyn, North Wales (see Figure 2.5 for location, Chapter 2). Collections were undertaken at four intervals per year during 2017 to 2019 (July, October, January, and April) to allow for investigation into seasonal effects on shell repair rates. From here on in this chapter these whelks will be referred to as mature wild (MW) whelks (>45 mm) and juvenile wild (JW) whelks (<45 mm).

The seasonally caught whelks were divided into either MW or JW whelks. This separation was probabilistically determined using existing size at maturity estimations (Hollyman, 2017). The size separation was to reduce size variability and any possible age and size differences in shell repair and growth rates. JW whelks were also collected opportunistically at other times of the year when required for additional laboratory experiments i.e., between summer 2017 and winter 2019. Each whelk pot was modified by replacing the existing netting (mesh size 20 mm) on the base of the pot with wire mesh (mesh size 3 mm) to retain all whelk sizes. Dispensation for the collection of undersized whelks was obtained from the Welsh Government (Appendix 4). Pots were baited with a mixture of crushed frozen shore crab (*Carcinus maenas*) and frozen mackerel (*Scomber scombrus*) and deployed for 24 hours. Upon retrieval the pots contained a wide range of whelk sizes (11 to 118 mm total shell length).



Figure 3.4: Inkwell pots used for whelk collection.

Following capture, whelks were transferred to the laboratory in seawater and placed into 175 L holding tanks supplied with flowing ambient temperature seawater and acclimated for 5 days to laboratory conditions. These whelks were further acclimated for 10 days in either 8 L or 15 L tanks (Figures 3.2 and 3.3) covered with mesh lids and supplied with ambient temperature seawater before any experiments were undertaken. The position of the tanks in the seawater table was rotated daily, position being determined using a randomly generated number. The bottom of the tank was cleaned weekly using a siphon to remove any accumulated detritus. Every two days, seven freshly shucked mussels (40 to 60 mm) in half shell were placed in each tank to excess as a food source, any uneaten food was removed when new mussels were introduced.

Tank based experiments

In experiments where the whelks were grown, and their shells repaired under different seawater temperatures a different tank set up and acclimation protocol were employed. Tank reared juvenile (TRJ) whelks were transferred into 15 L tanks, which were placed into 175 L tanks, whereas mature and juvenile wild caught (MW and JW) whelks were transferred directly into the 175 L tanks (Figure 3.5). Each large tank was supplied with a trickle flow ($<0.5 \text{ L} \cdot \text{hr}^{-1}$) of ambient temperature seawater, aeration, and the tank electrically heated and cooled to maintain the seawater at a temperature of $\pm 1^\circ\text{C}$ of the desired temperature (chosen based on known seawater bottom temperatures and optimal ranges). Whelks were fed (as described for TRJ, MW and JW whelks above), the tanks cleaned, and tank positions rotated daily in the 175 L tank. Where the required temperature was above or below the ambient seawater temperature, the seawater temperature was raised by heating or lowered (cooled by chiller) by 1°C every 2 days to allow the whelks to acclimate slowly to their new seawater temperature. Seawater temperature was monitored hourly using several 'Tinytag' temperature loggers deployed in representative small and large tanks. These data were subsequently downloaded into Excel and the seawater temperature records checked daily for consistency. There were some issues with the reliability of recording this way and measurements were also supplemented by daily manual seawater temperature measurements.

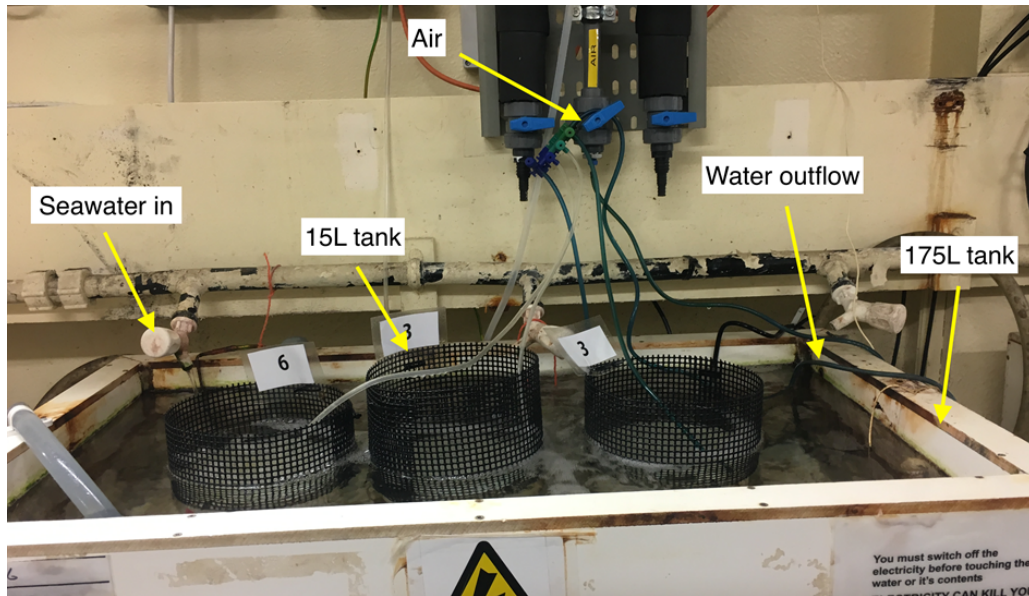


Figure 3.5: Experimental tank set up for those whelks placed in temperature-controlled conditions. The 175 L tank was either connected to a heater or chiller, depending on the seawater temperature required and time of year.

Labelling of whelks

Groups of laboratory reared whelks (11 to 21 mm total shell length) of known age were selected from the fortnightly hatchings to ensure that the whelks had an approximately similar age. For each experiment wild-caught juvenile and adult whelks were selected from the large 175 L acclimatisation tank. The number of whelks used in each experiment is shown in Table 3.1. Each whelk was labelled with an identification number. The surface of each whelk was blotted dry with absorbent paper and a thin layer of superglue applied to the shell surface. A printed paper number was attached to the glued shell surface (Figure 3.6) and a watertight seal was formed over the number by applying a second layer of glue. Labelling each individual whelk in this way allowed any individual to be tracked during shell repair and shell growth. Labelled whelks were held for ~20 minutes in a shallow tray of seawater, sufficient to keep the whelk's tissue moist but shallow enough for the numbers and glue to air dry. The process of shell drying, gluing, labelling, and re-gluing was carried out in <1 hour, to minimise stress to the whelks and avoid the risk of desiccation. Once the glue and labels were dry several dimensions of the whelk's shell were measured with vernier callipers (± 0.1 mm) to obtain total shell length (TSL), minimum width (W) and aperture length (ApL) (Figure 3.6). Total wet weight (i.e., shell and tissues) determined using a top loading balance (± 0.01 g). Any shell damage was recorded using the five-point scale ((0) *undamaged* (no obvious repairs) to (4) *severe damage* (entire shell is

badly scarred and covered with major shell repairs) detailed in Chapter 2 and Figure 2.5. To ensure that each whelk was responsive before experimentation it was gently touched with a blunt ended seeker. Whelks that were unresponsive were not used in any experiments, and during this process retraction of the whelk into its shell was assessed on a scale of 1 to 4. This scale was based on 1 being able to fully retract into the shell to 4 no retractability seen beyond shell lip (see Figure 3.7). Further whelks of similar size were labelled to make up for any shortfall in numbers.

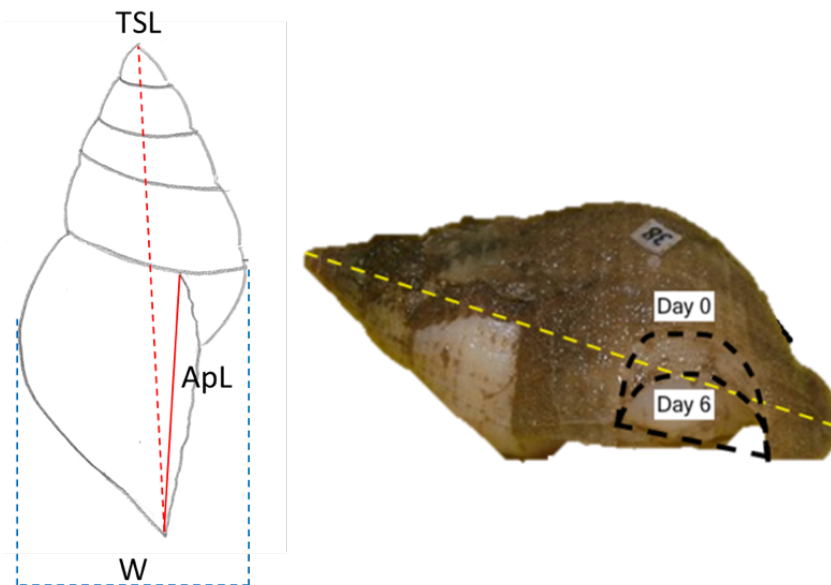


Figure 3.6: Representation of a *Buccinum undatum* shell (Left) with total shell length (TSL) (red dashed line) aperture length (ApL) (solid red line) and minimum width (W) (blue dashed lines). *B. undatum*, number 38 (Right) with TSL (yellow dashed line) and an approximate square area of shell removed with a Dremel cutting wheel (black dotted line) (Day 0) and repair (Day 6). In this whelk complete repair took 21 days.

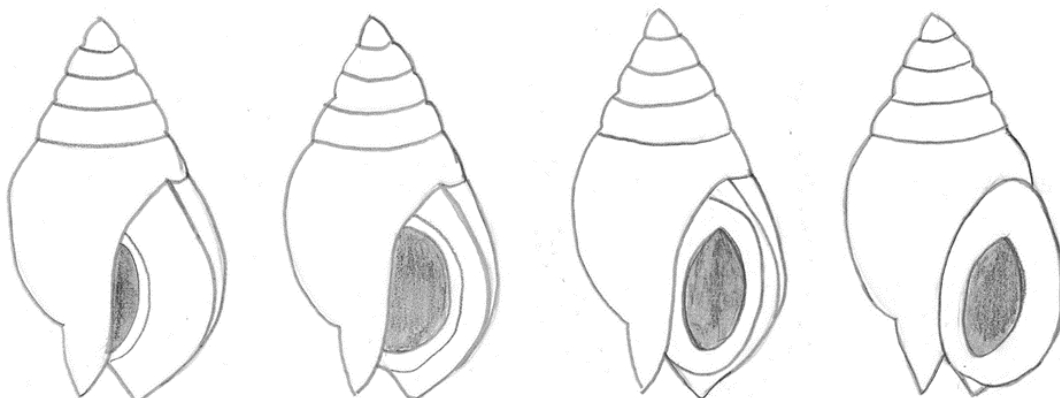


Figure 3.7: Diagrammatic representation of how retraction of the whelk body into the shell was scored from 1-4; left to right. The further the whelk retracted into the shell, the lower the score.

Shell damage and measurement of shell repair

Following a 10-day acclimatisation period in the different experimental tanks, each whelk was removed in turn and an approximate square of shell removed from the shell lip (Figure 3.6). The amount of shell cut out using a Dremel 3000 rotary tool, with cutting wheel attachment, was made as a proportion of approximately 40% of the aperture length (Figure 3.6). To ensure the body and mantle remained un-touched and avoided the heat from the saw blade during cutting, BluTack was carefully pushed inside the shell to hold the whelk's foot back. About 40% of whelks were treated in the same way as the damaged whelks i.e., handled and BluTack inserted, but their shells were left uncut; these whelks served as a shell growth control comparison. The excised shell squares were removed and retained; some of these shell pieces had been used earlier to study variations in shell colour (see Chapter 2).

Periodically each whelk was removed from its experimental tank. The shell, including the area of shell where damage had been inflicted was photographed against a measurable linear scale and the data recorded for analysis using the image analysis programme ImageJ, to determine the proportion of shell removed and repaired. Photographed whelks were returned to their tank within 10 minutes to ensure minimal disruption to shell growth. Whilst whelks were removed for photography, tank cleaning and water changes occurred. Following calibration of the measuring tool in ImageJ with a linear scale, measurements of whelk shell length (TSL) and the area damaged were calculated to an accuracy of $\pm 0.01 \text{ mm}^2$ using the straight line and freehand selections tools respectively (see outlines in Figure 3.6). The frequency of photography and computed measurements varied between groups. For the TRJ whelks this was every 3 days, the JW whelks 6 days, and the MW whelks 7 days. Photographs and measurements continued until the end of the experiment (see Table 3.1 for experiment duration). The time between photography and measurement and length of the experiment was largely based on observations of the speed of shell repair or when the majority of shells were repaired and when natural mortality began to increase. Shell growth and repair in juvenile whelks, particularly the TRJ whelks was rapid, thus photographs and measurements were taken more frequently. Percentage repair rates and cumulative growth (mm) were calculated for each whelk and average rates determined for each group of whelks in each experiment. At the end of each experiment whelks were individually frozen at -20°C .

Determination of sexual maturity

Following experimental damage and repair, each whelk was dissected to ascertain their sex, and sexual maturity (Figure 3.8 and Table 3.2). Whelks were thawed for 12 hours in a cold room until fully defrosted, then the body was carefully removed from their shell, avoiding damage to the delicate shell margin. This was achieved using forceps to grip and pull the foot, and at the same time twisting the shell to ease movement and release the mantle from the central columella muscle. If the body broke during this process, a tap was used to remove the remaining parts. The presence of a penis indicated a male whelk and there was no evidence of imposex in the populations studied (Ten Hallers-Tjabbes *et al.*, 1994; Strand and Jacobsen, 2002). Gonad maturity was assessed using the methods described in Haig *et al.* (2015) and Hollyman (2017) where maturity is assessed by gonad tissue presence on the digestive gland. A binary maturity scale was used where 1 was assigned to those showing signs of current or past maturity and 0 for those that were non-mature.

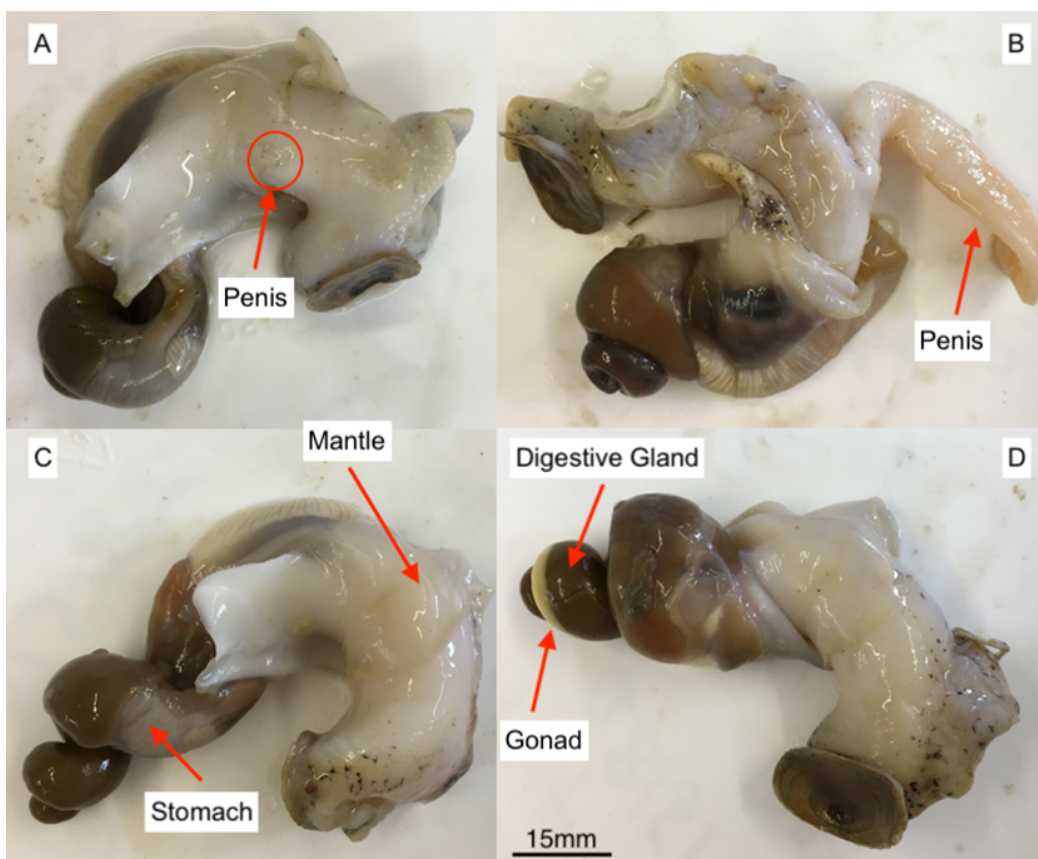


Figure 3.8: Dissected body of *Buccinum undatum*. A and B) juvenile male with small penis (A), mature male with large penis (B), C and D) females with gonad and digestive gland visible.

Statistical analysis

The methods for statistical analyses below follow those of Colvin *et al.* (2022b).

From the measurements of TSL and damage area, cumulative rates of increase in TSL and percentage shell repair were calculated for each individual for the experiment period and daily rates calculated from these final values as percentage repair and growth per day ($\text{mm}^2.\text{day}^{-1}$ and $\text{mm}.\text{day}^{-1}$ respectively). Statistics were performed in R Studio (version 1.3.1). Linear Models were used to test whether shell growth and shell repair were significantly influenced by environmental variables. Depending on treatment (Table 3.1 and 3.2; Experimental Factor), response variables were either percentage repair (%) or TSL growth day^{-1} (mm); explanatory variables include age (TRJ, JW, MW), food (unfed, daily, or weekly) and temperature (5, 10 or 15 °C). Response variables were modelled as continuous variables, and explanatory variables were modelled as categorical variables. Statistical significance (p-values) was obtained from F-tests, and backwards model selection based on p-values was applied (Zuur *et al.*, 2009). When interaction terms were non-significant in the full model, they were replaced with a non-interactive term and the process restarted. Diagnostic plots of residuals were checked for fit.

For graphical representation, the cumulative values were plotted in place of actual rates for a clearer comparative view of shell growth and shell repair between treatment groups. TSL was presented graphically using an average cumulative growth, taken as the average increase in shell length, and percentage repair as the average proportion of shell repaired out of 100% for all individuals per measured day. Due to differences in experiment length, with adult whelk studies running for longer periods than juveniles, and disparity in the degree of shell repair recorded, with some whelks attaining 100% repaired shell long before the end of the experiment, the values have not been taken as a final day measure. To resolve this, for statistical purposes, experiment duration for measures of repair rate have been taken as the day at which the first 75% of individuals from one single experiment have repaired to 100%.

Table 3.1: Summary of the experimental design and set up for the *Buccinum undatum* laboratory-controlled shell damage experiments.

Experimental factor	Life stage	Whelk size (mm)*	Initial no. of whelks *	Tank size (litres)	Tank arrangement*	Length (days)	Food quantity	Seawater temperature
Life stage July-August 2018	Juvenile (TRJ)	11-21	80	8 with 400 µm mesh bases in 15 holding tanks	4 tanks of 20	39		Ambient (Flow-through)
	< UK SOM (JW)	<45	80	15	8 tanks of 10	49		
	> UK SOM (MW)	>45	80	15		70		
Temperature December-January 2018-2019	Juvenile (TRJ)	11-21	90	10.26 in 175 holding tank	2 tanks of 15 for each temperature	15		5, 10 and 15°C (Static)
	> UK SOM (MW)	>45	160	10.26 in 175 holding tank	8 tanks of 10 for each temperature	21		5 and 10°C (Static)
Natural Seasonality January, April, July, October 2017-2019	Juvenile (TRJ)	11-21	80	15	8L with 400 µm mesh base of 20 suspended in 15L tanks	39	Daily	Ambient (Flow-through)
	< UK SOM (JW)	<45	80	15	4 15L tanks of 10 for each food level	49		
	> UK SOM (MW)	>45	80	15		70		
Temperature Controlled Seasonality January, April, July, October 2017-2019	Juvenile (TRJ)	11-21	80	5 in 175 holding tanks	8 L tanks of 10	39		10°C ±1.5 (Static)
	< UK SOM (JW)	<45	80	175	Split over 4 175L tanks	49		
	> UK SOM (MW)	>45	80			70		
Food availability July-August	Juvenile (TRJ)	11-21	90	8 with 400 µm mesh base suspended in 15	3 8L tanks of 10 for each food level	15	Unfed, once weekly, daily	Ambient (Flow-through)
	> UK SOM (MW)	>45	120	15	4 15L tanks of 10 for each food level	21		

*Numbers change from initial arrangement due to natural mortality. Random individual tank rotation with imaging for every tank. Mature and juvenile wild caught whelk were classed as greater than and below the average UK size at maturity when initially landed (>/< UK SOM).

Table 3.2: Summary table listing the additional measures taken.

Experiment	Group	Data collection method
Sex		Visual assessment and dissection
Maturity	Whelks < and > UK SOM	Visual assessment based on percentage maturity of gonads on dissection of whelk. If sign of maturity present whelk assigned a binary value of 1, no sign of prior maturation, a binary value of 0
Retractability		Visual assessment pre-experimental damage based on how far an individual could retreat within the shell. Retractability scale 1-4
Previous damage		Visual assessment of the shell pre-experimental damage. Values based on damage scale 0-4

Results

Prior shell damage and Retractability of body

All whelks used in the experiments were carefully examined prior to introduction into the experimental conditions to assess whether previous shell damage might influence the rate of shell repair and shell growth when they were damaged experimentally. Examination of cumulative % repair over time demonstrated that whelks that had previously received substantial damage to their shells displayed an overall increased shell repair rate but a decreased rate of total shell length increase, with similar results for both adult (MW) and juvenile whelks (JW) (Figure 3.9), although the differences were non-significant ($p > 0.05$; Table 3.3). These whelks were also assessed for retractability into the shell prior to damage. In general, whelks that retracted $>50\%$ into their shell displayed slower rates of shell growth and repair (Figure 3.10 A and B), however this response was non-significant for both ($p > 0.05$; Table 3.3). In all shell repair experiments, prior shell damage and the ability to retract within the shell aperture were similarly not found to significantly impact rates of shell repair and shell growth.

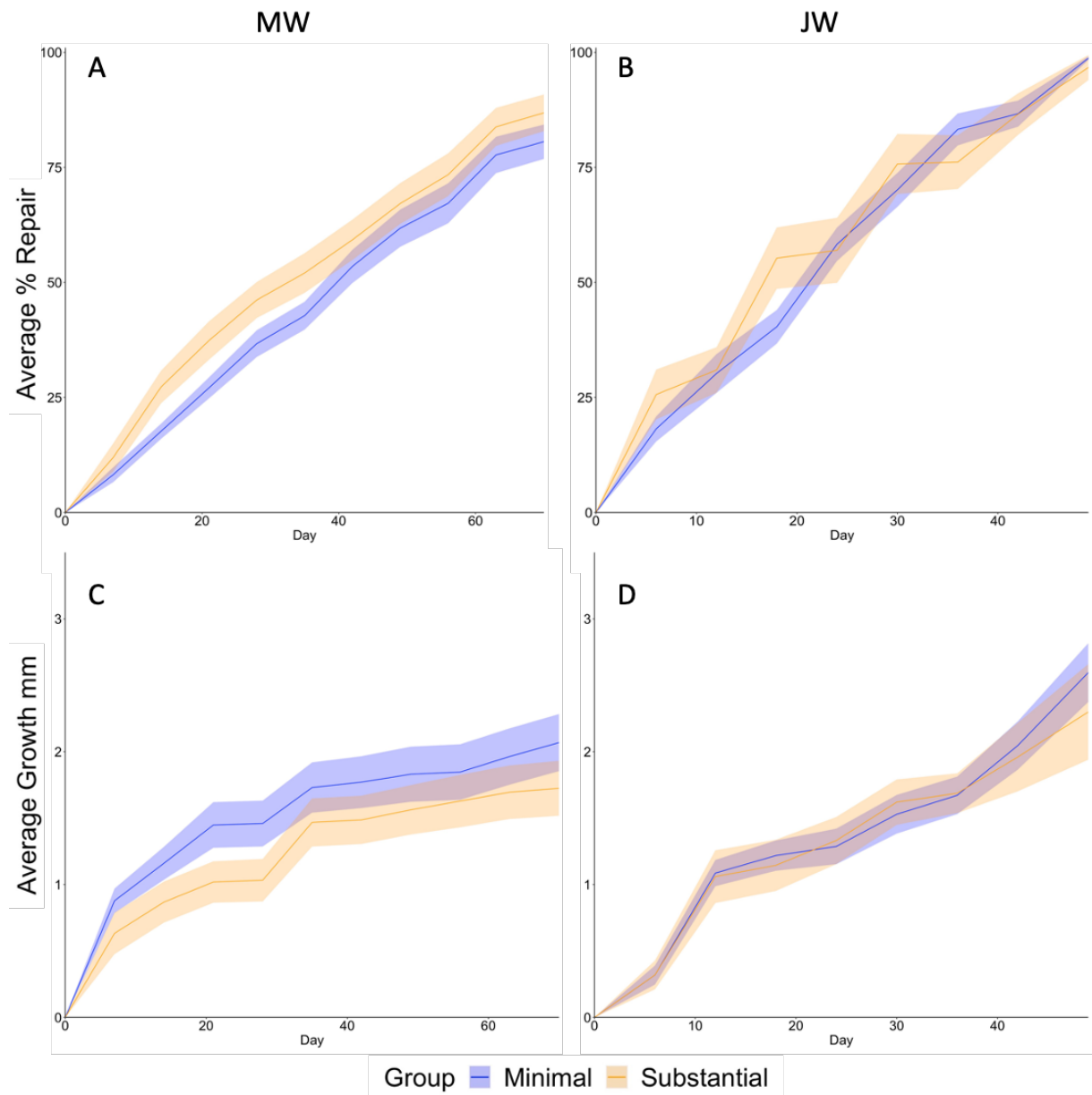


Figure 3.9: A and B) Average cumulative % repair (± 1 SE ribbon) and C and D) average cumulative growth (± 1 SE ribbon) with time for > and < SOM *Buccinum undatum* that had received minimal (blue) and substantial (orange) natural damage to their shells prior to their inclusion in the experiments and before the whelks were experimentally-damaged. Each line represents a level of previous natural shell damage that had been assessed on a scale of 0-4 (0 = no damage, 4 = > 4 events of shell damage), with 0-1 as minimal damage and >2 substantial previous damage.

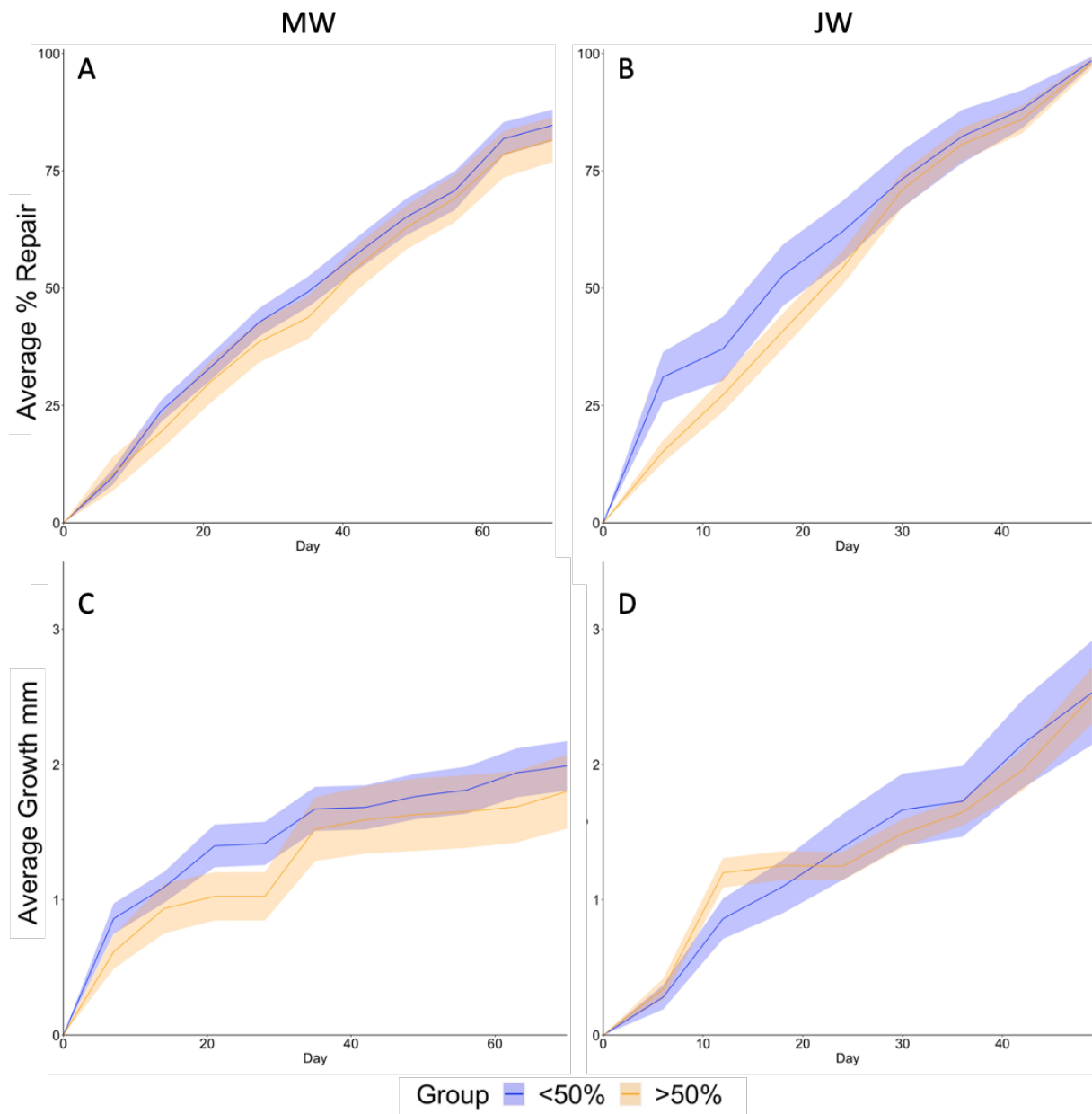


Figure 3.10: A and B) average cumulative % repair (± 1 SE ribbon) C and D) average cumulative growth (± 1 SE ribbon) with time for > and < SOM *Buccinum undatum*. Each line corresponds to a measure of retractability into the shell of the individual whelk prior to experimental shell damage, <50 retraction into the shell or >50%.

Table 3.3: Summary table of repair rates ($\text{mm}^2.\text{day}^{-1}$) and growth rates ($\text{mm}.\text{day}^{-1}$) of experimentally-damaged *Buccinum undatum*. Damaged vs control individuals were non-significant for all growth (TSL increase) experiments.

Natural damage		Mean \pm Standard Error								ANOVA	Where within group?
Group	Minimal				Substantial						
	MW	MW Control	JW	JW Control	MW	MW Control	JW	JW Control			
Repair Rate	1.151 ± 0.053	-	2.275 ± 0.095	-	1.241 ± 0.057	-	2.203 ± 0.176	-	Age: F= 122.81, p<0.001 Group: F= 0.019, p>0.05 Age*Group: F= 0.63, p>0.05	None	
Growth Rate	0.030 ± 0.004	0.029 ± 0.006	0.044 ± 0.005	0.054 ± 0.005	0.024 ± 0.003	0.027 ± 0.010	0.043 ± 0.005	0.059 ± 0.003	Age: F= 24.46, p<0.001 Group: F= 0.34, p>0.05 Age*Group: F= 0.3, p>0.05	None	
Retractability		Mean \pm Standard Error								ANOVA	Where within group?
Group	<50%				>50%						
	MW	MW Control	JW	JW Control	MW	MW Control	JW	JW Control			
Repair Rate	1.210 ± 0.048	-	2.320 ± 0.133	-	1.166 ± 0.068	-	2.224 ± 0.106	-	Age: F= 122.7, p<0.001 Group: F= 0.484, p>0.05 Age*Group: F= 0.069, p>0.05	None	
Growth Rate	0.027 ± 0.003	0.033 ± 0.006	0.047 ± 0.010	0.050 ± 0.007	0.028 ± 0.005	0.018 ± 0.007	0.042 ± 0.003	0.060 ± 0.004	Age: F= 24.61, p<0.001 Group: F= 0.378, p>0.05 Age*Group: F= 0.006, p>0.05	None	

Life Stage

Average repair rate over time decreased with increasing age (Figure 3.11 A), with a total range in rates of 2.1% day⁻¹ across the groups (tank-reared juvenile (TRJ), wild-caught <SOM (JW), wild-caught >SOM (MW)). Although both TRJ and JW whelks were classed as juveniles, both age and size of individual further came into effect with these rates with TRJ being on average a younger age than JW whelks. The greatest response to shell repair was seen within TRJ (TSL 11.5-21.25 mm) where the majority of shells were repaired within a 30-day period. JW and MW whelks repaired at a much slower rate. For JW whelks, similar results were not seen until day 49 and for MW whelks at day 63 no whelk had fully repaired their shell. Cumulative increase in total shell length for the three groups of whelks (Figure 3.11 B) showed a similar trend to that of shell repair rate over time. Repair rate and increase in total shell length were significantly different between age groups, ($p < 0.001$; Table 3.4). Compared with the experimentally-damaged whelks the undamaged control whelks generally achieved a larger total length (Figure 3.11 B), although this was not statistically significantly different ($p > 0.05$; Table 3.4).

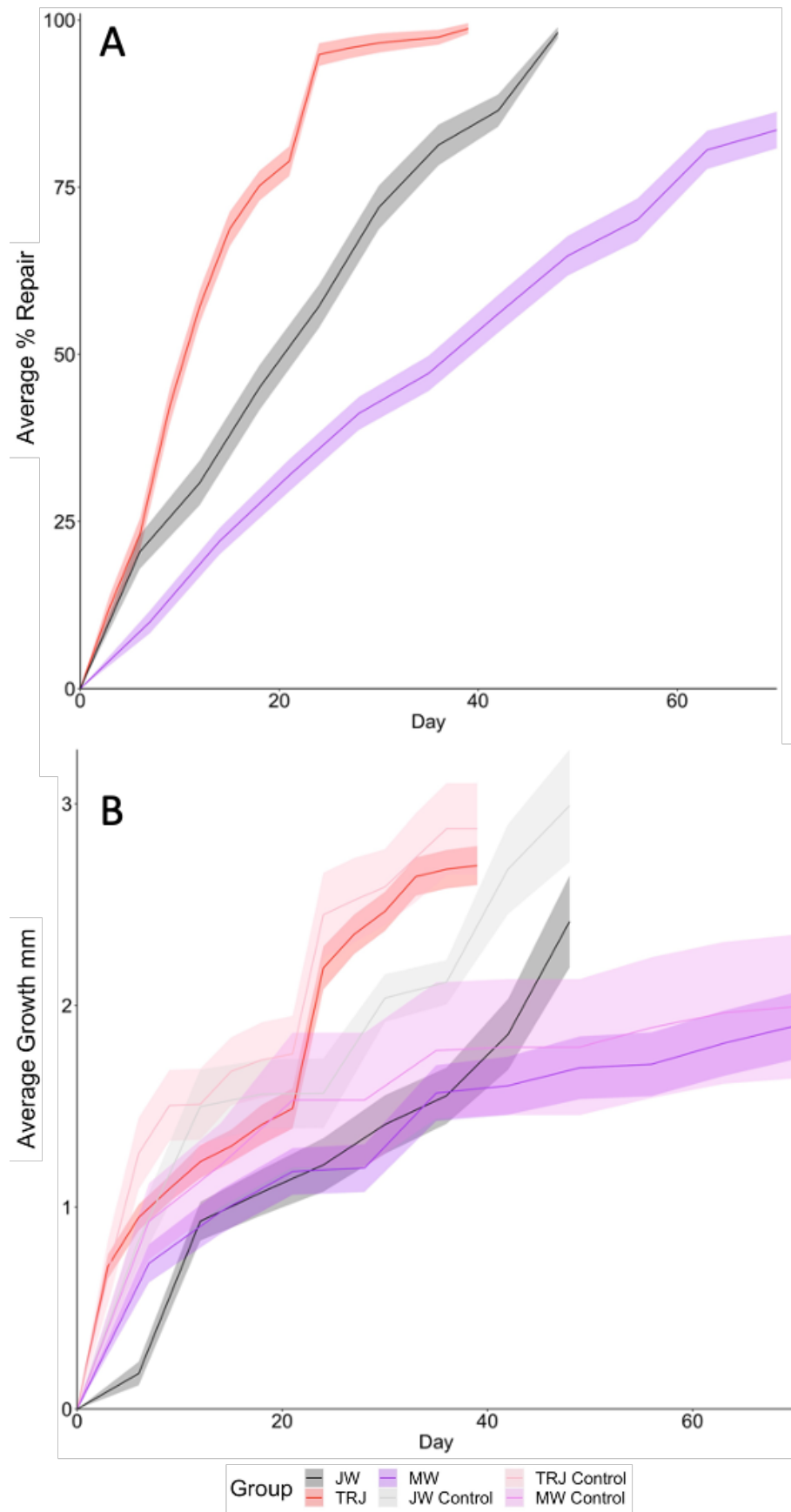


Figure 3.11: A) average cumulative % repair (± 1 SE ribbon) and B) average cumulative growth (± 1 SE ribbon) with time for three different age groups of *Buccinum undatum*.

Sex and Maturity

When the maturity data were combined for both sexes (Figure 3.12), although some whelk caught >SOM were found to be non-mature, the average TSL for both non-mature and mature whelks were similar ($78.8 \text{ mm} \pm 11.3 \text{ SD}$ and $80.1 \text{ mm} \pm 11.5 \text{ SD}$ respectively). For JW whelk, the average TSL was $36.3 \text{ mm} \pm 4 \text{ SD}$. TSL increase between all groups initially showed little difference, however the JW whelks had maximum shell growth over the experimental period.

Following this, a comparison of shell growth and shell repair in male and female whelks during both summer and winter months showed fastest rates of shell repair during the summer, with 100% repair reached before day 30 in all JW whelk (Figures 3.13 A and B). On average, those >SOM showed significantly faster overall rates of repair in experiments carried out during the winter than during the summer months (Table 3.4). Further differences were seen with a reversed response between mature males and females during the winter and summer months for both shell repair and TSL increase, whereby faster rates were seen for males in winter and fastest rates for females during the summer months. TSL increase, and shell repair both saw an opposite response in juveniles. Assessed maturity saw significant differences in rates of shell growth and shell repair ($p < 0.001$; Table 3.4). However, differences were non-significant for whelk sex ($p > 0.05$; Table 3.4).

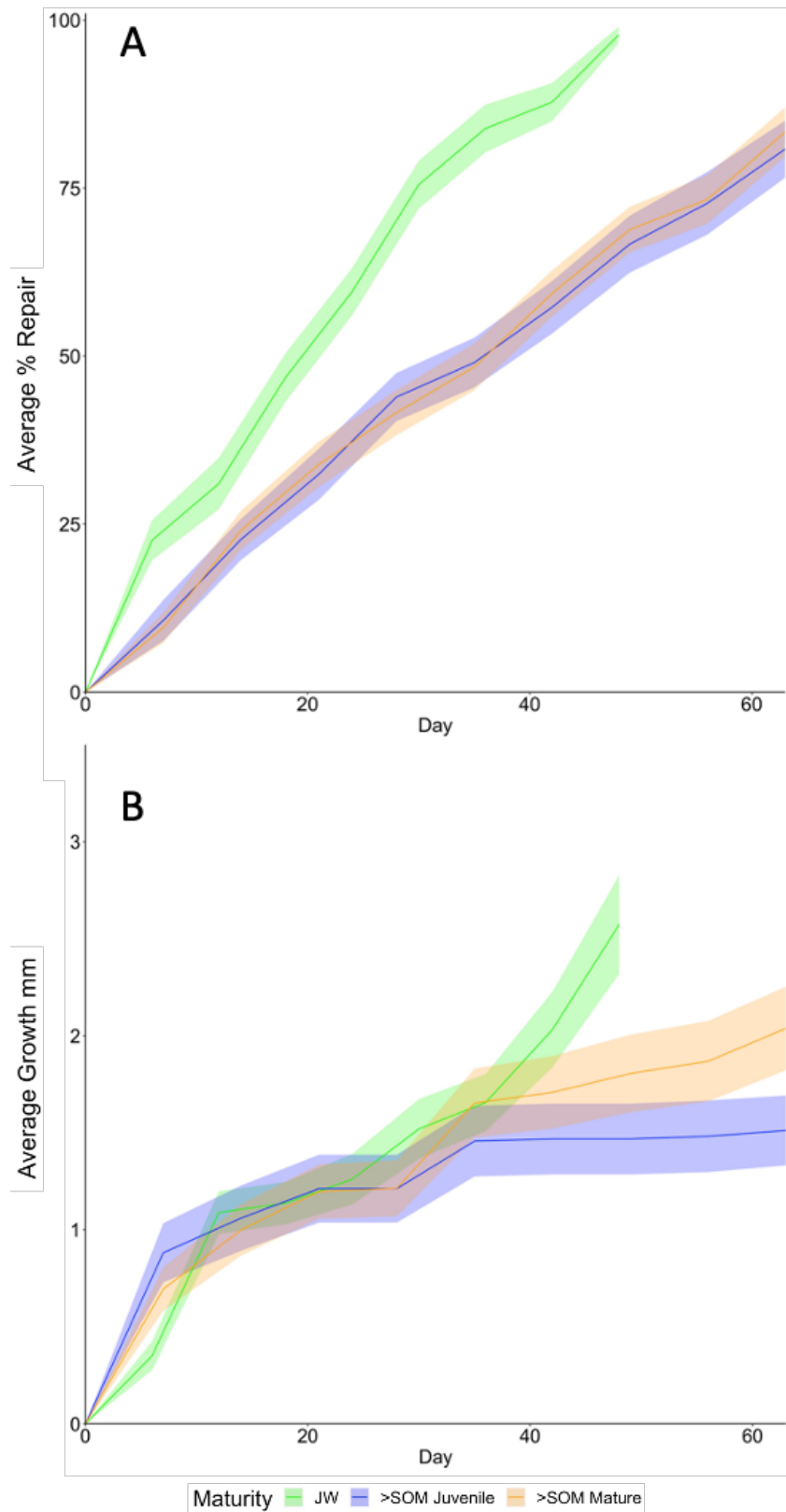


Figure 3.12 A) average cumulative % shell repair (± 1 SE ribbon) and B) average cumulative shell growth (± 1 SE ribbon) with time for wild caught *Buccinum undatum*. Binary maturity assessed during winter months as yes (1) or no (0). Maturity groups: <SOM juvenile (JW), >SOM but juvenile and >SOM mature.

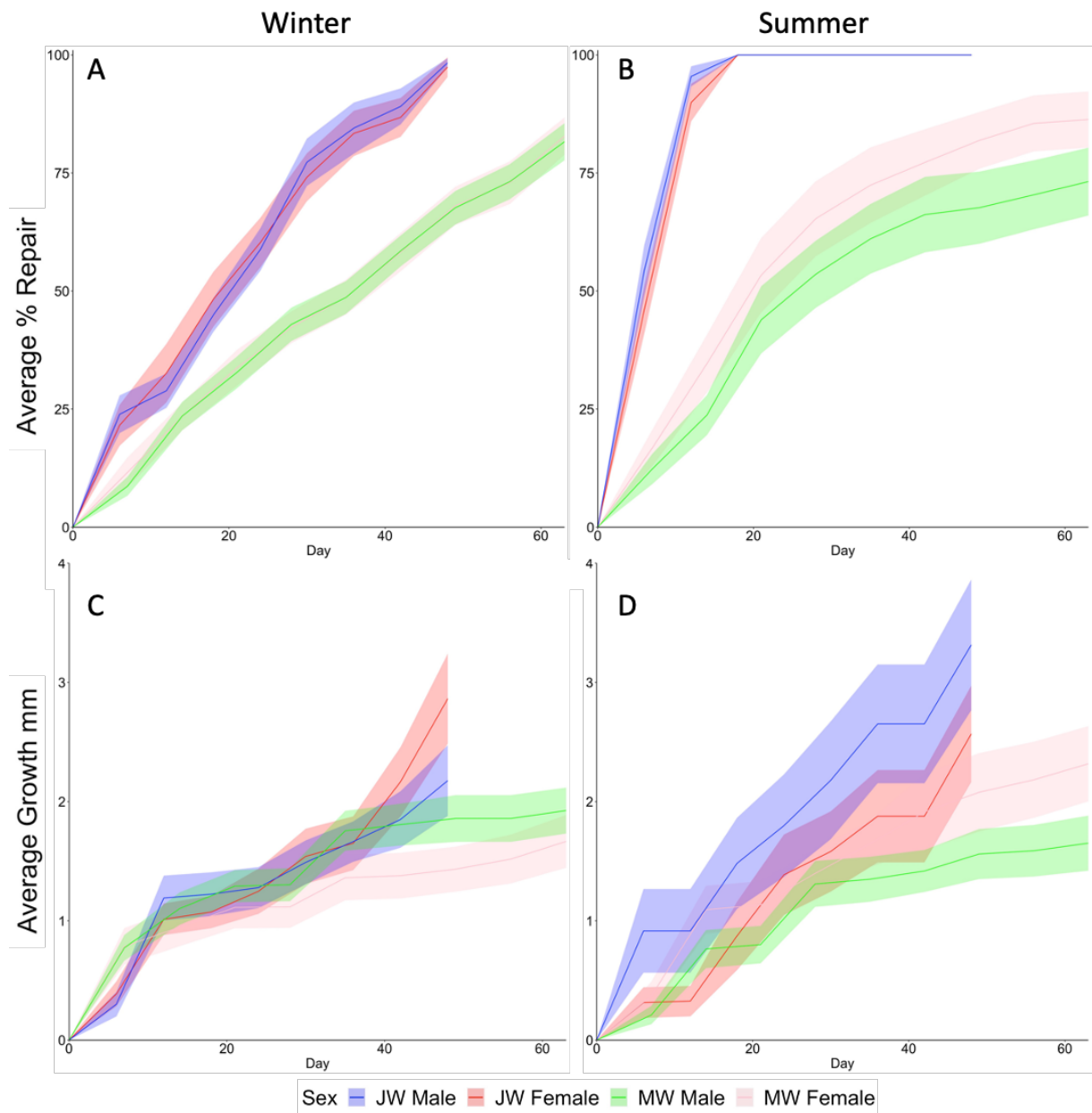


Figure 3.13: Average cumulative % shell repair rates (A and C) (± 1 SE ribbon) and average cumulative shell growth (B and D) (± 1 SE ribbon) in experimentally-damaged *Buccinum undatum* during the winter (A and C) and summer (B and D). Whelk sex determined through the presence or absence of a penis. JW refers to a wild caught juvenile whelk and MW a wild caught mature whelk.

Table 3.4: Summary of repair rates ($\text{mm}^2.\text{day}^{-1}$) and growth rates ($\text{mm}.\text{day}^{-1}$) of experimentally-damaged *Buccinum undatum*. Damaged vs control individuals were non-significant for all growth (TSL increase) experiments.

Life Stage		Mean \pm Standard Error						ANOVA	Where within group?
Group	Tank-reared Juvenile (TRJ)		Juvenile Wild (JW)		Mature Wild (MW)				
	Damaged	Control	Damaged	Control	Damaged	Control			
Repair Rate	3.951 ± 0.071	-	2.044 ± 0.017	-	1.933 ± 0.039	-		Life stage: F= 865, p<0.001	All
Growth Rate	0.091 ± 0.004	0.102 ± 0.009	0.050 ± 0.005	0.062 ± 0.006	0.027 ± 0.002	0.029 ± 0.005		Life stage: F= 90.6, p<0.001	All

Sex		Mean \pm Standard Error								ANOVA	Where within group?
Group	Summer				Winter						
	Female	Female Control	Male	Male Control	Female	Female Control	Male	Male Control			
Repair Rate	4.085 ± 0.335	-	4.018 ± 0.338	-	1.655 ± 0.065	-	1.499 ± 0.075	-	Season: F= 114.97, p<0.001 Sex: F= 0.11, p>0.05 Season*Sex: F= 0.002, p>0.05	Season	
Growth Rate	0.044 ± 0.012	0.039 ± 0.021	0.065 ± 0.016	0.625 ± 0.028	0.040 ± 0.005	0.042 ± 0.009	0.034 ± 0.004	0.425 ± 0.007	Season: F= 3.16, p>0.05 Sex: F= 0.54, p>0.05 Season*Sex: F= 2.04, p>0.05	None	

Assessed Maturity		Mean \pm Standard Error								ANOVA	Where within group?
Group	Summer				Winter						
	Mature	Mature Control	Juvenile	Juvenile Control	Mature	Mature Control	Juvenile	Juvenile Control			
Repair Rate	1.262 ± 0.076	-	5.556 ± 0.000	-	1.220 ± 0.037	-	2.035 ± 0.026	-	Season: F= 4920.5, p<0.001 Maturity: F= 4373.9, p<0.001 Season*Maturity: F= 2318.4, p<0.001	All	
Growth Rate	0.035 ± 0.004	0.029 ± 0.011	0.065 ± 0.015	0.0736 ± 0.033	0.026 ± 0.003	0.026 ± 0.004	0.051 ± 0.006	0.063 ± 0.009	Season: F= 3.29, p>0.05 Maturity: F= 11.68, p<0.001 Season*Maturity: F= 0.14, >0.05	Maturity	

Feeding Regime

Figure 3.14 shows the cumulative % shell repair (A) and shell growth (B) for the experimentally-damaged whelks maintained in different food regimes. Daily fed and unfed juvenile whelks (TRJ) repaired their damaged shells faster than whelks fed only once a week (Figure 3.14 A). However, for rates of repair, the only significance was found between life stage (see Table 3.5). MW whelks (wild caught > UK SOM) fed once weekly repaired their shells at a similar rate to that of TRJ whelks fed only once a week (Figure 3.14 A). When this group of whelks were fed daily or unfed, their rates of shell repair were slower than the TRJ and other MW whelks (Figure 3.14 A). When the effect of food regime on cumulative growth was investigated (Figure 3.14 B), TRJ whelks grew notably faster when fed once a week compared with those fed daily or were unfed. MW whelks, whose shells were undamaged and fed daily and the MW damaged whelks fed daily grew more slowly (0.027 and $0.028 \text{ mm.day}^{-1} \pm 0.009$ and 0.014 SE respectively) than all other whelk groups which ranged between approximately 0.075 to 0.09 mm.day^{-1} . The effect of feeding regime and the interaction between feeding and age were both significant for TSL increase ($p < 0.05$; see Table 3.5).

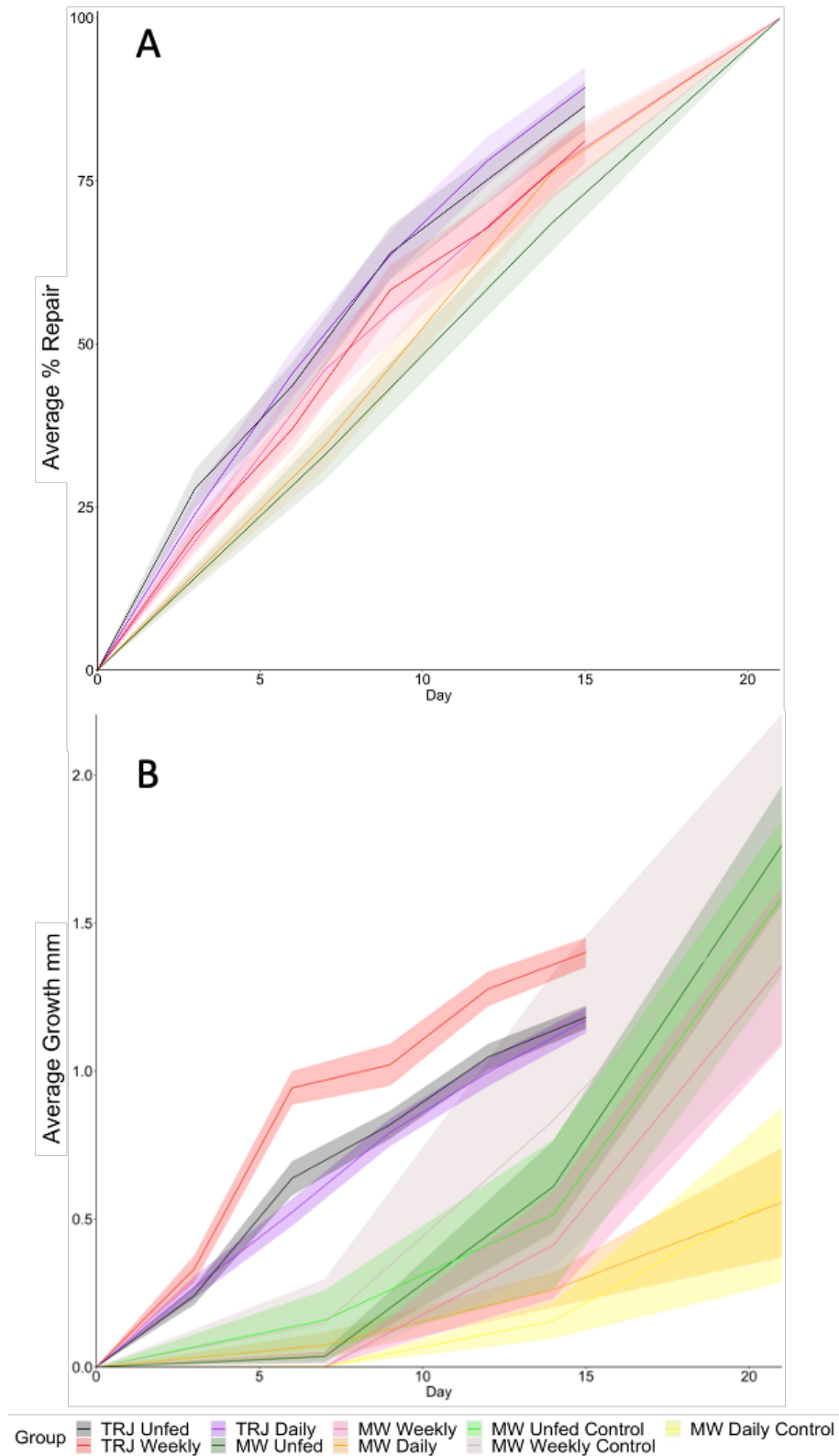


Figure 3.14: A) Average cumulative % repair (± 1 SE ribbon) and B) average cumulative growth (± 1 SE ribbon) for *Buccinum undatum* presented with different feeding regimes (daily, once weekly, unfed). Two groups of whelks were used, tank-reared juvenile (TRJ) and wild-caught >SOM (MW). The TRJ and MW experiments continued for 15 days and 21 days respectively.

Table 3.5: Summary of repair rates ($\text{mm}^2.\text{day}^{-1}$) and growth rates ($\text{mm}.\text{day}^{-1}$) of experimentally-damaged *Buccinum undatum*. Damaged vs control individuals were non-significant for all growth (TSL increase) experiments.

Food		Mean \pm Standard Error									ANOVA	Where within group?
Group	Unfed			Once Weekly			Daily					
	TRJ Damaged	MW Damaged	MW Control	TRJ Damaged	MW Damaged	MW Control	TRJ Damaged	MW Damaged	MW Control			
Repair Rate	5.765 ± 0.025	4.756 ± 0.002	-	5.405 ± 0.226	4.760 ± 0.001	-	5.954 ± 0.203	4.761 ± 0.001	-	Age: F= 54.6, p<0.001 Food: F= 1.87, p>0.05 Age*Food: F= 2.01, p>0.05	None	
Growth Rate	0.079 ± 0.003	0.084 ± 0.010	0.075 ± 0.012	0.093 ± 0.003	0.065 ± 0.013	0.079 ± 0.026	0.078 ± 0.003	0.027 ± 0.009	0.028 ± 0.014	Age: F= 17.2, p<0.001 Food: F= 11.1, p<0.001 Age*Food: F= 6.53, p<0.05	Daily:Unfed Daily:Weekly	

Seawater Temperature

Across all seawater temperatures, experimentally-damaged TRJ whelks repaired and grew their shells at the fastest rates (Figure 3.15). At 15°C TRJ whelks repaired their shells on average at $10.4 \text{ mm}^2 \cdot \text{day}^{-1}$ ($\pm 0.253 \text{ SE}$) with >90% seeing full shell repair by day 9, a rate almost double that of TRJ whelks reared at 5°C and 10°C (Figure 3.15 A). For TRJ whelks at 5 and 10°C rates were slower, with only 70% repair seen during the same time period. Between days 0 and 12 an initial faster rate in TRJ whelks was observed under 5°C conditions when compared with 10°C. By day 20 MW (wild caught > UK SOM) whelks had repaired 75% of their damaged shells at 10°C and 50% at 5°C (Figure 3.15 A). The effect of seawater temperature and its interaction with age were both found to be significant for rates of shell repair ($p < 0.001$ and $p < 0.05$ respectively; Table 3.6).

Variation in shell growth between the TRJ whelks under the three temperature regimes was tightly constrained (Figure 3.15 B), with all whelks growing at similar rates. The largest overall increase in TSL during the 15-day experiment was observed at 15°C. By contrast there was greater variation in growth amongst the MW wild-caught whelks under two different temperature regimes (Figure 3.15 B). MW Whelks reared at 15°C did not survive. Up until day 7 shell growth was initially, rapid, and similar to the growth rate in the TRJ whelks. However, following a period of rapid growth shell deposition slowed resulting in a small increase ($\sim 0.5 \text{ mm}$) for the remaining 13 days of the experiment. The fastest rates of shell growth of the MW whelks were observed at 10°C compared with those held at 5°C both for experimentally-damaged and control (undamaged) whelks (Figure 3.15 B). The effect of seawater temperature on TSL was found to be significant ($p < 0.05$; Table 3.6), however its interaction with age was non-significant ($p > 0.05$; Table 3.6).

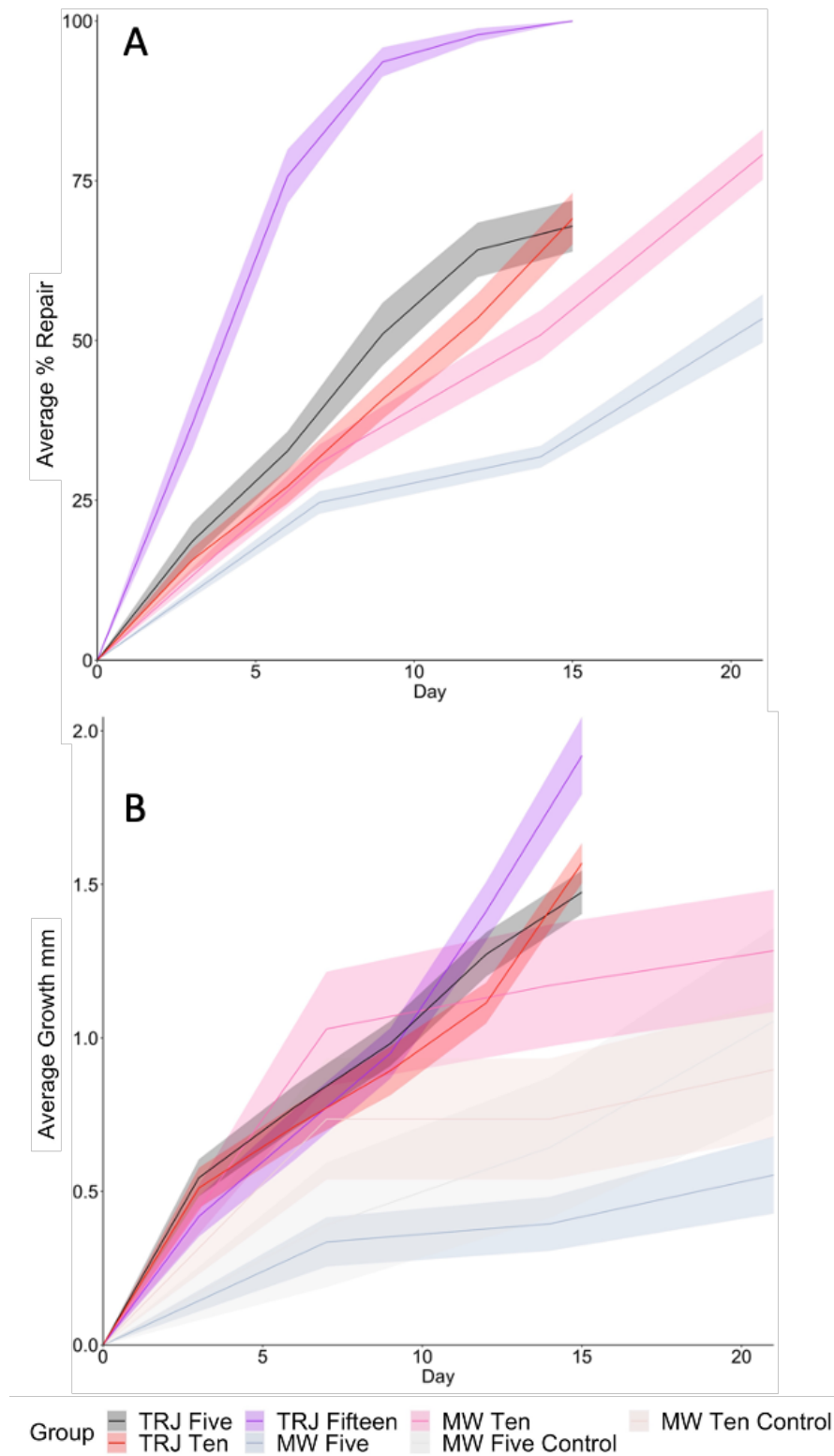


Figure 3.15: A) Average cumulative % repair (± 1 SE ribbon) and B) average cumulative growth (± 1 SE ribbon) with time for *Buccinum undatum*. Two groups of whelks were used, tank-reared juvenile (TRJ) and wild caught >SOM (MW). TRJ experiments ran for 15 days at 5, 10 and 15°C and MW for 21 days at 5 and 10°C. No survival of MW whelks occurred at 15°C in both control groups and under experimental conditions.

Seasonal Variation

For the seasonal variation experiments on shell repair and shell growth using wild-caught whelks > UK SOM, no significant difference was found between the ambient and temperature-controlled systems ($p > 0.05$; Table 3.6), however for the < UK SOM and TRJ whelks a significant difference was seen between both ($p < 0.05$; Table 3.6). Wild-caught whelks >SOM showed the fastest rates of shell repair during the spring months under both controlled and ambient seawater temperatures (Figure 3.16 A and B), with all whelks completely repairing their shells during the experimental period. Under controlled conditions the spring and winter whelks repaired their shells faster than those whelks that repaired in the summer and autumn (Figure 3.16 A). The repair rates of damaged shells in whelks > UK SOM under ambient seawater temperatures (Figure 3.16 B) were different to those maintained under controlled conditions. Damaged whelks under these conditions repaired their shells faster in the spring and autumn and more slowly in the summer and winter (Figure 3.16 B). In the summer, whelks had an initial slow period of growth when maintained at a controlled temperature, followed by a rapid increase after day 20 compared with a steady increase under ambient conditions (Figure 3.16 C and D). Amongst the shell repair and TSL increase experiments significant differences were found between all the seasons except for summer/ winter and autumn/ spring comparisons respectively ($p < 0.001$; Table 3.6).

Shell repair rates of wild-caught < UK SOM whelks were slowest during the spring under both temperature-controlled and ambient seawater conditions (Figure 3.17 A and B). Repair rates were fastest in the summer, autumn, and winter under temperature-controlled conditions (Figure 3.17 A) and only fastest in summer in ambient seawater (Figure 3.17 B). Shell repair rates saw similar patterns in the spring, autumn, and winter in ambient seawater (Figure 3.17 B). Shell growth rates generally mirrored shell repair rates under both conditions with fastest growth during the summer and slowest growth in the spring (Figure 3.17 C and D). < UK SOM whelks grew twice as fast during the summer and spring under controlled conditions than they did under ambient conditions (Figure 3.17 C and D) and demonstrated a significant difference ($p < 0.001$; Table 3.6) in shell repair rates and shell growth under temperature controlled and ambient conditions apart from in the autumn/spring. Further significant differences were seen for all seasons of shell growth, with the exception of autumn/spring and autumn/winter ($p < 0.001$; Table 3.6).

Shell repair in tank-reared juvenile (TRJ) whelks maintained under controlled temperatures was similar throughout the year and completed very rapidly (Figure 3.18). However, under ambient conditions, rates of shell repair were much slower during the winter (Figure 3.18 B and D). At other times of the year the shell was repaired at a similar rate to those whelks maintained under controlled conditions (Figure 3.18 A and B). Shell growth was rapid during the summer, and to a lesser extent in the spring under controlled conditions (Figure 3.18 C). Similarly shell growth was rapid under summer ambient water temperatures, but the rate of growth was almost twice as fast as growth under controlled conditions, and three times as fast as shell growth in the autumn, winter, and spring. In these experiments TRJ whelks demonstrated rapid rates of shell repair ($16 \text{ \%} \cdot \text{day}^{-1}$) and a growth rate of $0.41 \text{ mm} \cdot \text{day}^{-1}$ (Figure 3.18 A-D). TRJ whelks demonstrated significant results for both season and tank system, with the exception of autumn/winter for both rates of shell repair and TSL increase ($p < 0.001$; Table 3.6).

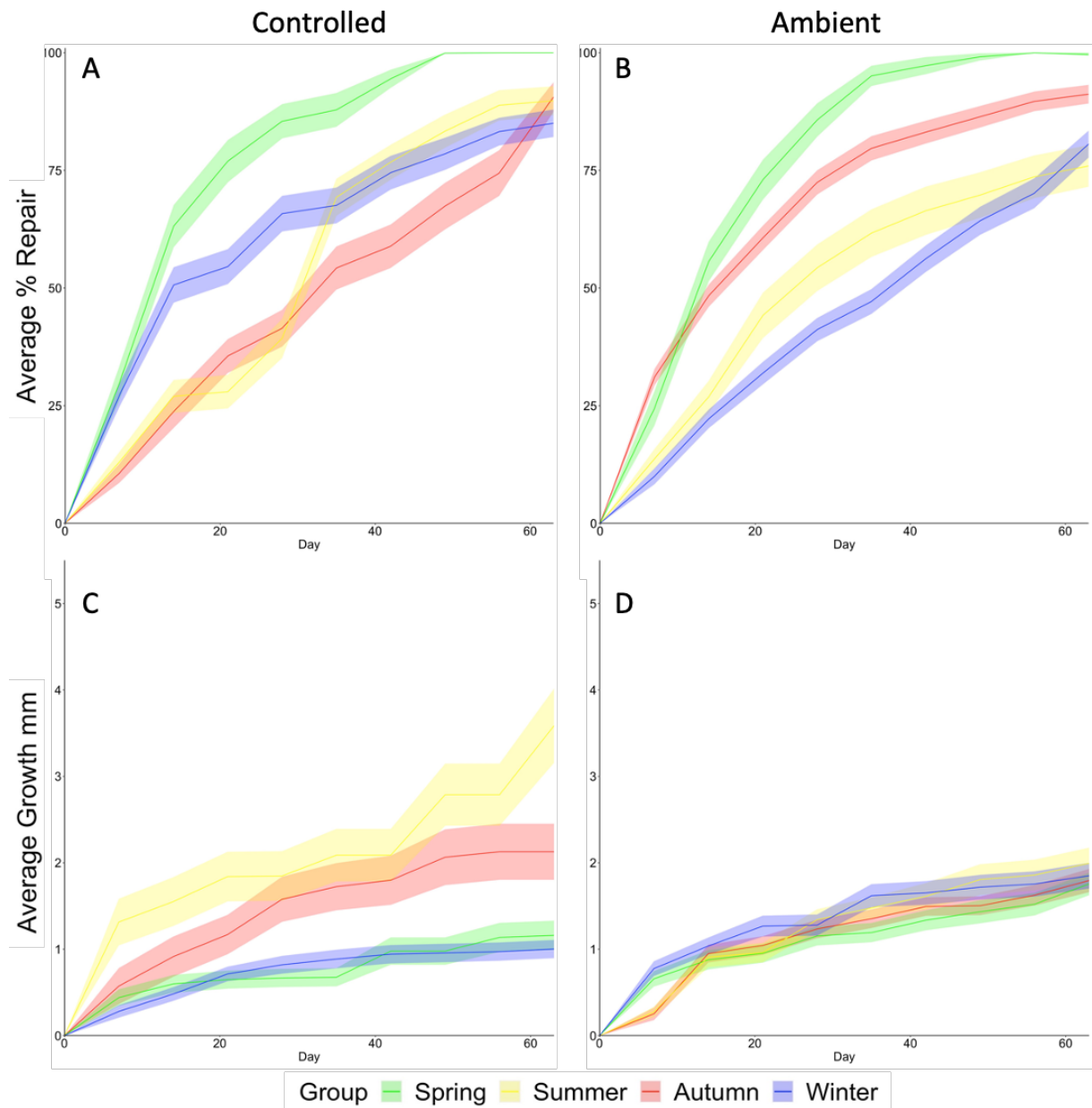


Figure 3.16: A and B average (± 1 SE ribbon) cumulative % repair and C and D average (± 1 SE ribbon) cumulative growth for mature wild-caught *Buccinum undatum* maintained under temperature-controlled regimes (A and C) and under ambient conditions (B and D) during four seasons of the year (spring, summer, autumn, and winter). Each line represents a different season when the experiment was undertaken.

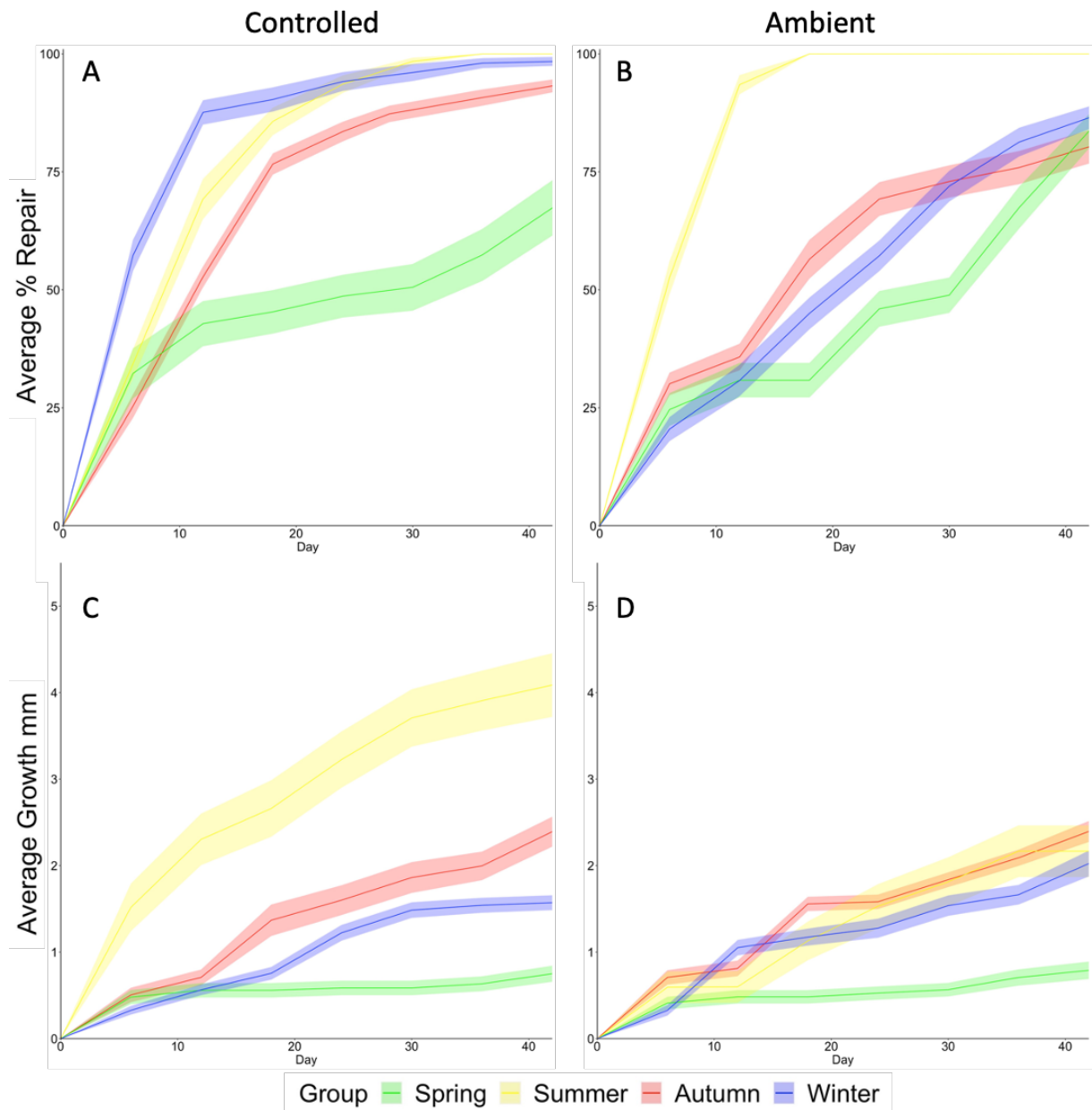


Figure 3.17: A and B Average ($\pm 1SE$ ribbon) cumulative % repair and C and D average ($\pm 1SE$ ribbon) cumulative shell growth for juvenile wild-caught *Buccinum undatum* maintained under temperature-controlled regimes (A and C) and under ambient conditions (B and D) during four seasons of the year (spring, summer, autumn, and winter). Each line represents a different season when the experiment was undertaken.

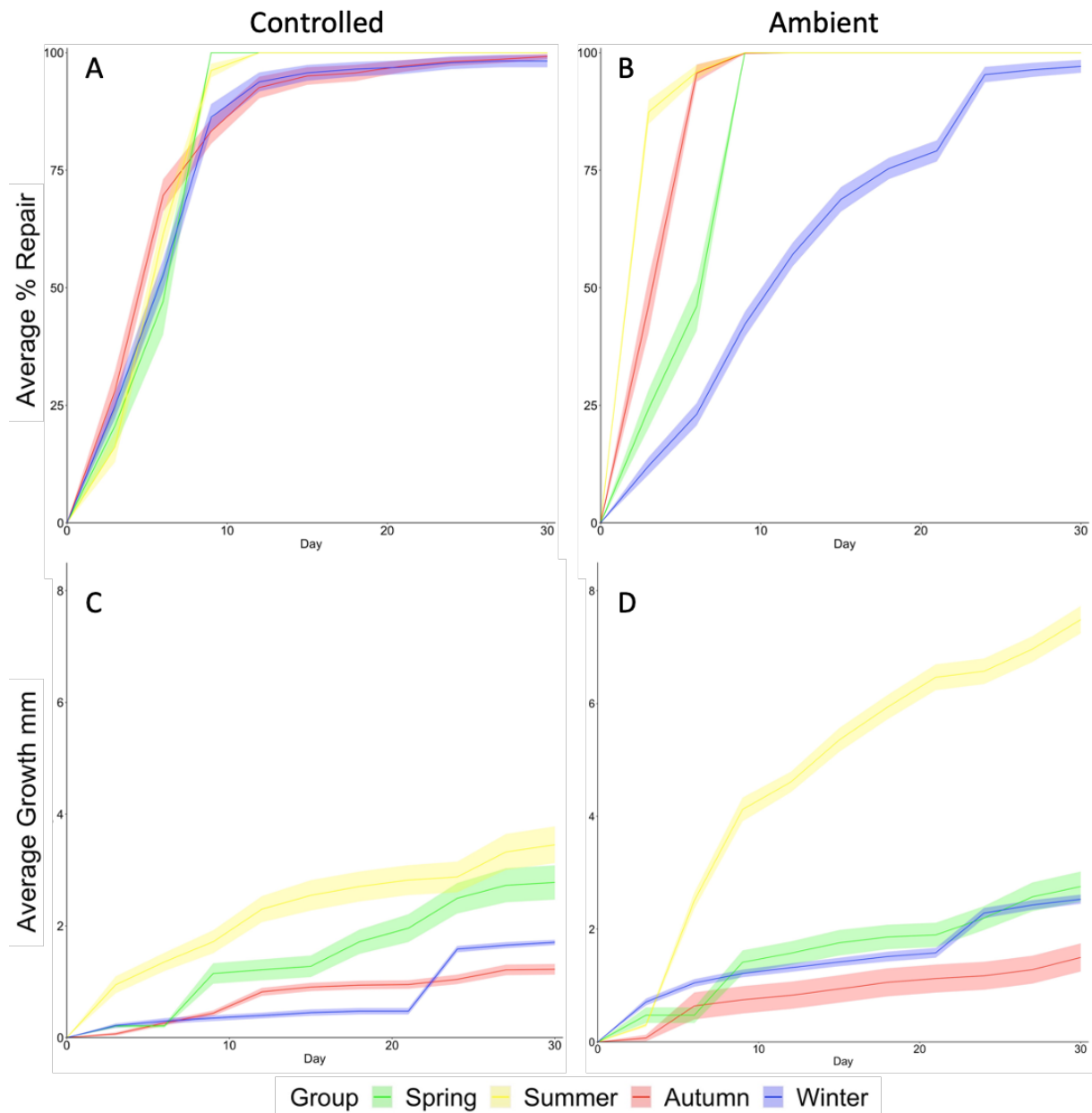


Figure 3.18: A and B Average (± 1 SE ribbon) cumulative % shell repair and C and D average cumulative shell growth for tank-reared juvenile *Buccinum undatum* maintained under temperature-controlled regimes (A and C) and under ambient conditions (B and D) (during four seasons of the year (spring, summer, autumn, and winter). Each line represents a different season when the experiment was undertaken.

Table 3.6: Summary of repair rates ($\text{mm}^2.\text{day}^{-1}$) and growth rates ($\text{mm}.\text{day}^{-1}$) of experimentally-damaged *Buccinum undatum*. Damaged vs control individuals were non-significant for all growth (TSL increase) experiments.

Temperature		Mean \pm Standard Error						ANOVA	Where within group?
Group	5°C			10°C			15°C		
	TRJ Damaged	MW Damaged	MW Control	TRJ Damaged	MW Damaged	MW Control	TRJ Damaged		
Repair Rate	4.527 ± 0.266	2.545 ± 0.179	-	4.605 ± 0.269	3.766 ± 0.186	-	10.397 ± 0.253	Age: F= 296, p<0.001 Group: F= 183, p<0.001 Age*Temp: F= 6.47, p<0.05	All
Growth Rate	0.098 ± 0.005	0.026 ± 0.006	0.050 ± 0.014	0.105 ± 0.004	0.061 ± 0.009	0.045 ± 0.010	0.106 ± 0.009	Age: F= 72.7, p<0.001 Group: F= 3.41, p<0.05 Age*Temp: F= 1.05, p>0.05	All

Wild-caught >SOM Seasonal																		ANOVA	Where within group?
Group	Spring Ambient		Spring Temp Control		Summer Ambient		Summer Temp Control		Autumn Ambient		Autumn Temp Control		Winter Ambient		Winter Temp Control				
	Damaged	Control	Damaged	Control	Damaged	Control	Damaged	Control	Damaged	Control	Damaged	Control	Damaged	Control	Damaged	Control			
Repair Rate	2.717 ±0.062	-	2.249 ±0.046	-	1.205 ±0.070	-	1.401 ±0.055	-	1.447 ±0.031	-	1.438 ±0.050	-	1.193 ±0.039	-	1.349 ±0.046	-	System: F= 2.79, p>0.05 Season: F= 280.48, p<0.001 System*Season: F= 18.15, p<0.001	All except Summer:Winter	
Growth Rate	0.038 ±0.003	0.024 ±0.007	0.032 ±0.004	0.000 ±0.000	0.038 ±0.003	0.017 ±0.003	0.045 ±0.009	0.067 ±0.010	0.029 ±0.003	0.028 ±0.004	0.035 ±0.006	0.029 ±0.006	0.027 ±0.002	0.029 ±0.005	0.016 ±0.002	0.016 ±0.003	System: F= 1.029, p>0.05 Season: F= 15.67, p<0.001 System*Season: F= 10.41, p<0.001	All except Autumn:Spring	
Wild-caught <SOM Seasonal																		ANOVA	Where within group?
Group	Spring Ambient		Spring Temp Control		Summer Ambient		Summer Temp Control		Autumn Ambient		Autumn Temp Control		Winter Ambient		Winter Temp Control				
	Damaged	Control	Damaged	Control	Damaged	Control	Damaged	Control	Damaged	Control	Damaged	Control	Damaged	Control	Damaged	Control			
Repair Rate	1.990 ±0.086	-	1.604 ±0.140	-	5.556 ±0.000	-	3.899 ±0.077	-	1.886 ±0.057	-	1.988 ±0.024	-	2.044 ±0.017	-	3.202 ±0.060	-	System: F=13.33, p<0.05 Season: F= 1009.1, p<0.001 System*Season: F= 181.13, p<0.001	All except: Autumn:Spring	
Growth Rate	0.019 ±0.003	0.018 ±0.006	0.017 ±0.003	0.021 ±0.004	0.060 ±0.014	0.071 ±0.027	0.140 ±0.014	0.119 ±0.034	0.009 ±0.030	0.047 ±0.005	0.048 ±0.004	0.064 ±0.009	0.050 ±0.005	0.059 ±0.006	0.051 ±0.003	0.048 ±0.006	System: F= 12.43, p<0.001 Season: F= 19.54, p<0.001 System*Season: F= 5.82, p<0.001	All except: Autumn:Spring Autumn:Winter	
TRJ Seasonal																		ANOVA	Where within group?
Group	Spring Ambient		Spring Temp Control		Summer Ambient		Summer Temp Control		Autumn Ambient		Autumn Temp Control		Winter Ambient		Winter Temp Control				
	Damaged	Control	Damaged	Control	Damaged	Control	Damaged	Control	Damaged	Control	Damaged	Control	Damaged	Control	Damaged	Control			
Repair Rate	11.111 ±0.000	-	11.111 ±0.000	-	15.987 ±0.247	-	10.687 ±0.164	-	15.941 ±0.305	-	6.336 ±0.125	-	3.568 ±0.055	-	6.381 ±0.112	-	System: F= 723.3, p<0.001 Season: F= 1042.58, p<0.001 System*Season: F= 544.66, p<0.001	All except: Autumn:Winter	
Growth Rate	0.126 ±0.022	0.243 ±0.061	0.146 ±0.027	0.100 ±0.031	0.411 ±0.018	0.436 ±0.078	0.218 ±0.031	0.135 ±0.027	0.110 ±0.057	0.096 ±0.019	0.059 ±0.006	0.064 ±0.010	0.089 ±0.003	0.093 ±0.008	0.025 ±0.004	0.051 ±0.008	System: F=4 8.8, p<0.001 Season: F= 62.55, p<0.001 System*Season: F= 9.12, p<0.001	All except: Autumn:Winter	

Discussion

This chapter investigated the variability and success of shell growth and shell repair in *Buccinum undatum* under different environmental conditions, whilst assessing their life history parameters and how these interact with growth through a series of laboratory-controlled experiments. Understanding the variability in response rate will help us better understand how individual whelks respond to periods of shell damage in the natural environment, for example mechanical (e.g., from towed fishing gears) and from natural damage such as when gastropods are dislodged from rocks and tumbled around on the seabed through wave action. Shell damage might also arise as a direct result of the gastropod shell lip impacting the edge of their prey during feeding. These data are needed to understand how whelks respond to these damage incidents and further how damage repair is affected by an individual's age and physiology.

B. undatum is well known for having a highly varied morphology, and this is observed throughout their distribution (Hollyman, 2017; Magnúsdóttir *et al.*, 2018). Many of these characteristics are seen to change in relation to water depth (Ten Hallers-Tjabbes, 1979; Magnúsdóttir, 2010; Mariani *et al.*, 2012), along with the local environment and hydrological conditions (Golikov, 1968; Trussell and Etter, 2001). Furthermore, local adaptations are often seen leading to divergence between populations, as has been noted in other gastropods such as *Littorina* sp. (Yamada, 1987; Johannesson, 1988; Valentinsson *et al.*, 1999; Weetman, *et al.*, 2006; Bell, 2008). Predation pressure and the combination of substratum type and biotic composition often influences changes to the shape and growth of marine molluscs, which has been noted in the dog whelk *Nucella lapillus* (Palmer, 1990) as well as in Canadian populations of *B. undatum* (Thomas and Himmelman, 1988; Rochette and Himmelman, 1996; Weetman *et al.*, 2006), and often these changes can occur because of prey behaviour and predator-induced morphological defences (Bourdeau and Johansson, 2012).

It was shown that whelks increased their total shell length continually throughout periods of shell repair following experimental damage. Interestingly, when shell growth of damaged and undamaged 'control' whelks was compared, damaged whelks generally grew more quickly, but not significantly so, than undamaged whelks over the same period. It had been expected that undamaged whelks would increase in length more quickly than repairing

shells due to the re-allocation of energy resources, that would normally be utilised during shell deposition, into shell repair. Despite shell repair being a priority for the damaged whelks, they continued to increase in shell length during the repair processes under all the experimental growth conditions. This is likely down to an evolutionary advantage to ensure that a whelk's shell continues to grow in length during any repair to its shell so that it reaches a size (length) refuge where it is no longer at danger from predators. Research into this area is limited, however it has been shown that Antarctic brachiopods *Liothyrella uva* (Cross *et al.*, 2015) and *B. undatum* (Colvin *et al.*, 2022b), can continue shell growth and formation even during periods of environmental or localised stress. Additionally, through the process of shell repair (regrowth and thickening) the additional build-up of completely new shell layers (Chapter 4) could further promote the increase in total shell length, through increased localised biomineralization.

Results from the growth experiments using different life stages (tank reared juveniles, non-mature and mature wild caught whelks </> UK SOM; 45 mm respectively) and sex, showed differences in shell growth and shell repair rates. Juvenile whelks grew twice as fast during the summer and spring under controlled conditions than they did under ambient conditions and were the only life stage to demonstrate a significant difference in shell repair rates and shell growth rates under temperature-controlled and ambient conditions. Although there were no sex differences in shell growth or repair rates, there were distinct seasonal differences in cumulative shell repair and shell growth in the larger (older) whelks over time, where shell growth under temperature-controlled conditions was slowest in the winter and spring with the fastest rates during the summer and autumn. Under ambient conditions there was less of a difference in growth response seasonally although growth in the spring was slower compared with the fastest growth in winter. These results show shell repair rates are higher when shell growth is lowest during winter and spring, and possibly suggests that energy reserves for growth are limited in these seasons and that the whelks are prioritising shell repair over an increase in shell length. However, this seasonal pattern of shell repair and shell growth was not so obvious in whelks reared under ambient seawater temperatures. Nonetheless, shell growth rates generally mirrored shell repair rates under both temperature-controlled and ambient conditions with fastest growth during the summer and slowest growth in the spring.

Individual size (age) and its effects on shell growth have been a well-studied factor in many taxa (Von Bertalanffy, 1938; Richardson, 2001; West *et al.*, 2012; Sibly *et al.*, 2015). *Buccinum undatum* classified as adult (> UK SOM; 45 mm) displayed slower rates of shell growth and shell repair, compared with juvenile individuals from the same population, with the fastest rates observed in the youngest individuals (TRJ). These different growth trajectories in molluscs are often associated with constraints to overall size and metabolic cost, with older individuals having additional trade-offs with energy diverted away from shell growth into gamete maturation and reproductive output (Tanabe, 1988; Palmer, 1990; Kideys, 1996; Richardson, 2001; Thomsen *et al.*, 2013; Colvin *et al.*, 2022b). Smaller whelks initially show rapid shell growth to enable them to reach a size refuge beyond which they are likely safe from the attention of predatory attacks (Chase, 1999; Karythis *et al.*, 2020). Regardless of individual size and age, a whelk's capacity for retraction and protection into the shell aperture is fundamental for protecting the delicate soft body tissues from predators (Palmer, 1990; Seed and Hughes, 1995; Kideys, 1996).

Due to the distinct stages in the whelk's maturity cycle with the development of eggs occurring between August and December in Welsh waters (Hollyman pers. comm.), whelk sex and maturity were investigated during both winter and summer data collection periods. Small juvenile non-mature whelks displayed faster rates of shell repair than larger (older) non-mature individuals indicating that size is an important factor. Maturity and sex proved to be significant factors affecting shell repair and were seasonally significant. However, no effect of maturity and season on shell length increase was observed. Males displayed the fastest rates of shell repair during the winter months, whilst females generally repaired their shells faster during the summer. For juveniles this response was reversed. These results appear consistent with female whelks having high metabolic expenses in the winter during the egg laying and encapsulation processes at a time of the year when they are feeding less, so energy reserves for shell repair would be further stretched (Martel *et al.*, 1986).

In this chapter my initial hypothesis, was that there would be a direct link between food availability and shell repair and shell growth in *B. undatum* i.e., faster rates of shell repair and shell growth would occur in whelks fed more frequently than those rationed or completely deprived of food. Both somatic and skeletal (shell) growth in organisms is a highly energetically costly metabolic activity and the availability and allocation of energy resources are needed to

ensure the whelks have the maximum chances of growth and survival. My results showed that food availability had mixed effects on shell repair rates. Surprisingly, whelks fed a daily regime of freshly shucked mussels (*Mytilus edulis*) repaired their shells at a similar rate to those that were unfed. However, significant differences were observed in overall shell repair rates when whelks were fed daily, unfed, or fed weekly. Larger (MW) whelks fed once weekly repaired their shells at a similar rate to that of juvenile whelks fed only once a week. However, when this group of whelks were fed daily or unfed, their rates of shell repair were slower than the juveniles and larger (MW) whelks. The observed differences in shell repair rates may reflect a vital need to rebuild a damaged shell and this metabolic process must be completed rapidly despite the lack of food availability. Presumably, any stored energy reserves are utilised to complete this task. Juvenile whelks fed once a week that repaired their shells more slowly than those fed daily or unfed significantly increased their total shell length compared with those fed daily or were unfed. This suggests that increase in shell size took precedence over shell repair when food is infrequently available (i.e., once weekly).

Although these responses to shell damage were not as expected it is likely that many terrestrial and marine organisms reserve their energy resources during periods of low food availability until conditions become more favourable (Tomanek and Somero, 1999; Stillman, 2003; Melzner *et al.*, 2011). Palmer, (1983), has shown that gastropods have the capability to use body reserves, and additional energy sources for the needs of shell growth. This is often in the form of protein catabolism, which although continues during normal conditions, is more heavily relied upon during periods of reduced food availability. However, without full knowledge of an individual whelk's prior feeding behaviours and food availability in the wild prior to capture, it is uncertain whether the unfed whelks might still have had some energy reserves that could have been used in shell repair or if they were using protein catabolism for shell growth and re-growth during experimental conditions (Colvin *et al.*, 2022b). Unexpectedly, groups of MW whelks whose shells were both undamaged and damaged and fed daily grew more slowly than undamaged and repairing whelks fed weekly or unfed. These findings may possibly be the result of the whelks over-eating, with those fed daily demonstrating the slowest growth rates. No signs of distress or increased mortality were observed with the fed groups suggesting that they were in 'good' condition. Experiments were carried out during the summer months and warmer seawater temperatures increased food consumption (pers. obs.). Consequently, during the summer, daily fed individuals may have had

more energy reserves to allocate from feeding to gametogenesis prior to reproduction in the autumn and this took priority instead of allocating these reserves to shell growth. Previous research by Nasution and Roberts (2004) also reported increased feeding during the summer months, and importantly found up to 97% of *B. undatum* starved for 40 days survived. This supports the conclusion that opportunistic scavenging whelks have considerable energy resources to maintain their normal physiological processes.

The results of this chapter demonstrated seawater temperature to have a significant effect on shell repair and shell growth in all *B. undatum* experiments. Temperatures were determined through known maximum and minimum sea bottom temperatures observed within Welsh waters. The fastest rates of shell repair and shell growth were observed in juvenile whelks maintained at 15°C, whereas the slowest repairing and growing whelks were adults at a low (winter) temperature of 5°C. Although adult whelks could not also be tested at 15°C due to increased mortality as the thermal limit was reached, the same patterns in growth were observed, with seawater temperature at 10°C seeing increases in rates of shell repair and TSL increase. Whelks reared at 15°C all died during the experiment probably because of the warmer temperatures seeing increased heat stress during the summer months. This temperature was likely at the limit of their thermal tolerances. Wild-caught whelks reared in the laboratory during the summer months consistently show high mortality rates (Hollyman pers. comm.). In the natural environment adult whelks are rarely found in shallow coastal waters during the summer months (pers. obs.), a habitat that is frequently the preserve of juvenile whelks which appear to be better adapted to warm summer coastal temperatures.

The effects of temperature are key when trying to understand individual success and physiological processes as a response to a perturbation to homeostasis. Changes in temperature can see dramatic effects in marine organisms, with a range of adjustments to metabolic processes observed (Page and Hubbard, 1987; Prosser *et al.*, 1991; Sokolova and Pörtner, 2003; Harley *et al.*, 2006). Benthic organisms often see increased responses to thermal stressors, (Foster, 1971; Harley *et al.*, 2006), with further impact seen based on individual size (Pechenik *et al.*, 2019; Levinton, 2020), whereby smaller individuals see more notable changes, as reflected within this chapter. The relationship seen between temperature and growth, whereby an increased temperature saw increases in rates of shell growth and repair, supports previous work examining the links between temperature and metabolism (Emmerson *et al.*,

2020; Borsetti *et al.*, 2021). Furthermore, in some gastropod species different environmental conditions have been found to relate to observable differences in morphology, including size and structure, for example the rough periwinkle (*Littorina saxatilis*) and the gold-ringed cowry (*Monetaria annulus*), whereby increased temperatures saw adverse effects on growth, due to disruptions to metabolism, health, and thermal stress (Himmelman and Hamel, 1993; Sokolova *et al.*, 2000b; Irie and Fischer, 2009; Melatunan *et al.*, 2013).

Patterns of shell repair and shell growth are consistent with the expected responses to age, whereby younger individuals displayed accelerated rates throughout the experiments. The seasonal experiments showed distinct differences in shell repair and shell growth rates in juvenile whelks and further differences in shell repair and shell growth under ambient seawater conditions and those held in temperature-controlled systems where generally faster rates were seen. This difference was not found in mature wild-caught whelks. In spring, juvenile and mature wild-caught whelks grew more slowly in shell length, however shell repair rates increased. Juvenile whelks displayed faster shell repair and shell growth rates during the warmer, summer months whilst the largest variation in shell repair and shell growth rates occurred in the autumn amongst the different life stages investigated. In the winter and spring, the observed lower shell repair and shell growth rates may have been the result of depleted energy stores and insufficient resources to complete the shell repair processes. In spring the collected wild-caught whelks had just experienced a period of reproductive development in the autumn and reproductive output, with egg laying in Welsh waters being completed in late winter (pers. obs.). This likely had caused depletion of energy stores for shell repair and shell growth. Nevertheless, shell repair was still prioritised. Developmental changes in marine molluscs affected by seasonal change are often those relying on the interaction between food availability, temperature, reproduction, and growth (Gabbott, 1983; Colvin *et al.*, 2022b). For example, during the summer months, when there is a greater food supply, energy is often re-directed to growth to attain a size refuge and increase reproductive success, for example *Geukensia demissa* (Hillard and Walters, 2009).

Further implications

All organisms require specific adaptations to survive and thrive in their particular environments that allow them to cope with environmental changes from normal conditions

(Clark *et al.*, 2008). Although shell regeneration is linked with hormonal and neurosecretory responses (Saleuddin and Wilbur 1983; Watabe, 1983), the full mechanisms are not fully yet understood. In an unpublished study, Colvin (2016) subjected fast and slow growing juvenile whelks to repeated shell damage. Following a first damage incident and following shell repair a secondary damage incident evoked an increased response in shell repair. The whelks repaired the damaged shell more quickly following the second incident than during the first incident. In this experiment and those undertaken and reported here during periods of rapid shell repair there was a decrease in TSL growth. Although there are many intrinsic and extrinsic factors affecting the rate of shell growth in molluscs, there are many factors still to understand, including genetics and predatory interactions.

In summary, this chapter has demonstrated that there are significant factors that affect the rates of shell repair and shell growth in *B. undatum* following experimental shell damage. Although shell growth was seen at all life stages, the rates of change varied, and seemingly depended on additional metabolic processes and thermal stress. Within the marine environment, many organisms are subjected to considerable risk, for example, from the impact of climate changes and seasonal exposure to significantly raised or lower seawater temperatures. As such, understanding the recovery capabilities of whelks exposed to damage helps us to better monitor and mitigate disturbance within a fishery management and conservation setting. In the next chapters I will examine the process of shell growth itself (Chapter 4) and the mechanisms and incorporation of elements into the repairing shell (Chapter 5).

Chapter 4 – Shell structure of *Buccinum undatum*

Work from this chapter has been published in the Journal of Experimental Marine Biology and Ecology
(June 2022) <https://doi.org/10.1016/j.jembe.2022.151720>

See Appendix 10

Figures

Figure 4.1: Laterally sectioned <i>Buccinum undatum</i> shell showing shell coils around the central internal columella (X), arrow marks opercular opening.	119
Figure 4.2: Simplified diagrammatic representation of the organic matrix, within the mineral CaCO ₃ shell layers. Image adapted from Weiner and Traub, 1984 and Furuhashi <i>et al.</i> , 2009.	121
Figure 4.3: Simplified diagrammatic representation of the general processes involved in shell biomineralization in gastropod molluscs. Note that under certain circumstances, when the processes fall out of equilibrium a reverse reaction can occur in all phases of the equation.	123
Figure 4.4: <i>Buccinum undatum</i> shells placed in silicon resin moulds, aligned and the resin ready to cure.	125
Figure 4.5: Cured and hardened resin blocks containing whole <i>Buccinum undatum</i> ready for thin section preparation.	125
Figure 4.6: A) pre-polished embedded sectioned whelk shell and B) polished embedded sectioned whelk shell sample ready for analyses. Dotted red arrow shows direction of shell growth and the blue arrows indicate the region of newly-deposited rapid shell growth.	126
Figure 4.7: A) thin polished sections of <i>Buccinum undatum</i> shell and B) glass viewing dish with 10mm depth of acetone, used to dissolve the resin and superglue from the thin shell section.	127
Figure 4.8: Thin shell sections of <i>Buccinum undatum</i> adhered to Kapton tape on custom microscope slides for μ XRD analysis.	128
Figure 4.9: Preparation of <i>Buccinum undatum</i> shell sections. A and F show thin sections, B and G polished resin blocks and C-E and H fractured shell samples. Samples A and F are on carbon tabs attached to the aluminium disc.	131
Figure 4.10: Scanning electron microscope used, with red arrow indicating where the samples were added onto the stage as shown in Figure 4.11.	132
Figure 4.11: Various shell samples shown in Figure 4.9 on the SEM stage. Aluminium discs, carbon tabs and silver bridges are indicated. Carbon sputter is not visible in these images. .	132
Figure 4.12: D spacing and relative intensity (arbitrary units) for A) a shell section with original and re-grown shell from the outer layer to the inner crossed-lamellar layer, B) outer to inner shell layers of a re-grown shell section C) crushed shell samples of two separate shells (shells 1	

and 2) and calcite and aragonite standards. Black points show the established primary d-spacing values for aragonite samples and green points for calcite.....134

Figure 4.13: Photomicrographs of shell sections of *B. undatum* viewed under reflected light. A) section showing an undamaged shell, B) shell with laboratory mechanical damage, C) shell displaying a natural damage incident in a wild caught whelk. The inner and outer shell layers are indicated with 'in' and 'out'. Two different microstructures are indicated with P (prismatic) and X (cross-lamellar). Red arrows indicate area of damage.136

Figure 4.14: Thin sections of the shells of *Buccinum undatum*. A and C) Photomicrographs taken under transmitted light and B and D) in blue light. Red arrows show area of shell damage, with subsequent repair marked with blue. Thin white arrows show areas of calcein incorporation, thick white arrows, absorption onto shell surface. Two different microstructures are indicated with P (prismatic) and X (cross-lamellar).137

Figure 4.15: SEM images of *Buccinum undatum* shells. A) outer shell and apex showing shell whorls and wave shell sculpture. B) area of mechanical damage with original shell and area of re-growth marked and C) shows area of re-growth. Initial cut marked with red line. Pe marks the periostracum.139

Figure 4.16: SEM images of internal shell structure of *Buccinum undatum*. Two different microstructures are shown: prismatic (P), crossed-lamellar (X) and periostracum (Pe). Double-ended arrow shows the full width of the crossed-lamellar layer. Red arrow marks point of old/new divide from damage and re-growth.140

Figure 4.17: SEM images showing the microstructure of the prismatic layer with distinct aragonitic prisms. DOG marks direction of growth, from the outer to inner shell.....141

Figure 4.18: *Buccinum undatum*. SEM images showing the microstructure of the crossed-lamellar layers with lamellae shown in different directional plains.142

Figure 4.19: *Buccinum undatum*. Higher magnification of crossed-lamellar layer showing distinct crossed patterning and lamellae travelling in alternate directions.....143

Introduction

This chapter investigates the shell structure and general mechanism of formation of the shell of *Buccinum undatum* with the aim of understanding how a damaged shell is successfully re-grown (Chapter 3). This will lead onto further analysis of trace element incorporation into the repairing shell in Chapter 5. Over the years, research into shell structure has played an integral part in literature of the phylum Mollusca. Key aspects of this include crystallography, biochemistry, taxonomy as well as calcification and growth studies (Wilbur and Owen, 1964; Harper, 2000; Bonucci, 2007; Harper *et al.*, 2009; Hammond, 2015).

The shell of a marine gastropod provides protection for the soft body tissues. When they are withdrawn inside the shell, the aperture is blocked by a retracted foot and often by an attached organic operculum as exemplified in *B. undatum*. The gastropod shell is a rigid calcareous exoskeleton distributed within an organic matrix (Wilbur and Owen 1964; Simkiss and Wilbur, 1989; Palmer, 1991). Molluscan shells are typically composed of several different microstructures, forming shell layers, which can vary between species along with the type of calcium carbonate present (Harper *et al.*, 2009). The shell of *B. undatum* is a hollow structure, formed around the columella (Figure 4.1), the base of which forms the aperture (Ruppert *et al.*, 2004). Hollyman (2017), described the shell as being formed of four shell layers composed of aragonitic calcium carbonate (CaCO_3) that typically form structures of prisms and sheets (Checa, 2018; Clark *et al.*, 2020).



Figure 4.1: Laterally sectioned *Buccinum undatum* shell showing shell coils around the central internal columella (X), arrow marks opercular opening.

Typically, shells are formed of a stiff mineral phase of between 95-99% calcium carbonate within up to 5% softer organic matrix (Sleight *et al.*, 2015; Clark *et al.*, 2020). Although the organic component of the shell structure only comprises a small percentage of the overall shell, it plays an important role in determining the shell's microstructure (Clark *et al.*, 2020) and is often used to regulate the size, structure, and orientation of the calcium carbonate crystals (Currey, 1977; Hayashi *et al.*, 2011). The linking of these different materials produces a material with elaborate microstructures and properties, including tensile strength, structure, and the lightweight nature of the shell (Chateigner *et al.*, 2000; de Paula and Silveira, 2009; Crippa *et al.*, 2020). During mineralisation and orientation of the crystalline structure, the organic matrix secreted from the mantle epithelium is key to the formation of the molluscan shell (Miyamoto *et al.*, 2005), and is seen to vary interspecifically (Wilbur and Watabe, 1963; Travis *et al.*, 1967; Levi-Kalishman *et al.*, 2001). Furthermore, the texture patterns of microstructural layers of aragonite are seen to vary by species and environment, (Chateigner *et al.*, 2000), and it is believed that the formation of these distinct microstructures is not only a result of inorganic processes, but also because of the organic matrix and proteins within the shell itself (Travis *et al.*, 1967; Palmer, 1983; Weiner and Traub 1984; Suzuki *et al.*, 2010).

The shell's organic matrix is formed of a heterogeneous amalgamation of carbohydrate and protein components, with suggestions that it contains α and β -keratin, chitin, and acidic glycoproteins (Figure 4.2) (Wilbur and Watabe, 1963; Travis *et al.*, 1967; Levi-Kalishman *et al.*, 2001; Furuhashi *et al.*, 2009). The matrix is typically formed from complex interactions between chitinous substances, tissue proteins, and an array of macromolecules containing both covalent and non-covalent bonds; although this is not universally seen in all molluscan species (Weiner and Traub, 1984; Nudelman *et al.*, 2006). These arrays of components are all fundamentally involved in the intricate processes controlling nucleation, growth, and adaptation of the shell structure (Weissbuch *et al.*, 1991; Weiner and Addadi, 1997). The organic matrix and a silk-fibroin like protein are thought to enhance mechanical properties of the shell, such as strength, in addition to the integral framework structure within which the mineral phase forms through calcification (Weiner and Traub, 1984; Falini *et al.*, 1996).

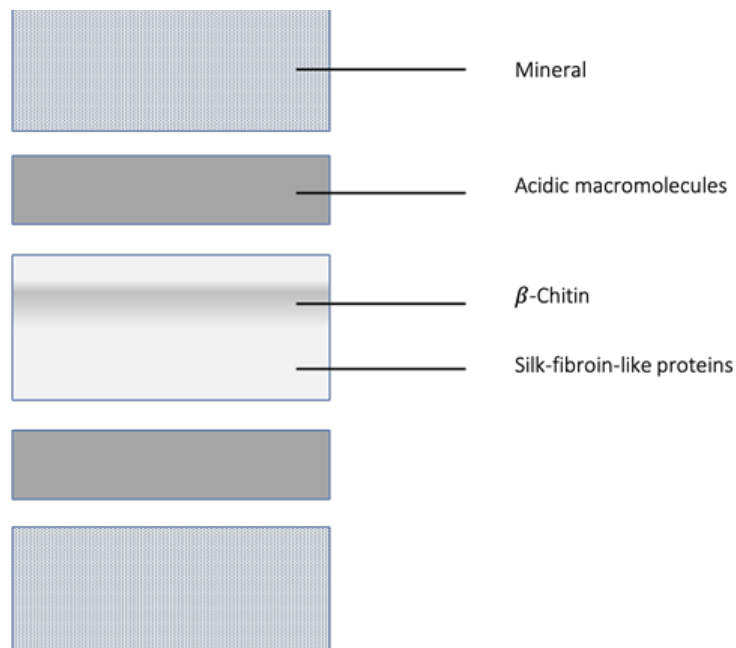


Figure 4.2: Simplified diagrammatic representation of the organic matrix, within the mineral CaCO_3 shell layers. Image adapted from Weiner and Traub, 1984 and Furuhashi *et al.*, 2009.

Calcium Carbonate (CaCO_3)

Shell growth and shell repair occur as a result of CaCO_3 secretions from the mantle epidermis (Simkiss and Wilbur, 1989; Findlay *et al.*, 2011; Clark *et al.*, 2020). The process is a cellular one, involving ion transport, protein synthesis, and physiochemical mechanisms of CaCO_3 crystal formation and orientation within an organic matrix (Saleuddin and Wilbur, 1983). The actual method of shell formation is still not fully understood but appears to be made up of three major processes, (1) CaCO_3 production, and the creation of the organic matrix, (2) mantle secretions, (3) crystal growth and orientation within the newly formed shell surface (Saleuddin and Wilbur, 1983).

Calcium carbonate (CaCO_3) is of scientific importance within both the biological and physical environment (Carlson, 1983; Gong *et al.*, 2012), for example in biology (biomineralization), geology (Addadi and Weiner, 2003), and the earth's atmospheric conditions, chiefly through sea water chemistry. CaCO_3 occurs within the natural environment as three main crystalline mineral polymorphs, calcite, aragonite and vaterite, as well as an amorphous calcium carbonate form (ACC) (Watabe, *et al.*, 1976; Bonucci, 1992; Gebauer *et al.*, 2008; Gong *et al.*, 2012). The polymorph vaterite is formed of a hexagonal system. Calcite and

aragonite have similar crystal structures, with the differences lying in the alignment and association of the molecular structure, whereby calcite presents as a trigonal crystal form, while aragonite is formed of an orthorhombic structure (Bonucci, 1992; Falini *et al.*, 1996; Ropp, 2013). In molluscs, the CaCO_3 crystals in newly deposited and repaired shell are generally either aragonite or calcite, with vaterite primarily occurring in patches or repairs (Carlson, 1983; Falini *et al.*, 1996; Thompson *et al.*, 2000; Gong *et al.*, 2012; Nehrke *et al.*, 2012; Clark *et al.*, 2020). It has been shown that newly repaired shell often has a different and characteristic crystal type to that of normally deposited shell (Watabe, 1983; Nehrke *et al.*, 2012; Loftus *et al.*, 2015). However, in repaired and non-repaired shells the different crystal polymorphs can coexist, or occur in individual shell layers (Watabe, 1983). The least common polymorph is vaterite, due to it being the most thermodynamically unstable crystal form at typical environmental temperatures and pressures. Although found in egg cases (Meenakshi *et al.*, 1974), insect larval stages and eggshells, it is not present in normal molluscan shells (Gould, 1972; Watabe, 1983).

Mollusc shell formation

Biomineralization is a fundamental process for organismal life, with the production of hard structures, including that of endo- and exoskeletal structures seen in both fauna and flora (Bonucci, 1992; Falini *et al.*, 1996). Although the need for calcification is clear, the processes involved are relatively unknown in molluscs (Wheeler, 1992; McConnaghey and Gillikin, 2008). In molluscs, shell mineralisation begins in the extra-pallial cavity (EPC), an area lined with the mantle epithelium in which the extra-pallial fluid (EPF) is contained. The cells of the mantle epithelium are involved in formation of the newly mineralising shell (Wheeler, 1992; McConnaghey and Gillikin, 2008). However, due to the morphological variation at a cellular level within the mantle, determining the exact cells used during shell formation is complex (Tsuji *et al.*, 1958; Wheeler, 1992). In some taxa initial mineralization also occurs within the periostracum, muscle, haemolymph vessels, and calcium carbonate (CaCO_3) spherules (Richardson *et al.*, 1981; Watabe, 1983; Checa and Harper, 2010; Clark *et al.*, 2020). During the production of CaCO_3 , carbonic acid (H_2CO_3) is formed from the reaction of water (H_2O) with carbon dioxide (CO_2), a process which is catalysed by the enzyme carbonic anhydrase (Figure 4.3). Following this, H_2CO_3 loses a hydrogen ion (H^+) resulting in the formation of bicarbonate (HCO_3^-) which further breaks down with the loss of H^+ to form a carbonate ion (CO_3^{2-}). These components are then transported into the EPF (Saleuddin and Wilbur, 1983), where

subsequent reactions with calcium ions (Ca^{2+}) occur to form CaCO_3 (Figure 4.3) (Mount *et al.*, 2004; Addadi *et al.*, 2006).

In many molluscan species the uptake of calcium (Ca^{2+}) from seawater occurs directly through the mantle, via either calcium channels, or achieved using the enzyme pump Ca^{2+} ATPase, with additional transport through bodily fluids (Ruppert *et al.*, 2004; Findlay *et al.*, 2011). This process occurs in direct correspondence with the concentration gradient of the EPF and the surrounding environment, whereby an increase in sea water Ca^{2+} sees an increase in the productivity of calcium deposition, until levels plateau, and a maximum rate is determined (Bevelander and Benzer, 1948; Watson *et al.*, 1971; McConnaughey, 1989). Furthermore, it is not clear as to what extent additional HCO_3^- and CO_3^{2-} , from the surrounding environment also reach the crystallization site to help in the calcification process (Saleuddin and Wilbur, 1983). The overall efficiency of shell carbonate formation is reliant on the rate of reactions occurring, along with the shell structure itself and although marine molluscs need carbonate ions to build their shells, an increase in dissolved CO_2 in seawater shifts the equilibrium and a reverse reaction occurs, with the H^+ reacting with the $\text{CO}_3^{2-} \rightarrow \text{HCO}_3^-$. When combined with an increased temperature this can see an increase in solubility in the shells of aragonitic organisms due to a decrease in supply of CO_3^{2-} ions (Saleuddin and Wilbur, 1983; Madin, 2010, Watson *et al.*, 2013).

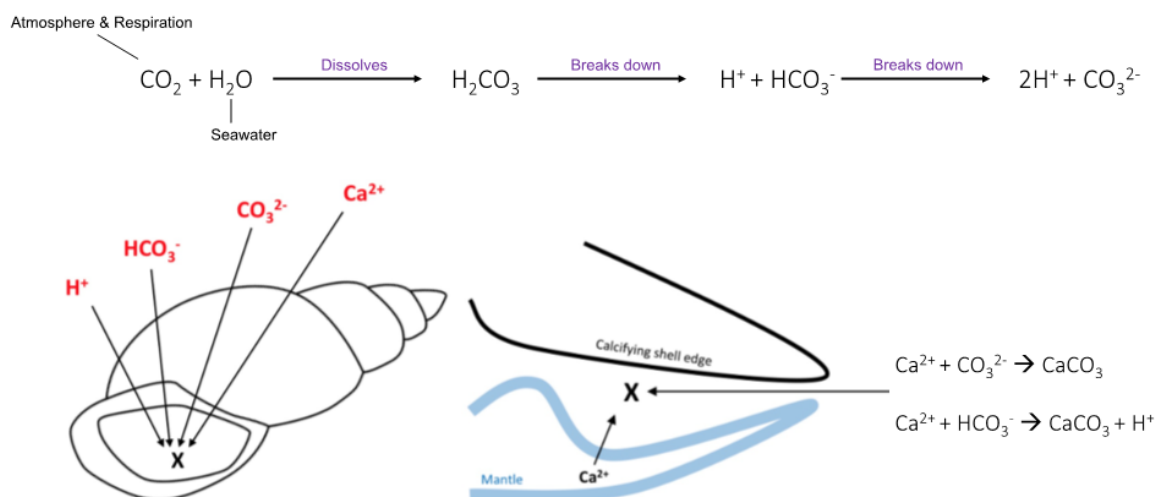


Figure 4.3: Simplified diagrammatic representation of the general processes involved in shell biomineralization in gastropod molluscs. Note that under certain circumstances, when the processes fall out of equilibrium a reverse reaction can occur in all phases of the equation.

In this chapter the aim is to examine the structure of the internal shell layers of *B. undatum* during shell growth and shell repair. This was achieved through visual observations and analyses using a series of microscopy techniques. It is hypothesised that the *B. undatum* shell is formed of multiple layers, and where re-growth and shell scarring occurs following shell damage, the shells will have deposited new shell layers beneath the original shell to repair the missing areas.

Materials and Methods

To understand the crystal structure of the shell of *Buccinum undatum* during shell growth and shell repair, a series of techniques were used. The shell material for the investigations was provided from the laboratory-reared and wild-caught whelks studied in Chapters 2 and 3. See these chapters for details of the experiments undertaken. The shell material used in the analyses was selected based on the quality of the shell structure and sample surface post-preparation (see below for techniques).

Sample preparation

Shell Embedding

To prepare the shell samples, silicon resin moulds were pre-coated with silicon grease and allowed to air dry to prevent resin sticking to the mould during the hardening process. To identify individual shells, paper labels, containing abbreviated details of the experiment number and growing conditions, were placed on the bottom of the moulds. Klear-set™ polyester casting resin was prepared using proportions of 6 drops hardener to 10 ml resin, and a base layer of ~5 mm depth was poured into each mould. The base layer was left to cure for 24 hours. Whole whelk shells were placed on top of the cured base layers. Resin was poured into the opercular opening and the shell slowly filled with resin whilst being twisted around to allow resin to pass into all the chambers and reduce the chances of air becoming trapped inside the shell chambers and forming bubbles in the hardened resin. Once the liquid resin had filled the entire shell it was allowed to spill over and fill the remainder of the mould up to the top so encasing the shell in resin (Figure 4.4). Each shell was manipulated so that the opercular opening lay uppermost in the mould, and the resin then allowed to cure and harden in a fume

cupboard for 48 hours at room temperature before the resin blocks were removed (see Figure 4.5).



Figure 4.4: *Buccinum undatum* shells placed in silicon resin moulds, aligned and the resin ready to cure.



Figure 4.5: Cured and hardened resin blocks containing whole *Buccinum undatum* ready for thin section preparation.

Block preparation

Once the resin-embedded shell was removed from the mould it was trimmed to remove surplus resin around the shell using a coarse cut diamond saw. A second cut along the direction of growth (DOG) was made just off centre using a Buehler Isomet 5000 linear precision diamond saw with a 0.76 mm blade attachment to allow space for further polishing. Following cutting, the block was turned through 180° and the other half of the shell and resin removed using the saw to make a thin ~10 mm slice of shell in a rectangular resin block (Figure 4.6 A). Thin sections and polished blocks were made of each selected whelk ready for further preparation and analysis.

The cut surfaces of the shell sections were ground smooth and flat by hand using progressively finer waterproof silicon carbide grinding papers P80-4000 (grit size), mounted on a Struers rotation grinder with a slow water flow onto the grinding plate to lubricate the process and to ensure even polishing of the surface. Samples were frequently monitored to check position along the damaged edge of the shell and growth lines. Once the shell surfaces were ground smooth, with no visible or large scratches, they were polished on a cloth soaked with a 3 µm diamond suspension on a Mecapol P230 rotation polisher, until the block surface was glass-like and clear of any scratches. Shell sections were thoroughly washed in detergent to remove any grease or polishing components on the block surface, rinsed in tap water, and left to air dry (Figure 4.6 B). Finally, samples were labelled with a unique code using a diamond scribe to ensure that the samples could be identified during analysis.

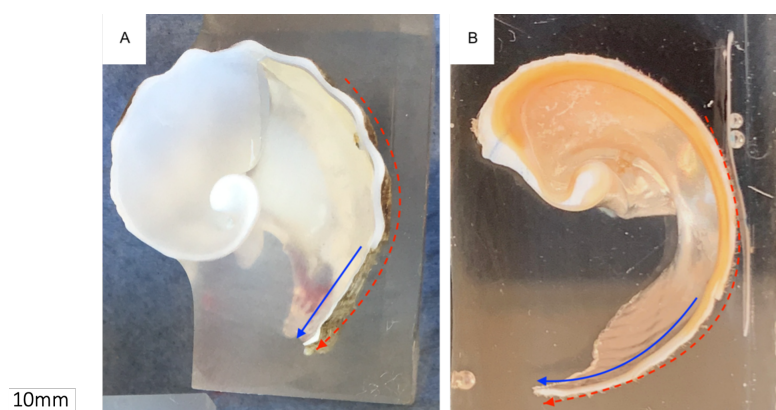


Figure 4.6: A) pre-polished embedded sectioned whelk shell and B) polished embedded sectioned whelk shell sample ready for analyses. Dotted red arrow shows direction of shell growth and the blue arrows indicate the region of newly-deposited rapid shell growth.

Thin sections

The remaining half of each block from experimental whelk was ground using successively finer silicon carbide abrasive papers and polished on a rotating cloth impregnated with 3 μm diamond paste. Once polished, this side was superglued to a microscope slide and surplus resin and shell cut off using the Buehler Isomet 5000 linear precision diamond saw to leave a thin-0.5 mm section along the direction of shell growth (DOG), attached to the glass slide. This newly cut surface was ground and polished to give a double-sided polished shell section with the best optical transparency (Figure 4.7 A). Optical transparency was carefully monitored throughout the grinding process by observing the section at intervals under a dissection microscope until light could completely pass through the entire shell section whilst ensuring the thin newly repaired shell did not break away from the original shell growth. To allow for the best quality X-ray transmission through the shell section, the resin and superglue, were removed from each section and from the glass slide by soaking in a covered glass dish containing acetone to a depth of 10 mm. A glass lid was used to avoid evaporation of the solvent. The dish and shell section were placed under a fume hood for 30 minutes before examining if the glue and remaining resin had dissolved from the shell surface or if more time was required (Figure 4.7 B). Once detached, sections of the shell were carefully removed from the dish using a scalpel blade and placed into a second dish filled with distilled water to flush off any chemical traces before being left to air dry on a clean labelled plastic surface.

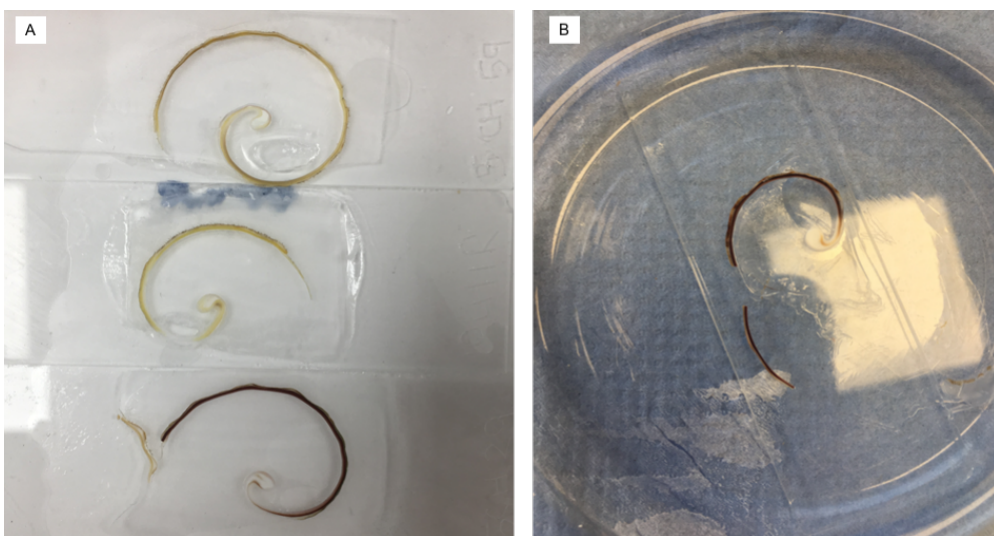


Figure 4.7: A) thin polished sections of *Buccinum undatum* shell and B) glass viewing dish with 10mm depth of acetone, used to dissolve the resin and superglue from the thin shell section.

Dry sections were placed under a dissection microscope on a clean slide. For cases where sections had broken apart, individual pieces were placed carefully to re-form the complete shell. Shells were assessed to identify the best side for analysis based on clarity of lines and freedom from surface defects. The dried sections were then adhered to Kapton (poly (4,4'-oxydiphenylene-pyromellitimide)) tape placed over 'windows' in custom microscope slides (75 x 25 x 3 mm slides, windows 25 x 18 x 3 mm) to allow interference free transmission (Hollyman, 2017) (Figure 4.8). For each slide different samples could be added with space between them provided they were clearly labelled, and samples were covered with a clean glass cover to protect and prevent dust settling.



Figure 4.8: Thin shell sections of *Buccinum undatum* adhered to Kapton tape on custom microscope slides for μ XRD analysis.

Transmission synchrotron analysis (μ XRD)

μ XRD analysis of the prepared thin shell sections was undertaken on the i18 beamline at Diamond Light Source, Oxford, to determine the mineralogy of the whelk shell CaCO_3 phase. For transmission synchrotron analysis, a thin shell of even thickness was required to provide the best X-ray transmission. The μ XRD signal comes from the whole path traversed by X-rays

through the sample, so longitudinal resolution will decrease with increasing thickness (see Appendices 5-9 for technical details).

μ XRD traces were run between and within the shell layers in the shell section together with μ XRD of a crushed powder shell sample. The use of a powdered sample allowed all possible reflections to be seen in a diffractogram due to the varied crystal orientations and helps eliminate any polymorph changes in crystal structure that might have arisen from the grinding process during preparation of the thin sections. Known calcite and aragonite standards were also analysed to allow a direct comparison between samples. A LaB₆ (lanthanum hexaboride 660C SRM) was analysed as a calibration standard as it provided a simple μ XRD spectrum with very well characterised peaks across a wide angular range.

A beam energy of 1200 eV was used with a 5-micron spot size and a step size of 30 μ m between spots to create the desired line profile within each sample. A Photonic Science Scientific sCMOS (scientific complementary metal oxide semiconductor) detector was used to collect the images, with a 5 second CMOS exposure per spot. Data collected from the XRD determinations were analysed using DAWN 2.11.0 (2018). Data were visualised and exported to Excel for graphical analysis. Once processed, the data were cropped between 1.2-4.5 d-spacing on the x-axis (distance between atomic layers), as for assessment of CaCO₃ makeup, in particular calcite and aragonite peaks, no further range was required (Chenery pers. comms). The Y-axis did not require cropping as it represents relative intensity (arbitrary units, a.u.)

Reflection and transmission microscopy

Thin shell sections were examined in transmitted light, and polished blocks with reflected light using a Meiji Techno Industry compound microscope with a Lumenera Infinity 3 CCD camera at x10 zoom. To examine the shell structure, consecutive photomicrographs of the shell sections and blocks were taken, and composite images prepared using Adobe Photoshop. Final composite images were examined to gain an insight into the shell structure. This was undertaken using a selection of undamaged small whelk shells and those that had been experimentally-damaged once and the shell allowed to repair (see Chapter 3), together with larger wild caught whelk shells that had sustained damage in their environment and repaired their shells resulting in shell scarring.

Calcein staining and fluorescence microscopy

Calcein is a calcium-dependant fluorescent molecule and is used for the fluorometric detection of calcium (Sigma-Aldrich P/N: C0875-5G). It combines with the mineralising shell to form a fluorescent mark (Kaehler and McQuaid, 1999). Calcein line formation can therefore be used as a time marker to determine any subsequent, shell growth and shell repair, such as deliberate shell damage. An initial trial demonstrated calcein was incorporated into the mineralising whelk shell when they were immersed for 24 hours in a 50 mgL⁻¹ calcein/seawater solution.

Twenty small (<45 mm) whelks whose shell lips had been mechanically-damaged (See Chapter 3 for methods) were immediately immersed in the calcein solution to mark the point of damage, before being on-grown and fed for 7 days in a flow-through ambient seawater system in an 8L tank suspended in a larger 15 L holding tank (see Chapter 3). After 7 days, ten whelks were removed and frozen at -20°C. The remaining ten whelks were damaged for a second time and left to repair for a further 7 days. At the end of the experiment, these whelks were frozen at -20°C. After 48 hours at -20°C, all whelks were carefully dissected and the flesh removed, avoiding damage to the delicate repaired shell margins. Dissected shells were soaked in a 10% NaOH solution for 24 hours, to remove any remaining organic matter within and on the shells, rinsed in distilled water, and air-dried before being embedded in Kleer-set™ polyester casting resin, as described above.

Once dry the block was cut in two halves and prepared into a thin section (approximately 0.2 – 0.5 mm). Under transmitted light, sequential photographic images of the shell structure, using thin sections of the shell, were taken on a Meiji Techno Industry microscope with a Lumenera, Infinity 3 CCD camera at x10 zoom. The same sections were viewed in a Nikon Optiphot fluorescent microscope with blue light (470-509 nm), (at x10 zoom) and imaged using an eyepiece CCD camera to visualise the fluorescent calcein line. For each shell, the shell section images and calcein line images were matched together, and composite images constructed to ascertain the position where the shell was experimentally-damaged following calcein incorporation.

Scanning Electron Microscopy (SEM)

To image the crystal microstructure of the *Buccinum undatum* shells, scanning electron microscopy (SEM) was undertaken at the Department of Earth Sciences, Cambridge University. Several shell samples were selected to display a range of shell angles and factors which could lead to variations in shell structure. These included undamaged and mechanically-damaged shells to assess the microstructure of the shell. Shell sections and resin-embedded shell blocks were prepared to allow the internal shell layers to be visible for analysis (Figure 4.9 B and G). Empty *B. undatum* shells were taken and fractured roughly along the direction of growth at multiple points on the shell (Figure 4.9 C, D, E and H). The thin shell sections used in the μ XRD analyses, were carefully removed from their Kapton tape, and adhered onto 25 mm carbon tabs (Figure 4.8 and 4.9 A and F). Prior to being placed on the SEM stage, all shell preparations were ultrasonically cleaned and air dried. Once prepared, a carbon sputter (approximately 10 nm amorphous carbon particles) was coated onto the surfaces along with a silver paint to make conductivity bridges from the samples to the aluminium disc. Samples were placed into the SEM (Figures 4.10 and 11), and once stage positions were set and the sample focussed along the XYZ axis, images were taken.

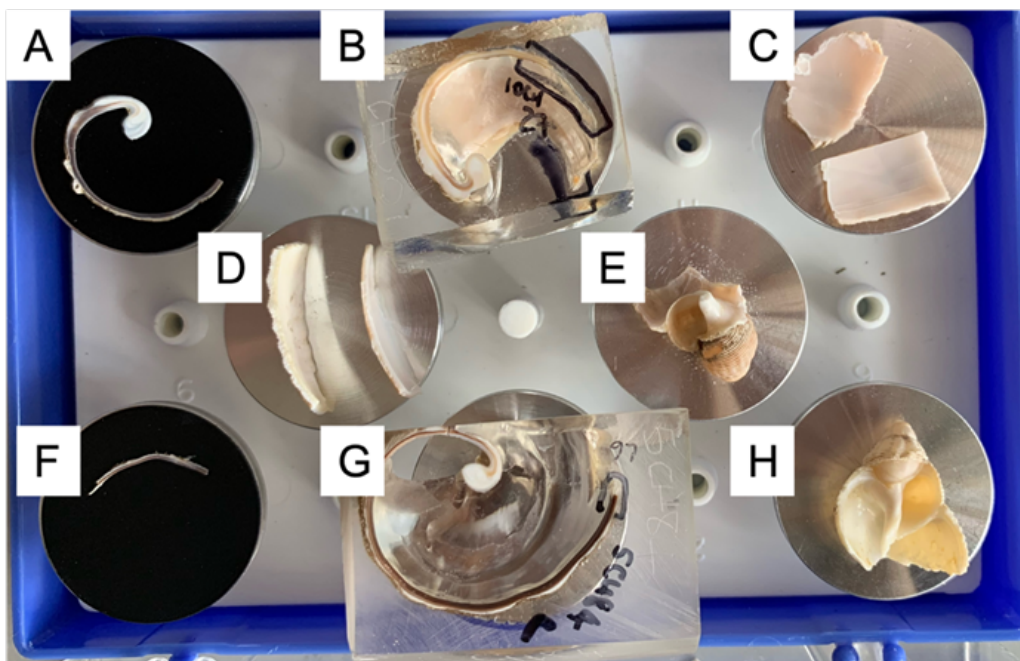


Figure 4.9: Preparation of *Buccinum undatum* shell sections. A and F show thin sections, B and G polished resin blocks and C-E and H fractured shell samples. Samples A and F are on carbon tabs attached to the aluminium disc.

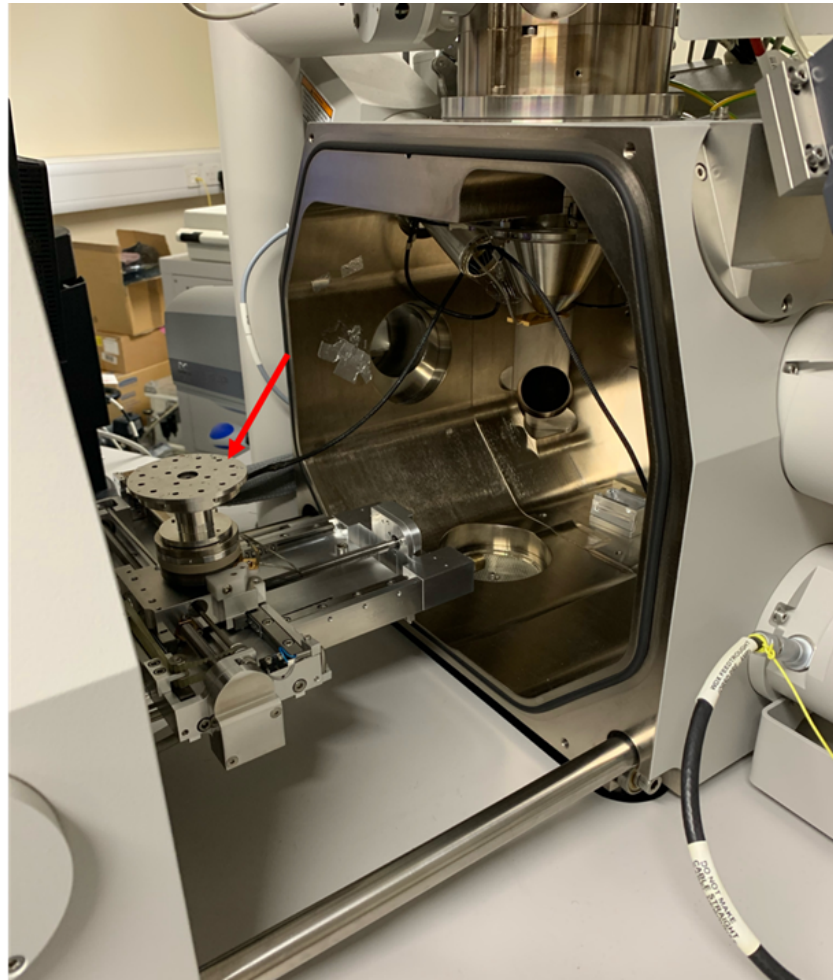


Figure 4.10: Scanning electron microscope used, with red arrow indicating where the samples were added onto the stage as shown in Figure 4.11.

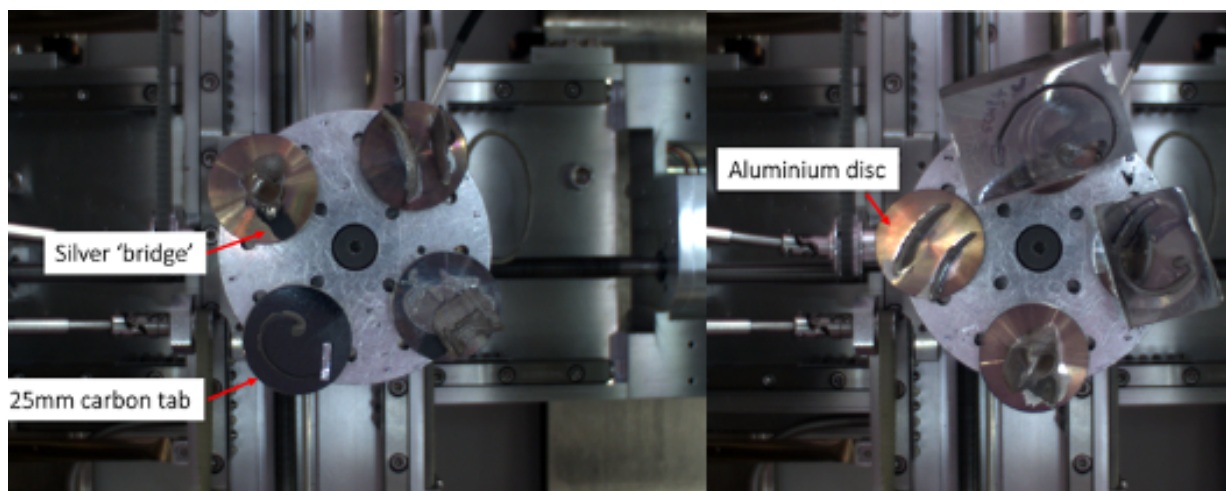


Figure 4.11: Various shell samples shown in Figure 4.9 on the SEM stage. Aluminium discs, carbon tabs and silver bridges are indicated. Carbon sputter is not visible in these images.

Results

Micro X-ray Diffraction (μ XRD)

μ XRD techniques revealed the shells of *B. undatum* to be wholly composed of aragonite. When the known primary d-spacing values for both calcite and aragonite were superimposed upon the calcite and aragonite standard spectra (Figure 4.12), together with the spectrum from the crushed shell samples, key peaks were observed at points 1-3 for aragonite for both whelk shells 1 and 2. This was then confirmed further through plotting spectra from the internal shell layers, showing consistency in values throughout the shells (Figure 4.12). These findings demonstrate that there is no evidence for micro-crystallites of calcite or vaterite. The only structural mineral detected was aragonite.

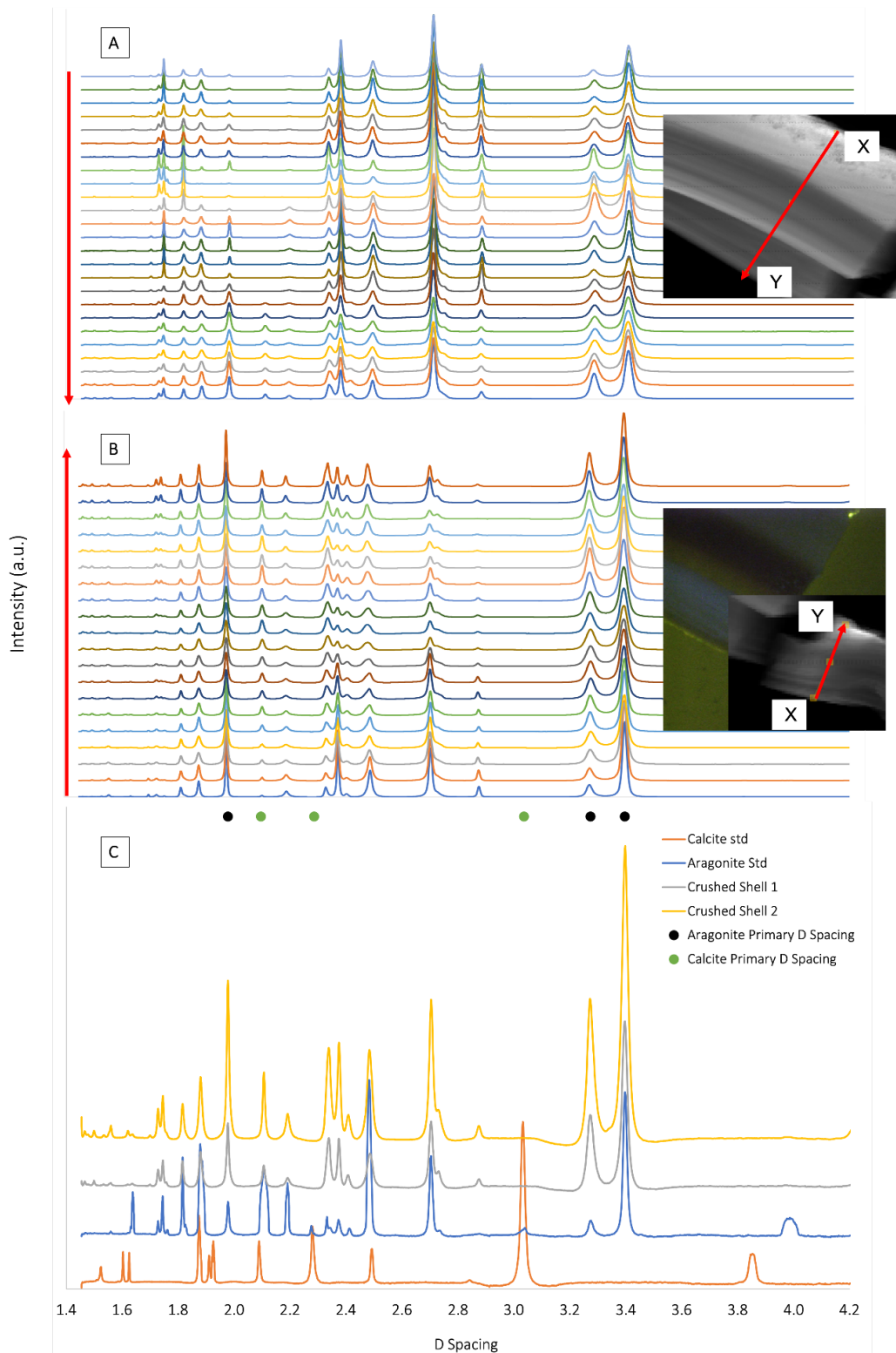


Figure 4.12: D spacing and relative intensity (arbitrary units) for A) a shell section with original and re-grown shell from the outer layer to the inner crossed-lamellar layer, B) outer to inner shell layers of a re-grown shell section C) crushed shell samples of two separate shells (shells 1 and 2) and calcite and aragonite standards. Black points show the established primary d-spacing values for aragonite samples and green points for calcite.

Reflection, transmission, and fluorescence microscopy

Images taken under reflected light show the shells of *B. undatum* are formed of two distinct microstructures, labelled P and X in Figure 4.13. An initial microscopic assessment suggested these were outer prismatic and inner crossed-lamellar layers and were later confirmed through SEM analysis. The structure of both undamaged (Figure 4.13 A) and damaged shells, with period of re-growth (shell repair) appeared to be structurally similar with shell layers completely re-forming to repair the area removed. At the point of damage (red arrows on Figure 4.13), the repair of the shell begins to form further back from the point of damage and attached to the inner shell layer. As the damaged shell is repaired the initial re-growth shows thickening over time. This can be seen in Figure 4.13 B during a short period of shell repair compared with a sample of natural shell damage, with further subsequent growth to the lip of the shell having a much thicker structure, to match the initial shell thickness (Figure 4.13 C).

The mechanics of shell re-growth were elucidated further using calcein staining, during which rapid shell re-growth, following marking, was identified through the bright fluorescence of the dye incorporated into the mineralising shell following damage. The new shell growth forms further back into the shell, away from the damaged area (Figure 4.14 B and C). The thin white arrows in Figure 4.14 show the point of calcein incorporation. Following calcein exposure, the dye was actively absorbed onto the outer periostracum giving an overall fluorescence (thick white arrows); however, these areas are not relevant to the growth of the shell. A similar shell calcification response was shown following a second period of damage to the shell and calcein staining, with the two calcein exposures presenting the same pattern within the shell (Figure 4.14 D). For comparison the same fluorescing shell section is imaged under transmitted light, with the single and double damage shown (Figure 4.14 A and C). Both images are typical of the response to damage and show similar thickening of the damaged area as a result of the period of re-growth during rapid shell deposition. As shown in Figure 4.14 B and C under reflected light, this re-growth (Figure 4.14 A and C) can be seen within both the prismatic and crossed lamellar layers of the shell and appear to be initially deposited as a thin layer to cover the excised shell area before this layer is thickened over time.

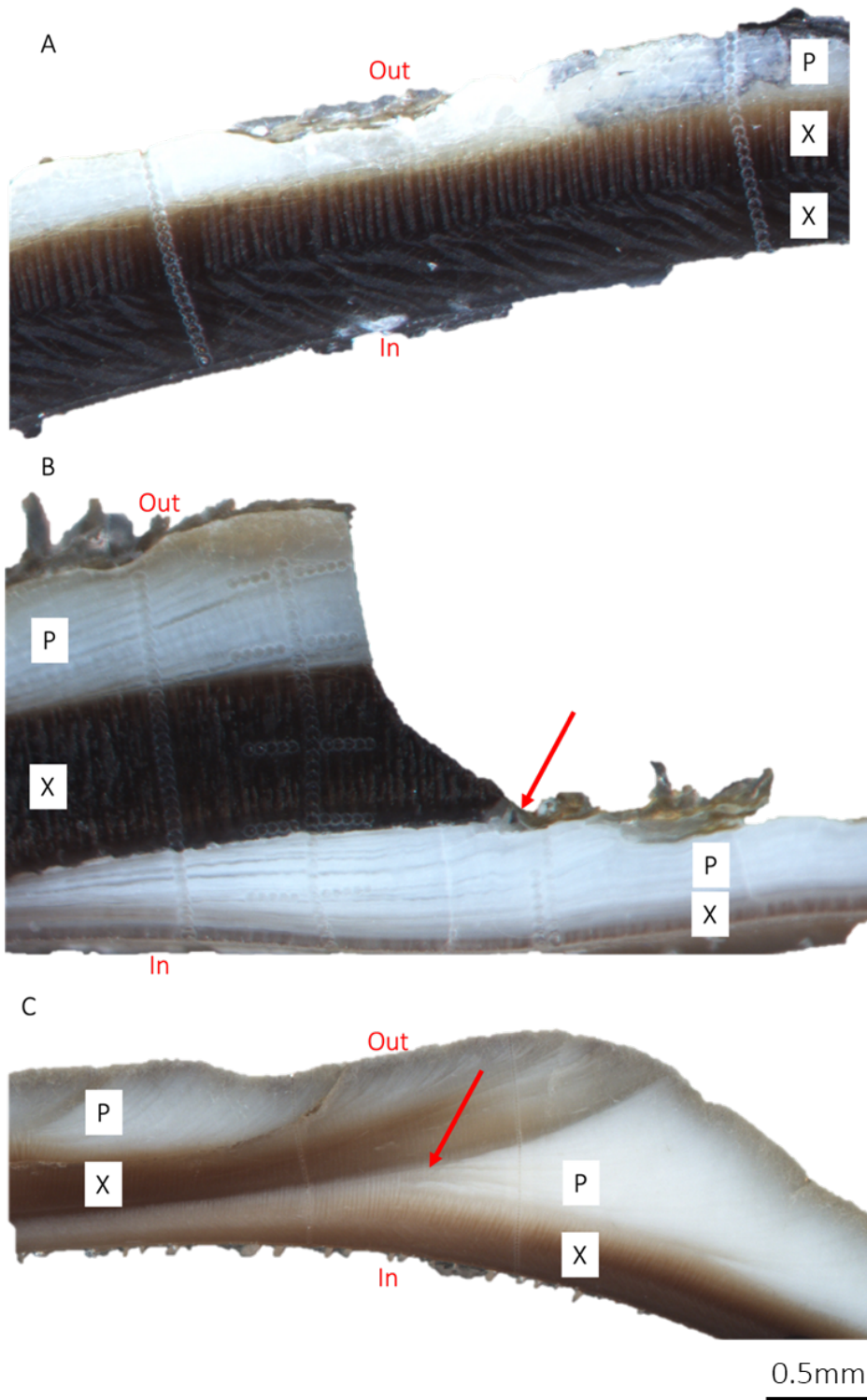


Figure 4.13: Photomicrographs of shell sections of *B. undatum* viewed under reflected light. A) section showing an undamaged shell, B) shell with laboratory mechanical damage, C) shell displaying a natural damage incident in a wild caught whelk. The inner and outer shell layers are indicated with 'in' and 'out'. Two different microstructures are indicated with P (prismatic) and X (cross-lamellar). Red arrows indicate area of damage.

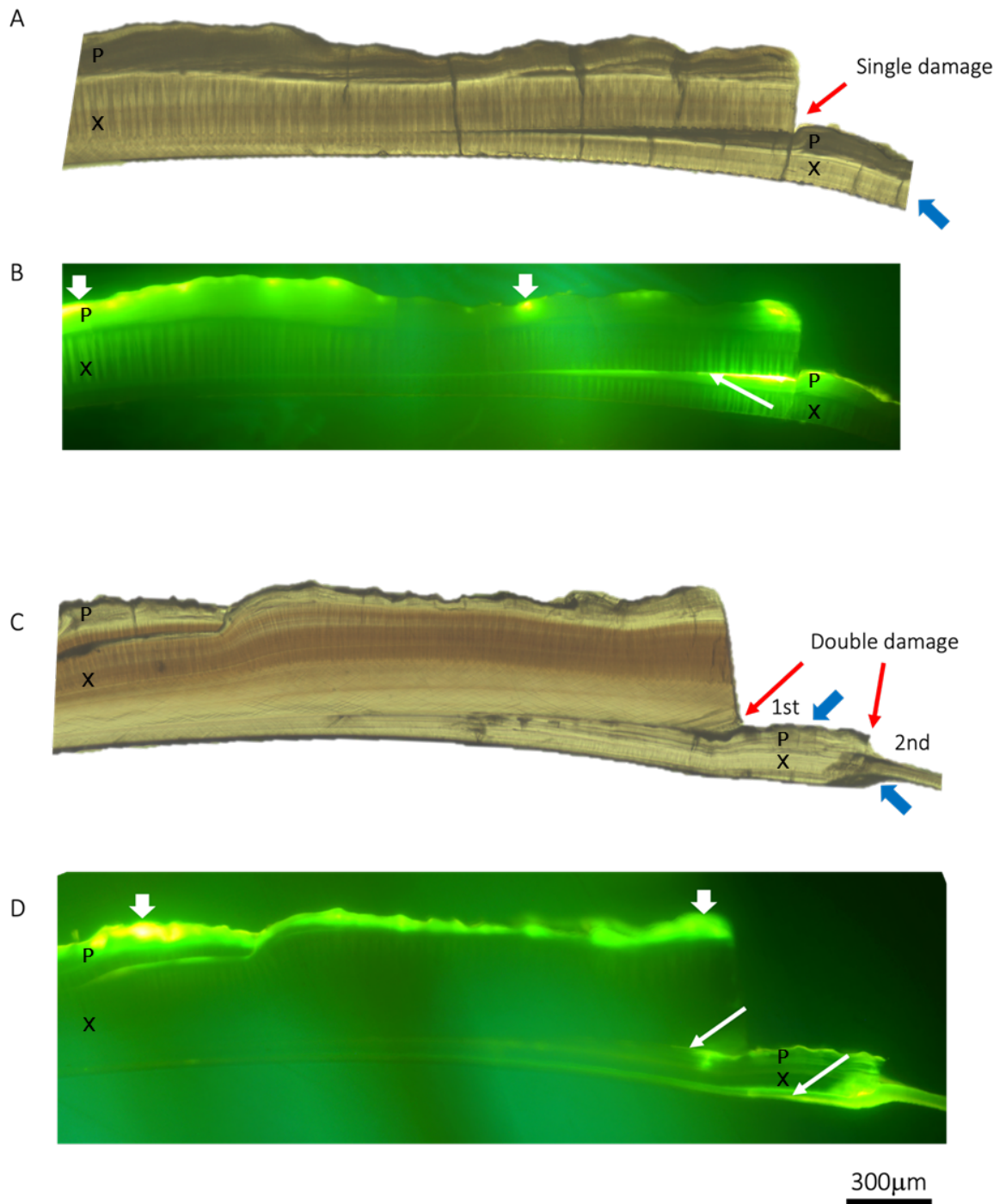


Figure 4.14: Thin sections of the shells of *Buccinum undatum*. A and C) Photomicrographs taken under transmitted light and B and D) in blue light. Red arrows show area of shell damage, with subsequent repair marked with blue. Thin white arrows show areas of calcein incorporation, thick white arrows, absorption onto shell surface. Two different microstructures are indicated with P (prismatic) and X (cross-lamellar).

Scanning Electron Microscopy (SEM)

The external structure of the shell of *B. undatum*, with the whorls and wave sculpture is shown in Figure 4.15 A. These structures are consistent across the external surface of the shell through to the apex. Imaging further confirmed the previous findings from the light microscopy and calcein staining imaging, that in the areas of re-growth of the shell, the new growth calcifies back beneath the previous shell (under-plating), along with re-growth to the sides of the 'gap' in the shell (Figure 4.15 B). This can be seen where the area of re-growth has formed under the original shell layers before mineralisation (Figure 4.15 C red arrow). The outer periostracum subsequently grows over the repaired shell surface, whilst filling in the joint between the original shell and the newly mineralised repaired shell in the area of damage (Figure 4.15 C). SEM analysis shows that the shells of *B. undatum* are constructed of two distinct microstructures (Figure 4.16). The outer layer is an aragonite prismatic layer (Figure 4.17), and an inner layer, the internal crossed-lamellar structure (Figures 4.18 and 4.19). It can appear as if there are more layers in the shell structure, this is due to the variation in angle of crystal formation, found within the crossed-lamellar layers and different angles of fracture will display different numbers and arrangement of these variations (Figures 4.18 and 4.19).

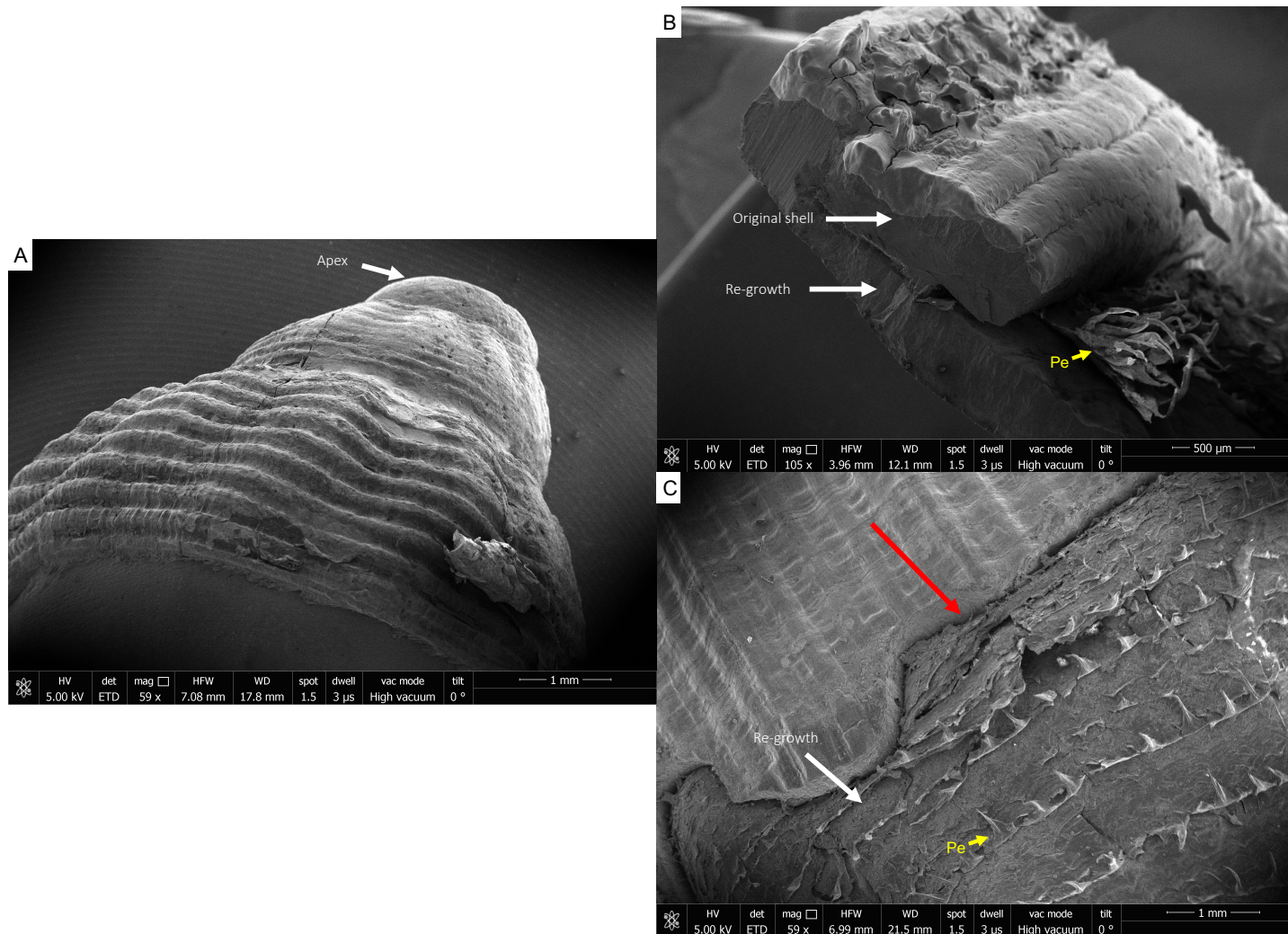


Figure 4.15: SEM images of *Buccinum undatum* shells. A) outer shell and apex showing shell whorls and wave shell sculpture. B) area of mechanical damage with original shell and area of re-growth marked and C) shows area of re-growth. Initial cut marked with red line. Pe marks the periostracum.

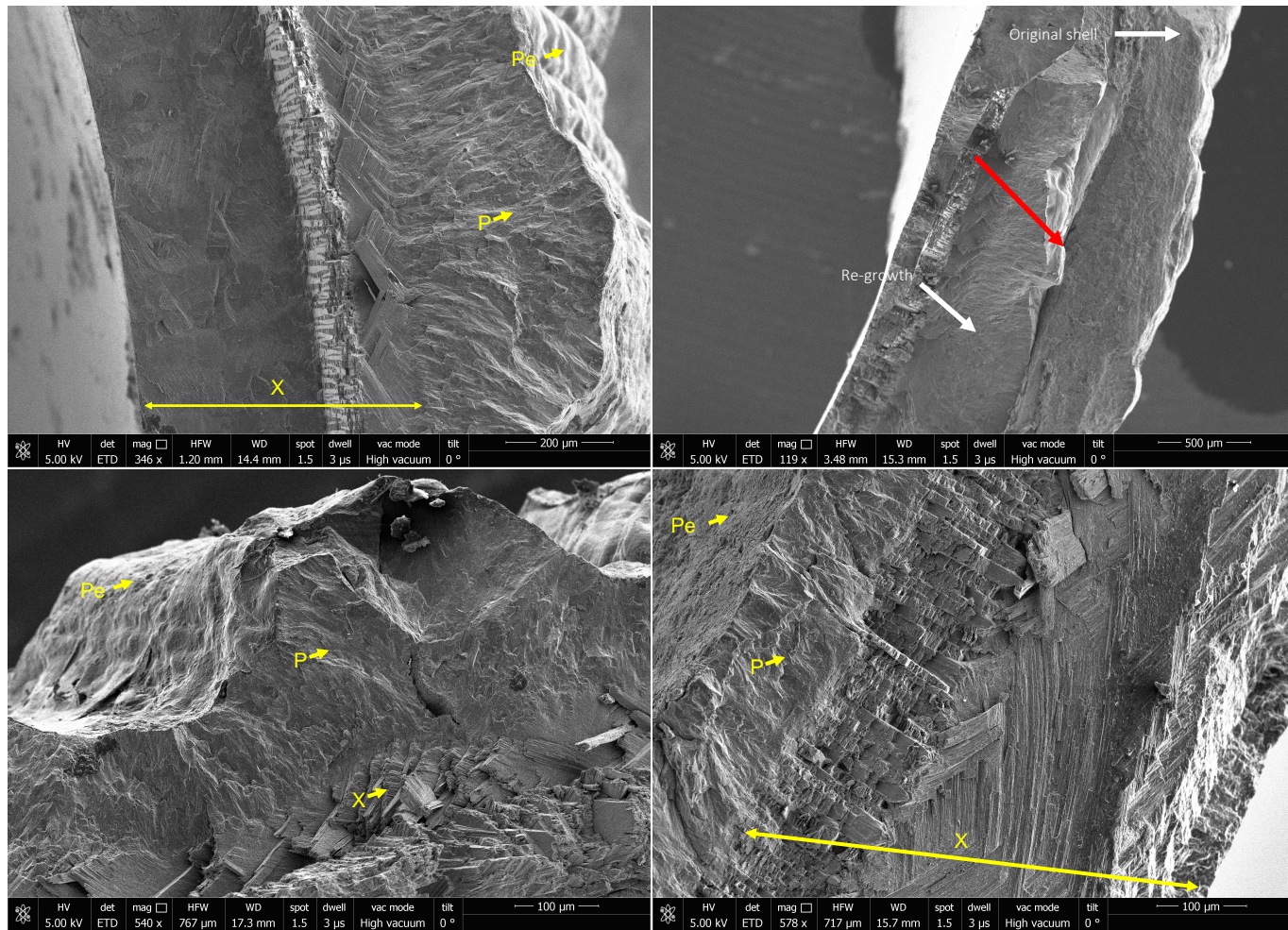


Figure 4.16: SEM images of internal shell structure of *Buccinum undatum*. Two different microstructures are shown: prismatic (P), crossed-lamellar (X) and periostracum (Pe). Double-headed arrow shows the full width of the crossed-lamellar layer. Red arrow marks point of old/ new divide from damage and re-growth.

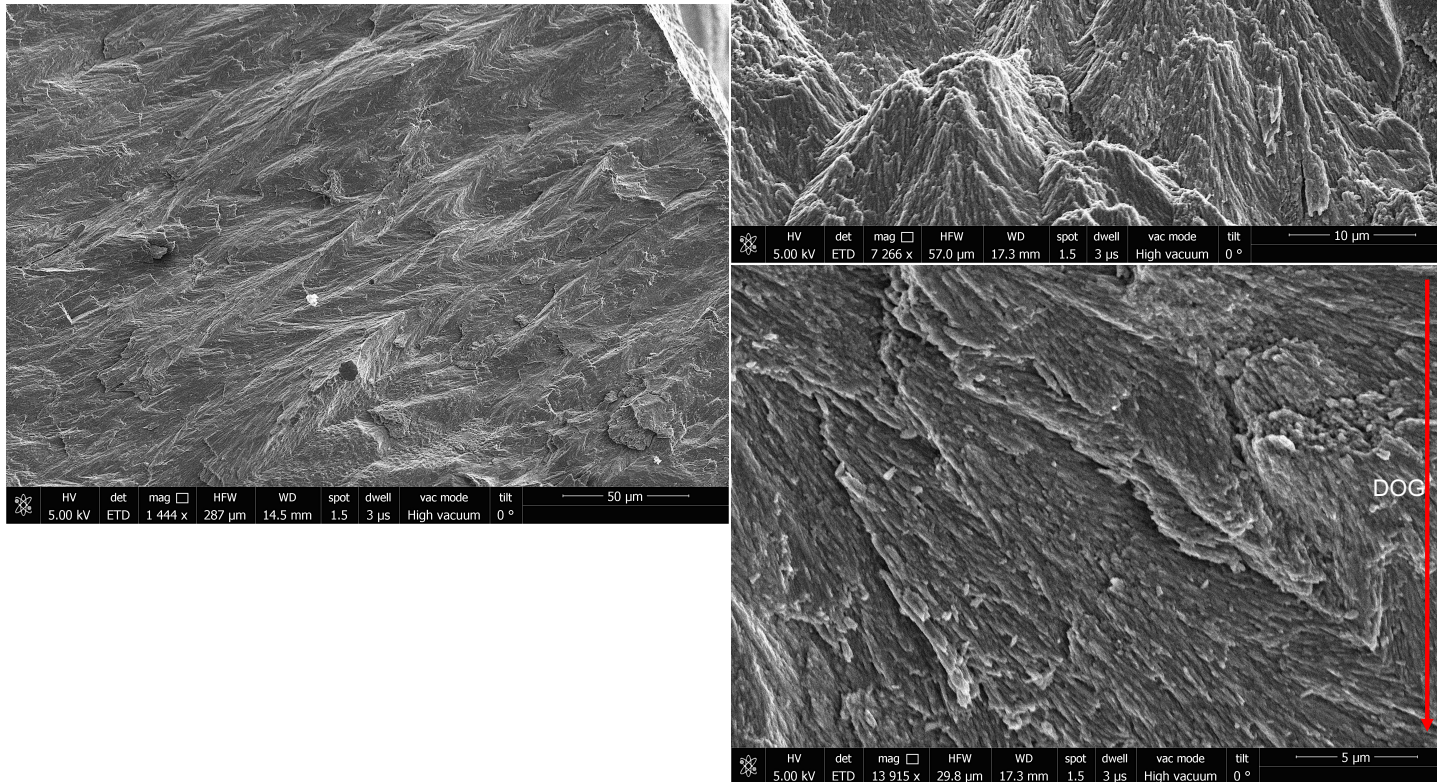


Figure 4.17: SEM images showing the microstructure of the prismatic layer with distinct aragonitic prisms. DOG marks direction of growth, from the outer to inner shell.

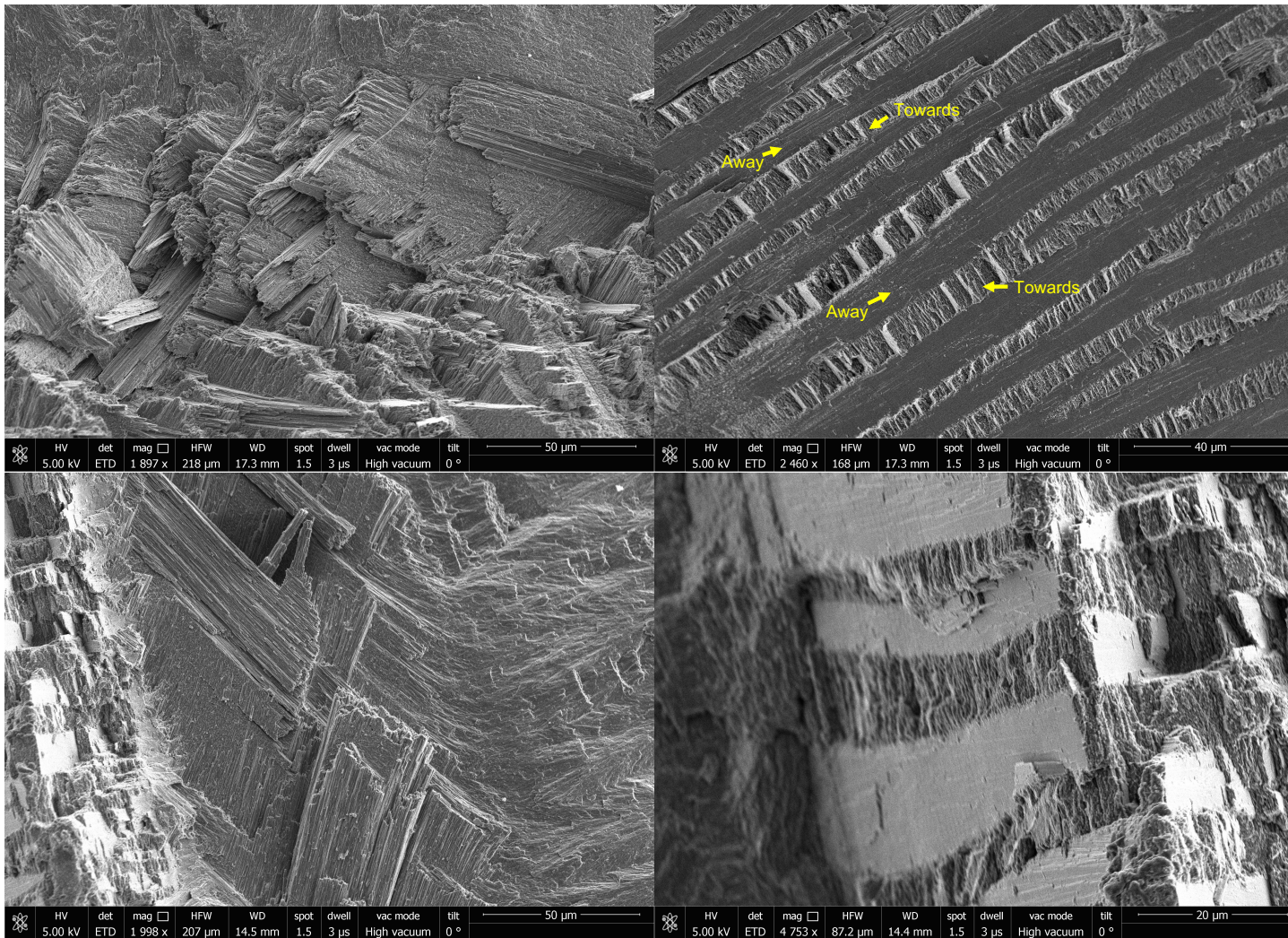


Figure 4.18: *Buccinum undatum*. SEM images showing the microstructure of the crossed-lamellar layers with lamellae shown in different directional planes.

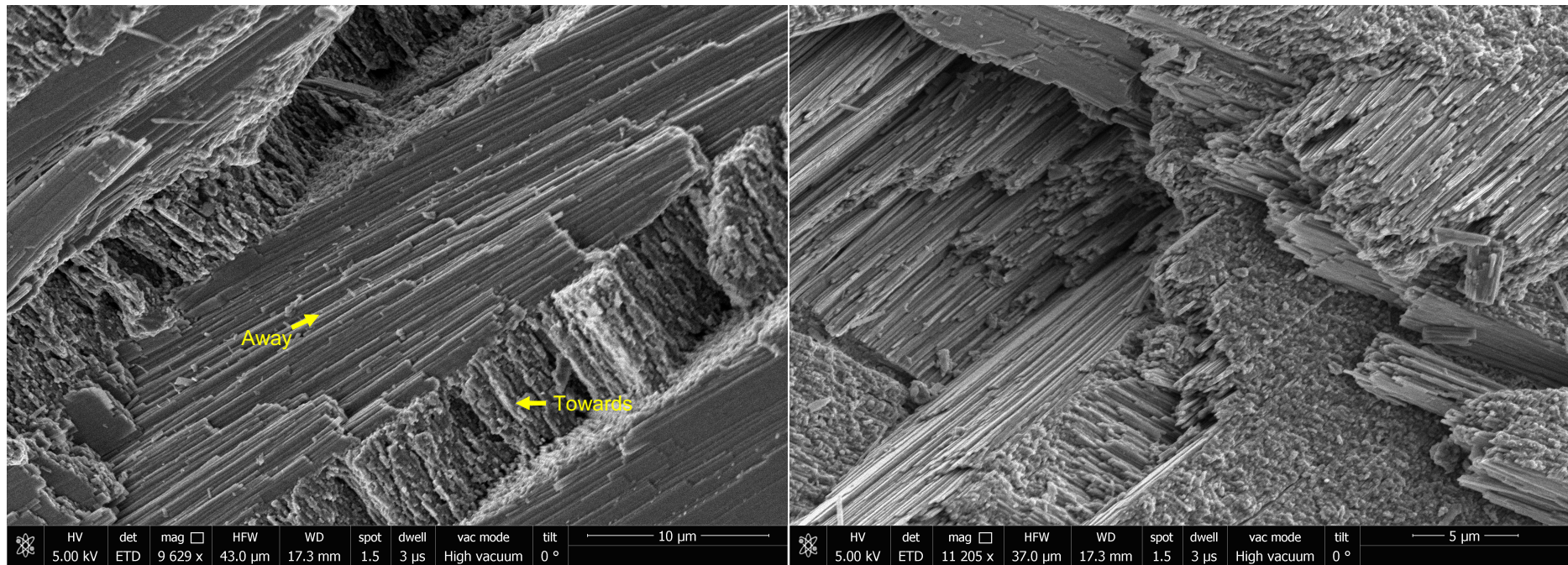


Figure 4.19: *Buccinum undatum*. Higher magnification of crossed-lamellar layer showing distinct crossed patterning and lamellae travelling in alternate directions.

Discussion

In this chapter, I have demonstrated that the shell of *Buccinum undatum* is composed entirely of aragonitic calcium carbonate with two distinct microstructures present; prismatic and crossed-lamellar. During periods of shell repair *B. undatum* re-grows the same shell structures to those formed during normal shell deposition. New shell is deposited on the existing inner shell back from the site of shell damage, and further shell is mineralised to fill in the area around the damage. A timeline of shell re-growth was confirmed using calcein-marked shells following experimental shell damage. Re-growth of the shell back beyond the damaged area further adds to variations in shell morphology seen in wild-collected populations of *B. undatum*. The shell becomes thickened along the edge of repair, frequently forming shell scars. This pattern of shell deposition post-shell damage also helps explain why there is an initial slow start to growth frequently observed in whelks recovering from experimentally inflicted shell damage reported in Chapter 3.

It is essential for organisms such as bivalves and gastropods that secrete an external exoskeleton, such as a shell, to be able to rapidly repair these structures if they become damaged. The re-grown shell also needs to have the same structural integrity as the original shell and the repair needs to provide an additional layer that underpins the original shell. However, although this thickening of the shell will increase the structural integrity, it could potentially lead to heavier shells over time (Kaiser *et al.*, 2000; Mensink *et al.*, 2000; Colvin *et al.*, 2022b). A period of rapid re-growth with an initial thin shell section allows an individual to quickly cover the damaged area, protecting the soft tissues within from external pressures. The obvious pressure to whelks is predation from foraging crabs and starfish that would be able to penetrate the shell and access the soft internal tissues through the damaged area. Once the damaged shell opening is repaired the whelks can subsequently focus on thickening the shell at the same time. I have demonstrated in this chapter that although the repaired areas of the shell initially appear thinner, they still consist of the same microstructural layers and calcium carbonate composition as the original shell growth.

Molluscan shells are formed of a hard substance, primarily calcium carbonate and, as established in this chapter, for *B. undatum* this is aragonite with no traces of calcite found, both during original growth, and through periods of rapid re-growth. This finding was supported by

the Raman spectrometry results presented in Chapter 2, where I showed that peaks in the Raman spectra in the shell microstructure of all *B. undatum* shell sections, and shell layers examined were consistent with the spectra seen in aragonite standards. There are many structures and combination of structures that can occur in mollusc shells, and these are seen to vary both within and between molluscan taxa (Kobayashi and Samata, 2006; Suzuki *et al.*, 2010). The outermost layer covering the shell of *B. undatum* is the periostracum, an uncalcified protein and lipid layer that is partially mineralised and serves multiple purposes, such as protection to the outer shell layer. Whilst it is commonly present as additional protection to the shell surface it is often eroded over time. Nonetheless, due to the periostracum, being attached to the mantle margin, another role in molluscs is to define a space in which the processes of shell secretion can begin, allowing mineralising shell deposition to occur at the shell edge (Bubel, 1973; Hunt and Oates, 1978; Richardson *et al.*, 1981; de Paula and Silveira, 2009; Clark *et al.*, 2020). Beneath the periostracum is the outer aragonite prismatic layer(s), these structures are clearly seen in molluscan shells, and although often described as being ‘primitive’ in comparison to other shell layers, they are formed of laterally arranged polygonal aragonite prisms (Suzuki and Uozumi, 1981; Kobayashi and Samata, 2006). The most common aragonite layer is that of crossed-lamellar structure, often referred to as the ‘building blocks of the shell’ and this structure has been noted to occur in many molluscan classes (Kogure *et al.*, 2014). I have demonstrated in the whelk’s shell that the crossed-lamellar structure forms the inner most shell layer. Crossed-lamellar is a multi-layered structure and is one of the most complex structures seen in mollusc shells as it is constructed of a sophisticated 3D hierarchical arrangement of lamellae orientations. Within this, elongate rectangular rods are aligned parallel to each other, and form in opposing directions, creating the crossing pattern seen within the aragonite crystal structure (Kobayashi and Samata, 2006; Nouet *et al.*, 2012; Crippa *et al.*, 2020). Each different microstructure provides a distinct property to the shell, often increasing its structural integrity and helping to reduce the frequency of shell fracturing over time (de Paula and Silveira, 2009; Rodriguez-Navarro *et al.*, 2012).

Summary

The shell of *B. undatum* is formed solely of aragonitic calcium carbonate and is deposited both during periods of ‘normal’ shell growth (linear increase in shell length) and during rapid re-growth (shell repair) following damage to the shell. The shell is formed of two

distinct microstructures: the outer prismatic layer and inner crossed-lamellar layer. These layers are replicated during shell damage and re-growth at all stages of shell growth (i.e., both in juveniles and adults). The findings of this chapter build on the knowledge of shell growth and shell repair reported in Chapters 2 and 3. The last chapter (Chapter 5) will examine further the processes of shell repair by studying the elemental composition of the shell layers and what, if any, elemental differences there are between normal shell growth and shell repair. Molluscan shells are complex bio-composite materials, whose formation is controlled by several factors including habitat, local environment, and genetics. However, the contribution of these is still relatively unknown, with regards to the synthesis and maintenance of the shell (Palmer, 1981; Clark *et al.*, 2020).

There is a growing interest in the understanding of the structure of shells, and their formation (de Paula and Silveira, 2009; Sleight *et al.*, 2015; Colvin *et al.*, 2022b), in addition to the future impacts on the shell from changes in environmental pressures (see Chapter 3 for more details). Although not within the scope of this thesis, further investigations into the mechanisms of shell re-growth including any immune responses and genetic makeup would be beneficial in furthering the understanding of the implications and processes involved in shell re-growth following periods of shell damage (Sleight *et al.*, 2015). Additionally, understanding the incorporation of elements into the aragonitic shell structure, which will be investigated in Chapter 5, and the organic matrix formation is key to understanding the mechanisms of shell growth and shell repair. The overall formation of shell carbonates and the organic components is an energetically costly process (Palmer, 1992), and it is important to understand how calcified structures and the energetic implications might respond to a changing marine environment, from events such as climate change and ocean acidification. Further work to investigate the impacts of such events are imperative to the overall understanding of impacts on shell growth and shell repair under further different environmental conditions (Colvin *et al.*, 2022b). Continued research into the structure and formation of the molluscan shell is important, not only in terms of impact to the species themselves, but is key to underpin the theories, applications, and mechanisms behind bio-mimetic structural materials for use in industry (Ji *et al.*, 2017).

Chapter 5 – Trace element incorporation in
Buccinum undatum shells

Figures

- Figure 5.1: Molecular structure, showing the lattice arrangement of aragonitic CaCO₃ showing Ca (green), C (grey), O (red) atoms and a substituted atom from group 2 e.g., Sr (blue circle) within the lattice. Image adapted from The Virtual Museum of Minerals and Molecules.....151
- Figure 5.2: Tank arrangement for controlled experimental damage used in all the experiments. Labelled whelks were held in the 10 L tanks held within the 175 L static water bath system. Temperatures maintained by controlled room temperatures and circulation and filtration through the pump and overhead piping system.161
- Figure 5.3: Diagrammatic representation of measurements taken at DLS. Green and purple arrows show traces run with μ XRD (Chapter 4) and black spots show examples of how μ EXAFS were taken through marked points. The black dotted rectangles show μ XRF selection areas for each mapped scan (5 μ m spots at 10 μ m step size). Solid rectangles represent the original (red) and (purple) re-grown shell.....163
- Figure 5.4: Diagrammatic representation of the whelk shell (red) with new growth (purple) and transects marked for ablation. Shell layers marked with dashed lines, purple arrow direction from outer to inner shell layers used for vertical laser traces and green arrows the laser ablation tracks horizontally within individual shell layers.....164
- Figure 5.5: A) Raw μ EXAFS data for inorganic aragonite and shell in energy domain, showing strong Sr absorption edge, followed by minor oscillations from surrounding atoms. B) Transformed data in radial domain with theoretical O, C and Ca atom scattering and C) for inorganic aragonite and shell showing very similar peak shapes. Radial distance (\AA) is a measure of the distance between the centres of atoms present.166
- Figure 5.6: Frequency histograms of bond length (\AA) for Sr-C, Sr-Ca, and Sr-O, under experiments indicated on right hand Y-axis. Sr doped and Sr non-doped combine 5 and 10°C, and original shell growth is shell material prior to damage. All data are average values for each experiment. Difference in colours between bars identifies individual bond lengths presented.167
- Figure 5.7: Typical examples of μ XRF element maps for normalised Sr/Ca concentrations in shell sections of *Buccinum undatum* shells. Direction of shell growth left to right. Black arrows indicate the point where the shells were experimentally-damaged. A and B) experimentally-damaged and repaired shells in non-doped seawater respectively. C) experimentally-damaged

and repaired shell under Sr doped seawater conditions. Scales (Y axes) represent different ranges of concentration of Sr (a.u.) in the shell sections.169

Figure 5.8: A) Photomicrograph of a typical *Buccinum undatum* shell section showing the LA-ICP-MS ablation spots (25 μ spot size) (right of the red dotted track line) through the outer prismatic layer and into the inner crossed-lamellar layer and B) Mg, Sr, Na and Ba traces plotted below the shell section. Grey dashed line marks point of interface between the outer prismatic and the crossed lamellar layers. Units of concentration are ppm.171

Figure 5.9: A) Photomicrograph of an experimentally-damaged *Buccinum undatum* shell section showing the temporal LA-ICP-MS ablation tracks (25 μ spot size) beneath the horizontal red arrows in five areas (1-5) of the shell. Areas 1 and 2 prismatic shell, areas 3 and 4 crossed-lamellar layer and area 5 newly repaired prismatic shell and B) Mg, Sr, Na and Ba concentrations following LA-ICP-MS analyses in different areas of the shell section showing temporal variations in concentrations along the red arrows through areas 1-5 and through the different structural layers. Red lines show partition between traces and arrows reflect direction of travel for the laser through the shell. Units of concentration are ppm.172

Figure 5.10: A) Photomicrograph of experimentally-damaged *Buccinum undatum* shell with a section of earlier, normally deposited shell (A1). Five vertical LA-ICP-MS ablation tracks (25 μ spot size) along different parts of the shell, from the outer prismatic to the inner crossed-lamellar are shown (red arrows). B) Mg, Sr, Na and Ba concentrations (ppm) along the laser traces (red lines) and across the different microstructure (grey dashed lines). C) 1; normally deposited prismatic and crossed-lamellar shell, 2 and 3; prismatic and crossed-lamellar layers of normally deposited and re-grown shell, 4; crossed-lamellar of normally deposited, and re-grown prismatic and crossed-lamellar shell, 5; regrown prismatic and crossed-lamellar shell.174

Figure 5.11: A) Photomicrograph of a naturally damaged wild-caught *Buccinum undatum* shell section showing four vertical LA-ICP-MS transects (1-4) across the prismatic and crossed-lamellar shell layers. Natural shell damage occurred in transects 1-3 (black arrows) whilst no shell damage occurred along 4, B) Mg, Sr, Na and Ba concentrations (ppm) along the laser traces (25 μ spot size) (red arrows) are enlarged in C. Vertical red lines in (B) distinguish the four traces, and the red arrows reflect the direction of travel of the laser through the shell.....176

Tables

Table 5.1: Equipment parameters used for μ EXAFS.....	162
Table 5.2: Settings used for LA-ICP-MS. Laser power was varied to give a typical fluence of 3-5.35 J. cm ⁻²	164
Table 5.3: Summary of bond lengths (Å) for Sr-O, Sr-C and Sr-Ca in an aragonite standard, in the original shell and repaired shell (new shell) determined using bulk μ EXAFS. 'Total' represents average bond length values across a whole shell section, 'Original' is bond length data from areas of no shell damage and 'new shell' is re-growth and shell repair.	167
Table 5.4: Summary of strontium (Sr, ppm) concentrations from LA-ICP-MS in repaired and normally deposited <i>Buccinum undatum</i> shells. Data for the shells from the doped experiments are the combined values from the double and triple concentrations as only a few shells were analysed. Number of ablation spots (n_{spot}) taken from different shell samples (n_{shell}).	177
Table 5.5: Summary of bond lengths (angstroms Å) determined using synchrotron analyses in inorganic aragonite standard material, damaged and repaired <i>B. undatum</i> shell fragments (this thesis) and various invertebrate calcified material published in the literature (table adapted from Chenery <i>et al.</i> , 2019).	179

Introduction

This final experimental chapter aims to build on the data collected and presented in Chapter 4, in which the crystal structure of the shell and calcium carbonate (aragonite) matrix were examined. In this final chapter, the incorporation of trace elements into the shell structure will be investigated using a variety of analytical techniques to examine if there are differences between normal shell deposition and rapidly re-grown shell following shell damage along with variations between shell microstructures.

Bond length and crystal structure

Mineralogical structure has a major control on trace element incorporation, atomic structure, and the typical bond lengths between constituent atoms and their neighbours (Soldati *et al.*, 2016). In molluscan shells mineralogical structure can be determined through extended X-ray absorption fine structure (EXAFS), providing knowledge of the bond lengths, and allowing a better insight into the lattice arrangement (Figure 5.1) (Weiss *et al.*, 2002; Weiner *et al.*, 2003).

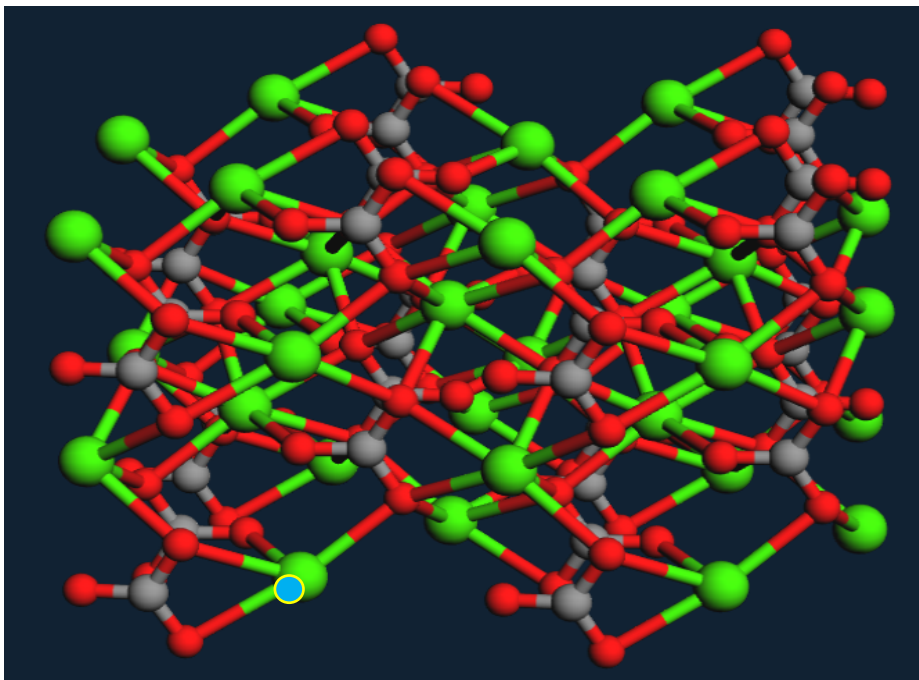


Figure 5.1: Molecular structure, showing the lattice arrangement of aragonitic CaCO_3 showing Ca (green), C (grey), O (red) atoms and a substituted atom from group 2 e.g., Sr (blue circle) within the lattice. Image adapted from The Virtual Museum of Minerals and Molecules.

Whilst bond lengths can be assessed using micro-X-ray diffraction (μ XRD), which uses the theory of diffraction to recreate the structure of a material, EXAFS enables micro-scale analysis through the targeting of certain elements, allowing an assessment of these at a biological structural level and identifies how specific bond lengths are compared to others (Parsons *et al.*, 2002). For further details on experimental techniques, see Appendices 6-9.

Trace element incorporation

Trace elements can be incorporated into the CaCO_3 crystal matrix as substitutions for Ca^{2+} (Hollyman, 2017; Zhao *et al.*, 2017b). This can occur when elements have similar electrochemical properties to the calcium ion allowing the replacement to be made (Figure 5.1). Other elements, which have a similar radius, but different charge may also incorporate into the matrix, and additional substituted ions will be needed to balance out the overall charge. This however can lead to complications when interpreting trace element incorporation in the shells, with increased concentrations of trace elements potentially recorded in areas of increased organic matter, for example in organic rich growth lines (Schöne *et al.*, 2010; Hollyman, 2017).

There are a number of trace elements which are incorporated into the shells of marine molluscs, but two of the most abundant, and consequently well studied are strontium (Sr) and magnesium (Mg). Their significant concentrations in seawater and position in the Periodic Table as Group 2 elements, above and below Ca gives them similar physico-chemical properties and allows them to easily substitute Ca into the matrix of CaCO_3 . Nonetheless, many elements can be incorporated in varying amounts into the CaCO_3 (aragonite) matrix (e.g., Mg, Sr, Ba and Na). These element incorporations have been shown to be influenced by a range of environmental parameters, for example Mg and Sr incorporation is influenced by seawater temperature (Freitas *et al.*, 2006), Ba productivity (Zhao *et al.*, 2017a), and Na incorporation is influenced by salinity (Mezger *et al.*, 2019), with different levels of incorporation often reflective of the concentrations in the extrapallial fluid surrounding the mineralising shell. Further variations in elemental incorporations can occur between species groups for a variety of reasons, for example due to variations in growth rates and shell structure (Schöne *et al.*, 2010; Markulin *et al.*, 2019; Wannamaker and Gillikin, 2019). Although clear links have been demonstrated amongst different species of foraminifera and corals, correlations between environmental

factors, trace element composition and the structure of molluscan shells are still relatively limited (e.g., Wannamaker and Gillikin, 2019). Thus, through an understanding of the element to calcium ratios in molluscan shells, a variety of environmental information can be gleaned from the shells such as proxies for seawater temperature, salinity, and productivity (Marali *et al.*, 2017b). Furthermore, the overall composition of the structures has been shown to reflect an individual's early life, allowing further information on ontogeny, connectivity, and habitats to be obtained (Norrie *et al.*, 2019). With recent advances in analytical technology, it has been possible to investigate not only elemental concentrations in shells but to obtain high spatial resolution maps of many trace elements in calcareous organisms (Chew *et al.*, 2021). Elemental analyses are widely used in paleo-environmental research, alongside stable isotopic analysis, to give a highly detailed and sensitive record of an organism's surrounding environment, thus allowing reconstruction of local environments and climate (Hausmann *et al.*, 2019; Höche *et al.*, 2022). Often these element concentrations are used as proxies in relation to temperature, however, they can also include changes in pH, freshwater input, upwelling and growth, in addition to that of nutrient distribution (Freitas *et al.*, 2006; Soldati *et al.*, 2016; Hollyman, 2017; Zhao *et al.*, 2017a; Mezger *et al.*, 2019). They can consequently be used to establish localised variation within and between different populations and can be pieced together to form chronologies allowing reconstructions of past climate changes to be studied (Höche *et al.*, 2022).

In this chapter, data on trace element concentration and inter-atomic bond lengths in the shell structures of *Buccinum undatum* were obtained. For this, synchrotron analysis including both micro-X-ray fluorescence (μ XRF) along with laser ablation-inductively coupled plasma-mass spectrometry (LA-ICP-MS) were used to determine spatially-resolved trace element incorporation into the shell. By using a combination of these techniques, that have differing capabilities in terms of available elements and detection limits, information from different regions of the whelk's shell, and in normally deposited and repaired shell, were obtained. Both techniques involved micro-sampling at a sub-100-micron scale (see Appendices 6-9 for technical details).

μ XRF is a non-destructive technique that measures the fluorescence from X-rays on emission from the sample (Kanngießer, 2003). This response occurs when an incident ray is absorbed by the atom giving rise to the promotion of an inner core electron, then the

subsequent relaxation of that electron with the loss of energy through fluorescence. Each element presents a unique characteristic fluorescence, allowing both qualitative and quantitative analysis of materials (Fitzgerald, 2008; Streltsov *et al.*, 2019). Although μ XRF provides a clear image of elemental changes within a structure, through relative level maps, μ XRF on the i18 beamline at the Diamond Light Source, Oxford (DLS) is not capable of measuring elements lighter than nominally mass 30. (i.e., Mg, Na and Li) due to a combination of self-absorption and air absorption of the soft X-rays from low mass elements. Although calibration of μ XRF on the i18 beamline to produce quantitative concentrations is possible, this was not possible within the scope and time frame of the current study.

Although LA-ICP-MS is destructive at the micro scale, the LA-ICP-MS at the British Geological Survey (BGS) can detect elements of lower mass (e.g., Ba, Mn Mg and Sr). The process of LA-ICP-MS itself uses the interaction between the laser and sample surface to break up the surface of the sample (ablation), and this sample vapour is then carried by a stream of helium gas to the ICP-MS for analysis. At this point a plasma is used (ICP), which ionises the elements present, and the subsequent ions are then measured based on mass/ charge ratio using the mass spectrometer (MS). Due to the methods of detection, counting the individual ions, and the ability to readily calibrate the instrument using standards, LA-ICP-MS further confirms the presence of elements and can calculate concentrations (reported in ppm, i.e., mg/kg) of the elements present and found within XRF, providing a more quantitative analysis of materials.

Strontium and Magnesium

Strontium (Sr) and Magnesium (Mg) are two well-studied trace elements occurring within carbonate structures (Schöne *et al.*, 2010). Differences in degrees of incorporation and composition are often seen in different bio-carbonate structures such as molluscan shells. This is due to Sr and Mg ion size and the calcium carbonate polymorph structure, altering the readiness to incorporate the ions (Mg^{2+} and Sr^{2+}) (Speer, 1983; Dietzel *et al.*, 2004; Schöne *et al.*, 2010). Moreover, it is also thought that there may be a further genetic influence on Sr and Mg, seen in concentration differences between taxonomic groups of marine organisms (Chave, 1954; Turekian and Armstrong 1960; Dodd, 1967). The concentrations of these ions are relatively temporally stable within open ocean seawater (Broecker and Peng, 1982; Kastner, 1999), with incorporation into the calcium carbonate lattice thought to occur at physio-

chemical equilibrium for most molluscs (Holail and Tony, 1995). This equilibrium is affected by a change in seawater temperature amongst other factors, and therefore elemental concentrations can often be reflective of these. Further differences in rates of incorporation can be observed between differing calcium carbonate polymorph structures i.e., calcite and aragonite (Wood *et al.*, 2022). Furthermore, due to the reduction in diagenetic alteration with skeletal porosity in molluscan shells, they provide an advance over many other carbonate structures, i.e., corals, as they less readily dissolve and therefore retain more reliable climate variability records (Ivany *et al.*, 2004; Warter *et al.*, 2018).

Although Mg/Ca and Sr/Ca concentrations have been used in temperature reconstructions in some corals and benthic foraminifera (Rosenthal *et al.*, 1997; Raddatz *et al.*, 2013; Fowell *et al.*, 2016), their applicability in molluscan species remains contentious (Marali *et al.*, 2017a). This has been due to the lack of reproducibility and consistency in data, whereby Mg/Ca and Sr/Ca ratios do not reliably reflect ambient seawater temperature, with little variations even under sudden change (Wannamaker and Gillikin, 2019). However, Mg and Sr ratios see a decrease with an increase in water depth for calcite and aragonite structures (Rosenthal *et al.*, 1997). Thus, this suggests that for some organisms, the effect is more likely due to pressure dependence on incorporation (Rosenthal *et al.*, 1997). Identifying patterns and drawing clear links between seawater temperature and Mg/Ca or Sr/Ca ratios is further complicated due to the underlying physiological processes that occur during biomineralization (Wanamaker and Gillikin, 2019). Factors such as growth rates and ontogeny in bivalve species have been noted to directly relate to both Mg and Sr incorporation, reflective in shell growth patterns, such as growth lines and periods of rapid shell growth (Marali *et al.*, 2017a). In conclusion, under different situations, the calcium carbonate polymorph, seawater temperature and pressure can all influence Sr/Ca and Mg/Ca ratios as well as vital effects such as growth rate and ontogeny.

Barium

As with Mg/Ca and Sr/Ca ratios, Ba/Ca ratios see further variation in incorporation into calcium carbonate structures, with an array of influencing factors. Previous studies have noted that Ba/Ca ratios have an inverse relationship to water salinity, with levels in the mollusc shell closely following water ratios (Poulain *et al.*, 2015). Further influencing factors of temperature and individual growth can additionally change incorporation rate (Poulain *et al.*, 2015;

Wanamaker and Gillikin, 2019). Links to a change in salinity and ocean productivity have also been noted, with sharp peaks occurring in relation to ocean upwelling events in coral biomineralization (Gonneea *et al.*, 2017) and further changes with increased chlorophyll and diatom blooms. An example of such is seen in the clam *Arctica islandica* (Thébault *et al.*, 2009a; Wanamaker and Gillikin, 2019), potentially allowing Ba to be an effective method of tracing high primary productivity (Toland *et al.*, 2000).

Other trace elements

There are many other trace elements which are incorporated into or adsorbed onto the shells of marine molluscs, often reflecting their natural environment, and changes in growth rates and ontogeny (Hüssy *et al.*, 2021). Elements including lithium (Li), manganese (Mn) and sodium (Na) are examples of such elements. A very low inter-individual variation in Li/Ca ratios, is further suggestive of strong environmental control on incorporation (Thébault and Chauvaud, 2013). Examples of such include a weak inverse relationship with seawater temperatures seen in aragonitic coralline structures (Marriott *et al.*, 2004; Thébault *et al.*, 2009b; Thébault and Chauvaud, 2013) and a stronger association with phytoplankton blooms, for example in the scallop *Pecten maximus* (Thébault and Chauvaud, 2013) along with calcification and shell micro growth rates (Thébault *et al.*, 2009b). Further alterations in rates of Li incorporation have been shown to be associated with river discharge, salinity, and seasonal variations and fluxes of dissolved materials i.e., from the chemical and mechanical weathering of silicates (Thébault *et al.*, 2009b; Thébault and Chauvaud, 2013).

In general, Mn incorporation into the shells is reflective of the relative Mn concentrations within seawater which are dependent on biogeochemical episodes (Barats *et al.*, 2008). Examples of such include it being a potential proxy for freshwater runoff and for phytoplankton blooms, due to its association with the processes involved during photosynthesis (Langlet *et al.*, 2006; Soldati *et al.*, 2016; Kelemen *et al.*, 2019). As with Mn, Na is occasionally reflective of freshwater input, with changes in Na/Ca ratios associated with a changing salinity (Devriendt *et al.*, 2021). Furthermore, variation has been shown to occur with pH and ocean acidification events within some molluscan species, whereby mussel species showed a change in Na incorporation, however scallop species did not (Zhao *et al.*, 2017b). Nonetheless, rates of incorporation cannot solely be associated with environmental factors, with individual vital effects and microstructures often displaying a strong correlation with

element incorporation, as seen in aragonite coral skeletons (Rollion-Bard and Blamart, 2015). The overall influencing factors on incorporation into biogenic carbonates are complex and still relatively unknown (Hollyman *et al.*, 2019).

Vital effects

'Vital' (i.e., metabolic, and kinetic) effects are those arising from biological controls on the process of calcification reflected in geochemical signatures (Purton *et al.*, 1999; Gillikin *et al.*, 2005). It is a 'catch-all' term often used to describe the complex biochemical mechanisms occurring within the shells and used to explain deviations from expected inorganic physico-chemical equilibrium values, under 'normal' conditions, such as ambient seawater temperatures. However, as vital effects have been studied in more detail over the last two decades, they have been broken down into several areas including metabolic effects and kinetic effects. Frequently, these effects can be seen as a change in element/Ca ratios from predicted values for inorganic calcium carbonate precipitation at defined temperatures and pressures, an example of this is that of Sr/Ca and Mg/Ca in seawater, where it is thought that growth rates and ontogeny further impact these concentration ratios (Buchardt and Fritz, 1978; Palacios *et al.*, 1994; Wannamaker and Gillikin, 2019). Additionally, other physiological factors, for example metabolism, has been noted to affect the rates of incorporation into the shells of the bivalves (e.g., the clam, *Arctica islandica*), (Gillikin *et al.*, 2005; Schöne *et al.*, 2010; Hahn *et al.*, 2012).

Chapter 5 focusses on assessing the differences in trace element incorporation in the shells of *B. undatum*, both within and between the shell layers of the originally deposited and newly repaired damaged shell areas. It is hypothesised that as the whelk repairs and re-grows its shell, due to rapid shell mineralisation following the shell damage observed in Chapter 3 compared to normally deposited shell, it is expected that a change in crystal structure and trace element incorporation will occur. To try and disentangle repair effects from simple environmental controls, experiments were undertaken at two different seawater temperatures and with artificially elevated strontium concentrations in the seawater. Although it is noted that mechanisms such as vital effects are important functions, and of great interest, this is potentially a very large area of research, and a detailed investigation into these processes was outside the time frame of the current PhD research. It is also hypothesised that bond length would differ between rapidly growing shell material, compared with original 'normal' shell

growth, either because of kinetic limitations or if the biological structure (matrix) on which the calcium carbonate was growing was different. If differences are observed, then it is further hypothesised that differences in trace element incorporation will occur as a result.

Materials and Methods

For determination of the spatial and temporal compositional differences in the shells of *Buccinum undatum*, a series of analytical techniques were carried out. Several methods were used to give an overview of the internal shell structure, particularly focussing on areas of shell damage and repair. At the i18 micro-spectroscopy beamline at Diamond Light Source (DLS); Micro X-Ray Diffraction (μ XRD) (Chapter 4), Micro X-Ray Fluorescence (μ XRF) and Micro Extended X-Ray Absorption Fine Structure, (μ EXAFS) were used to assess micro-scale trace element incorporation and crystal structure. Further in-depth trace-element analyses were performed using Laser Ablation Inductively Coupled Plasma Mass Spectrometry (LA-ICP-MS) at the British Geological Survey (BGS). See Appendices 6-9 for description of background to the analytical techniques used.

Whelk shells that had been damaged and grown at different seawater temperatures were selected from previous growth experiments reported in Chapter 3 and their elemental composition investigated. Additionally, seawater chemical composition experiments were undertaken, to investigate element incorporation into whelk's shell growth and shell repair when the surrounding environmental conditions were manipulated and held constant with no external seawater input. Wild-caught whelks were grown in seawater doped with elevated concentrations of strontium (Sr) to study whether newly mineralising shell or repairing shell area contained elevated levels of Sr or whether the whelks were able to control Sr incorporation. Wild-caught whelk shells, from archived samples, that displayed prior heavy natural damage, and clear shell scarring were also chosen for analysis to assess whether naturally damaged and repaired shells displayed similar changes in element incorporation to the experimentally-damaged and repaired shells. Samples examined at DLS (reported in Chapter 4) were also re-analysed by LA-ICP-MS to allow direct and full comparative measurement within individuals using both DLS and LA-ICP-MS analyses.

Temperature-controlled and manipulated seawater chemical composition experiments

To provide constant environmental conditions during whelk shell growth and shell repair experiments, four 175 L tanks were used as water baths and held in two temperature-controlled rooms (approximately 10°C and 5°C with two tanks per room). An external filter was attached to each tank with the capacity to filter 900 L h⁻¹ of seawater and an efficiency to filter particles <1 µm and control particulate material entering each tank. The system was left for four weeks to stabilise prior to experimentation. Water volume within the system at any one time was maintained at ca. 137 L. An overhead pipe system delivered the filtered seawater into five smaller 10 L tanks suspended within each 175 L tank (Figure 5.2). This pipe system in combination with drainage holes 2.5 cm from the rim of each small tank allowed the flow of water entering and leaving to aerate each individual tank.

Once the tank system and filters had matured, whelks were collected during September and December 2018 using baited inkwell pots deployed and left to soak for 24 hours off Brynisiencyn in the Menai Strait, North Wales (53°09'30.4' N 4°16'46.6' W). Whelks (size range 45-55 mm TSL) were held for ten days, fed, and left to acclimatise to the controlled experimental conditions allowing natural shell growth to occur. A total of 140 whelks were used across two temperatures 5 and 10°C, with 7 whelks per 10 L tank. From collection to the end of the experimental period, whelks were fed a daily diet of mussel (*Mytilus edulis*) tissue. The system received regular water changes of approximately 10 L every three days, and water samples were taken from each 175 L tank daily and frozen to assess baseline Sr levels. Seawater samples were filtered using Isopore membrane 0.2 µm GTP filters into LDPE plastic bottles. Bottles used were new, and it has previously been demonstrated with in-house checks at BGS that they do not produce measurable contamination for the elements of interest. All water taken was replaced from a store of appropriately filtered and aged seawater in large holding tanks, that were filled and left in each temperature-controlled room to adjust to the required temperature before adding to the experiment tank.

Superglue was used to attach a paper number to each whelk shell. By placing a thin layer both beneath and on top of the label it formed a watertight seal and allowed the tag to remain throughout the experiment thus allowing the growth of each individual whelk to be

tracked. Once the labels had dried and before returning the whelks to their tanks, seawater from their tanks was taken during a water change and used to soak and then rinse individuals to ensure minimal chemical residue entered the system. Whelks were left for a further seven days before experimental damage. Cuts were made as a proportion of aperture size, calculated as approximately 40% of the total aperture opening of each whelk to account for variability within individual size. This was achieved using the Dremel 3000 with cutting wheel attachment (see Chapter 3 Methodology). Before returning the labelled whelks to their tanks, photographs were taken against a measurable scale and aperture size cut area and total shell length measurements made using ImageJ. Measurements were to 3 decimal places and repeated every 7 days until the end of the experiment period of 21 days. At the end of the experiment, whelks were removed from their tanks and frozen at -20°C for 48 hours as a means of dispatch. To prepare samples for analysis, whelks were carefully dissected out of the shell in order not to damage the fragile repaired shell margin. Shells were soaked overnight, rinsed in distilled water, and left to completely air dry for 72 hours.

The above experiment was repeated, but this time the seawater was doped with extra Sr to investigate if a proportional uptake of Sr could be detected in the new shell growth. This was achieved by dosing one of the 175 L tanks with twice the normal seawater concentration of Sr and another of the 175 L tanks with three times the concentration of Sr. To reach these concentrations, 2.91 g (2x) and 5.83 g (3x) of powdered strontium chloride hexahydrate (Sigma-Aldrich P/N:255521) were used. A litre of seawater was collected from the required tank, so as not to change the experimental water volume, and warmed by placing in a large beaker in a water bath at ~40°C. The powdered strontium chloride was then added to the warmed water which was stirred until fully dissolved. This solution was then slowly added back into the 175 L tank over 10 minutes, with vigorous mixing, and the process was repeated for each tank. No seawater flowed into the tanks during the experiment to ensure the element concentrations remained constant. Water collection and water changes occurred as before in the 10°C room to maintain water quality at this temperature, whereas the 5°C tanks received no water changes, due to improved water quality at this lower temperature. Whelks were given the same acclimation periods before shell cutting, and during this period of natural shell growth, three water changes were conducted prior to shell damage.

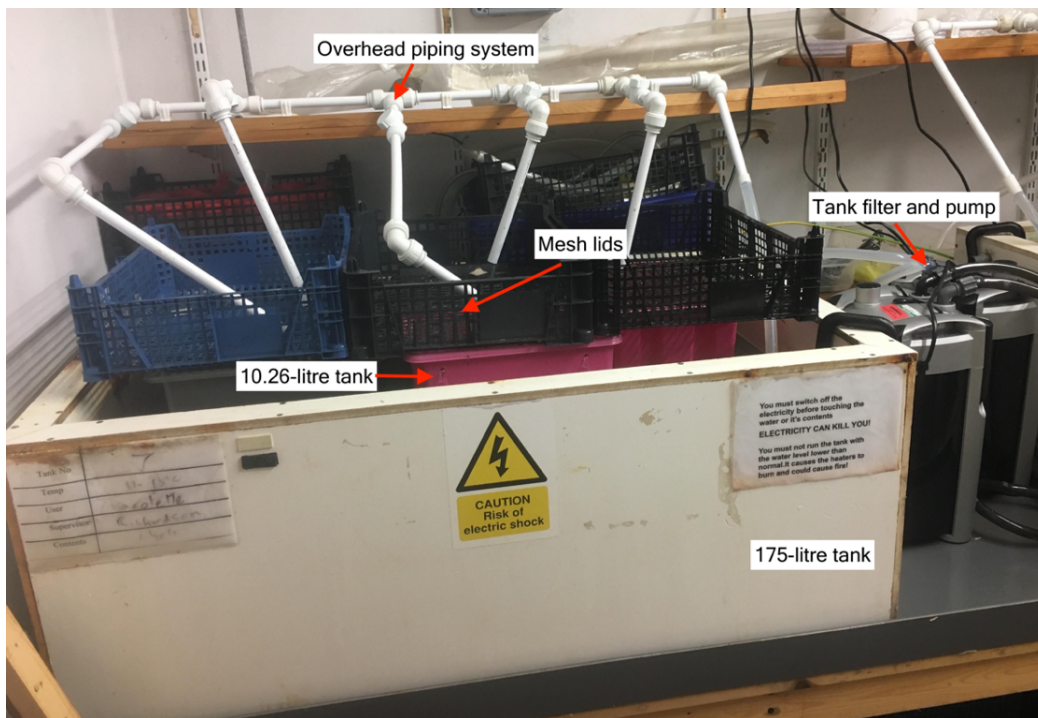


Figure 5.2: Tank arrangement for controlled experimental damage used in all the experiments. Labelled whelks were held in the 10 L tanks held within the 175 L static water bath system. Temperatures maintained by controlled room temperatures and circulation and filtration through the pump and overhead piping system.

Sample preparation

Thin sections (100 μm) and polished blocks (~10 mm thick) were prepared from each whelk shell margin along the direction of growth for analysis at BGS and DLS following methods in Chapter 4.

Diamond Light Source

Following successful application to the Diamond Light Source (DLS) committee (Appendix 5), analyses of sectioned whelk shell samples were undertaken using the i18 micro-diffraction beamline at the synchrotron facility. The beamline uses a 27 mm-period undulator to produce a bright energy x-ray microbeam to allow in-depth sample analysis, using the specific techniques outlined below. All primary data analyses were carried out using Dawn (v2.27) software (Basham *et al.*, 2015), with element maps further processed in Excel and visualised through ImageJ. An in-depth overview of each technique and the data analysis used, including XRF masking and analysis, can be found in Appendices 6-9.

μEXAFS – Micro Extended X-Ray Absorption Fine Structure

XAS (X-ray absorption spectroscopy) was used at DLS to assess whether the process of rapid shell growth brought about changes in the crystal lattice, particularly changes in bond lengths that might create incorporation site distortions thus influencing trace element substitution. The method of XAS used was μEXAFS (micro extended X-ray absorption fine structure). The EXAFS spectra were collected as a series of analytical spots along the areas of shell damage, shell repair and natural shell growth. The sampling strategy is illustrated diagrammatically in Figure 5.3. The equipment parameters for collection of μEXAFS spectra are given in Table 5.1.

The data collected were processed to retrieve the inter-atomic distances (as measured from R-space spectra) of the nearest Ca, O and C atoms to the Sr atoms in the aragonite crystals of the *B. undatum* shells. The arrangement of these atoms and their inter-atomic distance around the Sr induce the EXAFS fine structure in the energy (E) space spectra due to scattering paths. Data output from the Diamond synchrotron collected for μEXAFS were processed using the DEMETER package of software programs (ATHENA, ARTEMIS, HEPHAESTUS) (Ravel and Newville, 2005). Further information on data processing can be found in Appendix 7.

Table 5.1: Equipment parameters used for μEXAFS

Parameter	Value
Sr X-ray Collection Time	1-5 s
Nominal Sr edge energy	15590 eV
Pre Edge-Energy Step	5 eV
Pre Edge Time Step	1 s
Edge Energy Step	0.5 eV
Edge Time Step	1s
EXAFS Step	0.040 Å ⁻¹

μXRF – Micro X-Ray Fluorescence

μXRF was used to investigate spatial differences in elemental concentrations within the internal shell surface. This was carried out to help improve the understanding of compositional variation through elemental maps between the original shell and rapid re-growth. The elements analysed were those suitably detectable within the eV range. The elements collected from the following emission lines (energies) from the excitation were Ca – Kα – 3.692 keV; Mn – Kα – 5.899 keV; Fe – Kα – 6.404 keV; Sr – Kα – 14.165 keV; Ba – Lα- 4.466 keV and U - Lα-

13.6414 keV. Samples were excited with an energy of 16 keV, except U which was excited with 17.5 keV. Angles were set at 45 degrees to each sample between the Incident X-ray beam and Vortex™ ME-4 Si drift detector. The flat surface of the block was required to create maps of pre-damage and re-growth, at the highest possible resolution. Desired beam current was set to provide appropriate XRF count rates without damaging the shell. 5 μm spots at 10 μm step size (Figure 5.3) was used to create the element maps, and to achieve this spatial resolution, KB mirrors focussed the X-ray beam profile down to 4 μm in both directions. For analysis, shells from those damaged in the temperature-controlled experiments were compared between 5°C (±1.5) and 10°C (±1.5). For experiments where Sr doping took place, 5 and 10°C could not be directly compared due to the regular water changes in the 10°C room.

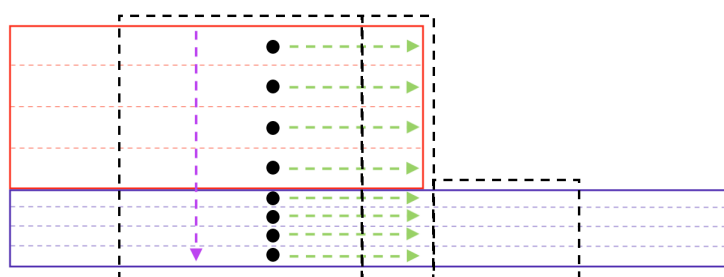


Figure 5.3: Diagrammatic representation of measurements taken at DLS. Green and purple arrows show traces run with μXRD (Chapter 4) and black spots show examples of how μEXAFS were taken through marked points. The black dotted rectangles show μXRF selection areas for each mapped scan (5 μm spots at 10 μm step size). Solid rectangles represent the original (red) and (purple) re-grown shell.

British Geological Survey

Laser Ablation-Inductively Coupled Plasma-Mass Spectrometry (LA-ICP-MS)

To analyse the spatial distribution of elements within the samples, multi-element analysis was performed by Laser Ablation-Inductively Coupled Plasma-Mass Spectrometry (LA-ICP-MS), with the focus on trace element incorporation. This consisted of a NewWave UP193FX excimer (193 nm) laser system with built-in microscope, coupled to an Agilent 7500 series ICP-MS. Whelk shell samples were presented as 10 mm thick polished blocks selected for analysis based on quality of preparation. The use of laser ablation allowed the samples to be analysed in a solid form, retaining the spatial component of measurements within the samples. Before

entering the ICP-MS, the block was secured in the sample tray of the ablation chamber, aligned, and levelled to ensure a flat surface using a combination of blocks and Blu-tack™; along with two homogenous silicate glass reference samples (NIST SRM610 and NIST SRM612) for calibration and quality control respectively. Lolite v2.5 software was used for data reduction and calibration. Concentrations in the calibration and QC standards were taken from the GeoREM on-line database (Jochum *et al.*, 2005). The tray was placed in the gas-tight ablation chamber, before being locked into place. Laser settings were set (Table 5.2) and a stream of helium gas was used to carry the ablated material through to the ICP-MS.

Table 5.2: Settings used for LA-ICP-MS. Laser power was varied to give a typical fluence of 3-5.35 J. cm⁻².

Ablation crater size (μm)	Repetition rate (Hz)	Power (%)	Fluence (Jcm ⁻²)	Irradiance (GWcm ⁻²)	Dwell time (s)	Analytical session
25	10	72	5.35	1.07		2
25	10	75			20	1
50	10	75			30	1
50	10	75			20	1

Data were collected in a time-resolved analysis mode, with individual points set to measure both the calibration SRM610 and quality control SRM612 standards before and after a series of ablations on samples (Figure 5.4). Measurements were taken both along layers and between layers interspersed with points from the SRM 610 standard (n = 3); the standard points being used to regularly, approximately every one hour, to update the calibration. Collected data were analysed from the laser output using the Lolite software and processed with methods outlined in Appendix 9.



Figure 5.4: Diagrammatic representation of the whelk shell (red) with new growth (purple) and transects marked for ablation. Shell layers marked with dashed lines, purple arrow direction from outer to inner shell layers used for vertical laser traces and green arrows the laser ablation tracks horizontally within individual shell layers.

Results

Crystal structure and bond length studies (μ EXAFS)

The work undertaken using μ EXAFS, to determine crystal structure and bond lengths, were intended to investigate (i) if any structural differences occurred between normally growing shells, damage, and re-grown shells and (ii) if the impact of a changed temperature and Sr concentration result in structural differences. It was hypothesised that such structural changes would result in changes in the concentrations of incorporated elements. The μ EXAFS data collected on crystal structure and bond length from the shells of *B. undatum* confirmed the μ XRD data that the calcium carbonate present in the shells is aragonite within both original and rapid shell re-growth (Figure 5.5). Figure 5.5 A demonstrates that the clear peaks within the μ EXAFS data align almost exactly with the peaks of the aragonite standard. Strontium was the strongest element signal detected so it was used to ascertain any potential structural changes as a result of bond length and trace element incorporation. Figure 5.5 B presents the individual theoretical spectra for the bond lengths of Sr-O, Sr-Ca, and Sr-C. Once these are combined, they give the fitted spectra for the analysed sample (Figure 5.5 C).

Table 5.3 summarises these bond lengths for Sr-O, Sr-C and Sr-Ca where there appears to be no obvious difference in the range of values and with the range in bond lengths being replicable between the original and regrown shell sections, along with the known aragonite standard. The bond lengths from a natural aragonite standard showed that the sample was pure aragonite, and this allows a comparison with original (non-damaged) and mechanically-damaged and re-grown whelk shells. These data were then explored further within Figure 5.6, whereby frequency histograms of the bond lengths were assessed against individual experimental set ups. Results show a similar pattern of bond length frequencies for the Sr-O, Sr-C and Sr-Ca bond lengths at temperatures of 5 and 10°C, as well as the original and regrown shell. Those shells growing in the Sr doped seawater had a greater frequency of bond lengths at 2.85 Å compared with at 2.86 Å and the shell regrowth had a very low frequency at 2.56 Å compared with the frequencies in the other growing conditions (Figure 5.6).

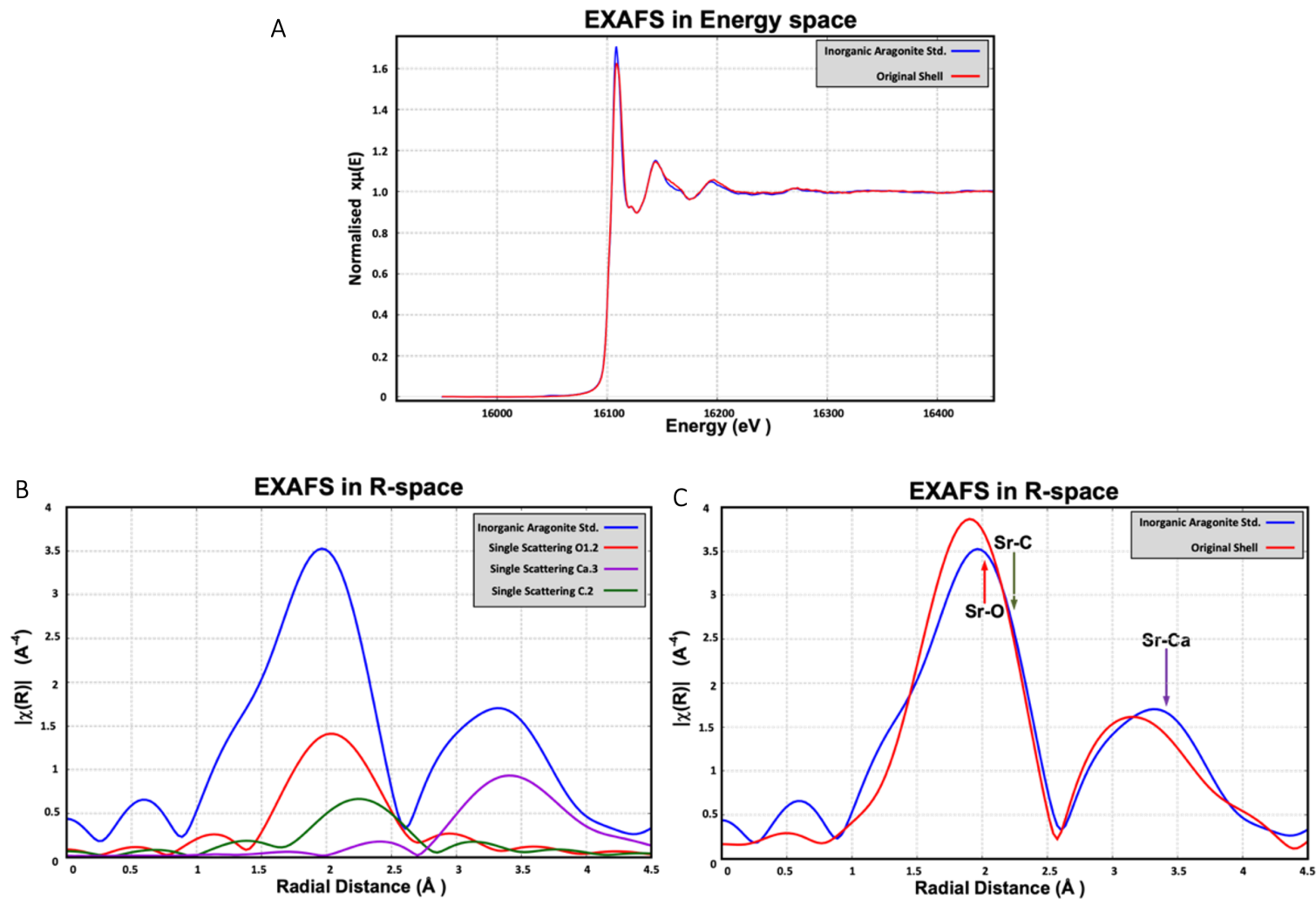


Figure 5.5: A) Raw μ EXAFS data for inorganic aragonite and shell in energy domain, showing strong Sr absorption edge, followed by minor oscillations from surrounding atoms. B) Transformed data in radial domain with theoretical O, C and Ca atom scattering and C) for inorganic aragonite and shell showing very similar peak shapes. Radial distance (\AA) is a measure of the distance between the centres of atoms present.

Table 5.3: Summary of bond lengths (Å) for Sr-O, Sr-C and Sr-Ca in an aragonite standard, in the original shell and repaired shell (new shell) determined using bulk μ EXAFS. ‘Total’ represents average bond length values across a whole shell section, ‘Original’ is bond length data from areas of no shell damage and ‘new shell’ is re-growth and shell repair.

Sample	Sample size	Sr-O	Sr-C	Sr-Ca
Aragonite std.	n = 8	2.57-2.60	2.85-2.89	4.03-4.06
Original shell	n = 36	2.55-2.59	2.84-2.87	4.01-4.05
New shell	n = 28	2.56-2.59	2.84-2.87	4.02-4.04
Total	n = 98	2.56-2.59	2.84-2.87	4.01-4.05

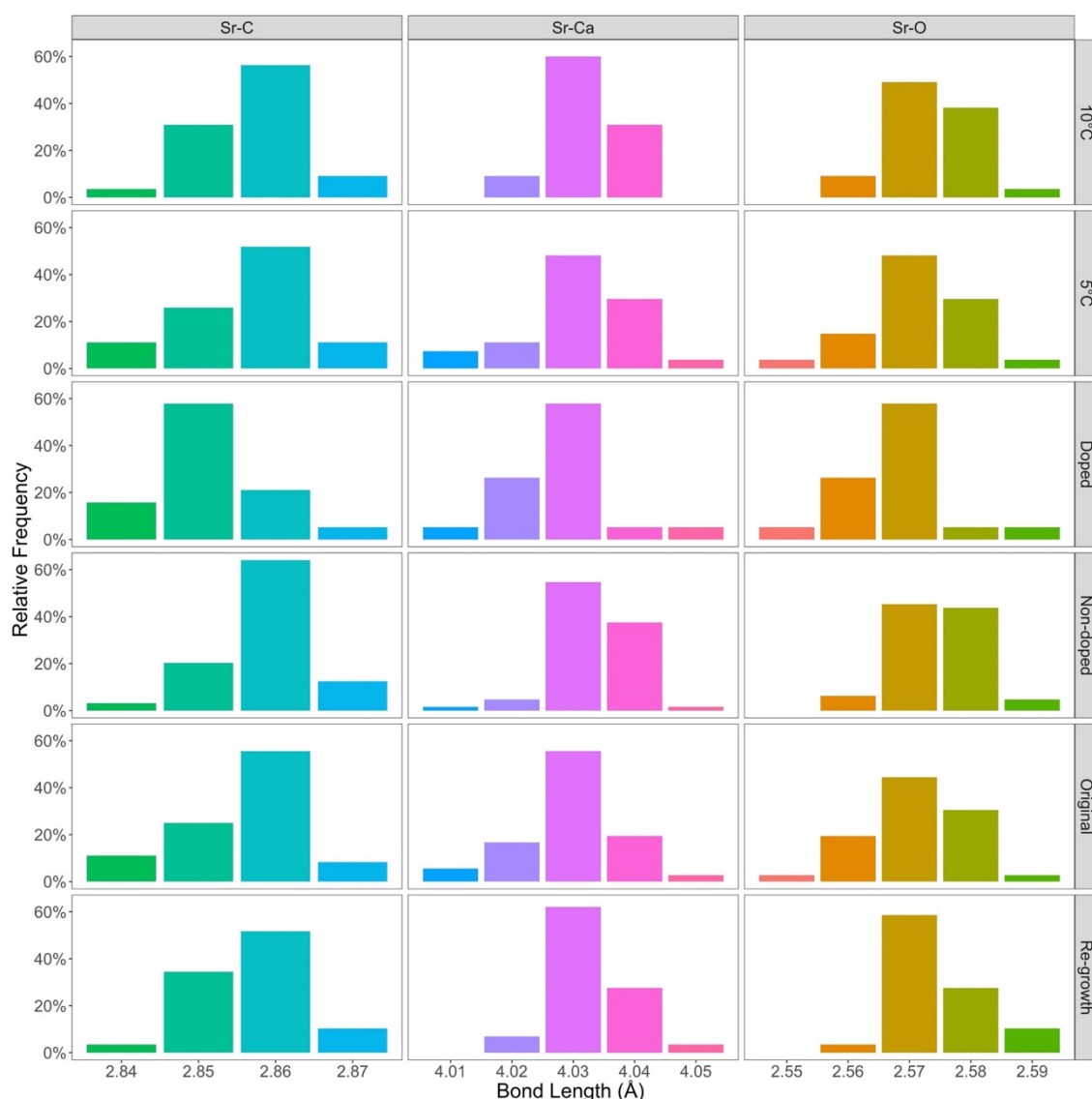


Figure 5.6: Frequency histograms of bond length (Å) for Sr-C, Sr-Ca, and Sr-O, under experiments indicated on right hand Y-axis. Sr doped and Sr non-doped combine 5 and 10°C, and original shell growth is shell material prior to damage. All data are average values for each experiment. Difference in colours between bars identifies individual bond lengths presented.

Trace element incorporation (μ XRF and LA-ICP-MS)

μ XRF

Elemental mapping by micro X-ray fluorescence assessed the spatial distribution of Sr within normal and repaired *B. undatum* shell and investigated any changes in incorporation as a result of strontium doping of the seawater and changing the Sr seawater concentration. X-ray fluorescence data were normalised, and the edge of the shell was defined by where the Ca signal started to decline, and the data for all elements beyond this point were removed from the elemental maps (masked to Ca). The strontium elemental maps produced (Figure 5.7) are colour-coded by relative Sr concentration. The analyses indicated that the outer prismatic layers consistently contained higher Sr concentrations throughout all the shell sections examined. Lowest concentrations were seen in the inner crossed-lamellar layer (Figure 5.7 A–C) with a general trend of decreasing Sr concentrations from the outer surface shell layer into the inner layers. The relative concentration difference is consistent across all examples i.e., the outer layer Sr concentration is approximately 3x the inner layer concentration and the middle layer is approximately 2x the inner layer concentrations (Figure 5.7 A-C). The pre- and post-damage Sr concentrations in the different shell layers are relatively similar. For areas of shell repair and re-growth in whelks growing in the non-doped seawater, there is less strontium in the outer prismatic outer layer than seen in the pre-damage shell (Figure 5.7 A and B). However, in the Sr doped whelk shells the Sr concentrations appear to be relatively similar in the pre- and post-damaged shell growth even though the new repaired shell growth is narrower than the pre-damage shell. The repaired prismatic shell deposited directly beneath the original inner shell layer contained lower concentrations of Sr compared with the prismatic layer in the previous normal shell growth (Figure 5.7 A-C). As each whelk's shell growth was monitored during shell repair it was possible to relate the changes in Sr concentrations to the point when shell repair began.

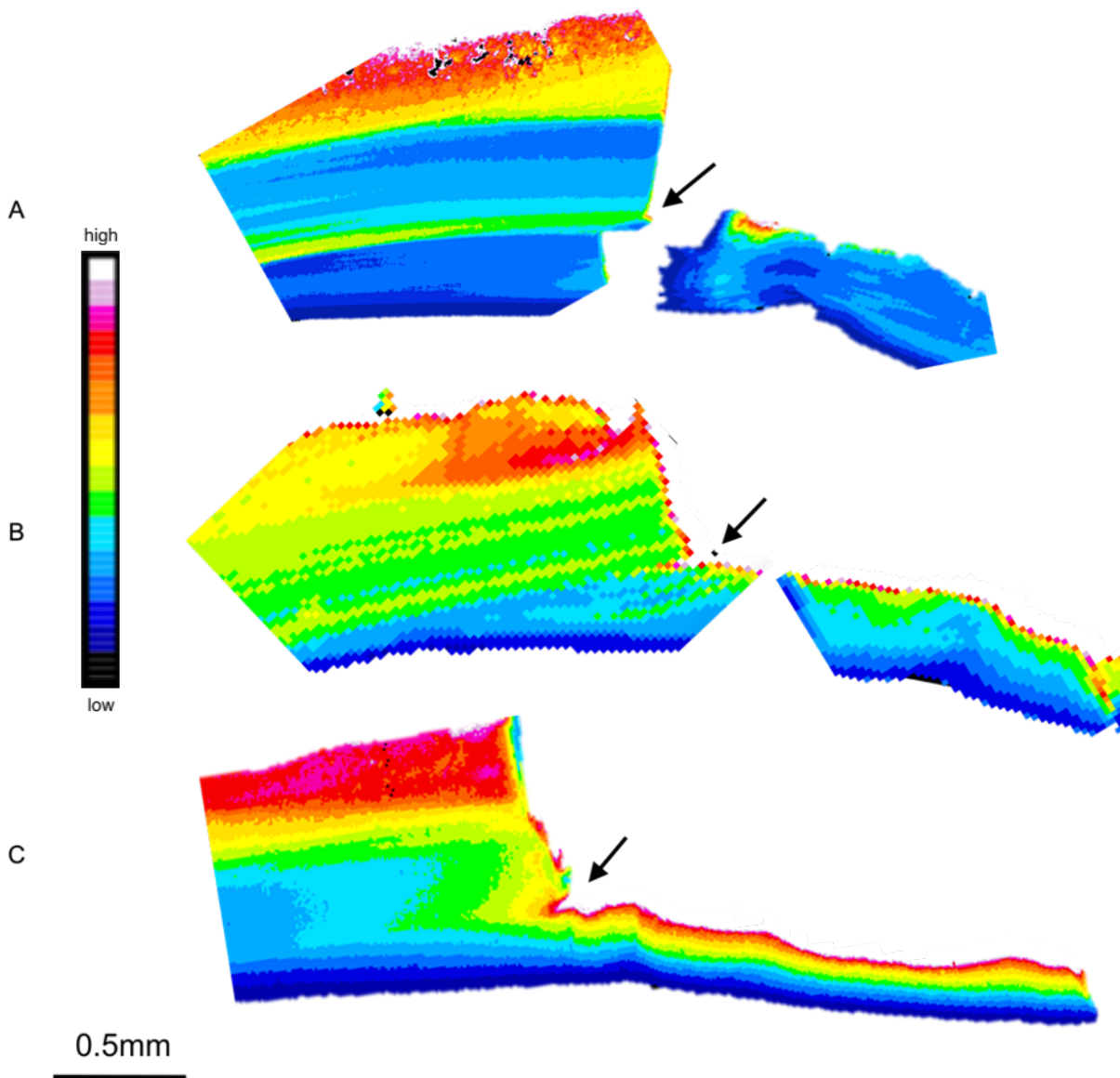


Figure 5.7: Typical examples of μ XRF element maps for normalised Sr/Ca concentrations in shell sections of *Buccinum undatum* shells. Direction of shell growth left to right. Black arrows indicate the point where the shells were experimentally-damaged. A and B) experimentally-damaged and repaired shells in non-doped seawater respectively. C) experimentally-damaged and repaired shell under Sr doped seawater conditions. Scales (Y axes) represent different ranges of concentration of Sr (a.u.) in the shell sections.

LA-ICP-MS

To further understand variations in the elemental composition across the two microstructural layers in the *B. undatum* shells LA-ICP-MS analyses were undertaken across a transect through the outer prismatic into the inner crossed-lamellar layer (see shell section in

Figure 5.8). Only those key elements that were above detection limits (Mg, Sr, Na and Ba) have been plotted in Figure 5.8; Li and Mn data are not shown as their values were below or close to the detection limits. The most obvious result is the abrupt decline in Sr, Mg and Ba concentrations at the interface between the prismatic and crossed-lamellar layers. Sodium concentrations on the other hand increased from the outer prismatic layer to the transition to the crossed-lamellar layer where the values remained stable (Figure 5.8). Although the y-axis scales for each element concentration (ppm) are different, in general, barium showed the greatest variation with the largest relative concentration change per value. The variations in Sr observed agree with the μ XRF analysis maps shown in Figure 5.7; highest concentrations of Sr were observed in the outermost layer of the prismatic microstructure and declined towards the inner crossed-lamellar layer.

To investigate elemental differences in the newly repaired shell following experimental shell damage, sections of shell that encompassed both periods of normal growth and newly repaired growth were analysed using LA-ICP-MS. Horizontal tracks were made along the direction of shell growth in five areas of the shell microstructures to determine temporal consistency in concentrations and between the original deposited shell and repaired shell and re-growth (Figure 5.9). Within each individual microstructure (tracks 1-5, Figure 5.9), all elements showed temporal variability within the five areas, although the most noticeable variation was a decline in the barium concentrations in areas 1 and 2; Ba values were initially high (above 20 ppm) and then declined to 1 ppm (Figure 5.9). Ba concentrations in the crossed-lamellar layer and into the repaired prismatic shell layer were barely above detectable levels. Na displayed a high level of variability in all five areas with no consistent pattern. There were, however, distinct changes in Mg and Sr concentrations between the outer prismatic layer (areas 1 and 2) and crossed-lamellar layer (areas 3 and 4). Concentrations declined abruptly, particularly Mg concentrations in the crossed-lamellar layer (area 3 and 4). Magnesium levels rose again in the newly deposited repaired prismatic shell (area 5) reaching concentrations seen initially in the outer prismatic layers (area 1 and 2). By contrast Sr concentrations continued to decline in the repaired shell (area 5).

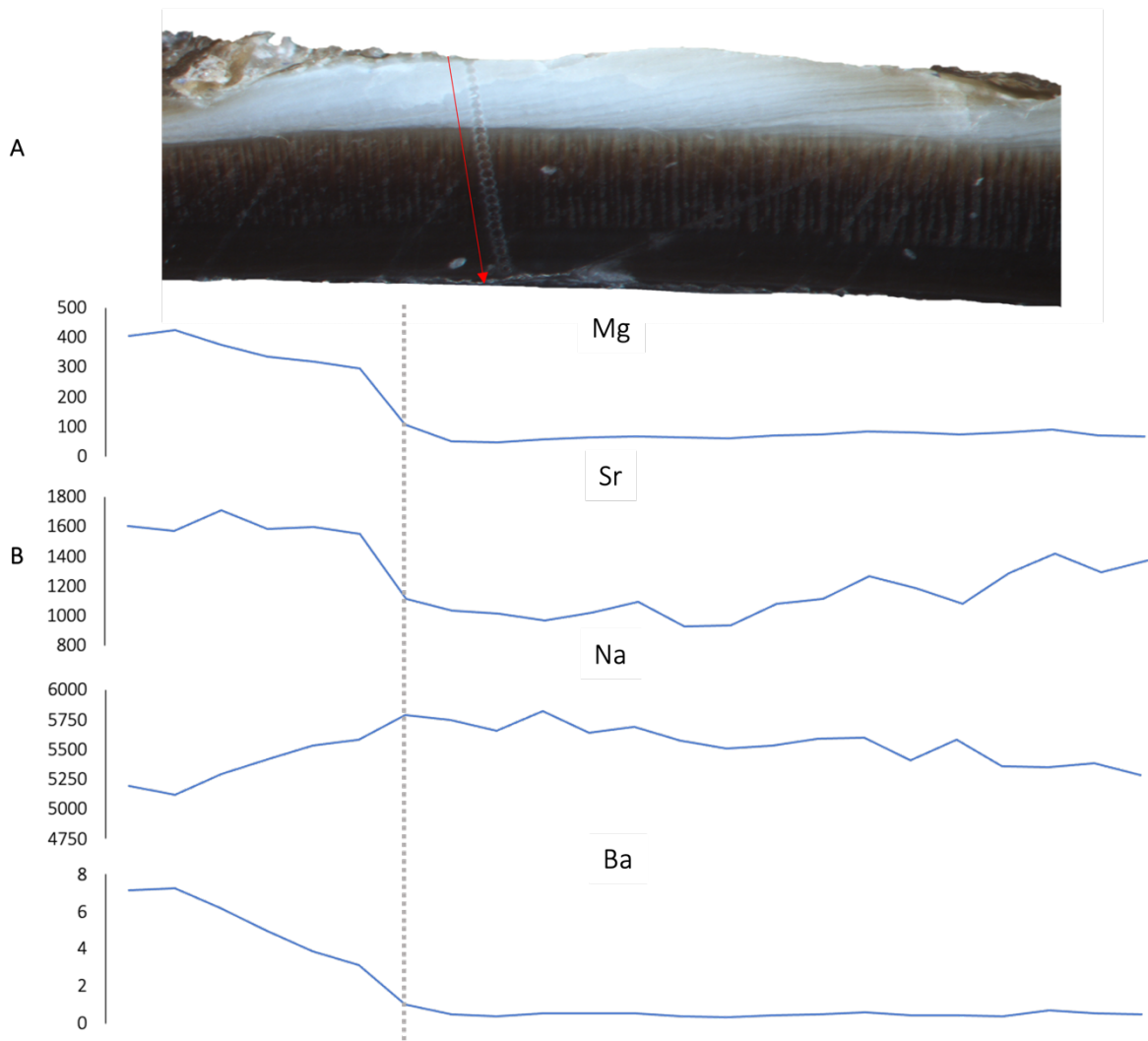


Figure 5.8: A) Photomicrograph of a typical *Buccinum undatum* shell section showing the LA-ICP-MS ablation spots (25 μ spot size) (right of the red dotted track line) through the outer prismatic layer and into the inner crossed-lamellar layer and B) Mg, Sr, Na and Ba traces plotted below the shell section. Grey dashed line marks point of interface between the outer prismatic and the crossed lamellar layers. Units of concentration are ppm.

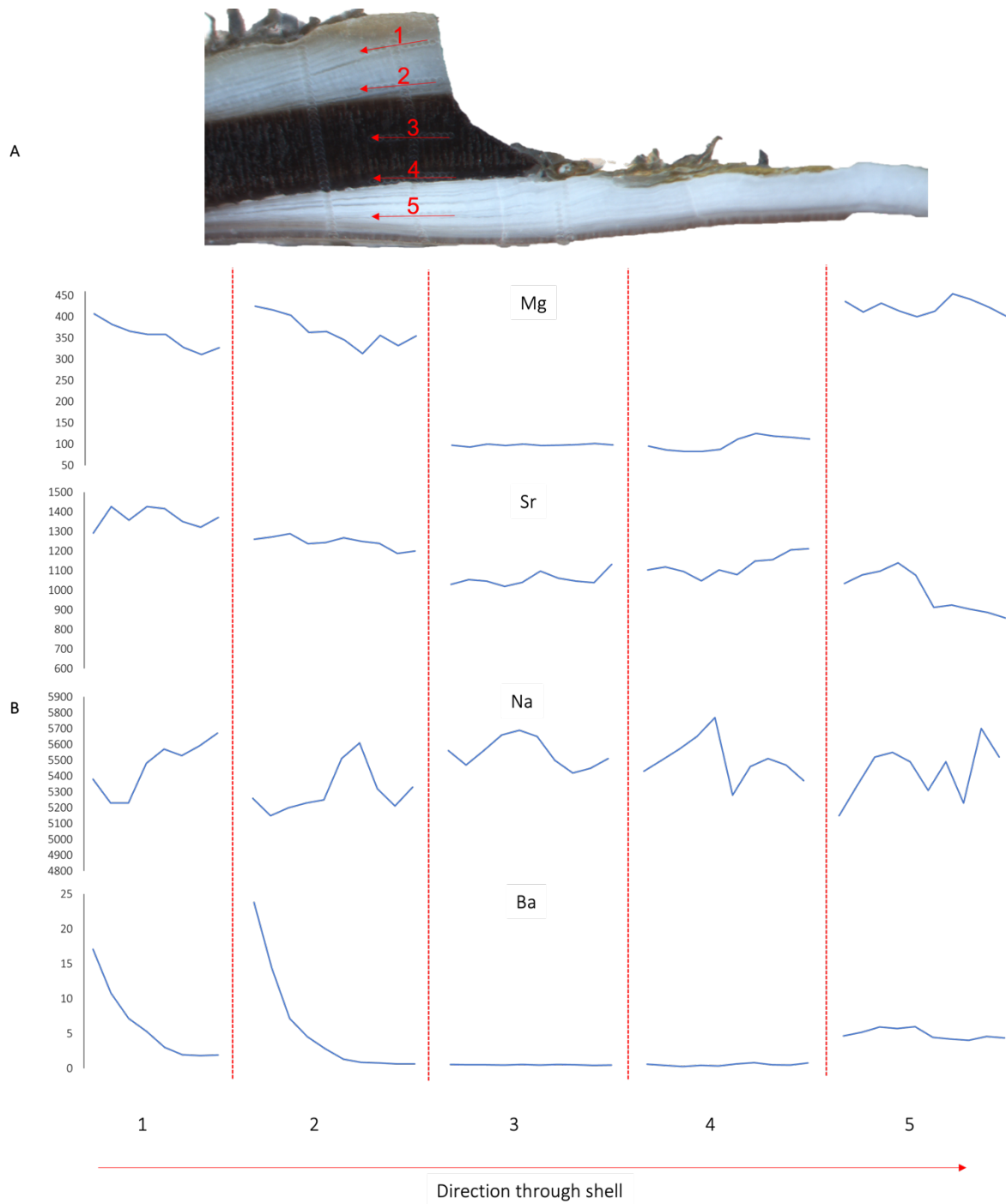


Figure 5.9: A) Photomicrograph of an experimentally-damaged *Buccinum undatum* shell section showing the temporal LA-ICP-MS ablation tracks (25 μ spot size) beneath the horizontal red arrows in five areas (1-5) of the shell. Areas 1 and 2 prismatic shell, areas 3 and 4 crossed-lamellar layer and area 5 newly repaired prismatic shell and B) Mg, Sr, Na and Ba concentrations following LA-ICP-MS analyses in different areas of the shell section showing temporal variations in concentrations along the red arrows through areas 1-5 and through the different structural layers. Red lines show partition between traces and arrows reflect direction of travel for the laser through the shell. Units of concentration are ppm.

Further LA-ICP-MS of the shell section analysed in Figure 5.9 was undertaken but using different orientations of sampling across the shell to investigate any differences in the elemental composition in the different structural parts of the shell i.e., prismatic, and crossed-lamellar layers and normal and repaired shell following shell damage. Figure 5.10 A shows the same section as illustrated in Figure 5.9 A plus an earlier part of the same shell (left image). Five independent tracks were analysed across the shell in different areas of the shell (Figure 5.10 A). Transect 1 tracked across the prismatic and crossed lamellar shell layers of normally deposited shell, transect 2 tracked through prismatic and crossed-lamellar layers of normally deposited shell and repaired prismatic and crossed-lamellar shell, transect 3 tracked through prismatic and crossed-lamellar layers of normally deposited shell and repaired prismatic and crossed-lamellar shell, transect 4 crossed through the crossed-lamellar layer of normally deposited shell and repaired prismatic and crossed-lamellar shell and transect 5 tracked through the repaired prismatic and crossed-lamellar shell (Figure 5.10 C).

The elemental composition of the prismatic and crossed-lamellar shell layers followed the same general pattern to those observed in the shell sections in Figure 5.8 and 5.9. Highest Mg concentrations were present in the prismatic shell layers compared to the crossed-lamellar layers with a marked decline and then rise in Mg concentrations at the prismatic/crossed-lamellar and crossed-lamellar/prismatic shell boundaries respectively (Figure 5.10 B and C). Mg concentrations were high in the outer surface of the newly repaired prismatic shell declining towards the inner shell surface (Figure 5.10 B and C). Variations in Sr and Na concentrations were not so clear cut as both elements displayed a downward trend (with variations) from the outer prismatic layer through the crossed-lamellar and prismatic layer to the inner surface of the shell (Figure 5.10 B and C). Barium concentrations were low (5 ppm) in both the normally deposited prismatic and crossed-lamellar shell layers (Figure 5.10 B for all shell sections 1-3). However, in the newly repaired prismatic shell Ba concentrations were initially elevated (>30 ppm) declining to 5 ppm towards the inner shell surface (Figure 5.10 B and C).

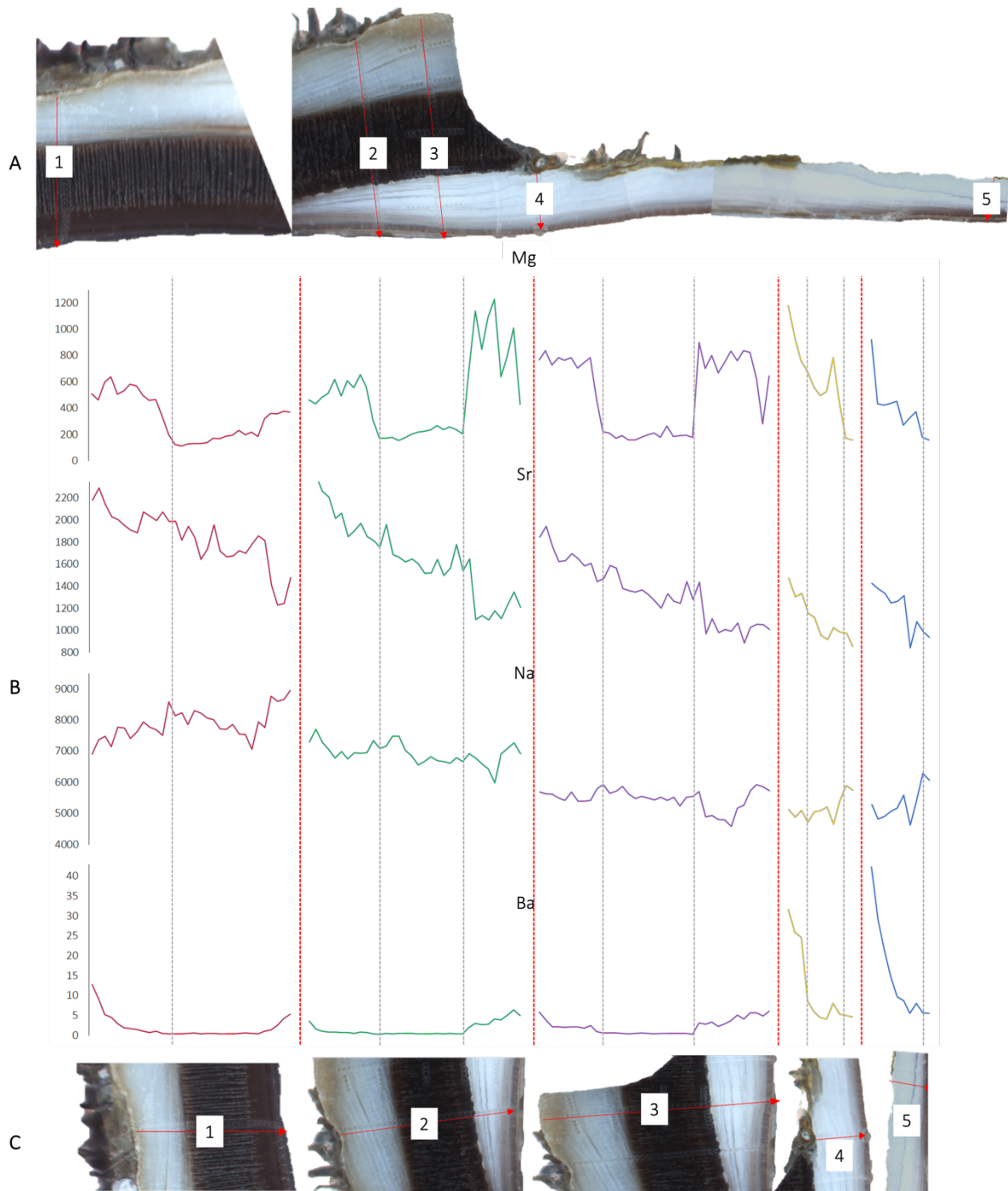


Figure 5.10: A) Photomicrograph of experimentally-damaged *Buccinum undatum* shell with a section of earlier, normally deposited shell (A1). Five vertical LA-ICP-MS ablation tracks (25 μ spot size) along different parts of the shell, from the outer prismatic to the inner crossed-lamellar are shown (red arrows). B) Mg, Sr, Na and Ba concentrations (ppm) along the laser traces (red lines) and across the different microstructure (grey dashed lines). C) 1; normally deposited prismatic and crossed-lamellar shell, 2 and 3; prismatic and crossed-lamellar layers of normally deposited and re-grown shell, 4; crossed-lamellar of normally deposited, and re-grown prismatic and crossed-lamellar shell, 5; regrown prismatic and crossed-lamellar shell.

The final LA-ICP-MS analysis of the *Buccinum undatum* shell sections involved an elemental investigation of regions of the shell of a wild-caught whelks that had been repeatedly damaged, and the shell damage subsequently repaired prior to capture in a baited pot (Figure 5.11). This was undertaken to understand if naturally incurred shell damage had a similar elemental composition to shells that had been experimentally-damaged in the laboratory. Magnesium concentrations were highest in the prismatic layers in all the sections and there was an obvious change in concentration at the prismatic/crossed-lamellar and crossed-lamellar/prismatic layer boundaries. The elemental data for transect 3 is compelling with an obvious increase in Mg where shell repair occurred, and prismatic shell was deposited. Changes in Sr concentrations at the shell layer boundaries almost mirrored the Mg concentration variations across the four transects. Sodium demonstrated similar variations across the four transects that had been observed in previous shell sections (i.e., Figures 5.9 and 5.10). Barium concentrations (>10 ppm) were recorded in the outer edges of the prismatic layer and declined into the crossed-lamellar layer. When prismatic shell was deposited following damage and repair (e.g., transect 3, black arrow) Ba levels of 20 ppm were recorded and then declined. These elemental patterns observed in the naturally damaged shell were similar to those observed in the experimentally-damaged shells (e.g., Mg, Sr and Ba, Figure 5.10 B transects 4 and 5).

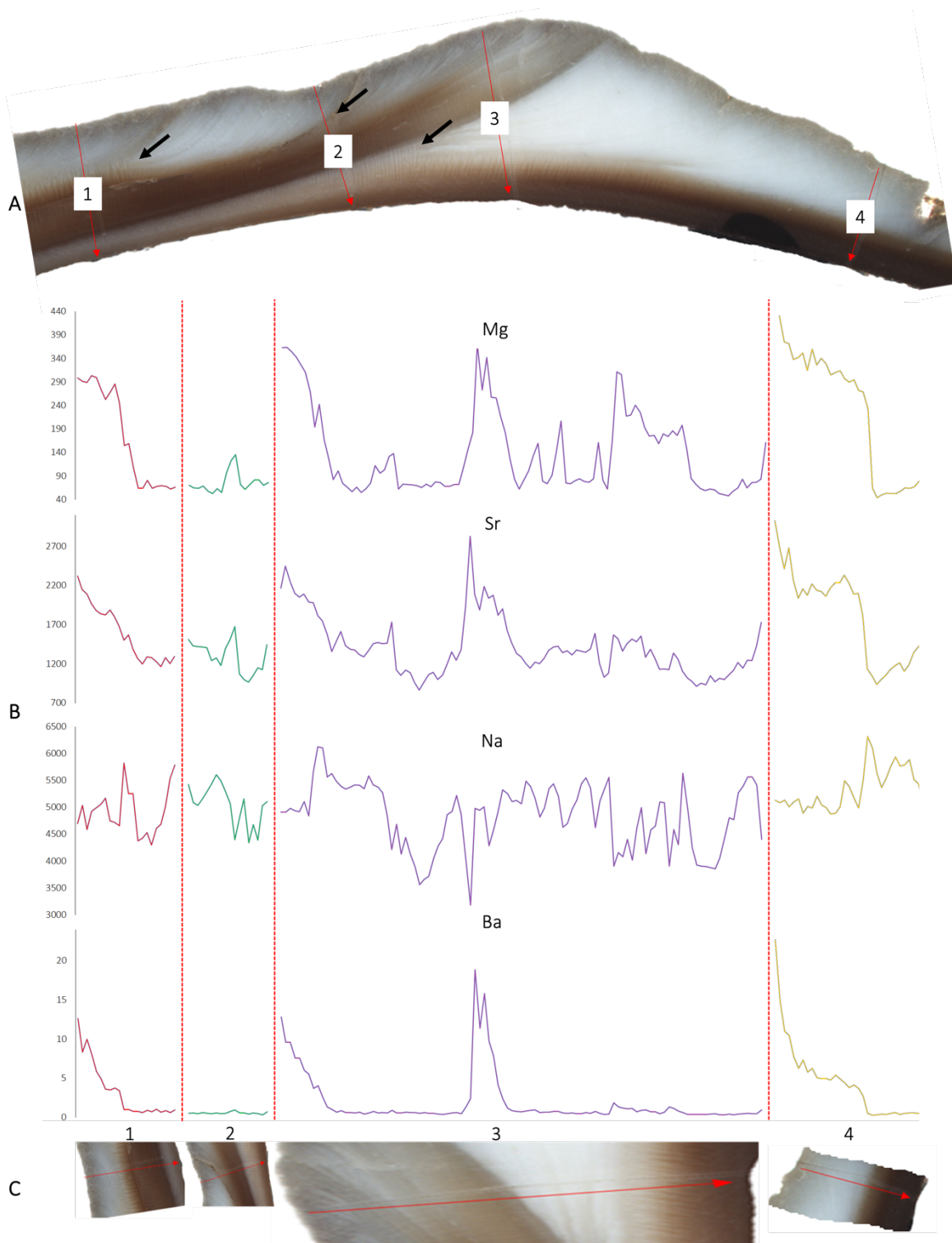


Figure 5.11: A) Photomicrograph of a naturally damaged wild-caught *Buccinum undatum* shell section showing four vertical LA-ICP-MS transects (1-4) across the prismatic and crossed-lamellar shell layers. Natural shell damage occurred in transects 1-3 (black arrows) whilst no shell damage occurred along 4, B) Mg, Sr, Na and Ba concentrations (ppm) along the laser traces (25 μ spot size) (red arrows) are enlarged in C. Vertical red lines in (B) distinguish the four traces, and the red arrows reflect the direction of travel of the laser through the shell.

Having ascertained there were visual differences and changes in elemental concentrations in the prismatic and crossed-lamellar shell structures and this was reflected in the repaired shell (Figures 5.8 – 5.11), Sr concentrations across these different structures were inspected in more detail (see Table 5.4). Data were averaged across shell microstructures to allow for investigation into the variation of experimental treatment under normal growth and rapid shell re-growth. Sr values recorded in the outer shell close to the periostracum were omitted from the data analysis because many of the values were outliers probably as a result of Sr absorption in the outer shell. In some areas of the shell sections very high values of Sr were recorded (e.g., 4304 ppm) and it is likely that these are more porous areas of the shell structure, resulting in increases in absorption within a single localised area. Although a large number of spots (n_{spot}) were taken, the number of shells (n_{shell}) was too few to determine statistically significant differences. However, it can be seen from Table 5.4 that there are clear differences between the Sr doped, and non-doped water, along with temperature on Sr incorporation, with raised levels of Sr and water temperature seeing corresponding increases in Sr ppm within the shell.

Table 5.4: Summary of strontium (Sr, ppm) concentrations from LA-ICP-MS in repaired and normally deposited *Buccinum undatum* shells. Data for the shells from the doped experiments are the combined values from the double and triple concentrations as only a few shells were analysed. Number of ablation spots (n_{spot}) taken from different shell samples (n_{shell}).

Experiment	n_{shell}	n_{spot}	Mean Sr ppm	± 1 StdDev	Mean Maximum Sr ppm	± 1 StdDev	Minimum Sr ppm	Maximum Sr ppm
Repaired shell								
10°C Sr doped	2	53	1834	754	3376	762	792	4304
5°C Sr doped	2	56	1569	575	3017	489	902	3363
10°C	2	116	1290	305	2563	724	808	2221
5°C	2	77	1329	392	2084	194	820	2790
Original shell								
10°C Sr doped	2	88	1587	447	2371	321	821	2796
5°C Sr doped	2	121	1371	237	1945	176	927	2207
10°C	3	344	1550	424	2420	NA	830	3350
5°C	1	101	1316	283	2670	170	929	2420

Discussion

Using a range of state-of-the-art analytical techniques, μ XRF, μ EXAFS and LA-ICP-MS the distribution of biogenic elements (Mg, Sr, Na and Ba) has been demonstrated in different structural parts using shell sections of *Buccinum undatum*. Damaging whelk shells and re-growing them at different seawater temperatures and with additional concentrations of strontium dosed into the seawater, provided a detailed insight and understanding of element distribution in the different shell structures. μ EXAFS analysis unequivocally demonstrated that both the normally deposited and repaired shell of *B. undatum* is aragonite. μ EXAFS undertaken at Diamond Light Source provided further information on atomic distances between the probed atom and their near neighbours. The information obtained allowed an understanding of the lattice arrangements and showed that the process of rapid shell growth during shell repair did not bring about changes in the crystal lattice and changes in bond lengths that might create incorporation site distortions and influence trace element substitution. μ EXAFS analyses showed that the strongest element signal detected was strontium. Using this element, no structural changes in bond length and trace element incorporation between normally deposited and repaired shell were detected. Bond length measurements for the elements Sr-O, Sr-C and Sr-Ca were replicable and similar both in original and regrown shell and to a known aragonite standard. However slight differences in bond length were observed in shells grown in Sr doped seawater where there was a greater frequency of bond lengths at 2.85 Å compared with at 2.86 Å whilst in newly repaired shell, a very low frequency of bond lengths at 2.56 Å compared with the frequencies in the other growing conditions were noted. Table 5 compares the bond-length data for standard aragonite and repaired whelk's shell presented in this chapter with those previously published in the literature (see Table 5.5). All the values are comparable and data in this thesis fall within the range of previously published values.

It has previously been suggested that the high concentrations of Sr in some bio-carbonates are the result of small amounts of the mineral strontianite (SrCO_3) present in the matrix, as opposed to the Sr ions directly substituting for the Ca in the bio-carbonate (Finch and Allison, 2007). These authors found the Sr-Ca bond distance in aragonite to be between 4.02 and 4.12 Å (mean 4.02 Table 5.5) for strontianite. There is no evidence in this thesis (μ XRD Chapter 4) or μ EXAFS (this chapter) to support their supposition. However, obtaining a definitive answer would require further complex analyses and are outside the scope of this

thesis. Nonetheless, the bond lengths in the *B. undatum* shells investigated in this chapter were between 4.01-4.05 Å (Table 5.5) which strongly suggests the element strontium displaces Ca in *B. undatum* shell aragonite.

Table 5.5: Summary of bond lengths (angstroms Å) determined using synchrotron analyses in inorganic aragonite standard material, damaged and repaired *B. undatum* shell fragments (this thesis) and various invertebrate calcified material published in the literature (table adapted from Chenery *et al.*, 2019).

Sample	Sr-O	Sr-C	Sr-Ca	References
Aragonite standard	2.57-2.60	2.85-2.89	4.03-4.06	This study (n = 8)
Aragonite standard	2.57	2.93	3.98	Cook <i>et al</i> , 2016
Aragonite standard	2.58	2.98	4.02	Finch <i>et al</i> , 2003
Whelks	2.56 - 2.59	2.84 - 2.87	4.01 - 4.04	This study (n = 98)
Otolith	2.55 - 2.58	2.85 - 3.01	3.96 - 3.99	Cook <i>et al</i> , 2016
Coral species	2.56 - 2.61	2.86 - 3.01	4.00 - 4.02	Finch <i>et al</i> , 2003
<i>Arctica islandica</i> shell	2.58 - 2.59	2.98 - 3.00	4.02	Foster <i>et al</i> , 2009
Otolith	2.57 - 2.61	2.93 - 2.97	3.97 - 4.01	Doubleday <i>et al</i> , 2014

A combination of techniques was used to visualise the distribution of trace element incorporation into the *B. undatum* shells. μ XRF allowed rapid elemental mapping at a small (5 micron) scale, and initial data on Sr incorporation were collected using these methods. Varying levels of element incorporation were observed in the different shell microstructures, with replication of patterns throughout the rapidly re-grown shell. All the analysed shell sections revealed clear elemental patterns of incorporation in the outer and inner shell layers and these patterns were replicated in both normally deposited shell and the rapidly re-grown shell. The strontium elemental maps showed relative Sr concentrations and indicated that the outer prismatic layer consistently contained higher Sr concentrations throughout all the shell sections examined. Lowest concentrations were seen in the inner crossed-lamellar layer with a general trend of decreasing Sr concentrations from the outer surface shell layer into the inner layers. The outer layer Sr concentration was approximately 3x the inner layer concentration and the middle layer was approximately 2x the inner layer concentrations. LA-ICP-MS allowed rapid and detailed mapping at sub-50-micron scales. These two techniques allowed for both relative concentrations of Sr (μ XRF mapping) and actual incorporation (LA-ICP-MS) of Mg, Sr, Na and Ba to be assessed. Although μ XRF was not calibrated to give an accurate ppm concentration,

using LA-ICP-MS gave a clearer picture of distinct individual changes in element concentrations within the shell structure.

LA-ICP-MS analysis showed there to be clear patterns of element incorporation between shell microstructures, with higher concentrations in the outer prismatic regions, and reducing levels towards the crossed-lamellar area. One of the main features found was that this elemental distribution was replicated within the new rapidly formed shell during periods of shell regeneration and repair. During this period, even though the newly formed prismatic structures are initially not on the exposed edge, due to being re-formed beneath the original shell layers, the highest trace element concentrations were still observed here. Although similar research has been carried out recently in whelks statoliths (Hollyman *et al.*, 2019), currently little is known about variations in trace element incorporation within the shell microstructures, particularly during periods of rapid re-growth in mineralising invertebrate species.

Previous research on the elemental composition of mollusc shells determined using LA-ICP-MS and investigating the element to calcium ratios within bivalve shells in relation to environmental conditions is well known (e.g., Richardson 2001; Foster *et al.*, 2009; Hollyman, 2017; Markulin *et al.*, 2019). However, there is a shortage of information relating to the impact of periods of shell damage (natural or anthropogenic) on elemental incorporation during shell repair. The data presented in this chapter goes a long way towards building on previously published accounts and understanding element incorporation into molluscan shells during periods of shell growth and shell repair. A detailed study of Sr distribution in whelks' shells found there was no obvious difference between normal shell growth and repaired shell growth with little variation under the two different temperature regimes or under Sr-doped water. Previously it has been noted that although annual variation and timing does see a slight effect within the data, due to shell formation occurring at different times of year, calcium carbonate structures formed at the same time should show the same geochemical signature along growth lines for trace element incorporation (Lazareth *et al.*, 2013). This provides a powerful insight into environmental responses at the time of shell formation. Furthermore, this understanding can allow quantification of larval dispersal through element fingerprinting (Honig *et al.*, 2020). However, as reflected within this thesis, previous research in bivalve species has noted that temperature itself only appears to have a minor influence on trace element incorporation into shell aragonite (Carré *et al.*, 2006; Warter *et al.*, 2018), with factors including light exposure

seeing additional impact, for example in laboratory reared *Tridacna crocea*. Nonetheless, for experiments run during this thesis all treatments experienced equal light exposure.

Although several different shell-forming species may co-exist in the same habitat, due to differences in physiology (for example feeding, respiration, reproduction, and rate of biomineralization), differences in shell geochemical composition can arise. An example of this can be with ontogeny and growth rates, whereby trace element incorporation sees positive correlations in some bivalve species. However, for others, for example the mussel *Mytilus edulis*, there are no distinct relationships between Sr/Ca ratios and growth rate (Carré *et al.*, 2006). Due to its importance as a key environmental tracer, and the consistency in results for Sr bonding found with this chapter for *B. undatum*, research into this commercial species would benefit further investigation, in particular with the relationship with seawater temperature and climate change (Doubleday *et al.*, 2014). For other calcifying marine species, where trace element analysis is being used to track environmental variables, these need to be validated if looking at a time-series analysis (Markulin *et al.*, 2019). Thus, allowing factors such as metabolic responses, temperature, and primary productivity to be determined, along with understanding individual growth rates and physiology of molluscan shells (VanPlantinga and Grossman 2019).

It is important to note that in areas of particularly high concentration of trace element, this does not absolutely suggest an increased rate of incorporation within biological carbonate structures, in particular molluscan shells, as it is possible that sudden spikes seen in the data are due more to the organic phase of mineralisation (Harriss, 1965; Nürnberg and Hemleben, 1996; Sinclair *et al.*, 1998; Fallon *et al.*, 1999; Schöne *et al.*, 2010). Although the organic matter within shells, both the insoluble chitin and soluble organic matrix, are not typically thought to contribute to trace element concentrations, it has previously been noted that there are occasional associations which are reflective of the fine scale heterogeneity seen within the shell microstructures, for example Mg within mussels (Lorens and Bender, 1980), and Mn, Cu, Zn and Cd in oyster shells (Carriker *et al.*, 1980). It is important to consider these factors, if using shell carbonates for environmental proxies (Takesue *et al.*, 2008). Deep investigation into the structure and composition of the organic matrix within *B. undatum* shells would be recommended for continued work into the investigations of shell re-growth and structure.

Conclusion

Within studies of sclerochronology, it is necessary to understand the drivers and influencing factors involved in shell chemistry. Through this understanding it will be easier to monitor and re-construct environmental conditions and validate environmental archives (VanPlantinga and Grossman, 2019). Through using experimental techniques of μ EXAFS, μ XRF and LA-ICP-MS, combining assessment of bond length and element concentration within the shells, we disproved the initial hypotheses that there would be a change in crystal structure and trace element incorporation in rapidly re-grown shell material. Results from the research presented in this Chapter did not find a change in concentration with changing mineralogical structure, and the visible difference in trace element incorporation between shell microstructural layers was mimicked within the rapid new shell growth. Nonetheless, the work in this chapter, better helps us to understand the implications of shell damage on whelks' growth, and potential interferences within their recovery capability. This chapter has built on the knowledge gained from Chapters 2-4 to build a complete picture of the mechanisms of shell growth and shell repair. To investigate this further, to see why we see a differing concentration between the shell microstructural layers identified in Chapter 4 using SEM, investigating the differences in crystal growth and how this impacts element concentration would be beneficial. Although this research has furthered our understanding on the element incorporation in the shells of *B. undatum* and the effect that periods of rapid shell re-growth have on this, it is a multifaceted process to disentangle the underlying mechanisms controlling trace element incorporation itself. It is likely that incorporation into the shell is controlled by a complex combination of both kinetic and biological processes (Foster *et al.*, 2009). Understanding the effects that seawater temperature has on seasonal growth dynamics of this commercial species is of importance going forwards, with results from this chapter providing an initial understanding and chemical baseline of data on the shells of *B. undatum*.

Chapter 6 – General Discussion

Below is a schematic to illustrate the relationship of each of the experimental thesis chapters.

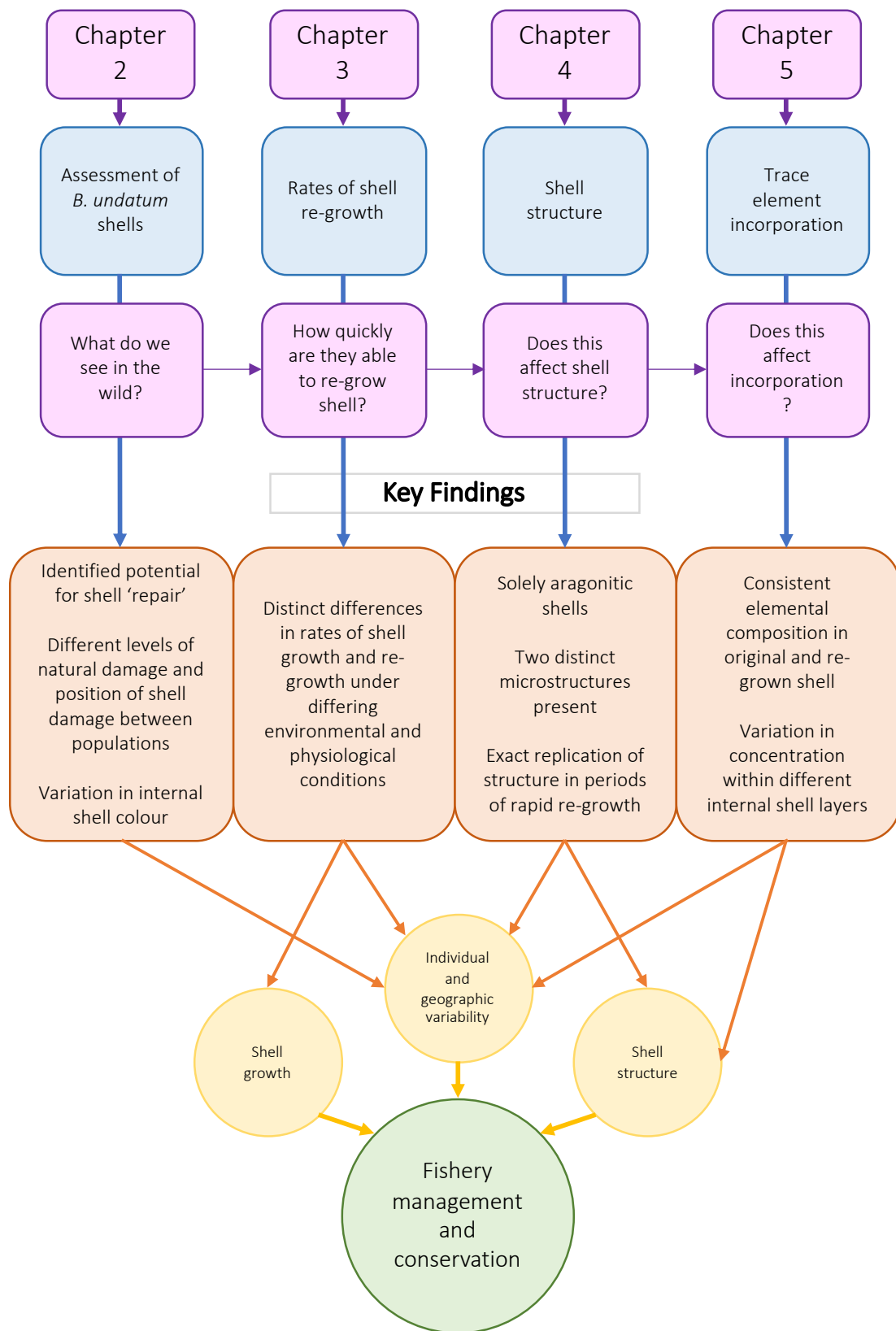


Figure 6.1: Summary diagram showing structure of the thesis with links between the experimental chapters and the overall impacts on the wider scale.

Throughout this thesis, I have investigated and detailed variations in the shell, and the impact of damage on *Buccinum undatum*. Within this framework, geographic variations in colour and damage incidences to the shell in wild populations have been documented along with the rates of shell growth, shell repair and shell structure in experimentally-damaged whelks. Whilst all these factors have their own significance, many have wider implications on the continued management and understanding of *B. undatum* stocks, a species under increasing scrutiny in UK fishery management plans. Figure 6.1 shows how each chapter is related, and how they each provide an understanding of the processes involved following damage to the shell of this key commercial species. Whilst Chapter 1 presents a synthesis of the older and up to date literature on *B. undatum*, places this information in the wider context of the biology of whelks, and identifies areas for the current research presented in this thesis, this general discussion will give an overview of each chapter followed by a summary of the findings within a wider context.

Understanding the variations in level of shell damage received by benthic organisms is key for being able to assess and monitor conservation efforts. In particular, understanding how these factors could directly impact a commercial species, will have clear linkages with the overall management of the fishery, to determine differences in potential growth and the recoverability of the stock in question. Previous reviews, for example Ramsay and Kaiser (1998), have researched the recovery capability of whelks following bottom fishing events, with respect to predation risks and escape capability. However, there had been very little research into the impact on the shell itself and variations seen between individuals and populations. In Chapter 2 I examined the shells of wild-caught *B. undatum* collected from commercial fishers around the UK to look for patterns of damage and any visual differences in the shell shape, colour, and structure. In this chapter, shells were examined for incidences of damage, recorded through scarring present on the shell surface and differences in the internal shell colour. This initial visual inspection allowed the quantification of damage from moderate to severe, leading to this chapter forming the basis of the identification of shell variation, different levels of natural damage to the shells of *B. undatum* along with variation in the position of damage and recognising the potential for shell repair to occur.

With the fishery for whelks being an all-year-round activity in many coastal areas, bettering our understanding of the seasonal impacts on shell growth and particularly recovery

and shell repair is of key importance to both monitor and mitigate negative impacts, for example changes in growth and survival. Furthermore, by studying how individual whelks might respond with increasing age and changing maturity status will allow a better understanding and help provide advice on management strategies. Whilst Chapter 2 explored the levels of shell damage seen in wild whelk populations and the prominence of damage and repair to the shell lip, Chapter 3 investigated variations in growth rate (total shell length increase) and shell re-growth (repair) of whelk in response to laboratory-controlled shell damage under various environmental factors (e.g., seawater temperature, food supply, season, and life stage). In this chapter, multiple and replicated tank-based experiments were undertaken and trials of experimental damage and repair in mature wild caught, juvenile wild-caught, and tank-reared juvenile whelks conducted. Several findings from this chapter, including the effects of seawater temperature, food availability and life stage on whelk growth and repair have been published recently in a peer-reviewed paper (Colvin *et al.*, 2022b; see Appendix 10).

Understanding shell growth and its structural components is becoming of greater importance, in furthering our knowledge of potential adjustments which may occur because of a changing environment. Having established and investigated variations in shell morphology (Chapter 2) and rates of shell growth and repair (Chapter 3), Chapter 4 investigated the internal crystal structure of *B. undatum* shells to identify if there were any variations and differences in structure during rapid shell re-growth (repair). This was achieved initially through μ XRD (X-ray diffraction), to identify the mineralogical form of calcium carbonate present in the shells and to determine if this structure differs in rapidly re-grown shell material. Light microscopy and calcein staining of the shell helped to establish the point of shell re-growth and damage and to understand the general shell formation and patterns of growth. The final assessment of the shell structure was achieved using scanning electron microscopy, to fully establish the whelk's shell microstructure and to investigate microstructural changes within the shell.

Progression through each chapter of this thesis has seen a finer-scale approach to investigating the variations in the shell and structure of *B. undatum*. Chapter 5 completes the study of the growth and structure of the *B. undatum* shell through an analysis of the shell at the elemental scale using the most up to date analytical techniques of: μ EXAFS for atomic bond length determinations, μ XRF to produce element maps, and LA-ICP-MS for establishing exact concentrations of trace element incorporation into the shell, (LA-ICP-MS), to ascertain actual

ppm concentration values in the shell. The research carried out in this chapter has provided a good understanding on element incorporation within whelk shells, and identified any variations observed under different environmental conditions and during periods of rapid shell re-growth. However, as stated within this chapter, disentangling the underlying processes has been a difficult task, with both kinetic and biological processes involved in the mechanisms of incorporation.

In conclusion, this thesis has answered three key questions (see Figure 6.2), the answers of which led into the bigger question of: how can we continue to sustainably manage this commercially-fished species?

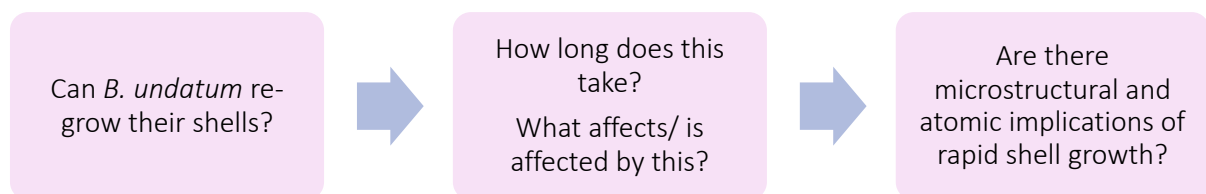


Figure 6.2: Chain of questions posed and then answered throughout the thesis.

Despite the large variability in shell type and structure, the general process of shell formation is shared between different mollusc species, whereby the outer mantle surface secretes the calcareous sheet onto the outer periostracum (e.g., Clark *et al.*, 2020). The molluscan shell is built up through secretions from the mantle during the process of biomineralization (Sleight *et al.*, 2015), and it is thought that the mantle is possibly divided into different areas for producing different types of microstructures (Sleight *et al.*, 2015). Although required for the continued protection and support of an organism, the processes of calcification, due to the transport and precipitation of CaCO₃ crystals, is a highly metabolic process (Palmer, 1992, Clark *et al.*, 2020), and therefore, the rapid periods of shell growth and repair following periods of damage are highly costly to the individual (Thomsen *et al.*, 2013; Colvin *et al.*, 2022b).

Within this thesis it has been determined that specific factors influence rates of shell growth and shell repair. However, it has been difficult to disentangle the complex interactions involved in the natural environment, for example, predatory risk and competition (see

Appendix 1). Nonetheless, all the underlying factors tested, outlined in Chapters 2, 3 and 4 of this thesis, help determine the mechanisms of shell growth and 'repair' whereby, differences in rates of growth occur, and a vast range in morphological features of the shell are observed, with differences noted both between and within a single population. Furthermore, Chapters 4 and 5 demonstrated that the internal microstructure, aragonitic composition and level of trace element incorporation remains consistent within both rapidly formed repaired shell growth and the original shell, under multiple experimental conditions, leading to further potential research into how and why the shell material can be rapidly deposited.

Whilst there is still considerable knowledge to be learned, including the mechanisms of calcium uptake into the shell, the formation of the organic matrix and the movements of biogenic elements involved in biomineralization into the shell (Richardson *et al.*, 1981; Simkiss and Wilbur, 1989; Miyamoto *et al.*, 2005; Kobayashi and Samata, 2006; Bonucci, 2007; Hollyman, 2017; Clark *et al.*, 2020; Colvin *et al.*, 2022b), it is recommended that in future studies, trace element and stable isotope incorporation into the shells of *B. undatum* are investigated with respect to geographic location and individual populations to look for differences in population growth. Furthermore, with an increasing concern on climate change and fishery pressures, using the knowledge gained from this thesis on growth rates and trace element incorporation into the shell, a baseline of data to continue research has been established thus gaining a further insight into how rapid shell growth can occur and its physiological implications to *B. undatum* and their enclosing shell. This research in particular will be carried out between 2023 to 2024 with a successful application to Fisheries Industry Science Partnerships scheme, using techniques and data from this thesis to investigate how both near- and long-term climate models could impact the whelk populations in UK waters. In having this information, we can better manage and advise fishery management plans, and in the greater scheme lead to enhanced social, economic and environmental sustainability of whelk fisheries through understanding how these populations recover and respond to changes in their environment and damage. Moreover, in developing the methodological techniques within this thesis, the methods could be applied to a wider range of marine molluscan species to ascertain recovery capabilities and investigate growth.

References

- Addadi, L., Joester, D., Nudelman, F., Weiner S., 2006. Mollusk shell formation: a source of new concepts for understanding biomineralization processes. *Chemistry – A European Journal*, 12, pp. 980–987.
- Addadi, L., Raz, S., Weiner, S., 2003. Taking advantage of disorder: amorphous calcium carbonate and its roles in biomineralization. *Advanced Materials*, 15(12), pp. 959-970.
- Almada-Villela, P.C., Davenport, J., Gruffydd, L.D., 1982. The effects of temperature on the shell growth of young *Mytilus edulis* L. *Journal of Experimental Marine Biology and Ecology*, 59(2-3), pp. 275-288.
- Arthur, M.A., Williams, D.F., Jones, D.S., 1983. Seasonal temperature-salinity changes and thermocline development in the mid-Atlantic Bight as recorded by the isotopic composition of bivalves. *Geology*, 11(11), pp. 655-659.
- Avanzi, C., Heer, K., Büntgen, U., Labriola, M., Leonardi, S., Opgenoorth, L., Piermattei, A., Urbinati, C., Vendramin, G.G., Piotti, A., 2020. Individual reproductive success in Norway spruce natural populations depends on growth rate, age and sensitivity to temperature. *Heredity*, 124(6), pp. 685-698.
- Barats, A., Amouroux, D., Pécheyran, C., Chauvaud, L., Donard, O.F.X., 2008. High-frequency archives of manganese inputs to coastal waters (Bay of Seine, France) resolved by the LA-ICP-MS analysis of calcitic growth layers along scallop shells (*Pecten maximus*). *Environmental Science & Technology*, 42(1), pp. 86-92.
- Basham, M., Filik, J., Wharmby, M.T., Chang, P.C., El Kassaby, B., Gerring, M., Aishima, J., Levik, K., Pulford, B.C., Sikharulidze, I., Sneddon, D., 2015. Data analysis workbench (DAWN). *Journal of Synchrotron Radiation*, 22(3), pp. 853-858.
- Bell, J.J., 2008. Similarity in connectivity patterns for two gastropod species lacking pelagic larvae. *Marine Ecology Progress Series*, 357, pp. 185-194.
- Benestan, L., 2020. Population genomics applied to fishery management and conservation. *Population genomics: Marine organisms*, pp. 399-421.
- Bennett, D.B., 1974. The effects of pot immersion time on catches of crabs, *Cancer pagurus* L. and lobsters, *Homarus gammarus* (L.). *ICES Journal of Marine Science*, 35(3), pp. 332-336.

- Bergmann, M., Beare, D.J., Moore, P.G., 2001. Damage sustained by epibenthic invertebrates discarded in the Nephrops fishery of the Clyde Sea area, Scotland. *Journal of Sea Research*, 45(2), pp. 105-118.
- Berry, R.J., Crothers, J.H., 1974. Visible variation in the dog whelk, *Nucella lapillus*. *Journal of Zoology*, 174(1), pp. 123-148.
- Bevelander, G., Benzer, P., 1948. Calcification in marine molluscs. *The Biological Bulletin*, 94(3), pp. 176-183.
- Bevelander, G., Nakahara, H., 1969. An electron microscope study of the formation of the nacreous layer in the shell of certain bivalve molluscs. *Calcified Tissue Research*, 3(1), pp. 84-92.
- Bonser, R.H., 1996. The mechanical properties of feather keratin. *Journal of Zoology*, 239(3), pp. 477-484.
- Bonucci, E., 1992. *Calcification in Biological Systems*. CRC Press, Boca Raton, Florida.
- Bonucci, E., 2007. *Biological Calcification: Normal and Pathological Processes in the Early Stages*. Springer Science and Business Media, New York.
- Borsetti, S., Hollyman, P.R., Munroe, D., 2021. Using a sclerochronological approach to determine a climate-growth relationship for waved whelk, *Buccinum undatum*, in the US Mid-Atlantic. *Estuarine, Coastal and Shelf Science*, 252, p. 107255.
- Borsetti, S., Munroe, D., Rudders, D., Chang, J.H., 2020. Timing of the reproductive cycle of waved whelk, *Buccinum undatum*, on the US Mid-Atlantic Bight. *Helgoland Marine Research*, 74(1), pp. 1-14.
- Borsetti, S., Munroe, D., Rudders, D.B., Dobson, C., Bochenek, E.A., 2018. Spatial variation in life history characteristics of waved whelk (*Buccinum undatum* L.) on the U.S. mid-Atlantic continental shelf. *Fisheries Research*, 198, pp. 129-137
- Bourdeau, P.E., Johansson, F., 2012. Predator-induced morphological defences as by-products of prey behaviour: A review and prospectus. *Oikos*, 121(8), pp. 1175-1190.
- Broecker, W.S., Peng, T.H., 1982. *Tracers in the Sea*. Palisades, New York: Lamont-Doherty Geological Observatory, Columbia University.
- Brokordt, K., Guderley, H., Guay M., Gaymer, C.F., Himmelman, J.H., 2003. Sex differences in reproductive investment: maternal care reduces escape response capacity in the whelk *Buccinum undatum*. *Journal of the Marine Biological Association of the United Kingdom*, 291, pp. 161-180

- Bubel, A., 1973. An electron-microscope study of periostracum formation in some marine bivalves. I. The origin of the periostracum. *Marine Biology*, 20(3), pp. 213-221.
- Buchardt, B., Fritz, P., 1978. Strontium uptake in shell aragonite from the freshwater gastropod *Limnaea stagnalis*. *Science*, 199(4326), pp. 291-292.
- Burgio, L., Clark, R.J., 2000. Comparative pigment analysis of six modern Egyptian papyri and an authentic one of the 13th century BC by Raman microscopy and other techniques. *Journal of Raman Spectroscopy*, 31(5). pp. 395-401.
- Burt, E.H., 1977 (ed.). Tips on wings and other things. In *The Behavioural Significance of Color*. STPM Press, New York. pp. 75–110.
- Cadée, G.C., 1999. Shell damage and shell repair in the Antarctic limpet *Nacella concinna* from King George Island. *Journal of Sea Research*, 41(1-2), pp. 149-161.
- Cadée, G.C., Boon, J.P., Fischer, C.V., Mensink, B.P., Ten Hallers-Tjabbes, C.C., 1995. Why the whelk (*Buccinum undatum*) has become extinct in the Dutch Wadden Sea. *Netherlands Journal of Sea Research*, 34(4), pp. 337-339.
- Carlson, W.D., 1983. The polymorphs of CaCO₃ and the aragonite-calcite transformation. *Reviews in Mineralogy and Geochemistry*, 11(1), pp. 191–225.
- Carré, M., Bentaleb, I., Bruguier, O., Ordinola, E., Barrett, N.T., Fontugne, M., 2006. Calcification rate influence on trace element concentrations in aragonitic bivalve shells: evidences and mechanisms. *Geochimica et Cosmochimica Acta*, 70(19), pp. 4906-4920.
- Carriker, M.R., Palmer, R.E., Sick, L.V., Johnson, C.C., 1980. Interaction of mineral elements in sea water and shell of oysters (*Crassostrea virginica* (Gmelin)) cultured in controlled and natural systems. *Journal of Experimental Marine Biology and Ecology*, 46(2), pp. 279-296.
- Chase, J.M., 1999. Food web effects of prey size refugia: variable interactions and alternative stable equilibria. *The American Naturalist*, 154(5), pp. 559-570.
- Chateigner, D., Hedegaard, C., Wenk, H.R., 2000. Mollusc shell microstructures and crystallographic textures. *Journal of Structural Geology*, 22(11-12), pp. 1723-1735.
- Chatzinikolaou, E., Richardson, C.A., 2007. Evaluating the growth and age of the netted whelk *Nassarius reticulatus* (gastropoda: nassaridae) from statolith growth rings. *Marine Ecological Progress Series*, 342, pp. 163-176.
- Chave, K.E., 1954. Aspects of the biogeochemistry of magnesium 1. Calcareous marine organisms. *The Journal of Geology*, 62(3), pp. 266-283.

- Checa, A., 1993. Non-predatory shell damage in recent deep-endobenthic bivalves from Spain. *Palaeogeography, Palaeoclimatology, Palaeoecology*, 100(3), pp. 309-331.
- Checa, A.G., 2018. Physical and biological determinants of the fabrication of molluscan shell microstructures. *Frontiers in Marine Science*, 5, p.353.
- Checa, A.G., Harper, E.M., 2010. Spikey bivalves: intra-periostracal crystal growth in anomalodesmatans. *The Biological Bulletin*, 219(3), pp. 231-248.
- Chew, D., Drost, K., Marsh, J.H., Petrus, J.A., 2021. LA-ICP-MS imaging in the geosciences and its applications to geochronology. *Chemical Geology*, 559, p.119917.
- Cintra-Buenrostro, C.E., 2007. Trampling, peeling and nibbling mussels: an experimental assessment of mechanical and predatory damage to shells of *Mytilus trossulus* (Mollusca: Mytilidae). *Journal of Shellfish Research*, 26(1), pp. 221-231.
- Clark, M.R., Althaus, F., Schlacher, T.A., Williams, A., Bowden, D.A., Rowden, A.A., 2016. The impacts of deep-sea fisheries on benthic communities: a review. *ICES Journal of Marine Science: Journal Du Conseil*, 73(suppl 1), i51-i69.
- Clark, M.S., Fraser, K.P., Peck, L.S., 2008. Antarctic marine molluscs do have an HSP70 heat shock response. *Cell Stress and Chaperones*, 13(1), pp. 39-49.
- Clark, M.S., Peck, L.S., Arivalagan, J., Backeljau, T., Berland, S., Cardoso, J.C.R., Caurcel, C., Chapelle, G., De Noia, M., Dupont, S., Gharbi, K., Hoffman, J.I., Last, K.S., Marie, A., Melzner, F., Michalek, K., Morris, J., Power, D.M., Ramesh, K., Sanders, T., Sillanpää, K., Sleight, V.A., Stewart-Sinclair, P.J., Sundell, K., Telesca, L., Vendrami, D.L.J., Ventura, A., Wilding, T.A., Yarra, T., Harper, E.M., 2020. Deciphering mollusc shell production: the roles of genetic mechanisms through to ecology, aquaculture and biomimetics. *Biological Reviews*, 95 pp. 1812-1837.
- Colvin, C.N., 2016. Timing of shell growth and repair in the whelk *Buccinum undatum* under experimental conditions. Unpublished Master of Marine Biology thesis, Bangor University.
- Colvin, C.N., Hold, N., Jones, M., Turner, R., Heney, C., Philips, E., 2022a. *Whelk: Stock Assessment*. Welsh Government Report
- Colvin, C.N., Hollyman, P.R., Richardson, C.A., Chenery, S.R.N., Waggitt, J.J., McCarthy, I.D., 2022b. The effect of environmental factors on shell growth and repair in *Buccinum undatum*. *Journal of Experimental Marine Biology and Ecology*, 551, p. 151720.
- Comfort, A., 1951. The pigmentation of molluscan shells. *Biological Reviews*, 26(3), pp. 285-301.

- Connell, J.H., 1974. Ecology: Field experiments in marine ecology. In: Mariscal. R., (ed.), *Experimental Marine Biology*, Academic Press, New York. pp. 21-54.
- Cook, L.M., 1986. Polymorphic snails on varied backgrounds. *Biological Journal of the Linnean Society*. 29, pp. 89-99.
- Cook, L.M., Kenyon, G., 1993. Shell strength of colour morphs of the mangrove snail *Littoraria pallescens*. *Journal of Molluscan Studies*, 59, pp. 29-34.
- Cook, P.K., Dufour, E., Languille, M.A., Mocuta, C., Réguer, S., Bertrand, L., 2016. Strontium speciation in archaeological otoliths. *Journal of Analytical Atomic Spectrometry*, 31(3), pp.700-711.
- Crawford, K.M., Whitney, K.D., 2010. Population genetic diversity influences colonization success. *Molecular Ecology*, 19(6), pp. 1253-1263.
- Crippa, G., Griesshaber, E., Checa, A.G., Harper, E.M., Roda, M.S., Schmahl, W.W., 2020. Orientation patterns of aragonitic crossed-lamellar, fibrous prismatic and myostracal microstructures of modern *Glycymeris* shells. *Journal of Structural Biology*, 212(3), p. 107653.
- Cross, E.L., Peck, L.S., Harper, E.M., 2015. Ocean acidification does not impact shell growth or repair of the Antarctic brachiopod *Liothyrella uva* (Broderip, 1833). *Journal of Experimental Marine Biology and Ecology*, 462, pp. 29-35.
- Cross, E.L., Peck, L.S., Lamare, M.D., Harper, E.M., 2016. No ocean acidification effects on shell growth and repair in the New Zealand brachiopod *Calloria inconspicua* (Sowerby, 1846). *ICES Journal of Marine Science*, 73(3), pp. 920-926.
- Crothers, J.H., 1983. Variation in dog-whelk shells in relation to wave action and crab predation. *Biological Journal of the Linnean Society*, 20(1), pp. 85-102.
- Currey, J.D., 1977. Mechanical properties of mother of pearl in tension. *Proceedings of the Royal society of London. Series B. Biological sciences*, 196(1125), pp. 443-463.
- Currey, J.D., Taylor, J.D., 1974. The mechanical behaviour of some molluscan hard tissues. *Journal of Zoology*, 173(3), pp. 395-406.
- Dakin, W. J., 2012. *Buccinum* (The whelk). Liverpool Marine Biological Committee., Memoir No. 20. London: William and Norgate.
- Dautzenberg, P., Fischer, H., 1912. *Mollusques provenant des campagnes de l'Hirondelle et de la Princesse-Alice dans les Mers du Nord*, Résultats des Campagnes Scientifiques Accomplies sur son Yacht par Albert Ier Prince Souverain de Monaco, Monaco: Imprimerie de Monaco

- Davies, P.S., 1966. Physiological ecology of *Patella*. I. the effect of body size and temperature on metabolic rate. *Journal of the Marine Biological Association of the United Kingdom*, 46(3), pp. 647-658.
- de Muizon, C.J., Iandolo, D., Nguyen, D.K., Al-Mourabit, A., Rousseau, M., 2022. Organic matrix and secondary metabolites in nacre. *Marine Biotechnology*, 24(5), pp. 831-842.
- de Paula, S.M., Silveira, M., 2009. Studies on molluscan shells: contributions from microscopic and analytical methods. *Micron*, 40(7), pp. 669-690.
- De Vooy, C., Van der Meer, J., 1998. Changes between 1931 and 1990 in by-catches of 27 animal species from the southern North Sea. *Journal of Sea Research*, 39(3-4), pp. 291-298.
- Devriendt, L.S., Mezger, E.M., Olsen, E.K., Watkins, J.M., Kaczmarek, K., Nehrke, G., De Nooijer, L.J., Reichart, G.J., 2021. Sodium incorporation into inorganic CaCO₃ and implications for biogenic carbonates. *Geochimica et Cosmochimica Acta*, 314, pp. 294-312.
- Dietl, G.P., 2004. Origins and circumstances of adaptive divergence in whelk feeding behavior. *Palaeogeography, Palaeoclimatology, Palaeoecology*, 208(3-4), pp. 279-291.
- Dietzel, M., Gussone, N., Eisenhauer, A., 2004. Co-precipitation of Sr²⁺ and Ba²⁺ with aragonite by membrane diffusion of CO₂ between 10 and 50°C. *Chemical Geology*, 203(1-2), pp. 139-151.
- Dodd, J.R., 1967. Magnesium and strontium in calcareous skeletons: a review. *Journal of Paleontology*, pp. 1313-1329.
- Dong, Y.W., Liao, M.L., Han, G.D., Somero, G.N., 2022. An integrated, multi-level analysis of thermal effects on intertidal molluscs for understanding species distribution patterns. *Biological Reviews*, 97(2), pp. 554-581.
- Dorsett, D. A., 1986. Brains to cells: the neuroanatomy of selected gastropod species. In: Willow, D.A.O., (eds.) *The Mollusca. Neurobiology and behaviour*, part II. Academic Press, New York. pp. 101-187.
- Doubleday, Z.A., Harris, H.H., Izzo, C., Gillanders, B.M., 2014. Strontium randomly substituting for calcium in fish otolith aragonite. *Analytical Chemistry*, 86(1), pp. 865-869.
- Dumont, C.P., Roy, J.S., Himmelman, J.H., 2008. Predation by the sea urchin *Strongylocentrotus droebachiensis* on capsular egg masses of the whelk *Buccinum undatum*. *Journal of the Marine Biological Association of the United Kingdom*. 88, pp. 1025-1031.
- Dyke, A., Dale, J., McNeely, R., 1996. Marine molluscs as indicators of environmental change in glaciated North America and Greenland during the last 18 000 years. *Géographie physique et Quaternaire*, 50(2), pp. 125-184.

- Ebert, T.A., 1968. Growth rates of the sea urchin *Strongylocentrotus purpuratus* related to food availability and spine abrasion. *Ecology*, 49(6), pp. 1075-1091.
- Eleftheriou, A., Robertson, M., 1992. The effects of experimental scallop dredging on the fauna and physical environment of a shallow sandy community. *Netherlands Journal of Sea Research*, 30, pp. 289-299.
- Emmerson, J.A., Hollyman, P.R., Bloor, I.S., Jenkins, S.R., 2020. Effect of temperature on the growth of the commercially fished common whelk (*Buccinum undatum*, L.): A regional analysis within the Irish Sea. *Fisheries Research*, 223, p. 105437.
- Endler, J.A., 1990. On the measurement and classification of colour in studies of animal colour patterns. *Biological Journal of the Linnean Society*, 41(4). pp. 315-352.
- Fisheries and aquaculture software. FishStatJ - software for fishery statistical time series. In: FAO Fisheries and Aquaculture Department [online]. Rome. Accessed 01/02/2023
- Fahy, E., 2001. Conflict between two inshore fisheries: for whelk (*Buccinum undatum*) and brown crab (*Cancer pagurus*), in the southwest Irish Sea. In *Coastal Shellfish — A Sustainable Resource*. Springer, Dordrecht. pp. 73-83.
- Fahy, E., Carroll, J., Hother-Parkes, L., O'Toole, M., Barry, C., 2005. Fishery associated changes in the Whelk *Buccinum undatum* stock in the southwest Irish Sea, 1995-2003. Dublin: Fisheries Science Services.
- Fahy, E., Masterson, E., Swords, D., Forrest, N., 2000. A Second Assessment of the whelk fishery *Buccinum undatum* in the southwest Irish Sea with particular reference to its history of management by size limit. Dublin: Fisheries Science Services.
- Fahy, E., Yalloway, G., Gleeson, P., 1995. Appraisal of the whelk *Buccinum undatum* fishery of the southern Irish sea with proposals for a management strategy. *Irish Fisheries Investigations*, Series B (Marine), 42.
- Falini, G., Albeck, S., Weiner, S., Addadi, L., 1996. Control of aragonite or calcite polymorphism by mollusk shell macromolecules. *Science*, 271(5245), pp. 67-69.
- Fallon, S.J., McCulloch, M.T., van Woesik, R., Sinclair, D.J., 1999. Corals at their latitudinal limits: laser ablation trace element systematics in *Porites* from Shirigai Bay, Japan. *Earth and Planetary Science Letters*, 172(3-4), pp. 221-238.
- Feder, H.M., 1963. Gastropod defensive responses and their effectiveness in reducing predation by starfishes. *Ecology*, 44(3), pp. 505-512.

- Finch, A.A., Allison, N., 2007. Coordination of Sr and Mg in calcite and aragonite. *Mineralogical Magazine*, 71(5), pp. 539-552.
- Finch, A.A., Allison, N., Sutton, S.R., Newville, M., 2003. Strontium in coral aragonite: 1. Characterization of Sr coordination by extended absorption X-ray fine structure. *Geochimica et Cosmochimica Acta*, 67(6), pp. 1197-1202.
- Findlay, H.S., Wood, H.L., Kendall, M.A., Spicer, J.I., Twitchett, R.J., Widdicombe, S., 2011. Comparing the impact of high CO₂ on calcium carbonate structures in different marine organisms. *Marine Biology Research*, 7(6), pp. 565-575.
- Fitzgerald, S., 2008. Non-destructive micro-analysis of art and archaeological objects using micro-XRF. *Archeometriai Műhely*, 3, pp.75-80.
- Fonds, M., 1991. Measurements of catch composition and survival of benthic animals in beam trawl fishery for sole in the southern North Sea. In: Effects of Beam Trawl Fishery on the Bottom Fauna in the North Sea, II, 1990 Studies, *BEON Report*, 13, pp. 85.
- Fonds, M., 1994. Mortality of fish and invertebrates in beam trawl catches and the survival chances of discards. In Environmental Impact of Bottom Gears on Benthic Fauna in Relation to Natural Resources Management and Protection of the North Sea, Netherlands Institute for Fisheries Research, *NIOZ Report*, 1994, pp. 131-146.
- Fonds, M., Verboom, B., Groeneveld, K., 1992. Catch composition and survival of fish and benthic invertebrates in commercial beam trawls for sole and plaice fishery in the southern North Sea. In Effects of Beam Trawl Fishery on the Bottom Fauna in the North Sea, III, 1991 Studies, *BEON Report*, 16, pp. 17-22.
- Foster, B., 1971. On the determinants of the upper limit of intertidal distribution of barnacles (Crustacea: Cirripedia). *The Journal of Animal Ecology*, 40(1), pp. 33-48.
- Foster, L.C., Allison, N., Finch, A.A., Andersson, C., 2009. Strontium distribution in the shell of the aragonite bivalve *Arctica islandica*. *Geochemistry, Geophysics, Geosystems*, 10(3).
- Fowell, S.E., Sandford, K., Stewart, J.A., Castillo, K.D., Ries, J.B., Foster, G.L., 2016. Intrareef variations in Li/Mg and Sr/Ca sea surface temperature proxies in the Caribbean reef-building coral *Siderastrea siderea*. *Paleoceanography*, 31(10), pp. 1315-1329.
- Freitas, P.S., Clarke, L.J., Kennedy, H., Richardson, C.A., Abrantes, F., 2006. Environmental and biological controls on elemental (Mg/Ca, Sr/Ca and Mn/Ca) ratios in shells of the king scallop *Pecten maximus*. *Geochimica et Cosmochimica Acta*, 70(20), pp. 5119-5133.

- Fretter, V., 1953. The transference of sperm from male to female prosobranch, with reference, also, to the pyramidellids. *Proceedings of the Linnean Society of London*, 164(2), pp. 217-224.
- Fretter, V., Graham, A., 1962. British prosobranch molluscs; Their functional anatomy and ecology. *Ray Society*, pp. 428, 483-485.
- Furuhashi, T., Schwarzinger, C., Miksik, I., Smrz, M., Beran, A., 2009. Molluscan shell evolution with review of shell calcification hypothesis. *Comparative Biochemistry and Physiology Part B: Biochemistry and Molecular Biology*, 154(3), pp. 351-371.
- Gabbott, P.A., 1983. Developmental and seasonal metabolic activities in marine molluscs. In *The Mollusca*. Hochachka, P.W., (ed.) Academic Press, New York. pp. 165-217.
- Gaspar, M.B., Richardson, C.A., Monteiro, C.A., 1994. The effects of dredging on shell formation in the razor clam, *Ensis siliqua* from Barrinha, southern Portugal. *Journal of the Marine Biological Association of the United Kingdom*, 74, pp. 927-938.
- Gebauer, D., Volkel, A., Colfen, H., 2008. Stable prenucleation calcium carbonate clusters. *Science*, 322(5909), pp. 1819-1822.
- Gendron, L., 1992. Determination of the size at sexual maturity of the waved whelk *Buccinum undatum* Linnaeus, 1758, in the Gulf of St. Lawrence, as a basis for the establishment of a minimum catchable size. *Journal of Shellfish Research*, 11, pp. 1-7.
- Gillikin, D.P., Lorrain, A., Navez, J., Taylor, J.W., André, L., Keppens, E., Baeyens, W., Dehairs, F., 2005. Strong biological controls on Sr/Ca ratios in aragonitic marine bivalve shells. *Geochemistry, Geophysics, Geosystems*, 6(5).
- Gołąbczak, M., Konstantynowicz, A., 2009. Raman spectra evaluation of the carbon layers with Voigt profile. *Journal of Achievements in Materials and Manufacturing Engineering*, 37(2), pp. 270-276.
- Golikov, A.N., 1968. Distribution and variability of long-lived benthic animals as indicators of currents and hydrological conditions. *Sarsia*, 34(1), pp. 199-208.
- Gong, Y.U.T., Killian, C.E., Olson, I.C., Appathurai, N.P., Amasino, A.L., Martin, M.C., Holt, L.J., Wilt, F.H., Gilbert, P.U.P.A., 2012. Phase transitions in biogenic amorphous calcium carbonate. *Proceedings of the National Academy of Sciences*, 109(16), pp. 6088-6093.
- Gonnea, M.E., Cohen, A.L., DeCarlo, T.M., Charette, M.A., 2017. Relationship between water and aragonite barium concentrations in aquaria reared juvenile corals. *Geochimica et Cosmochimica Acta*, 209, pp. 123-134.

Goodwin, D.H., Flessa, K.W., Schöne, B.R., Dettman, D.L. 2001. Cross-calibration of daily growth increments, stable isotope variation, and temperature in the Gulf of California bivalve mollusk *Chione cortezi*: Implications for paleoenvironmental analysis. *Palaios*, 16(4), pp. 387-398.

Gould, R.W., 1972. Brown pelican eggshells: X-ray diffraction studies. *Bulletin of Environmental Contamination and Toxicology*, 8(2), pp. 84-88.

Guerra-Varela, J., Colson, I., Backeljau, T., Breugelmans, K., Hughes, R.N., Rolán-Alvarez, E., 2009. The evolutionary mechanism maintaining shell shape and molecular differentiation between two ecotypes of the dogwhelk *Nucella lapillus*. *Evolutionary Ecology*, 23(2), pp. 261-280.

Hahn, S., Rodolfo-Metalpa, R., Griesshaber, E., Schmahl, W.W., Buhl, D., Hall-Spencer, J.M., Baggini, C., Fehr, K.T., Immenhauser, A., 2012. Marine bivalve shell geochemistry and ultrastructure from modern low pH environments: environmental effect versus experimental bias. *Biogeosciences*, 9(5), pp. 1897-1914.

Haig, J.A., Pantin, J.R., Salomonsen, H., Murray, L.G., Kaiser, M.J., 2015. Temporal and spatial variation in size at maturity of the common whelk (*Buccinum undatum*). *ICES Journal of Marine Science*, 72(9), pp. 2707-2719.

Hammond, C., 2015. *The Basics of Crystallography and Diffraction*, Fourth edition. Oxford: International Union of Crystallography, Oxford University Press.

Hancock, D.A., 1960. 2. The ecology of the molluscan enemies of the edible mollusc. *Journal of Molluscan Studies*, 34(3), pp. 123-143.

Hancock, D.A., 1963. Marking experiments with the commercial whelk (*Buccinum undatum*). *ICNAF Special Publication*, 4, pp. 176-187.

Harley, C.D., Randall Hughes, A., Hultgren, K.M., Miner, B.G., Sorte, C.J., Thornber, C.S., Rodriguez, L.F., Tomanek, L., Williams, S.L., 2006. The impacts of climate change in coastal marine systems. *Ecology Letters*, 9(2), pp. 228-241.

Harper, E.M., 2000. Are calcitic layers an effective adaptation against shell dissolution in the Bivalvia? *Journal of Zoology*, 251(2), pp. 179-186.

Harper, E.M., Checa, A.G., Rodríguez-Navarro, A.B., 2009. Organization and mode of secretion of the granular prismatic microstructure of *Entodesma navicula* (Bivalvia: Mollusca). *Acta Zoologica*, 90(2), pp. 132-141.

Harper, E.M., Clark, M.S., Hoffman, J.I., Philipp, E.E.R., Peck, L.S., Morley, S.A., 2012. Iceberg Scour and Shell Damage in the Antarctic Bivalve *Laternula elliptica*. *PLoS ONE*, 7(9): e46341.

- Harriss, R.C., 1965. Trace element distribution in molluscan skeletal material I. Magnesium, iron, manganese, and strontium. *Bulletin of Marine Science*, 15(2), pp. 265-273.
- Harvey, A.W., 1990. Sexual differences in contemporary selection acting on size in the hermit crab *Clibanarius digueti*. *The American Naturalist*, 136(3), pp. 292-304.
- Harvey, C., Garneau, F., Himmelman, J.H., 1987. Chemodetection of the predatory seastar *Leptasterias polaris* by the whelk *Buccinum undatum*. *Marine Ecology Progress Series*, 40(1-2), pp. 79-86.
- Harwood, J., 2001. Marine mammals and their environment in the twenty-first century. *Journal of Mammalogy*, 82(3), pp. 630-640.
- Hausmann, N., Prendergast, A.L., Lemonis, A., Zech, J., Roberts, P., Siozos, P., Anglos, D., 2019. Extensive elemental mapping unlocks Mg/Ca ratios as climate proxy in seasonal records of Mediterranean limpets. *Scientific reports*, 9(1), p. 3698.
- Hayashi, A., Yokoo, N., Nakamura, T., Watanabe, T., Nagasawa, H., Kogure, T., 2011. Crystallographic characterization of the crossed lamellar structure in the bivalve *Meretrix lamarckii* using electron beam techniques. *Journal of Structural Biology*, 176(1), pp. 91-96.
- Hayward, P.J., Ryland, J.S., (eds.) 2011. *Handbook of the Marine Fauna of North-West Europe*, Chapter 10: Molluscs. Oxford University Press, Oxford, p. 535.
- Hedegaard, C., Bardeau, J.F., Chateigner, D., 2006. Molluscan shell pigments: an *in-situ* resonance Raman study. *Journal of Molluscan Studies*, 72(2), pp. 157-162.
- Helgeson, H.C., Delany, J.M., Nesbitt, H.W., Bird, D.K., 1978. Summary and critique of the thermodynamic properties of rock-forming minerals. *American Journal of Science*, 278(A) pp. 1-229.
- Heude-Berthelin, C., Hégron-Macé, L., Legrand, V., Jouaux, A., Adeline, B., Mathieu, M., Kellner, K., 2011. Growth and reproduction of the common whelk *Buccinum undatum* in west Cotentin (Channel), France. *Aquatic Living Resources*, 24, pp. 317-327.
- Hieber, A.D., Mudalige-Jayawickrama, R.G., Kuehnle, A.R., 2006. Color genes in the orchid *Oncidium Gower Ramsey*: identification, expression, and potential genetic instability in an interspecific cross. *Planta*, 223(3), pp. 521-531
- Hillard, R., Walters, K., 2009. Prevalence, patterns, and effects of shell damage on *Geukensia demissa* in South Carolina estuarine habitats. *Marine Biology*, 156(10), pp. 2149-2160.
- Himmelman, J., 1988. Movement of whelks (*Buccinum undatum*) towards a baited trap. *Marine Biology*, 97(4), pp. 521-531.

Himmelman, J., Hamel, J., 1993. Diet, behaviour and reproduction of the whelk *Buccinum undatum* in the northern Gulf of St. Lawrence, eastern Canada. *Marine Biology*, 116(3), pp. 423-430.

Höche, N., Walliser, E.O., Schöne, B.R., 2022. Microstructural mapping of *Arctica islandica* shells reveals environmental and physiological controls on biomineral size. *Frontiers in Earth Science*, 9, p. 1350.

Holail, H., Tony, R., 1995. Mineralogical and geochemical compositions of modern bivalve shells from the Mediterranean coast of Egypt. *GeoJournal*, 35, pp. 481-486.

Hold, N., Colvin, C., Delargy, A., L Vay, L., 2021. *The use of catch limits in the management of whelk fishing in the Welsh zone*. Welsh Government Report

Hollyman, P.R., 2017. Age, growth and reproductive assessment of the whelk, *Buccinum undatum*, in coastal shelf seas. PhD thesis, Bangor University, pp. 404. <http://e.bangor.ac.uk/9872/>.

Hollyman, P.R., Chenery, S.R., Ignatyev, K., Laptikhovsky, V.V., Richardson, C.A., 2019. Micro-scale geochemical and crystallographic analysis of *Buccinum undatum* statoliths supports an annual periodicity of growth ring deposition. *Chemical Geology*, 526, pp. 153-164.

Hollyman, P.R., Chenery, S.R., Leng, M.J., Laptikhovsky, V.V., Colvin, C.N., Richardson, C.A., 2018. Age and growth rate estimations of the commercially fished gastropod *Buccinum undatum*. *ICES Journal of Marine Science*. 75(6), pp. 2129-2144.

Hollyman, P.R., Leng, M.J., Chenery, S.R., Sloane, H.J., Richardson, C.A., 2020. Calibration of shell $\delta^{18}\text{O}$ from the common whelk *Buccinum undatum* highlights potential for palaeoenvironmental reconstruction. *Palaeogeography, Palaeoclimatology, Palaeoecology*, 560, p.109995.

Honig, A., Etter, R., Pepperman, K., Morello, S., Hannigan, R., 2020. Site and age discrimination using trace element fingerprints in the blue mussel, *Mytilus edulis*. *Journal of Experimental Marine Biology and Ecology*, 522, p. 151249.

Hunt, S., Oates, K., 1978. Fine structure and molecular organization of the periostracum in a gastropod mollusc *Buccinum undatum* L. and its relation to similar structural protein systems in other invertebrates. *Philosophical Transactions of the Royal Society of London. B, Biological Sciences*, 283(998), pp. 417-459.

Hüssy, K., Limburg, K.E., de Pontual, H., Thomas, O.R., Cook, P.K., Heimbrand, Y., Blass, M., Sturrock, A.M., 2021. Trace element patterns in otoliths: the role of biomineralization. *Reviews in Fisheries Science & Aquaculture*, 29(4), pp. 445-477.

Irie, T., Fischer, K., 2009. Ectotherms with a calcareous exoskeleton follow the temperature-size rule—evidence from field survey. *Marine Ecology Progress Series*, 385, pp. 33-37.

Ivany, L.C., Peters, S.C., Wilkinson, B.H., Lohmann, K.C., Reimer, B.A., 2004. Composition of the early Oligocene Ocean from coral stable isotope and elemental chemistry. *Geobiology*, 2(2), pp. 97-106.

Jalbert, P., Himmelman, J.H., Béland, P., Thomas, B., 1989. Whelks (*Buccinum undatum*) and other subtidal invertebrate predators in the northern Gulf of St. Lawrence. *Le Naturaliste Canadien*, 116(1), pp. 1-15.

Jeffreys, J.G., 1867. *British Conchology: or, an Account of the Mollusca Which Now Inhabit the British Isles and the Surrounding Seas*. John Van Voorst, London.

Jennings, S., Kaiser, M.J., 1998. The Effects of Fishing on Marine Ecosystems. *Advances in Marine Biology*, 34, pp. 201-352.

Jennings, S., Kaiser, M.J., Reynolds, J.D., 2001. *Marine Fisheries Ecology*. Blackwell Science, Oxford.

Ji, H., Li, X., Chen, D., 2017. *Cymbiola nobilis* shell: Toughening mechanisms in a crossed-lamellar structure. *Scientific Reports*, 7(1), pp. 1-10.

Jochum, K.P., Nohl, U., Herwig, K., Lammel, E., Stoll, B., Hofmann, A.W., 2005. GeoReM: a new geochemical database for reference materials and isotopic standards. *Geostandards and Geoanalytical Research*, 29(3), pp. 333-338.

Johannesson, K., 1988. The paradox of Rockall: why is a brooding gastropod (*Littorina saxatilis*) more widespread than one having a planktonic larval dispersal stage (*Littorina littorea*)? *Marine Biology*, 99(4), pp. 507-513.

Johnsen, S., 2016. How to measure color using spectrometers and calibrated photographs. *Journal of Experimental Biology*, 219(6), pp. 772-778.

Kaehler, S., McQuaid, C.D., 1999. Use of the fluorochrome calcein as an in-situ growth marker in the brown mussel *Perna perna*. *Marine Biology*, 133(3), pp. 455-460.

Kaiser, M.J., Edwards, D.B., Armstrong, P.J., Radford, K., Lough, N.E.L., Flatt, R.P., Jones, H.D., 1998. Changes in megafaunal benthic communities in different habitats after trawling disturbance. *ICES Journal of Marine Science: Journal Du Conseil*, 55(3), pp. 353-361.

Kaiser, M.J., Ramsay, K., Richardson, C.A., Spence, F.E., Brand, A.R., 2000. Chronic fishing disturbance has changed shelf sea benthic community structure. *Journal of Animal Ecology*, 69(3), pp. 494-503.

- Kaiser, M.J., Spencer, B.E. 1995. Survival of by-catch from a beam trawl. *Marine Ecology Progress Series*, 126, pp. 31-38.
- Kaiser, M.J., Spencer, B.E., 1996. The effects of beam-trawl disturbance on infaunal communities in different habitats. *Journal of Animal Ecology*, 65(3), pp. 348-358.
- Kanngießler, B., 2003. Quantification procedures in micro-X-ray fluorescence analysis. *Spectrochimica Acta Part B: Atomic Spectroscopy*, 58(4), pp. 609-614.
- Karythis, S., Cornwell, T.O., Noya, L.G., McCarthy, I.D., Whiteley, N.M., Jenkins, S.R., 2020. Prey vulnerability and predation pressure shape predator-induced changes in O₂ consumption and antipredator behaviour. *Animal Behaviour*, 167, pp. 13-22.
- Kastner, M., 1999. Oceanic minerals: Their origin, nature of their environment, and significance. *Proceedings of the National Academy of Sciences*, 96(7), pp. 3380-3387.
- Kawecki, T.J., Ebert, D., 2004. Conceptual issues in local adaptation. *Ecology Letters*, 7(12), pp. 1225-1241.
- Kelemen, Z., Gillikin, D.P., Bouillon, S., 2019. Relationship between river water chemistry and shell chemistry of two tropical African freshwater bivalve species. *Chemical Geology*, 526, pp. 130-141.
- Kenchington, E., Glass, A., 1998. Local adaptation and sexual dimorphism in the waved whelk (*Buccinum undatum*) in Atlantic Nova Scotia with applications to fisheries management. Department of Fisheries and Oceans, Science Branch, Maritimes Region, Invertebrate Fisheries Division, Bedford Institute of Oceanography.
- Kideys, A.E., 1994. Effect of tagging on the growth rate of the neogastropod, *Buccinum undatum* in the laboratory. *Fisheries Research*, 20(2-3), pp. 283-289.
- Kideys, A.E., 1996. Determination of age and growth of *Buccinum undatum* L. (Gastropoda) off Douglas, Isle of Man. *Helgoländer Meeresuntersuchungen*, 50(3), pp. 353-368.
- Kideys, A.E., Hartnoll, R.G., 1991. Energetics of mucus production in the common whelk *Buccinum undatum* L. *Journal of Experimental Marine Biology and Ecology*, 150(1), pp. 91-105.
- Kideys, A.E., Nash, R.D.M., Hartnoll, R.G., 1993. Reproductive cycle and energetic cost of reproduction of the neogastropod *Buccinum undatum* in the Irish Sea. *Journal of the Marine Biological Association of the United Kingdom*, 73(2), pp. 391-403.
- Kobayashi, I., Samata, T., 2006. Bivalve shell structure and organic matrix. *Materials Science and Engineering: C*, 26(4), pp. 692-698.

- Kobluk, D.R., Mapes, R.H., 1989. The fossil record, function, and possible origins of shell color patterns in Paleozoic marine invertebrates. *Palaios*, 4(1), pp. 63-85.
- Kogure, T., Suzuki, M., Kim, H., Mukai, H., Checa, A.G., Sasaki, T., Nagasawa, H., 2014. Twin density of aragonite in molluscan shells characterized using X-ray diffraction and transmission electron microscopy. *Journal of crystal growth*, 397, pp. 39-46.
- Krantz, D.E., Jones, D.S., Williams, D.F., 1984. Growth rates of the sea scallop, *Placopecten magellanicus*, determined from the $^{18}\text{O}/^{16}\text{O}$ record in shell calcite. *The Biological Bulletin*, 167(1), pp. 186-199.
- Lalli, C.M., Gilmer, R.W., 1989. *Pelagic Snails: The Biology of Holoplanktonic Gastropod Mollusks*. Stanford University Press, Stanford, California.
- Lammens, J.J., 1967. Growth and reproduction in a tidal flat population of *Macoma balthica* (L.). *Netherlands Journal of Sea Research*, 3(3), pp. 315-382.
- Langlet, D., Alleman, L.Y., Plisnier, P.D., Hughes, H., André, L., 2006. Mn seasonal upwellings recorded in Lake Tanganyika mussels. *Biogeosciences Discussions*, 3(5), pp. 1453-1471.
- Laptikhovsky, V.V., 2014. Does starfish predation determine spawning seasonality in the whelk *Buccinum undatum* in the Gulf of St Lawrence? *Journal of Molluscan Studies*, 80(2), pp. 219-221.
- Large, S.I., Smee, D.L., 2013. Biogeographic variation in behavioral and morphological responses to predation risk. *Oecologia*, 171(4), pp. 961-969.
- Lawler, A., 2013 Determination of the size of maturity of the whelk *Buccinum undatum* in English waters – Defra Project MF0231
- Lazareth, C.E., Le Cornec, F., Candaudap, F., Freydier, R., 2013. Trace element heterogeneity along isochronous growth layers in bivalve shell: consequences for environmental reconstruction. *Palaeogeography, Palaeoclimatology, Palaeoecology*, 373, pp. 39-49.
- Lervik, A., Bedeaux, D., Kjelstrup, S., 2013. Active transport of the Ca^{2+} pump: introduction of the temperature difference as a driving force. *European Biophysics Journal*, 42(5), pp. 321-331.
- Levi-Kalishman, Y., Falini, G., Addadi, L., Weiner, S., 2001. Structure of the nacreous organic matrix of a bivalve mollusk shell examined in the hydrated state using cryo-TEM. *Journal of Structural Biology*, 135(1), pp. 8-17.
- Levin, S.A., 1992. The problem of pattern and scale in ecology: the Robert H. MacArthur award lecture. *Ecology*, 73(6), pp. 1943-1967.

- Levinton, J., 2020. Thermal stress: The role of body size and the giant major claw in survival and heat transfer of a fiddler crab (*Leptuca pugilator*). *Journal of Experimental Marine Biology and Ecology*, 530, p. 151428.
- Linhart, Y.B., Grant, M.C., 1996. Evolutionary significance of local genetic differentiation in plants. *Annual review of ecology and systematics*, 27(1), pp. 237-277.
- Loftus, E., Rogers, K., Lee-Thorp, J., 2015. A simple method to establish calcite: aragonite ratios in archaeological mollusc shells. *Journal of Quaternary Science*, 30(8), pp. 731-735.
- Lorens, R.B., Bender, M.L., 1980. The impact of solution chemistry on *Mytilus edulis* calcite and aragonite. *Geochimica et Cosmochimica Acta*, 44(9), pp. 1265-1278.
- Lutz, R.A., 1976. Annual growth patterns in the inner shell layer of *Mytilus edulis* L. *Journal of the Marine Biological Association of the United Kingdom*, 56(03), pp. 723-731.
- MacDonald, B.A., Thomas, M., 1980. Age determination of the soft-shell clam *Mya arenaria* using shell internal growth lines. *Marine Biology*, 58(2), pp. 105-109.
- Mackie, A.M., 1970. Avoidance reactions of marine invertebrates to either steroid glycosides of starfish or synthetic surface-active agents. *Journal of Experimental Marine Biology and Ecology*, 5(1), pp. 63-69.
- Mackie, A.M., Lasker, R., Grant, P.T., 1968. Avoidance reactions of a mollusc *Buccinum undatum* to saponin-like surface-active substances in extracts of the starfish *Asterias rubens* and *Marthasterias glacialis*. *Comparative Biochemistry and Physiology*, 26(2), pp. 415-418.
- Madin, K., 2010. Ocean acidification: A risky shell game. *Oceanus*, 48(1), pp. 6-8.
- Magnúsdóttir, H., 2010. The common whelk (*Buccinum undatum* L.): Life history traits and population structure. Magister Scientiarum degree thesis, University of Iceland
- Magnúsdóttir, H., Pálsson, S., Westfall, K.M., Jónsson, Z.O., Örnólfsdóttir, E.B., 2018. Shell morphology and color of the subtidal whelk *Buccinum undatum* exhibit fine-scaled spatial patterns. *Ecology and evolution*, 8(9), pp. 4552-4563.
- Magnúsdóttir, H., Pálsson, S., Westfall, K.M., Jónsson, Z.O., Örnólfsdóttir, E.B., 2019. Morphological variation in genetically divergent populations of the common whelk, *Buccinum undatum* (Gastropoda: Buccinidae), across the North Atlantic. *Biological Journal of the Linnean Society*, 128(1), pp. 93-106.
- Maia, R., Eliason, C.M., Bitton, P.P., Doucet, S.M., Shawkey, M.D., 2013. pavo: an R package for the analysis, visualization and organization of spectral data. *Methods in Ecology and Evolution*, 4(10), pp. 906-913.

Marali, S., Schöne, B.R., Mertz-Kraus, R., Griffin, S.M., Wanamaker Jr, A.D., Butler, P.G., Holland, H.A., Jochum, K.P., 2017a. Reproducibility of trace element time-series (Na/Ca, Mg/Ca, Mn/Ca, Sr/Ca, and Ba/Ca) within and between specimens of the bivalve *Arctica islandica*—A LA-ICP-MS line scan study. *Palaeogeography, Palaeoclimatology, Palaeoecology*, 484, pp. 109-128.

Marali, S., Schöne, B.R., Mertz-Kraus, R., Griffin, S.M., Wanamaker Jr, A.D., Matras, U., Butler, P.G., 2017b. Ba/Ca ratios in shells of *Arctica islandica*—potential environmental proxy and crossdating tool. *Palaeogeography, Palaeoclimatology, Palaeoecology*, 465, pp. 347-361.

Mariani, S., Peijnenburg, K.T., Weetman, D., 2012. Independence of neutral and adaptive divergence in a low dispersal marine mollusc. *Marine Ecology Progress Series*, 446, pp. 173-187.

Marine Management Organisation., 2018. *UK Sea Fisheries Statistics 2018*. Office for National Statistics, London

Marine Management Organisation., 2020. *UK Sea Fisheries Statistics 2020*. Office for National Statistics, London

Marine Management Organisation., 2022. *UK Sea Fisheries Statistics 2021*. Office for National Statistics, London

Markulin, K., Peharda, M., Mertz-Kraus, R., Schöne, B.R., Uvanović, H., Kovač, Ž., Janeković, I., 2019. Trace and minor element records in aragonitic bivalve shells as environmental proxies. *Chemical Geology*, 507, pp. 120-133.

Marriott, C.S., Henderson, G.M., Belshaw, N.S., Tudhope, A.W., 2004. Temperature dependence of $\delta^{7}\text{Li}$, $\delta^{44}\text{Ca}$ and Li/Ca during growth of calcium carbonate. *Earth and Planetary Science Letters*, 222(2), pp. 615-624.

Martel, A., Larrivé, D.H., Himmelman, J.H., 1986. Behaviour and timing of copulation and egg-laying in the neogastropod *Buccinum undatum* L. *Journal of Experimental Marine Biology and Ecology*, 96(1), pp. 27-42.

Martinelli, J.C., Lopes, H.M., Hauser, L., Jimenez-Hidalgo, I., King, T.L., Padilla-Gamiño, J.L., Rawson, P., Spencer, L.H., Williams, J.D., Wood, C.L., 2020. Confirmation of the shell-boring oyster parasite *Polydora websteri* (Polychaeta: Spionidae) in Washington State, USA. *Scientific Reports*, 10(1), p. 3961.

McConnaughey, T.A., 1989. ^{13}C and ^{18}O isotopic disequilibrium in biological carbonates: II. In vitro simulation of kinetic isotope effects. *Geochimica et Cosmochimica Acta*, 53(1), pp. 163-171.

- McConnaughey, T.A., Gillikin, D.P., 2008. Carbon isotopes in mollusk shell carbonates. *Geo-Marine Letters*, 28(5-6), pp. 287-299.
- McIntyre, R., Lawler, A., Masefield, R., 2015. Size of maturity of the common whelk, *Buccinum undatum*: Is the minimum landing size in England too low? *Fisheries Research*. 162, pp. 53–57.
- McNaught, M.K., Owens, I.P., 2002. Interspecific variation in plumage colour among birds: species recognition or light environment? *Journal of Evolutionary Biology*, 15(4), pp. 505-514.
- Meenakshi, V.R., Martin, A.W., Wilbur, K.M., 1974. Shell repair in *Nautilus macromphalus*. *Marine Biology*, 27(1), pp. 27-35.
- Melatunan, S., Calosi, P., Rundle, S.D., Widdicombe, S., Moody, A.J., 2013. Effects of ocean acidification and elevated temperature on shell plasticity and its energetic basis in an intertidal gastropod. *Marine Ecology Progress Series*, 472, pp. 155-168.
- Melzner, F., Stange, P., Trübenbach, K., Thomsen, J., Casties, I., Panknin, U., Gorb, S.N., Gutowska, M.A., 2011. Food supply and seawater pCO₂ impact calcification and internal shell dissolution in the Blue Mussel *Mytilus edulis*. *PloS One*, 6(9), e24223.
- Mensink, B.P., Fischer, C.V., Cadée, G.C., Fonds, M., Ten Hallers-Tjabbes, C.C., Boon, J.P., 2000. Shell damage and mortality in the common whelk *Buccinum undatum* caused by beam trawl fishery. *Journal of Sea Research*, 43(1), pp. 53-64.
- Mezger, E.M., De Nooijer, L.J., Bertlich, J., Bijma, J., Nürnberg, D., Reichart, G.J., 2019. Planktonic foraminiferal spine versus shell carbonate Na incorporation in relation to salinity. *Biogeosciences*, 16(6), pp. 1147-1165.
- Mitton, J.B., 1977. Shell colour and pattern variation in *Mytilus edulis* and its adaptive significance. *Chesapeake Science*, 18, pp. 387-390.
- Miura, O., Sasaki, Y., Chiba, S., 2012. Destruction of populations of *Batillaria attramentaria* (Caenogastropoda: Batillariidae) by tsunami waves of the 2011 Tohoku earthquake. *Journal of Molluscan Studies*, 78(4), pp. 377-380.
- Miyamoto, H., Miyoshi, F., Kohno, J., 2005. The carbonic anhydrase domain protein nacrein is expressed in the epithelial cells of the mantle and acts as a negative regulator in calcification in the mollusc *Pinctada fucata*. *Zoological Science*, 22(3), pp. 311-315.
- Molina, A.N., Pulgar, J.M., Rezende, E.L., Carter, M.J., 2022. Heat tolerance of marine ectotherms in a warming Antarctica. *Global Change Biology*, 29(1), pp. 179-188.
- Moore, H. B., 1936. The biology of *Purpura lapillus*. I. Shell variation in relation to environment. *Journal of the Marine Biological Association of the United Kingdom*, 21, pp. 61-89.

- Moore, P. G., Howarth, J., 1996. Foraging by marine scavengers: effects of relatedness, bait, damage and hunger. *Journal Sea Research*, 36(3/4) pp. 267-273.
- Morel, G.M., Bossy, S.F., 2004. Assessment of the whelk (*Buccinum undatum* L.) population around the Island of Jersey, Channel Isles. *Fisheries Research*, 68(1-3), pp. 283-291.
- Moschino, V., Deppieri, M., Marin, M.G., 2003. Evaluation of shell damage to the clam *Chamelea gallina* captured by hydraulic dredging in the Northern Adriatic Sea. *ICES Journal of Marine Science*, 60(2), pp. 393-401.
- Mount, A.S., Wheeler, A.P., Paradkar, R.P., Snider, D., 2004. Hemocyte-mediated shell mineralization in the Eastern Oyster. *Science*, 304(5668), pp. 297–300.
- Murray, L.G., Hinz, H., Hold, N., Kaiser, M.J., 2013. The effectiveness of using CPUE data derived from Vessel Monitoring Systems and fisheries logbooks to estimate scallop biomass. *ICES Journal of Marine Science*. 70, pp. 1330-1340.
- Nakahara, H., 1983. Calcification of gastropod nacre. *Biomineralization and Biological Metal Accumulation*. Springer, Dordrecht, Netherlands. pp. 225-230.
- Nasution, S., Roberts, D., 2004. Laboratory trials on the effects of different diets on growth and survival of the common whelk, *Buccinum undatum* L. 1758, as a candidate species for aquaculture. *Aquaculture International*, 12(6), pp. 509-521.
- Nehrke, G., Poigner, H., Wilhelms-Dick, D., Brey, T., Abele, D., 2012. Coexistence of three calcium carbonate polymorphs in the shell of the Antarctic clam *Laternula elliptica*. *Geochemistry, Geophysics, Geosystems*, 13(5).
- Nicholson, G.J., Evans, S.M., 1997. Anthropogenic impacts on the stocks of the common whelk *Buccinum undatum* (L.). *Marine Environmental Research*, 44(3), pp. 305-314.
- Nielsen, C., 1974. Observations on *Buccinum undatum* L. attacking bivalves and on prey responses, with a short review on attack methods of other prosobranchs. *Ophelia*, 13(1-2), pp. 87-108.
- Norrie, C.R., Dunphy, B.J., Ragg, N.L., Lundquist, C.J., 2019. Comparative influence of genetics, ontogeny and the environment on elemental fingerprints in the shell of *Perna canaliculus*. *Scientific Reports*, 9(1), p. 8533.
- Nouet, J., Baronnet, A., Howard, L., 2012. Crystallization in organo-mineral micro-domains in the crossed-lamellar layer of *Nerita undata* (Gastropoda, Neritopsina). *Micron*, 43(2-3), pp. 456-462.

Nudelman, F., Gotliv, B.A., Addadi, L., Weiner, S., 2006. Mollusk shell formation: Mapping the distribution of organic matrix components underlying a single aragonitic tablet in nacre. *Journal of Structural Biology*, 153(2), pp. 176-187.

Nürnberg, D., Bijma, J., Hemleben, C., 1996. Assessing the reliability of magnesium in foraminiferal calcite as a proxy for water mass temperatures. *Geochimica et Cosmochimica Acta*, 60(5), pp. 803-814.

Nuttall, C.P., 1969. Coloration. In: Moore, R.C., (ed.) *Treatise on Invertebrate Paleontology, N, Mollusca*. Volume 6. Geological Society of America and the University of Kansas Press, Lawrence, USA. pp. 70-72.

Owen, R., Kennedy, H., Richardson, C.A, 2002. Experimental investigation into partitioning of stable isotopes between scallop (*Pecten maximus*) shell calcite and sea water. *Palaeogeography, Palaeoclimatology, Palaeoecology*, 185(1-2), pp. 163-174.

Page, H.M., Hubbard, D.M., 1987. Temporal and spatial patterns of growth in mussels *Mytilus edulis* on an offshore platform: relationships to water temperature and food availability. *Journal of Experimental Marine Biology and Ecology*, 111(2), pp. 159-179.

Palacios, R., Orensanz, J.M., Armstrong, D.A., 1994. Seasonal and life-long variation of Sr/Ca ratio in shells of *Mya arenaria* from Grays Harbor (Washington)—an ancillary criterion in demographic studies. *Estuarine, Coastal and Shelf Science*, 39(4), pp. 313-327.

Palmer, A.R., 1981. Do carbonate skeletons limit the rate of body growth? *Nature*, 292(5819), pp. 150-152.

Palmer, A.R., 1983. Relative cost of producing skeletal organic matrix versus calcification: Evidence from marine gastropods. *Marine Biology*, 75(2-3), pp. 287-292.

Palmer, A.R., 1985. Quantum changes in gastropod shell morphology need not reflect speciation. *Evolution*, 39(3), pp. 699-705.

Palmer, A.R., 1990. Effect of crab effluent and scent of damaged conspecifics on feeding, growth, and shell morphology of the Atlantic dogwhelk *Nucella lapillus* (L.). *Hydrobiologia*, 193, pp. 155-182.

Palmer, A.R., 1992. Calcification in marine molluscs: how costly is it? *Proceedings of the National Academy of Sciences*, 89(4), pp. 1379-1382.

Pálsson, S., Magnúsdóttir, H., Reynisdóttir, S., Jónsson, Z. O., Örnólfssdóttir, E. B., 2014. Divergence and molecular variation in common whelk *Buccinum undatum* (Gastropoda:

Buccinidae) in Iceland: a trans-Atlantic comparison. *Biological Journal of the Linnean Society*, 111(1), pp. 145-159.

Parker, A.R., Mckenzie, D.R., Large, M.C., 1998. Multilayer reflectors in animals using green and gold beetles as contrasting examples. *Journal of Experimental Biology*, 201(9), pp. 1307-1313.

Parsonage, S., Hughes, J.M., 2002. Natural selection and the distribution of shell colour morphs in three species of *Littoraria* (Gastropoda: Littorinidae) in Moreton Bay, Queensland. *Biological Journal of the Linnean Society*, 75, pp. 219–232.

Parsons, J.G., Aldrich, M.V., Gardea-Torresdey, J.L., 2002. Environmental and biological applications of extended X-ray absorption fine structure (EXAFS) and X-ray absorption near edge structure (XANES) spectroscopies. *Applied Spectroscopy Reviews*, 37(2), pp. 187-222.

Pascoal, S., Carvalho, G., Creer, S., Mendo, S., Hughes, R.N., 2012. Plastic and heritable variation in shell thickness of the intertidal gastropod *Nucella lapillus* associated with risks of crab predation and wave action, and sexual maturation. *PLoS one*, 7(12), p.e. 52134.

Pechenik, J.A., Chaparro, O.R., Franklin, A., Mardones, M.L., Montory, J.A., 2019. Thermal tolerance of intertidal and subtidal adults and embryos of the marine gastropod *Crepidatella peruviana*. *Marine Ecology Progress Series*, 616, pp. 67-81.

Perron, F.E., 1981. The partitioning of reproductive energy between ova and protective capsules in marine gastropods of the genus *Conus*. *The American Naturalist*, 118(1), pp. 110-118.

Peterson, D.A., Hilborn, R., Hauser, L., 2014. Local adaptation limits lifetime reproductive success of dispersers in a wild salmon metapopulation. *Nature communications*, 5(1), pp. 1-7.

Phifer-Rixey, M., Heckman, M., Trussell, G.C., Schmidt, P.S., 2008. Maintenance of clinal variation for shell colour phenotype in the flat periwinkle *Littorina obtusata*. *Journal of Evolutionary Biology*, 21(4), pp. 966-978.

Philippart, C.J.M., 1998. Long-term impact of bottom fisheries on several by-catch species of demersal fish and benthic invertebrates in the south-eastern North Sea. *ICES Journal of Marine Science: Journal du Conseil*, 55(3), pp. 342-352.

Phillips, E., 2022. The density of *Buccinum undatum* (L. 1758) at Moelfre and Nefyn (North Wales, UK) and size selectivity of baited commercial pots. MSc thesis. Bangor: Bangor University.

- Piet, G.J., Rijnsdorp, A.D., Bergman, M.J.N., van Santbrink, J.W., Craeymeersch, J., Buijs, J., 2000. A quantitative evaluation of the impact of beam trawling on benthic fauna in the southern North Sea. *ICES Journal of Marine Science: Journal Du Conseil*, 57(5), pp. 1332-1339.
- Pons, G., Evangelisti, V., Capri, F., Mozzone, S., Viarengo, A. 2002. Cytochemical localization and quantification of plasma membrane Ca₂ -ATPase activity in mollusc digestive gland cells. *European Journal of Histochemistry*, 46(1), pp. 31-40.
- Poulain, C., Gillikin, D.P., Thébault, J., Munaron, J.M., Bohn, M., Robert, R., Paulet, Y.M., Lorrain, A., 2015. An evaluation of Mg/Ca, Sr/Ca, and Ba/Ca ratios as environmental proxies in aragonite bivalve shells. *Chemical geology*, 396, pp. 42-50.
- Preston, S.J., Roberts, D., 2007. Variation in shell morphology of *Calliostoma zizyphinum* (Gastropoda: Trochidae). *Journal of Molluscan Studies*, 73(1), pp. 101-104.
- Prosser, C.L., Graham, G., Galton, V., 1991. Hormonal regulation of temperature acclimation in catfish hepatocytes. *Journal of Comparative Physiology B*, 161(1), pp. 117-124.
- Purton, L.M., Shields, G.A., Brasier, M.D., Grime, G.W., 1999. Metabolism controls Sr/Ca ratios in fossil aragonitic mollusks. *Geology*, 27(12), pp. 1083-1086.
- Raddatz, J., Liebetrau, V., Rüggeberg, A., Hathorne, E., Krabbenhöft, A., Eisenhauer, A., Böhm, F., Vollstaedt, H., Fietzke, J., Correa, M.L., Freiwald, A., 2013. Stable Sr-isotope, Sr/Ca, Mg/Ca, Li/Ca and Mg/Li ratios in the scleractinian cold-water coral *Lophelia pertusa*. *Chemical Geology*, 352, pp. 143-152.
- Ramón, M., Abelló, P., Richardson, C.A., 1995. Population structure and growth of *Donax trunculus* (Bivalvia: Donacidae) in the western Mediterranean. *Marine Biology*, 121(4), pp. 665-671.
- Ramsay, K., Kaiser, M.J., 1998. Demersal fishing disturbance increases predation risk for whelks (*Buccinum undatum* L.). *Journal of Sea Research*, 39, pp. 299-304.
- Ramsay, K., Kaiser, M.J., Richardson, C.A., Veale, L.O., Brand, A.R., 2000. Can shell scars on dog cockles (*Glycymeris glycymeris* L.) be used as an indicator of fishing disturbance? *Journal of Sea Research*, 43(2), pp. 167-176.
- Ramsay, K., Richardson, C.A., Kaiser, M.J., 2001. Causes of shell scarring in dog cockles *Glycymeris glycymeris* L. *Journal of Sea Research*, 45(2), pp. 131-139.
- Ravel, B., Newville, M.A., 2005. ATHENA, ARTEMIS, HEPHAESTUS: data analysis for X-ray absorption spectroscopy using IFEFFIT. *Journal of synchrotron radiation*, 12(4), pp. 537-541.

Richardson, C.A., 2001. Molluscs as archives of environmental change. *Oceanography and Marine Biology: An Annual Review*, 39, pp. 103-164.

Richardson, C.A., Crisp, D.J., Runham, N.W., Gruffydd, L.D., 1980. The use of tidal growth bands in the shell of *Cerastoderma edule* to measure seasonal growth rates under cool temperate and sub-arctic conditions. *Journal of the Marine Biological Association of the United Kingdom*, 60(4), pp. 977-989.

Richardson, C.A., Peharda, M., Kennedy, H., Kennedy, P., Onofri, V., 2004. Age, growth rate and season of recruitment of *Pinna nobilis* (L) in the Croatian Adriatic determined from Mg: Ca and Sr: Ca shell profiles. *Journal of Experimental Marine Biology and Ecology*, 299(1), pp. 1-16.

Richardson, C.A., Runham, N.W., Crisp, D.J., 1981. A histological and ultrastructural study of the cells of the mantle edge of a marine bivalve *Cerastoderma edule*. *Tissue and Cell*, 13(4), pp. 715-730.

Riesen, W., Reise, K., 1982. Macrobenthos of the subtidal Wadden Sea: revisited after 55 years. *Helgoländer Meeresuntersuchungen*, 35(4), pp. 409-423.

Robinson, R.F., Richardson, C.A., 1998. The direct and indirect effects of suction dredging on a razor clam (*Ensis arcuatus*) population. *ICES Journal of Marine Science, Journal du Conseil*, 55(5), pp. 970-977.

Rochette, R., Himmelman, J.H., 1996. Does vulnerability influence trade-offs made by whelks between predation risk and feeding opportunities? *Animal Behaviour*, 52(4), pp. 783-794.

Rochette, R., Tétrault, F., Himmelman, J. H., 2001. Aggregation of whelks, *Buccinum undatum*, near feeding predators: the role of reproductive requirements. *Animal Behaviour*. 61, pp. 31-41.

Rodriguez-Navarro, A.B., Checa, A., Willinger, M.G., Bolmaro, R., Bonarski, J., 2012. Crystallographic relationships in the crossed lamellar microstructure of the shell of the gastropod *Conus marmoreus*. *Acta Biomaterialia*, 8(2), pp. 830-835.

Rollion-Bard, C., Blamart, D., 2015. Possible controls on Li, Na, and Mg incorporation into aragonite coral skeletons. *Chemical Geology*, 396, pp. 98-111.

Ropp, R.C., 2013. *Encyclopedia of the Alkaline Earth Compounds*. Elsevier Science, Oxford, UK.

Rosenthal, Y., Boyle, E.A., Slowey, N., 1997. Temperature control on the incorporation of magnesium, strontium, fluorine, and cadmium into benthic foraminiferal shells from Little Bahama Bank: Prospects for thermocline paleoceanography. *Geochimica et Cosmochimica Acta*, 61(17), pp. 3633-3643.

Ruppert, E.E., Fox, R.S., Barnes, R.D., 2004. *Invertebrate Zoology. Chapter 12: Mollusca*. Cengage Learning, Delhi. pp. 269-301

Saenko, S.V., Schilthuizen, M., 2021. Evo-devo of shell colour in gastropods and bivalves. *Current Opinion in Genetics and Development*, 69, pp. 1-5.

Saleuddin, A.S.M., Wilbur, K.M., (eds.) 1983. *Shell formation. The Mollusca. Volume 4: Physiology, Part 1*. Academic Press, New York. pp. 235-287.

Sanford, E., Kelly, M.W., 2011. Local adaptation in marine invertebrates. *Annual review of Marine Science*, 3, pp. 509-535.

Santarelli-Chaurand, L., 1985. Les pecheries de Buccin (*Buccinum undatum* L.: Gastropoda) du Golfe Normand- Breton. Eléments de gestion de la ressource. PhD thesis, L'Universite d'aix-Marseille.

Santarelli, L., Gros, P., 1985. Age and growth of the whelk *Buccinum undatum* L. (Gastropoda: Prosobranchia) using stable isotopes of the shell and operculum striae. *Oceanol Acta*. 8(2), pp. 221–229.

Schöne, B.R., Rodland, D.L., Wehrmann, A., Heidel, B., Oschmann, W., Zhang, Z., Fiebig, J., Beck, L., 2007. Combined sclerochronologic and oxygen isotope analysis of gastropod shells (*Gibbula cineraria*, North Sea): life-history traits and utility as a high-resolution environmental archive for kelp forests. *Marine Biology*. 150(6), pp. 1237-1252.

Schöne, B.R., Zhang, Z., Jacob, D., Gillikin, D.P., Tütken, T., Garbe-Schönberg, D., McConnaughey, T., Soldati, A., 2010. Effect of organic matrices on the determination of the trace element chemistry (Mg, Sr, Mg/Ca, Sr/Ca) of aragonitic bivalve shells (*Arctica islandica*)—Comparison of ICP-OES and LA-ICP-MS data. *Geochemical journal*, 44(1), pp. 23-37.

Schreier, F., 2018. Comments on the Voigt function implementation in the Astropy and SpectraPlot. com packages. *Journal of Quantitative Spectroscopy and Radiative Transfer*, 213, pp. 13-16.

Scolding, J.W.S., Richardson, C.A., Luckenbach, M.J., 2007. Predation of cockles (*Cerastoderma edule*) by the whelk (*Buccinum undatum*) under laboratory conditions. *Journal of Molluscan Studies*, 73(4), pp. 333-337.

Sebens, K.P., 1987. The ecology of indeterminate growth in animals. *Annual review of ecology and systematics*, 18(1), pp. 371-407.

Seed, R., 1968. Factors influencing shell shape in the mussel *Mytilus edulis*. *Journal of the Marine Biological Association of the United Kingdom*, 48(3), pp. 561-584.

Seed, R., Hughes, R.N., 1995. Criteria for prey size-selection in molluscivorous crabs with contrasting claw morphologies. *Journal of Experimental Marine Biology and Ecology*, 193(1-2), pp. 177-195.

Shelmerdine, R.L., Adamson, J., Laurenson, C.H., Leslie, B., 2007. Size variation of the common whelk, *Buccinum undatum*, over large and small spatial scales: Potential implications for micro-management within the fishery. *Fishery Research*. 86, pp. 201-206.

Sibly, R.M., Baker, J., Grady, J.M., Luna, S.M., Kodric-Brown, A., Venditti, C., Brown, J.H., 2015. Fundamental insights into ontogenetic growth from theory and fish. *Proceedings of the National Academy of Sciences*, 112, pp. 13934-13939.

Simkiss, K., Wilbur, K.M., 1989. Biomineralization: cell biology and mineral deposition, *Quarterly Review of Biology*, 14, p. 337.

Sinclair, D.J., Kinsley, L.P., McCulloch, M.T., 1998. High resolution analysis of trace elements in corals by laser ablation ICP-MS. *Geochimica et Cosmochimica acta*, 62(11), pp. 1889-1901.

Sleight, V.A., Thorne, M.A., Peck, L.S., Clark, M.S., 2015. Transcriptomic response to shell damage in the Antarctic clam, *Laternula elliptica*: time scales and spatial localisation. *Marine genomics*, 20, pp. 45-55.

Smith, K.E., Thatje, S., Hauton, C., 2013. Thermal tolerance during early ontogeny in the common whelk *Buccinum undatum* (Linnaeus 1785): Bioenergetics, nurse egg partitioning and developmental success. *Journal of Sea Research*. 79, pp. 32-39.

Sokolova, I.M., Berger, V.J., 2000. Physiological variation related to shell colour polymorphism in White Sea *Littorina saxatilis*. *Journal of Experimental Marine Biology and Ecology*, 245(1), pp. 1-23.

Sokolova, I.M., Bock, C., Pörtner, H.O., 2000a. Resistance to freshwater exposure in White Sea *Littorina* spp. I: Anaerobic metabolism and energetics. *Journal of Comparative Physiology B*, 170(2), pp. 91-103.

Sokolova, I.M., Granovitch, A.I., Berger, V.J., Johannesson, K., 2000b. Intraspecific physiological variability of the gastropod *Littorina saxatilis* related to the vertical shore gradient in the White and North Seas. *Marine Biology*, 137(2), pp. 297-308.

Sokolova, I.M., Pörtner, H.O., 2003. Metabolic plasticity and critical temperatures for aerobic scope in a eurythermal marine invertebrate (*Littorina saxatilis*, Gastropoda: Littorinidae) from different latitudes. *Journal of Experimental Biology*, 206(1), pp. 195-207.

Solas, M.R., Hughes, R.N., Márquez, F., Brante, A., 2015. Early plastic responses in the shell morphology of *Acanthina monodon* (Mollusca, Gastropoda) under predation risk and water turbulence. *Marine Ecology Progress Series*, 527, pp. 133-142.

Soldati, A.L., Jacob, D.E., Schöne, B.R., Bianchi, M.M., Hajduk, A., 2009. Seasonal periodicity of growth and composition in valves of *Diplodon chilensis patagonicus* (d'Orbigny, 1835). *Journal of Molluscan Studies*, 75(1), pp. 75-85.

Soldati, A.L., Jacob, D.E., Glatzel, P., Swarbrick, J.C., Geck, J., 2016. Element substitution by living organisms: the case of manganese in mollusc shell aragonite. *Scientific reports*, 6(1), pp. 1-9.

Speer, J.A., 1983. Crystal chemistry and phase relations of orthorhombic carbonates. In: *Carbonates: Mineralogy and chemistry*. Reeder, R.J., (ed.) Mineralogical Society of America. pp. 145–190.

State of Maine, department of marine resources (2016). <http://www.maine.gov/dmr/science-research/species/whelks.html> [Accessed, March 2017].

Stillman, J.H., 2003. Acclimation capacity underlies susceptibility to climate change. *Science* (New York), 301(5629), p. 65.

Strand, J., Jacobsen, J.A., 2002. Imposex in two sublittoral neogastropods from the Kattegat and Skagerrak: the common whelk *Buccinum undatum* and the red whelk *Neptunea antiqua*. *Marine Ecology Progress Series*, 244, pp. 171-177.

Streli, C., Rauwolf, M., Turyanskaya, A., Ingerle, D., Wobrauschek, P., 2019. Elemental imaging of trace elements in bone samples using micro and nano-X-ray fluorescence spectrometry. *Applied Radiation and Isotopes*, 149, pp. 200-205.

Stuart-Fox, D., Moussalli, A., 2009. Camouflage, communication and thermoregulation: lessons from colour changing organisms. *Philosophical Transactions of the Royal Society B: Biological Sciences*, 364(1516), pp. 463-470.

Sullivan, C.H., Mangel, T.K., 1984. Formation, organization, and composition of the egg capsule of the marine gastropod, *Ilyanassa obsoleta*. *The Biological Bulletin*, 167(2), pp. 378-389.

Sun, X., Yang, A., Wu, B., Zhou, L., Liu, Z., 2015. Characterization of the mantle transcriptome of yesso scallop (*Patinopecten yessoensis*): identification of genes potentially involved in biomineralization and pigmentation. *PloS one*, 10(4), p.e. 0122967.

Suzuki, M., Kameda, J., Sasaki, T., Saruwatari, K., Nagasawa, H., Kogure, T., 2010. Characterization of the multilayered shell of a limpet, *Lottia kogamogai* (Mollusca:

Patellogastropoda), using SEM–EBSD and FIB–TEM techniques. *Journal of structural biology*, 171(2), pp. 223-230.

Suzuki, S., Uozumi, S., 1981. Organic components of prismatic layers in molluscan shells. *Journal of the faculty of science Hokkaido University*, 20(1), pp. 7-20.

Sword, G.A., Simpson, S.J., 2000. Is there an intraspecific role for density-dependent colour change in the desert locust? *Animal Behaviour*, 59(4), pp. 861-870.

Takesue, R.K., Bacon, C.R., Thompson, J.K., 2008. Influences of organic matter and calcification rate on trace elements in aragonitic estuarine bivalve shells. *Geochimica et Cosmochimica Acta*, 72(22), pp. 5431-5445.

Tanabe, K., 1988. Age and growth rate determinations of an intertidal bivalve, *Phacosoma japonicum*, using internal shell increments. *Lethaia*, 21(3), pp. 231-241.

Ten Hallers-Tjabbes, C.C., 1979. The shell of the whelk *Buccinum undatum*: Shape analysis and sex discrimination. Groeningen, the Netherlands: University of Groeningen.

Ten Hallers-Tjabbes, C.C., Kemp, J.F., Boon, J.P., 1994. Imposex in whelks (*Buccinum undatum*) from the open North Sea: relation to shipping traffic intensities. *Marine Pollution Bulletin*, 28(5), pp. 311-313.

Thébault, J., Chauvaud, L., 2013. Li/Ca enrichments in great scallop shells (*Pecten maximus*) and their relationship with phytoplankton blooms. *Palaeogeography, Palaeoclimatology, Palaeoecology*, 373, pp. 108-122.

Thébault, J., Chauvaud, L., l'Helguen, S., Clavier, J., Barats, A., Jacquet, S., Pécheyran, C., Amouroux, D., 2009a. Barium and molybdenum records in bivalve shells: Geochemical proxies for phytoplankton dynamics in coastal environments? *Limnology and Oceanography*, 54(3), pp. 1002-1014.

Thébault, J., Schöne, B.R., Hallmann, N., Barth, M., Nunn, E.V., 2009b. Investigation of Li/Ca variations in aragonitic shells of the ocean quahog *Arctica islandica*, northeast Iceland. *Geochemistry, Geophysics, Geosystems*, 10(12).

Thomas, M.L.H., Himmelman, J.H., 1988. Influence of predation on shell morphology of *Buccinum undatum* L. on Atlantic coast of Canada. *Journal of Experimental Marine Biology and Ecology*, 115(3), pp. 221-236.

Thompson, J.B., Paloczi, G.T., Kindt, J.H., Michenfelder, M., Smith, B.L., Stucky, G., Morse, D.E., Hansma, P.K., 2000. Direct observation of the transition from calcite to aragonite growth as induced by abalone shell proteins. *Biophysical Journal*, 79(6), pp. 3307-3312.

- Thomsen, J., Casties, I., Pansch, C., Körtzinger, A., Melzner, F., 2013. Food availability outweighs ocean acidification effects in juvenile *Mytilus edulis*: Laboratory and field experiments. *Global Change Biology*, 19(4), pp. 1017-1027.
- Thomsen, J., Gutowska, M., Saphörster, J., Heinemann, A., Trübenbach, K., Fietzke, J., Hiebenthal, C., Eisenhauer, A., Körtzinger, A., Wahl, M., Melzner, F., 2010. Calcifying invertebrates succeed in a naturally CO₂ enriched coastal habitat but are threatened by high levels of future acidification. *Biogeosciences*, 7(11), pp. 3879-3891.
- Toland, H., Perkins, B., Pearce, N., Keenan, F., Leng, M.J., 2000. A study of sclerochronology by laser ablation ICP-MS. *Journal of Analytical Atomic Spectrometry*, 15(9), pp. 1143-1148.
- Tomanek, L., Somero, G.N., 1999. Evolutionary and acclimation-induced variation in the heat-shock responses of congeneric marine snails (genus *Tegula*) from different thermal habitats: implications for limits of thermotolerance and biogeography. *The Journal of Experimental Biology*, 202(21), pp. 2925-2936.
- Travis, D.F., François, C.J., Bonar, L.C., Glimcher, M.J., 1967. Comparative studies of the organic matrices of invertebrate mineralized tissues. *Journal of Ultrastructure Research*, 18(5-6), pp. 519-550.
- True, J.R., 2003. Insect melanism: the molecules matter. *Trends in ecology and evolution*, 18(12), pp. 640-647.
- Trussell, G.C., Etter, R.J., 2001. Integrating genetic and environmental forces that shape the evolution of geographic variation in a marine snail. In: Hendry, A.P., Kinnison, M.T., (eds.) *Microevolution Rate, Pattern, Process*. Contemporary Issues in Genetics and Evolution, Volume 8. Springer, Dordrecht.
- Tsuji, T., Sharp, D.G., Wilbur, K.M., 1958. Studies on shell formation. VII. The submicroscopic structure of the shell of the oyster *Crassostrea virginica*. *The Journal of Biophysical and Biochemical Cytology*, 4(3), pp. 275-280.
- Turekian, K.K., Armstrong, R.L., 1960. Magnesium, strontium and barium concentrations and calcite-aragonite ratios of some recent molluscan shells. *Journal of Marine Research*, 18, pp. 133-151.
- Underwood, A.J., Creese, R.G., 1976. Observations on the biology of the trochid gastropod *Austrocochlea constricta* (Lamarck) (Prosobranchia). II. The effects of available food on shell-banding pattern. *Journal of Experimental Marine Biology and Ecology*, 23(3), pp. 229-240.
- Valentinsson, D., 2002. Reproductive cycle and maternal effects on offspring size and number in the neogastropod *Buccinum undatum* (L.). *Marine Biology*, 140(6), pp. 1139-1147.

- Valentinsson, D., Sjödin, F., Jonsson, P.R., Nilsson, P., Wheatley, C., 1999. Appraisal of the potential for a future fishery on whelks (*Buccinum undatum*) in Swedish waters: CPUE and biological aspects. *Fisheries Research*, 42(3), pp. 215-227.
- Van Beek, F.A., van Leeuwen, P.I., Rijnsdorp, A.D., 1990. On the survival of plaice and sole discards in the otter-trawl and beam-trawl fisheries in the North Sea. *Netherlands Journal of Sea Research*, 26(1), pp. 151-160.
- Vandenabeele, P., Moens, L., Edwards, H.G.M., and Dams, R., 2000. Raman spectroscopic database of azo pigments and application to modern art studies. *Journal of Raman Spectroscopy*, 31(6), pp. 509-517.
- VanPlantinga, A.A., Grossman, E.L., 2019. Trace elements in mussel shells from the Brazos River, Texas: Environmental and biological control. *Biogeosciences Discussions*, pp. 1-27.
- Vasconcelos, P., Morgado-André, A., Morgado-André, C., Gaspar, M.B., 2011. Shell strength and fishing damage to the smooth clam (*Callista chione*): simulating impacts caused by bivalve dredging. *ICES Journal of Marine Science*, 68(1), pp. 32-42.
- Vermeij, G.J., 1973. Morphological patterns in high-intertidal gastropods: adaptive strategies and their limitations. *Marine Biology*, 20(4), pp. 319-346.
- Von Bertalanffy, L., 1938. A quantitative theory of organic growth (inquiries on growth laws. II). *Human Biology*, 10(2), pp. 181-213.
- Walker, P.A., Heessen, H.J.L., 1996. Long-term changes in ray populations in the North Sea. *ICES Journal of Marine Science: Journal du Conseil*, 53(6), pp. 1085-1093.
- Wanamaker, A.D., Gillikin, D.P., 2019. Strontium, magnesium, and barium incorporation in aragonitic shells of juvenile *Arctica islandica*: Insights from temperature controlled experiments. *Chemical Geology*, 526, pp. 117-129.
- Warter, V., Erez, J., Müller, W., 2018. Environmental and physiological controls on daily trace element incorporation in *Tridacna crocea* from combined laboratory culturing and ultra-high resolution LA-ICP-MS analysis. *Palaeogeography, Palaeoclimatology, Palaeoecology*, 496, pp. 32-47.
- Warton, D.I., Duursma, R.A., Falster, D.S., Taskinen, S., 2012. smatr 3—an R package for estimation and inference about allometric lines. *Methods in ecology and evolution*, 3(2), pp. 257-259.
- Watabe, N., 1983. Shell Repair. In: Saleuddin, A.S.M., Wilbur, K.M., (eds.) *The Mollusca*, Volume 4: Physiology. Academic Press, New York. pp. 289-316.

- Watabe, N., Meenakshi, V.R., Blackwelder, P.L., Kurtz, E.M., Dunkelberger, D.G., 1976. Calcareous spherules in the gastropod *Pomacea paludosa*. In: Watabe, N., Wilbur, K.M., (eds.) Mechanisms of mineralization in the invertebrates and plants. University South Carolina Press, Columbia, pp. 283–308.
- Watson, E.L., Vincenzi, F.F., Davis, P.W., 1971. Ca^{2+} activated membrane ATPase: selective inhibition by ruthenium red. *Biochimica et Biophysica Acta (BBA) - Biomembranes*, 249(2), pp. 606-610.
- Watson, S.A., Peck, L.S., Tyler, P.A., Southgate, P.C., Tan, K.S., Day, R.W., Morley, S.A., 2012. Marine invertebrate skeleton size varies with latitude, temperature and carbonate saturation: implications for global change and ocean acidification. *Global Change Biology*, 18(10), pp. 3026-3038.
- Weetman, D., Hauser, L., Bayes, M.K., Ellis, J.R., Shaw, P. W., 2006. Genetic population structure across a range of geographic scales in the commercially exploited marine gastropod *Buccinum undatum*. *Marine Ecological Progress Series*. 317, pp. 157-169.
- Weiner, S., Addadi, L., 1997. Design strategies in mineralized biological materials. *Journal of Materials Chemistry*, 7(5), pp. 689-702.
- Weiner, S., Levi-Kalishman, Y., Raz, S., Addadi, L., 2003. Biologically formed amorphous calcium carbonate. *Connective Tissue Research*, 44(1), pp. 214-218.
- Weiner, S., Traub, W., 1984. Macromolecules in mollusc shells and their functions in biomineralization. *Philosophical Transactions of the Royal Society B: Biological Sciences*, 304(1121), pp. 425-434.
- Weiss, C.A., Torres-Cancel, K., Moser, R.D., Allison, P.G., Gore, E.R., Chandler, M.Q., Malone, P.G., 2014. Influence of temperature on calcium carbonate polymorph formed from ammonium carbonate and calcium acetate. *Journal of Nanotechnology and Smart Materials*, 1, pp. 1-6.
- Weiss, I.M., Tuross, N., Addadi, L.I.A., Weiner, S., 2002. Mollusc larval shell formation: amorphous calcium carbonate is a precursor phase for aragonite. *Journal of Experimental Zoology*, 293(5), pp. 478-491.
- Weissbuch, I., Addadi, L., Leiserowitz, L., 1991. Molecular recognition at crystal interfaces. *Science*, 253(5020), pp. 637-645.
- West, G.B., Brown, J. H., Brian J. Enquist, B.J., 2012. A general model for ontogenetic growth. *Nature*, 413, pp. 628-631.

- Wheeler, A.P., 1992. Mechanisms of molluscan shell formation. In: Bonucci, E. (ed.) *Calcification in Biological Systems*. CRC Press, Boca Raton, Florida. pp. 179-216.
- White, T.E., Dalrymple, R.L., Noble, D.W., O'Hanlon, J.C., Zurek, D.B., Umbers, K.D., 2015. Reproducible research in the study of biological coloration. *Animal Behaviour*, 106(5), pp. 51-57.
- Wilbur, K.M., Owen, G., 1964. Growth. In: Wilbur, K.M., Yonge, C.M., (eds.) *The Mollusca*, Volume 1: Physiology of Mollusca. Academic Press, New York. pp. 211-242.
- Wilbur, K.M., Watabe, N., 1963. Experimental studies on calcification in molluscs and the alga *Coccolithus huxleyi*. *Annals of the New York Academy of Sciences*, 109(1), pp. 82-112.
- Williams, S.T., 2017. Molluscan shell colour. *Biological Reviews*, 92(2), pp. 1039-1058.
- Williams, S.T., Ito, S., Wakamatsu, K., Goral, T., Edwards, N.P., Wogelius, R.A., Henkel, T., de Oliveira, L.F.C., Maia, L.F., Strekopytov, S., Jeffries, T., 2016. Identification of shell colour pigments in marine snails *Clanculus pharaonius* and *Clanculus margaritarius* (Trochoidea; Gastropoda). *PLoS One*, 11(7), p.e. 0156664.
- Witbaard, R., Klein, R., 1994. Long-term trends on the effects of the southern North Sea beamtrawl fishery on the bivalve mollusc *Arctica islandica* L. (Mollusca, bivalvia). *ICES Journal of Marine Science*, 51(1), pp. 99-105.
- Wojdyr, M., 2010. Fityk: a general-purpose peak fitting program. *Journal of Applied Crystallography*, 43(5), pp. 1126-1128.
- Wolff, M., Garrido, J.P., 1991. Comparative study of growth and survival of two colour morphs of the Chilean scallop *Argopecten purpuratus* (Lamarck, 1819) in suspended culture. *Journal of Shellfish Research*, 10, pp. 47-53.
- Wood, R.S., Chakoumakos, B.C., Fortner, A.M., Gillies-Rector, K., Frontzek, M.D., Ivanov, I.N., Kah, L.C., Kennedy, B., Pracheil, B.M., 2022. Quantifying fish otolith mineralogy for trace-element chemistry studies. *Scientific Reports*, 12(1), pp. 1-10.
- Woods, P., Jonasson, J.P., 2017. Bayesian hierarchical surplus production model of the common whelk *Buccinum undatum* in Icelandic waters. *Fisheries Research*, 194, pp. 117-128.
- Yamada, S.B., 1987. Geographic variation in the growth rates of *Littorina littorea* and *L. saxatilis*. *Marine Biology*, 96(4), pp. 529-534.
- Zhao, L., Schöne, B.R., Mertz-Kraus, R., 2017a. Controls on strontium and barium incorporation into freshwater bivalve shells (*Corbicula fluminea*). *Palaeogeography, Palaeoclimatology, Palaeoecology*, 465, pp. 386-394.

Zhao, L., Schöne, B.R., Mertz-Kraus, R., Yang, F., 2017b. Insights from sodium into the impacts of elevated pCO₂ and temperature on bivalve shell formation. *Journal of Experimental Marine Biology and Ecology*, 486, pp. 148-154.

Zuur, A.F., Ieno, E.N., Walker, N., Saveliev, A.A., Smith, G.M., 2009. Mixed effects models and extensions in ecology with R. New York, USA: Springer. Available at: <https://doi.org/10.1007/978-0-387-87458-6>.

Appendices

Table of Contents

Appendix 1 – Atlas of shell damage	222
Appendix 2 – FITYK data processing method notes.....	229
Appendix 3 – Peak height, area, and full width half maximum under the 5 prominent peak positions used to fit spectra	241
Appendix 4 – DISP056 Dispensation for the collection of undersized whelks	242
Appendix 5 – Grant SP20234 Diamond Light Source.....	245
Appendix 6 – Overview of analytical techniques	249
Appendix 7 – Data processing; μ EXAFS - ATHENA.....	262
Appendix 8 – Methods used for processing μ XRF maps	263
Appendix 9 – Process for data analysis of laser output.....	266
Appendix 10 – Paper manuscript	268

Appendix 1 – Atlas of shell damage

This appendix provides background research into the variation in type of shell damage received by *Buccinum undatum*.

In their natural habitats marine molluscs frequently experience damage to their shells. This can be biological, in the form of predatory attacks with shells being chipped by the chelae of crushing crabs or drilling attempts by other predatory gastropods, for example *Nucella lapillus*. Further incidences can occur in some whelk species such as *Busycon carica* during feeding as they use their shell lip to abrade and open the shell valves of their prey along with accidental damage to the bivalve shell margin during the burrowing process (Ramsay *et al.*, 2001¹; Dietl, 2004²; Scolding and Richardson, 2007³). Abiotic factors such as storms (Miura *et al.*, 2012⁴), iceberg scour (Harper *et al.*, 2012⁵) and anthropogenic impacts from mechanical towed fishing gears can further result in damage incidences to the shell (Checa, 1993⁶; Gaspar *et al.*, 1994⁷; Witbaard and Klein, 1994⁸; Cadée, 1999⁹). Although there is variation in damage incidents, distinguishing these differences between anthropogenic and naturally induced incidents can be difficult (Figure A1.1). However, understanding these interactions and the causes of shell damage can provide useful information about the local environment (Cintra-Buenrostro, 2007¹⁰). The level and type of damage received to the shell will vary dependent on its cause. For example, the damage inflicted from feeding and burrowing to the edge of the shell lip, will differ from that of being knocked against by larger objects (e.g., mobile fishing gear). This could further be reflected through variations in geographical location, with differences in predator presence, exposure, and fishing activity across a range of sites.

¹ Ramsay, K., Richardson, C.A., Kaiser, M.J., 2001. Causes of shell scarring in dog cockles *Glycymeris glycymeris* L. *Journal of Sea Research*, 45(2), pp. 131-139.

² Dietl, G.P., 2004. Origins and circumstances of adaptive divergence in whelk feeding behavior. *Palaeogeography, Palaeoclimatology, Palaeoecology*, 208(3-4), pp. 279-291.

³ Scolding, J.W.S., Richardson, C.A., Luckenbach, M.J., 2007. Predation of cockles (*Cerastoderma edule*) by the whelk (*Buccinum undatum*) under laboratory conditions. *Journal of Molluscan Studies*, 73(4), pp. 333-337.

⁴ Miura, O., Sasaki, Y., Chiba, S., 2012. Destruction of populations of *Batillaria attramentaria* (Caenogastropoda: Batillariidae) by tsunami waves of the 2011 Tohoku earthquake. *Journal of Molluscan Studies*, 78(4), pp. 377-380.

⁵ Harper, E.M., Clark, M.S., Hoffman, J.J., Philipp, E.E.R., Peck, L.S., Morley, S.A., 2012. Iceberg Scour and Shell Damage in the Antarctic Bivalve *Laternula elliptica*. *PLoS ONE*, 7(9): e46341.

⁶ Checa, A., 1993. Non-predatory shell damage in recent deep-endobenthic bivalves from Spain. *Palaeogeography, Palaeoclimatology, Palaeoecology*, 100(3), pp. 309-331.

⁷ Gaspar, M.B., Richardson, C.A., Monteiro, C.A., 1994. The effects of dredging on shell formation in the razor clam, *Ensis siliqua* from Barrinha, southern Portugal. *Journal of the Marine Biological Association of the United Kingdom*, 74, pp. 927-938.

⁸ Witbaard, R., Klein, R., 1994. Long-term trends on the effects of the southern North Sea beamtrawl fishery on the bivalve mollusc *Arctica islandica* L. (Mollusca, bivalvia). *ICES Journal of Marine Science*, 51(1), pp. 99-105.

⁹ Cadée, G.C., 1999. Shell damage and shell repair in the Antarctic limpet *Nacella concinna* from King George Island. *Journal of Sea Research*, 41(1-2), pp. 149-161.

¹⁰ Cintra-Buenrostro, C.E., 2007. Trampling, peeling and nibbling mussels: an experimental assessment of mechanical and predatory damage to shells of *Mytilus trossulus* (Mollusca: Mytilidae). *Journal of Shellfish Research*, 26(1), pp. 221-231.



Figure A1.1: *Buccinum undatum* caught during time on commercial fishing boats. Shells clearly show signs of prior damage, with shell scarring evident in multiple places. Arrows indicate areas of shell damage and consequent scarring.

Investigations were carried out as part of this thesis to determine differing types of shell damage to *Buccinum undatum*. These trials have been carried out to attempt to identify specific patterns of shell damage and relate these findings to a single, whilst providing a baseline for further research. Data collected has been from both laboratory settings, along with observations on board commercial fishing vessels. Within this initial assessment of determining damage patterns to shells, predation, riddling (flat riddle and rotary), and otter trawling have been undertaken. These observations have further justified and highlighted the difficulty of quantifying individual damage causes to the shells, due to both the similarity in patterns of shell breakage, along with the un-known factor of prior shell damage and areas of shell weakness both within the laboratory trials, and field experiments. Further study would be recommended to also look at the additional impact of previous shell fracturing and re-growth, multiple damage incidences, along with disturbance incidences to ascertain if breakage to the shell is further enhanced by this process or to see if this affects where the breaks are made or how the shell falls away. It would further be beneficial to run longer term studies, rearing individuals within the laboratory and field, to ensure no prior shell damage has occurred and fully research

into the different causes of shell damage. Furthermore, to fully understand impacts of storms, turbulence, and trawling gears (i.e., scallop) over time, and determine the proportions of shell damage caused from these means, dive-based or underwater camera surveys would be necessary to assess immediate impact of those individuals on the sea floor. Additionally, it is recommended that any further research into spatial variations of shell damage incidences gathers information on fishing intensity, benthic ecology (i.e., predator abundance) and wave exposure and these are all considered to identify the causes of the differences in shell damage. It is likely that in areas of increased fishing activity, predation and exposure, more damaged shells will be encountered and there will be an increased variation in the type of damage to the shell.

Table A1.1: Methods used, and key observations found during damage trials.

Damage Type	Method	Observations	Figure
Predation	Live whelks were placed in a tank with unfed velvet swimming crabs. Tanks were checked hourly for 12 hours, and then again, a day later.	Initial chipping to shell lip, followed by siphonal canal and around shell whorls.	A1.2
Rotary riddle	Multiple trips on board commercial whelk fishing vessels between 2020-2023. Observations made on catch landed (oversized) and those returned to sea (undersized).	Chips to shell lip and siphonal canal, and occasional holes on different whorls.	A1.3
Flat riddle			A1.4
Beam trawl	Observational trips on board research vessel during beam trawls. It is key to note that very few whelks were caught over multiple trawls.	Chipping to shell lip and siphonal canal. However very few whelks were caught in trawls to fully investigate.	A1.5



Figure A1.2: A-C, Velvet swimming crab *Necora puber* feeding on live *Buccinum undatum*. D and E show predatory attacks by the crab with areas of shell chipped away from the crushing action of the claws marked by red arrows. F) shows a partly eaten *B. undatum* with continued chipping around the shell whorls and fleshy parts fully exposed, G) empty *B. undatum* shell after feeding process, shell lip, siphonal canal and whorls have been chipped away.



Figure A1. 3: Rotary riddle on board commercial whelk fishing boat. Yellow arrows indicate direction of whelk travelling through the metal frame. Red arrows show areas of shell damage from the riddling process.



Figure A1. 4: Flat riddle on board commercial whelk fishing boat. Red arrows show areas of shell damage from the riddling process.

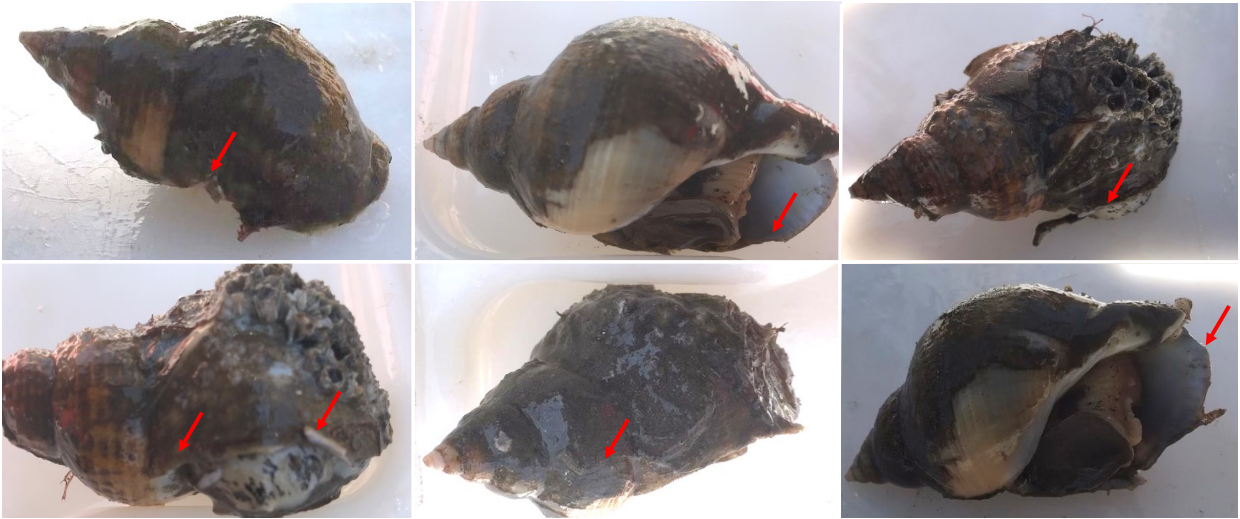


Figure A1. 5: *Buccinum undatum* caught during beam trawls. Damage to shells indicated by red arrows.

Appendix 2 – FITYK data processing method notes

Start with Excel spreadsheet “Modified Photospecwhelk V2.xlsx”

Sheets follow left to right order, start with sheet

“All combined” this comes from the data you sent me. WL (wavelength) is first column, then each analysis in columns afterwards. AT the top of each column, I have calculated the maximum value.

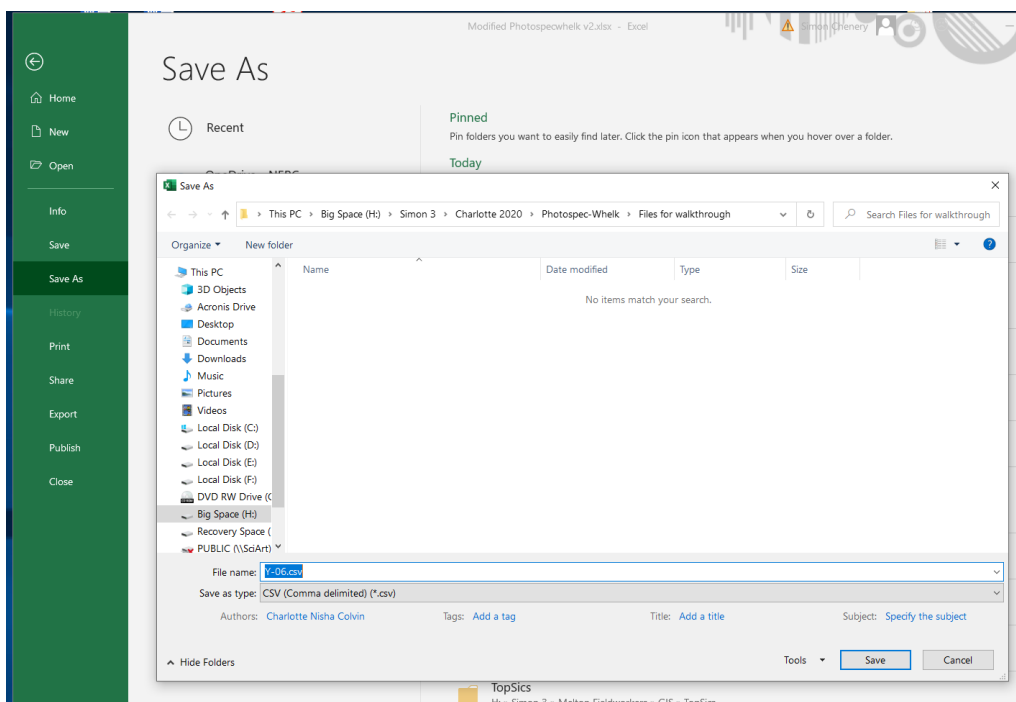
“All normed” takes the data from “All combined” and divides the values by the maximum and multiplies by 100. Thus, the resulting data points are normalised such that they are % of maximum.

“All norm Trim” takes columns from “All normed” (i) removes the lowest wavelength data 177.581 nm to 237.439 nm; (ii) names the individual shell data; (iii) creates new columns on the right-hand side of the data which are the mean and standard deviations for the first 6 shells of each colour e.g., “B-4-av” and “B-4-sd”.

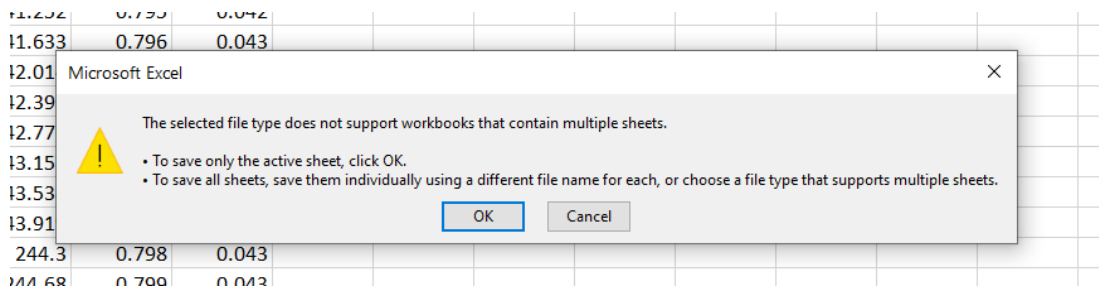
“Avg-sd” are the new mean and sd columns from “All norm Trim” pasted as values.

Fityk needs CSV files to read in and one spectra at a time so.... Example

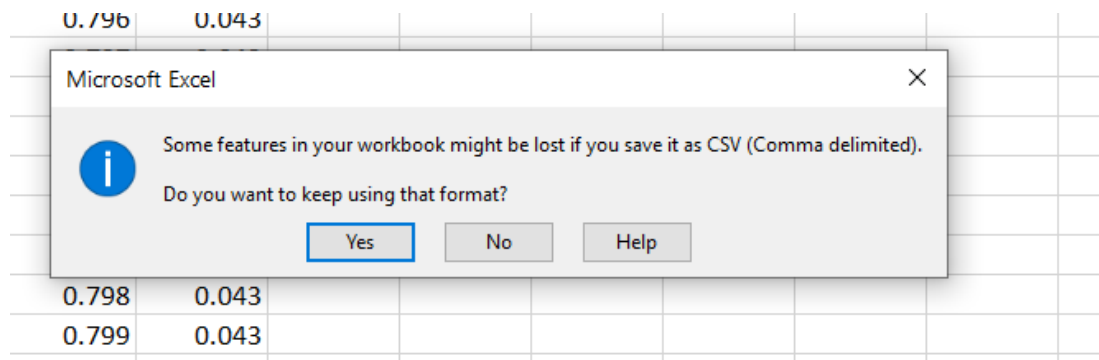
“Y06” copied wavelength column and then the average and sd columns for this shell Y-06 from “Avg-sd”. Save just this sheet by using



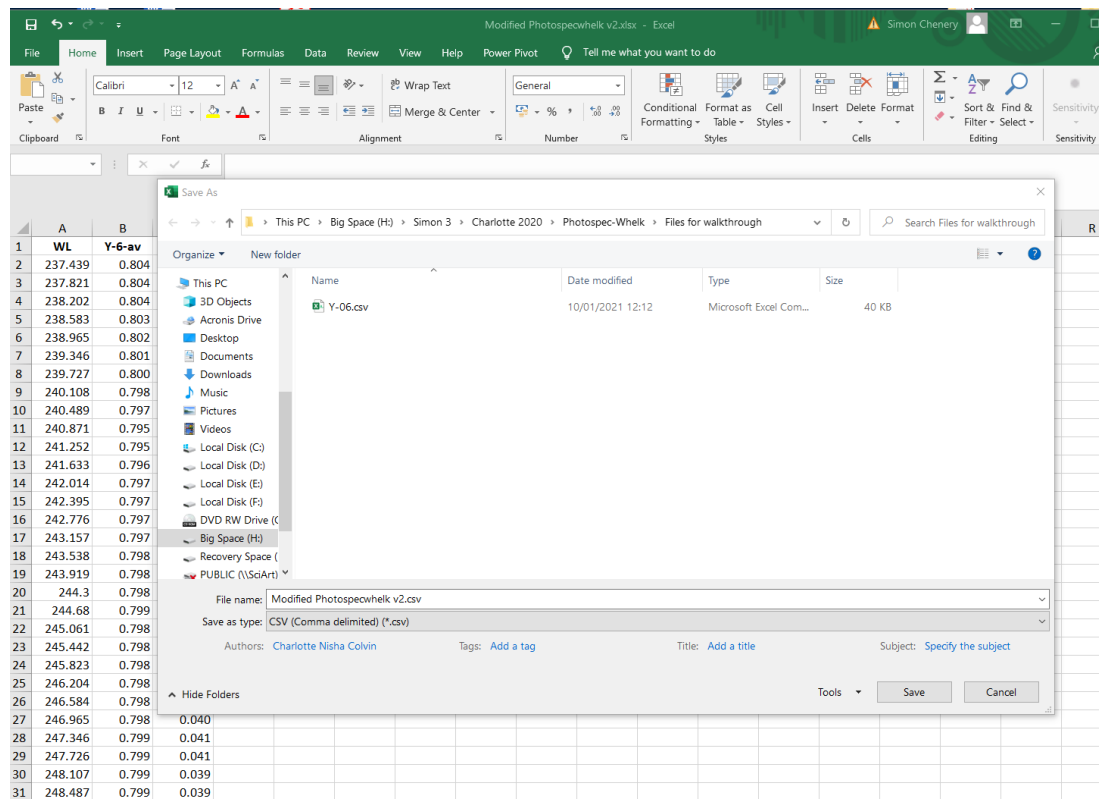
Then do OK to only save this sheet



Say “No” to keeping in CSV format, you want the original workbook to stay as XLSX



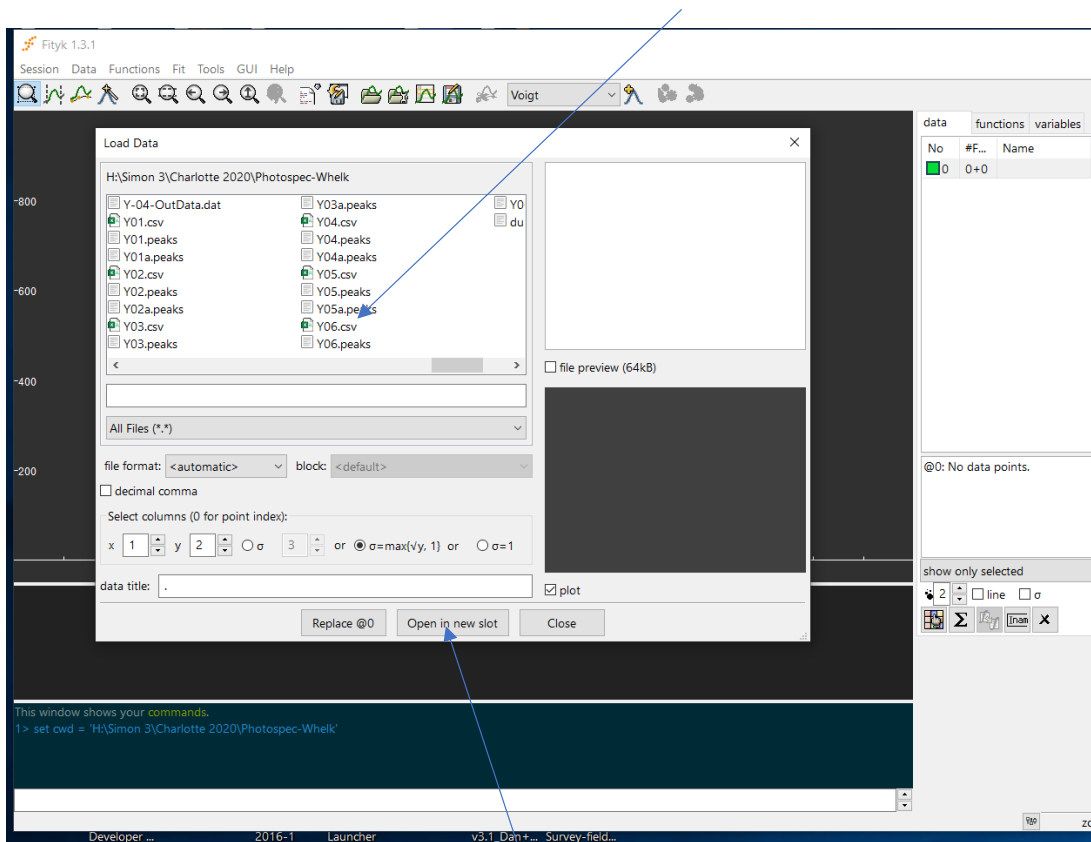
It will ask you to “save” again. Do not need to do this. Press “Cancel”



You can now proceed to replace “Y06” with the next shell data.

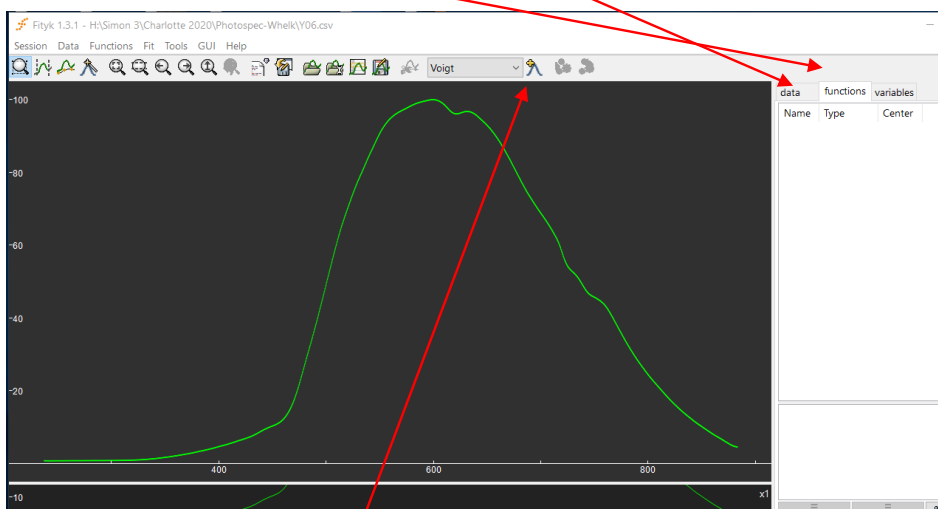
You are now ready to open Fityk and load CSV data file will use Y-06 as example.

Drop down menu "Data" and use "Load file" – in this case "Y-06.csv"



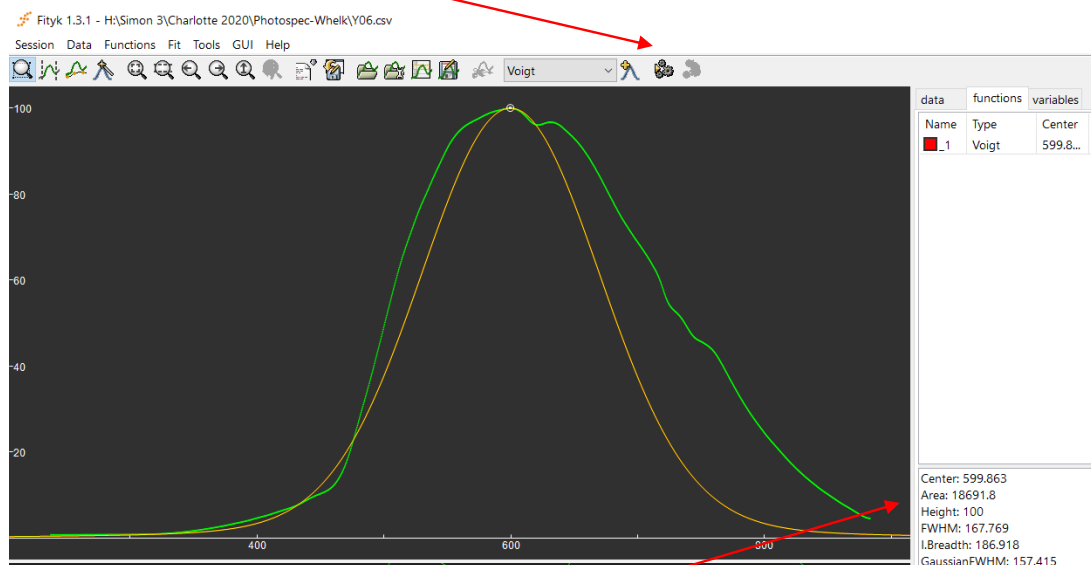
Use "Open in new slot" button at bottom of screen

Activate "functions" tab rather than "data" tab, so you can see what peaks you have added



Add first peak using button

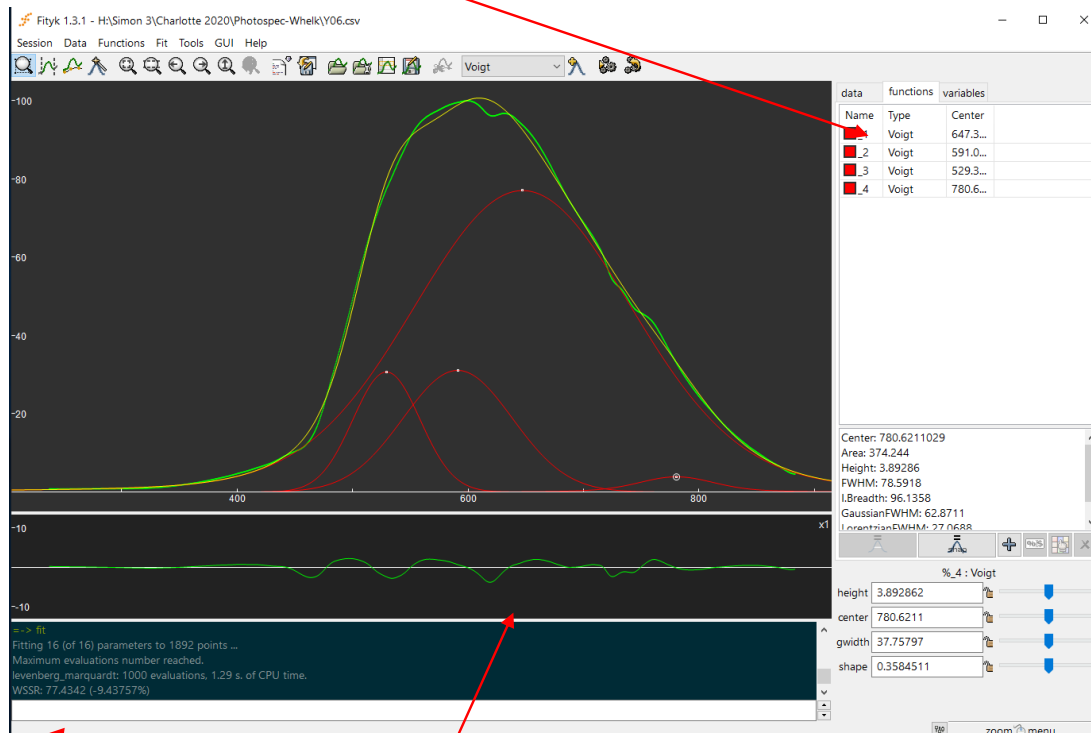
Press the "Fit" button



Note the fit parameters will change here

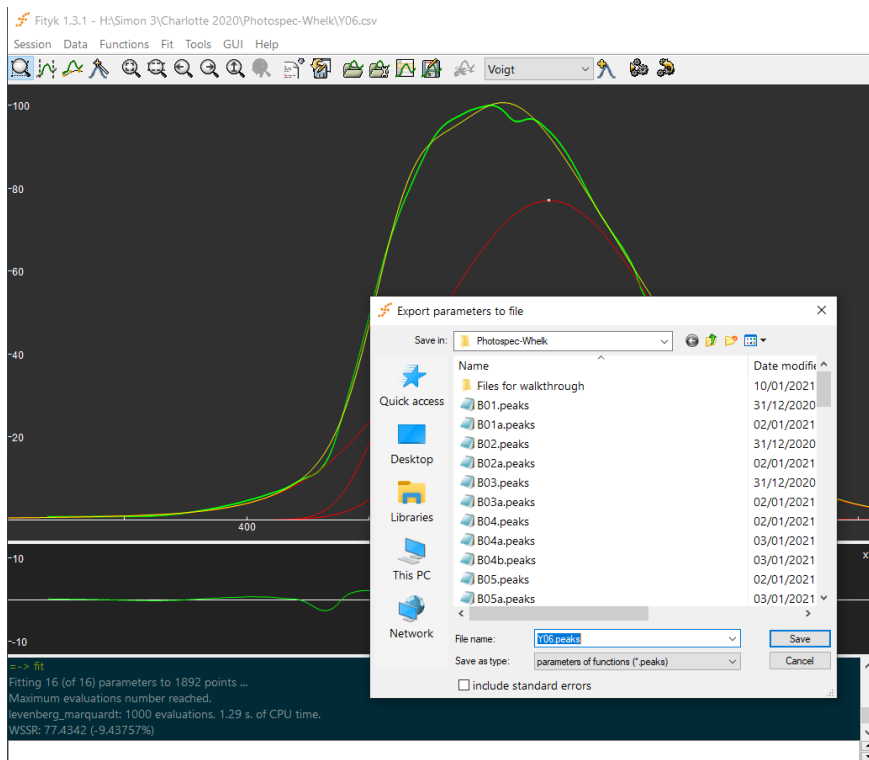
Repeat adding a peak and fitting each time you add a peak. Do this 4 times

You should see 4 functions



If the fit is reasonable the line showing the fit (original data in green – fitted data in yellow on the main window) should be "rippled" rather than "wavy" also the "WSSR" value will be less than about 200.

To save the data for each of the fitted peaks go to drop down menu “Functions” and choose “Export Peak Parameters” option. Save the peak data as “Y-06.peaks” etc



Next Excel spreadsheet is created from these” *. peaks” files. To get them into Excel open an empty Excel workbook and drag and drop on this.

It will then open a new workbook, if you are lucky or if it remembers from the last time, it will have everything ready in columns

# PeakType	Center	Height	Area	FWHM	parameters...
%_1 Voigt	647.329	77.0261	19375.7	224.435	77.0261 647.329 125.348 0.114106
%_2 Voigt	591.073	31.079	3690.28	111.453	31.079 591.073 66.9548 -0.000481089
%_3 Voigt	529.397	30.6792	2232.16	67.8796	30.6792 529.397 40.8685 -0.00391557
%_4 Voigt	780.621	3.89286	374.244	78.5918	3.89286 780.621 37.758 0.358451

If not, you will get text import wizard, you want “delimited” not “fixed width”

Text Import Wizard - Step 1 of 3

The Text Wizard has determined that your data is Delimited.
If this is correct, choose Next, or choose the data type that best describes your data.

Original data type

Choose the file type that best describes your data:

- Delimited - Characters such as commas or tabs separate each field.
- Fixed width - Fields are aligned in columns with spaces between each field.

Start import at row: 1 File origin: MS-DOS (PC-8)

My data has headers.

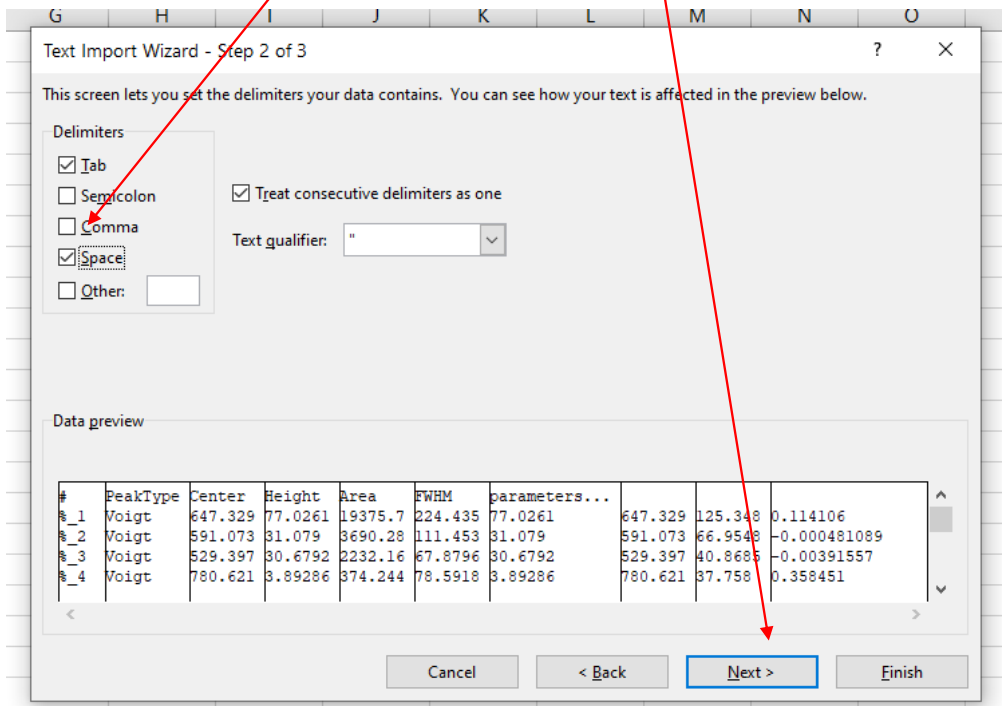
Preview of file H:\Simon 3\Charlotte 2020\Photospec-Wheelk\Files for walkthrough\Y06.peaks.

```

1 # PeakTypeCenterHeightAreaFWHMparameters...
2 %_1 Voigt647.32977.026119375.7224.435 77.0261 647.329 125.348 0.114106
3 %_2 Voigt591.07331.0793690.28111.453 31.079 591.073 66.9548 -0.000481089
4 %_3 Voigt529.39730.6792232.1667.8796 30.6792 529.397 40.8685 -0.00391557
5 %_4 Voigt780.6213.89286374.24478.5918 3.89286 780.621 37.758 0.358451

```

After you do "Next" tick "Space" under "Delimiters" . Then "Next" .

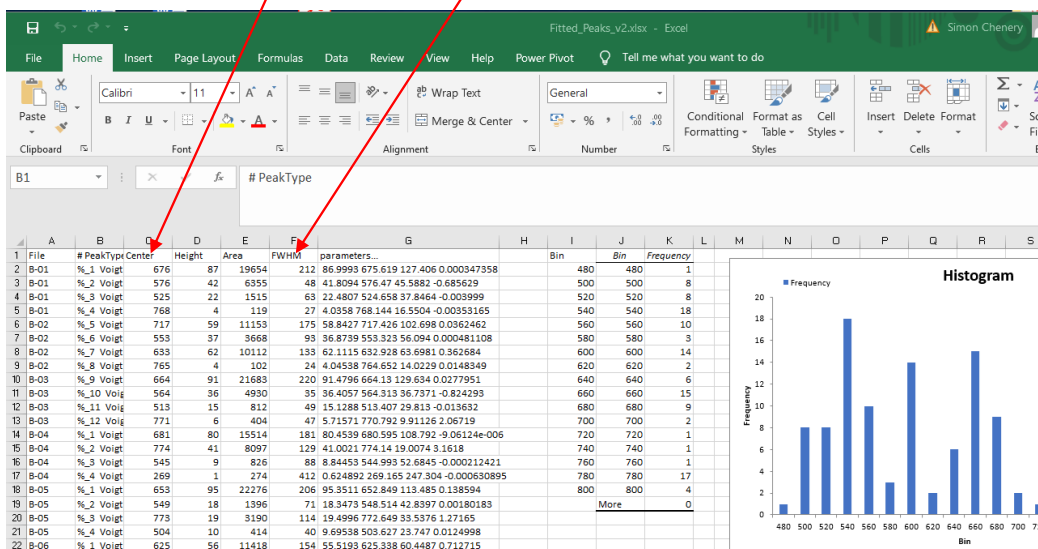


At following step just tick "Finish"

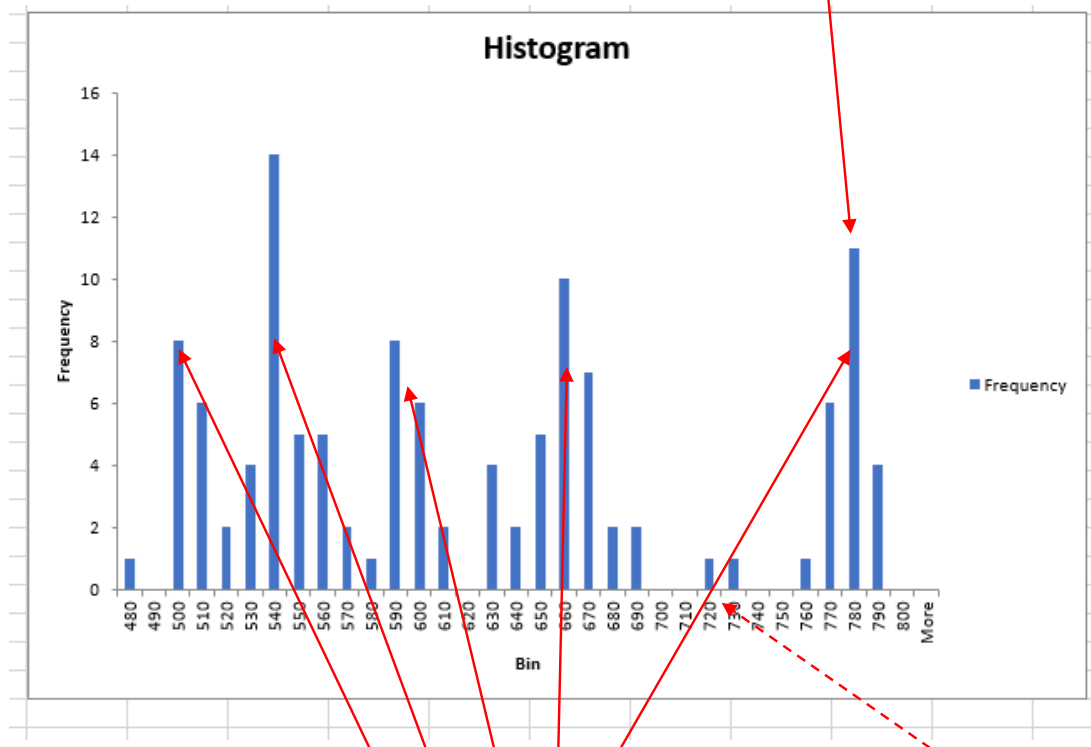
You can then cut and paste this data into a new compilation Excel spreadsheet.

This takes us to my next spreadsheet "Fitted Peaks v2.xlsx"

Start with sheet "Data1" this is a compilation of all the fitted peak data for the first 6 shells of each colour. Remember "Center" is the wavelength. FWHM is "Full Width Half Maximum" and is a measure of the fitted peak width



Make Histograms of the wavelength to decide on where primary peaks can be found in terms of wavelength



So, the 5 key wavelengths here were: 502; 539; 591; 655; 775.

As we discussed for the few peaks with a skewed to high wavelength shape needed to add 720 nm as 6th peak.

I have also plotted Center (wavelength) versus peak Height (Height Cht) and FWHM (FWHM cht) to help focus on what key wavelengths are and influence of colour

We can now go back to Fityk and re-fit with fixed peak points. You may want to use more than 6 shells per colour to produce a histogram with more data and your own chosen key wavelength.

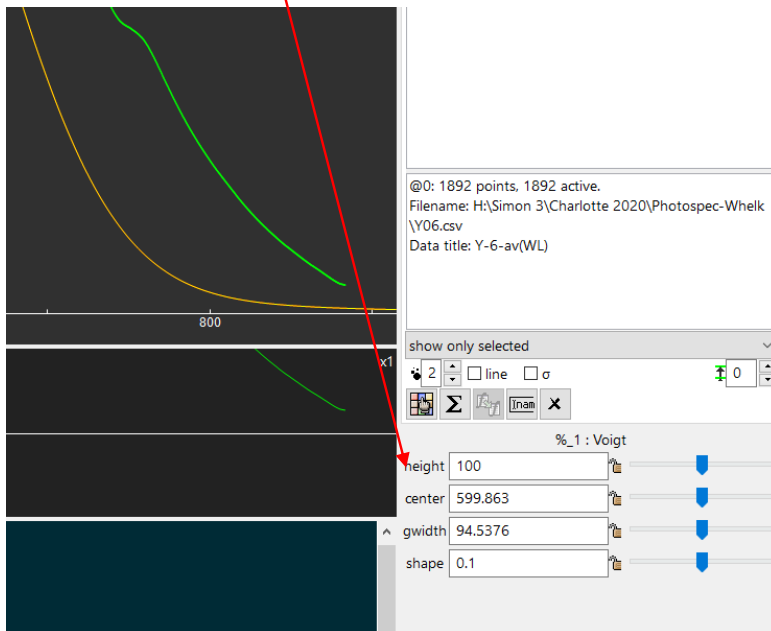
In Fityk, load the data file as before, we will use Y-06 as an example again.

High light the “functions” tab rather than “data” tab as before to see what you have done.

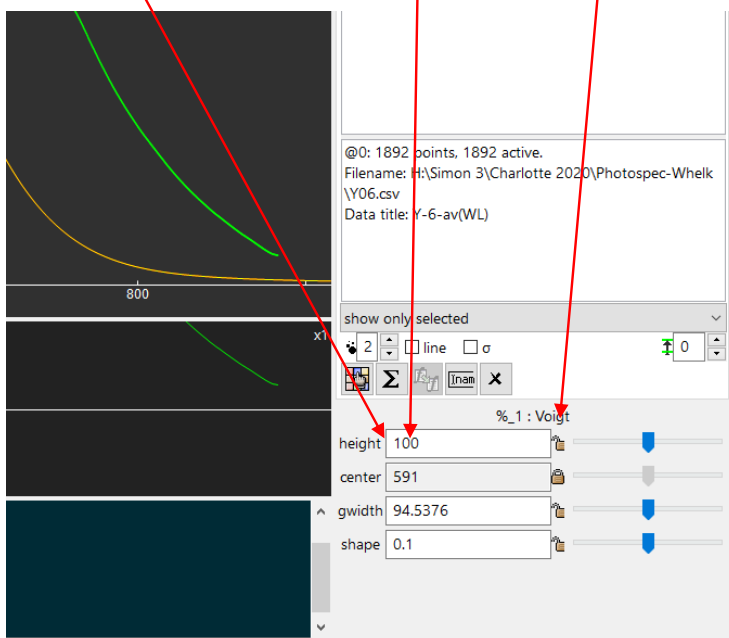
First, add a peak via the button as before, but **do not immediately** press the fit button.

Instead go to the peak data in the bottom left

Manually change center to the nearest peak value we want to fit, in this case the value is 599.863 and the nearest of our desired peak values is 591



When you have changed value to 591, click the little padlock to fix the value note. The value now has a grey background rather than white.



Now press the fit button.

Add another peak, this time it wants to go to 760.742, change this to 775

Now press the fit button.

Add another peak, this time it wants to go to 706.608, change this to 655

Now press the fit button.

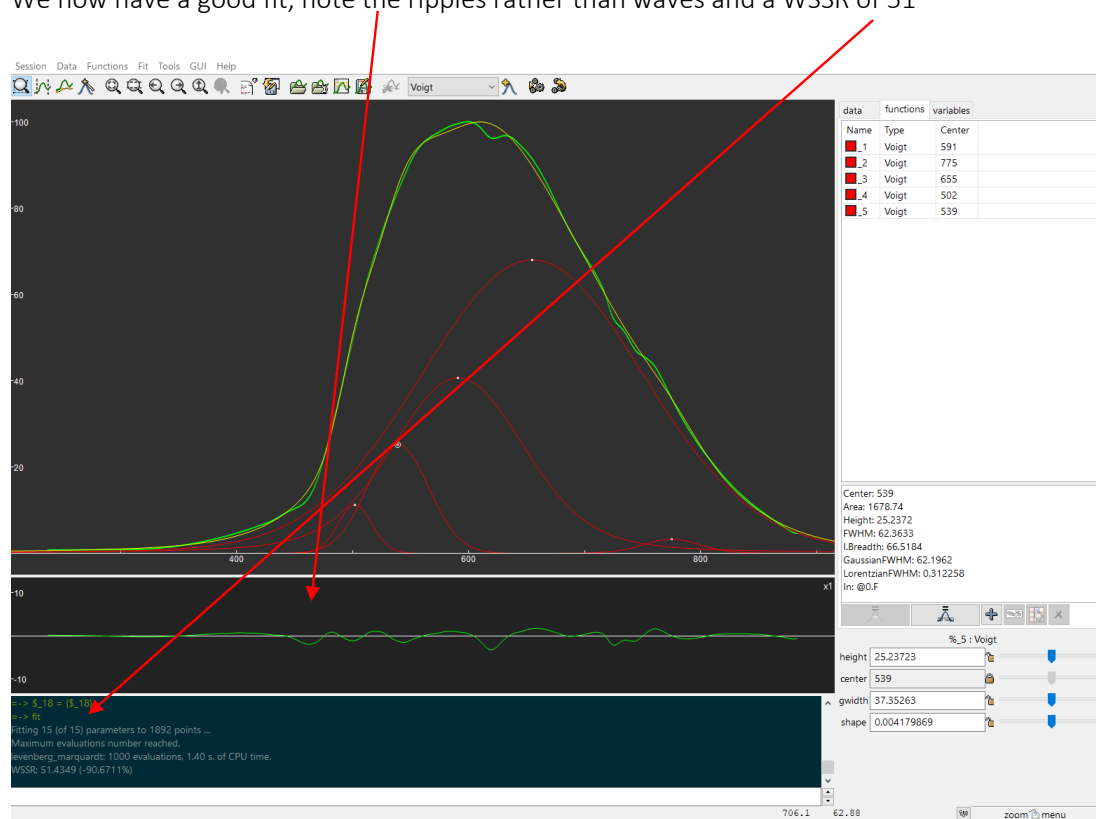
Add another peak, this time it wants to go to 514.703, change this to 502

Now press the fit button.

Add another peak, this time it wants to go to 535.466, change this to 539

Now press the fit button.

We now have a good fit, note the ripples rather than waves and a WSSR of 51



For the high wavelength skewed peaks you will need to add an extra 6th fixed peak of 720 nm

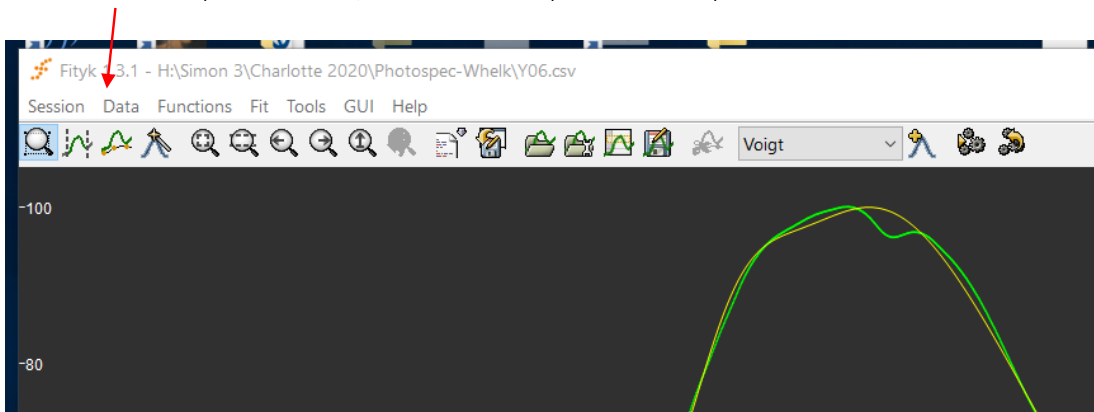
As before, to save the data for each of the fitted peaks go to drop down menu "Functions" and choose "Export Peak Parameters" option. Save the peak data as "Y-06A.peaks" etc I have save this as Y-06A.peaks so as not to overwrite the previous version.

Do not close Fityk yet!

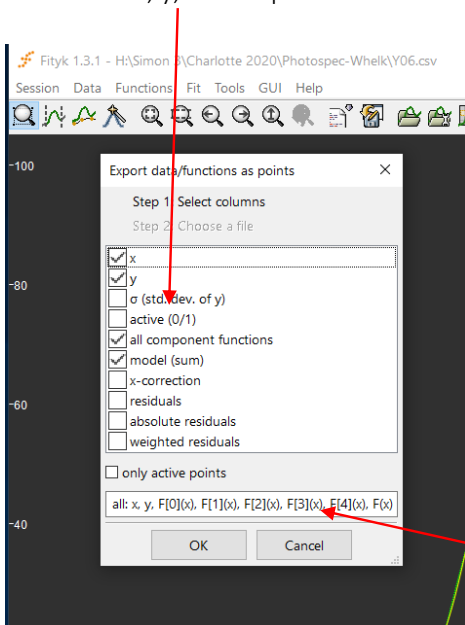
Next Excel spreadsheet is created from these "*.peaks" files. To get them into Excel open an empty Excel work book and drag and drop on this. But this time cut and paste into a second sheet in my case into "Fitted Peaks v2.xlsx" as sheet "Data2".

Once you have done this return to Fityk because we want to output the spectra to a data file to read into Excel to plot up nicely.

Go to "Data" dropdown menu, and choose "Export Points" option



Make sure x, y, all component functions, and model are ticked



Also, before clicking "OK" button copy the order they will appear in the output file from here i.e.

"x, y, F[0](x), F[1](x), F[2](x), F[3](x), F[4](x), F(x)"

Save the output points as something like "Y-06-Outdata.dat" to make it clear what this file is.

Note the *.dat extension.

Repeat all of the above for each shell you want to plot a nice output for!

In the same way we drag and dropped the "*.peaks" files onto a open Excel workbook to get it into a readable format you can do the same thing with the "*.dat" files. Again, you may have to use the Import text pop-ups to get the in.

You will need to add the column headers: x; y; F[0](x); F[1](x); F[2](x); F[3](x); F[4](x); F(x)" manually.

I have stacked all of these I did into "Out_Point_Data v2.xlsx".

Appendix 3 – Peak height, area, and full width half maximum under the 5 prominent peak positions used to fit spectra

Number of shells within peak group for each colour varies depending on if a peak was fitted. B, O, P, W, Y represent brown, orange, purple, white, and yellow shells respectively. Number after letter code is an individual shell identifier.

Center 520				Center 560				Center 620				Center 660				Center 780			
	Height	Area	FWHM		Height	Area	FWHM		Height	Area	FWHM		Height	Area	FWHM		Height	Area	FWHM
B11	8.28	610.11	68.21	B11	11.04	1149.80	97.62	B2	3.90	300.09	72.25	B11	55.37	14141.30	192.25	B11	74.31	13097.50	50.65
B2	6.11	357.59	54.94	B2	26.33	2389.94	85.26	O10	27.24	4142.75	75.22	B2	94.53	19015.10	179.73	B2	19.66	3187.61	118.65
B5	13.28	8.56E+02	6.04E+01	B4	1.29	5.46E+37	2.70E+37	O11	15.22	2352.18	99.83	B4	80.37	15517.90	181.39	B4	48.46	6710.20	130.08
B6	7.77	465.10	55.99	B5	17.90	2355.55	94.67	O2	86.54	18251.40	198.12	B5	93.44	21350.90	205.08	B5	16.24	2629.74	103.71
B9	7.32	401.43	51.52	B6	0.85	2.99E+24	2.25E+24	O6	35.20	8802.45	163.63	B6	97.40	21749.90	199.84	B6	25.55	3407.40	122.32
O10	11.02	727.47	62.02	B9	5.03	191.75	35.84	O9	25.45	2545.48	93.95	B9	84.17	20217.50	194.03	B9	50.91	6852.78	126.45
O11	6.99	406.85	54.66	O10	24.26	2203.32	85.31	P11	15.49	3250.75	133.76	O10	72.61	16310.90	203.12	O10	8.72	1394.41	102.19
O2	19.25	1030.66	50.30	O11	38.86	3693.97	89.24	P20	9.97	1185.43	111.74	O11	81.99	16145.30	179.59	O11	16.11	2911.33	119.73
O5	8.70	436.88	46.97	O2	18.31	974.68	50.02	P9	20.23	4786.22	161.35	O2	16.72	4473.38	171.81	O2	16.20	2021.88	117.24
O9	17.47	974.59	52.39	O5	68.79	9828.09	116.74	W10	96.73	21753.60	200.50	O5	75.89	12149.10	150.38	O5	19.36	3032.97	123.40
P10	5.76	395.18	64.18	O6	49.05	5211.39	99.80	W11	97.73	21864.00	199.54	O6	52.57	8131.59	145.30	O6	17.72	2761.46	114.00
P11	23.10	3041.76	86.23	O9	35.94	3383.31	60.24	W12	95.58	21757.50	203.42	O9	73.87	17344.70	220.59	O9	0.37	1.85E+61	-2.21E+60
P12	9.23	673.01	68.43	P10	2.94	1.95E+61	4.22E+60	W15	95.60	21844.50	193.52	P10	50.41	13314	203.02	P10	69.78	9864	132.78
P20	16.54	1073.58	60.97	P11	34.81	5520.24	116.05	W17	94.91	21397.20	179.98	P11	68.71	11593.70	158.51	P11	47.33	8043.74	139.55
P7	10.61	682.27	60.42	P12	10.02	910.26	85.15	W9	97.11	21992.90	201.70	P12	62.64	15969	186.14	P12	70.41	10743.10	128.17
P9	3.85	1.07E+43	1.77E+42	P20	23.97	4417.05	118.18	Y11	47.83	9471.88	177.42	P20	81.54	19841.50	228.59	P20	4.67	340.01	68.45
W10	23.72	1469.01	58.19	P7	8.56	783.63	3.26	Y12	17.89	1342.31	70.48	P7	95.49	23775.40	205.21	P7	31.50	4458.16	122.05
W11	23.39	1392.38	55.93	P9	15.88	1804.97	106.81	Y14	20.06	2063.66	96.66	P9	34.75	5168.29	116.17	P9	85.01	13142.80	145.24
W12	22.79	1387.45	57.20	W11	11.78	578.20	45.46	Y18	97.05	20804.60	192.19	Y11	49.41	11005.30	192.49	W10	16.04	2748.60	110.86
W15	26.94	1701.19	59.32	W12	14.12	989.94	47.98	Y20	75.45	15885.90	186.93	Y12	80.28	18644.20	196.28	W11	16.72	2863.58	110.06
W17	23.98	1488.84	58.32	W15	12.74	862.40	53.46					Y14	81.07	17764.30	185.99	W12	15.58	2728.12	112.47
W9	22.99	1412.75	57.72	W17	14.11	1014.49	54.48					Y19	76.42	12126.50	148.98	W15	13.72	2394.88	113.07
Y11	18.22	992.95	51.14	W9	12.18	669.82	27.06					Y20	19.75	3699.33	175.93	W17	15.12	2574.30	109.77
Y12	16.07	886.27	51.82	Y11	30.13	2551.73	79.55									W9	16.26	2813.83	111.38
Y14	14.55	902.07	58.23	Y12	44.35	3836.65	81.27									Y11	14.31	1988.84	73.51
Y18	23.24	1199.92	48.43	Y14	33.38	2787.23	78.43									Y12	10.96	1386.34	111.36
Y19	12.07	607.77	47.28	Y18	17.41	934.54	50.27									Y14	13.48	1972.28	114.67
Y20	17.02	880.21	48.60	Y19	69.34	9915.64	117.72									Y18	16.89	2594.03	115.81
				Y20	23.95	1762.42	69.12									Y19	20.74	3148.63	80.09
																Y20	18.09	3104.89	109.58

Appendix 4 – DISP056 Dispensation for the collection of undersized whelks

Is-adran Môr a Physgodfeydd / Marine & Fisheries Division



Llywodraeth Cymru
Welsh Government

Miss CN Colvin
School of Ocean Sciences
Bangor university
Menai Bridge
LL59 5AB

4 August 2017

Dear Miss Colvin

Project: Shell growth and repair in Whelk
Ref: DISP056

Thank you for your Exemption request received on 26 May 2017 regarding the collection of juvenile *Buccinum Undatum* in Welsh waters.

After due consideration of the details of the proposed research and all other relevant factors, the authorisations below are issued under authority of the Welsh Ministers, for the purposes of the legislation set out below.

These Authorisations:

1. are valid for the period 00:01 on 07 August 2017 to 23:59 on 01 June 2020;
2. only apply to the Research Vessel *The Mya* owned by *School of Ocean Sciences – Bangor University*;
3. only extend to the activities set out in your application documents received 26 May 2017; and
4. are subject to the Conditions set out below.

Uned Pysgodfeydd / Fisheries Unit
Llywodraeth Cymru / Welsh Government
Rhodfa Padarn,
Llanbadarn Fawr,
Aberystwyth,
Ceredigion, SY23 3UR

Ffôn/Tel 0300 062 2184
Marineandfisherieslegislation@wales.gsi.gov.uk
Gwefan/Website www.wales.gov.uk

The Authorisations

Council Regulation (EC) No 850/98 of 30 March 1998 for the conservation of fishery resources through technical measures for the protection of juveniles of marine organisms (“Council Regulation 850/98”).

The Activities which would otherwise be prohibited by Article 17, 18 and 19 of Council Regulation 850/98 are hereby authorised, subject to the Conditions below, pursuant to Article 43(1) of that Regulation (as being fishing operations conducted solely for the purpose of scientific investigations).

The activities set out in the application which would otherwise be covered by, **Byelaw 19: Specified Fish Sizes and Byelaw 30: Fishing for Lobster, Crawfish, Crab Prawn and Whelk** of the former North Western and North Wales Sea Fisheries Committee (NWNWSFC) are hereby authorised, subject to the conditions below, pursuant to Byelaw 1 of the NWNWSFC (fishing for sea fish for scientific purposes).

For information, the Byelaws of the Sea Fisheries Committees (SFCs) now have effect, as if made in a statutory instrument by the Welsh Ministers, by virtue of Article 13(1) of and Schedule 3 to the Marine and Coastal Access Act 2009 (Commencement No.1, Consequential, Transitional and Savings Provisions) (England and Wales) Order 2010 (S.I. 2010/630 (c.42)).

Conditions

1. The authorisations given above (“the Authorisations”) are valid for the period 00:01 on 07 August 2017 to 23:59 on 01 June 2020. The Authorisations expire automatically, if not terminated or withdrawn before that date.
2. The authorisations may only be exercised whilst on board the Research Vessel *The Mya*
3. The authorisations only extend to the Activities listed in your application.
4. Any species-
 - a. in respect of which a Special Area of Conservation (“SAC”) has been designated; and
 - b. which is caught as a result of undertaking the Activities within the relevant SAC, must be returned immediately to the sea, alive wherever possible.
5. No species caught as a result of undertaking the Activities can be offered for sale.
6. A copy of this letter must be kept on board the Research Vessel *The Mya* at all times whilst that vessel is exercising the Authorisations set out in this letter.
7. A copy of this letter must be presented upon request to any Welsh Government Fisheries Enforcement Officer and/or any Marine Enforcement Officer.
8. The Research Vessel *The Mya* and all crew on board must comply with all demands and instructions issued by any Welsh Government Fisheries Enforcement Officer and/or any Marine Enforcement Officer.
9. The Research Vessel *The Mya* and all crew on board must comply with all other relevant legislation (i.e. the Authorisations relate only to the legislation mentioned in the same).

10. The Welsh Government's Fisheries Enforcement Operations room must be notified at the beginning and again at the end of each day upon which activities will be undertaken in exercise of the Authorisations.

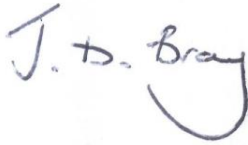
The Fisheries Enforcement Operations room can be contacted by telephone on 0300 025 7907 alternatively 0300 025 3500 or via email sent to fisheriesops@wales.gsi.gov.uk

11. If at any point during the authorisation period there are amendments to existing and/or the addition of any European Marine Site designation, the Habitat Regulation Assessment will need to be carried out again which may result in limitations/additional conditions. Welsh Government Officials will contact you if this situation arises.

12. The Welsh Ministers may in their absolute discretion withdraw these authorisations at any time. Where possible prior notice of withdrawal will be given, but in any of the following instances, this authorisation may be withdrawn without notice:

- (a) in the case of emergency;
- (b) if any of the Conditions set out in this letter are breached;
- (c) if the activities permitted by the Authorisations result or are likely to result in a significant effect to any European Marine Site (as defined by regulation 8(4) of the Conservation of Habitats and Species Regulations 2010 (SI 2010/490).

Yours sincerely

A handwritten signature in blue ink that reads "J. D. Bray". The signature is written in a cursive style with a large, sweeping flourish at the end.

Julian Bray
Head of Operations

Appendix 5 – Grant SP20234 Diamond Light Source

Dear Colleague,

Diamond is pleased to inform you that you have been successful with your proposal:
Proposal No [SP20234](#) "Determining spatial and temporal compositional variation in Buccinum undatum shells."
to be scheduled in the allocation period (AP) 24 from Oct 2018 - Apr 2019.

To help us with scheduling, please use this link [SP20234](#) to your proposal to **tell us your date preferences before Tue 3 Jul 2018**. Please ensure that you contact all your team members regarding this beamtime and scheduling. Please use this link to view the [AP24 schedule](#). Note that we will assume you are happy with any dates if we do not hear from you and will send you only a final schedule.

Further information on your proposal is given below.

Regards,

User Office
Diamond Light Source
Harwell Campus
Didcot
OX11 0DE
Tel: 01235 778571
Email: useroffice@diamond.ac.uk

Summary of the review of the proposal No: [SP20234](#)

Outcome: Number of shifts(s) 15 on I18: Microfocus Spectroscopy

The number of shifts awarded is provisional and is subject to scheduling constraints.

Comments:

Technical feasibility for I18: Microfocus Spectroscopy: Feasible : The investigators corresponded with Konstantin over the proposal. At that point they discussed doing 10 x 10 micron resolution XRD maps, which would take about 1.5 hrs, however in the proposal they discuss 2 x 2 micron maps, which for the same area take 25 times longer hence as written the proposal would take a long time, however I think a compromise on resolution & map size is achievable allowing a reasonable body of work to be obtained in 15 shifts.

Peer Review Panel comments:

The proposal was well received and should be awarded time.

Determining spatial and temporal compositional variation in *Buccinum undatum* shells.

Abstract – Trace element variations within mollusc shells have long been investigated as proxies for historical environmental conditions, e.g. seawater temperature. The efficacy of these proxies varies due to the influence of other factors such as physiological impacts and the mineralogy of the shells. Quantifying these factors is difficult due to the large unknowns in biologically mediated processes, such as shell growth rate. The whelk, *Buccinum undatum*, has a shell characterised by 4 distinct layers of the mineral aragonite but these layers exhibit distinctly different chemical compositions. Within areas of repaired shell, these differences are amplified, with significant changes in concentrations of key trace elements during periods of rapid shell expansion, seemingly unrelated to environmental effects. This project aims to quantify the influence of shell mineralogy and organic content on trace element incorporation during periods of rapid repair growth. This will be achieved by utilizing a suite of crystallographic (μ XRD), fluorescence (μ XRF) and absorption (μ XANES) techniques on the I-18 beamline to resolve differences in shell mineralogy, trace element concentrations and inorganic-organic coordination states of key trace at a high spatial resolution.

1. Scientific context - Calcium carbonate (CaCO_3) structures formed by marine molluscs incorporate trace elements during mineralization at detectable concentrations. There is much debate in the literature regarding the controlling factors behind trace element incorporation. There are clear differences both between and within species, likely depending on a range of environmental, physiological and structural factors (Gillikin et al., 2005; Schöne et al., 2010). Changes in environmental variables such as temperature, can control incorporation of particularly Mg and Sr which are at relatively steady concentrations in the water column throughout an annual cycle (Broecker & Peng, 1982; Kastner, 1999) (i.e. incorporation controlled by thermodynamic equilibrium). It has also been shown that physiology can likely mediate incorporation of certain elements such as Sr which increases with ontogenetic changes in growth for certain species (Hollyman et al., 2017). Mineralogical factors can influence trace element incorporation with differences in crystal structure and organic content potentially playing important roles. Mollusc shells are commonly found to be composed of two polymorphs of CaCO_3 , calcite and aragonite. The differences in crystal structure between these two forms causes clear differences in incorporation of elements, with aragonite incorporating Sr at concentrations orders of magnitude higher than calcite (Dietzel et al., 2004; Schöne et al., 2010). Whilst a majority of marine mollusc shells are comprised of aragonite, calcite shells are common and some structures can be comprised of both calcite and aragonite in a heterogenous matrix (Galante-Oliveria et al. 2014). The distinct structural differences between the layers of mollusc shells (in terms of crystal size, orientation and crystal microstructure) are thought to be regulated by differences in the organic matrix, used by molluscs to control shell deposition (Weiner & Traub, 1980; Levi-Kalishman et al., 2001). The organic component of mollusc shells is thought to represent between 1 and 5 % of the weight (Kaplan, 1998) and has been shown to either enrich (e.g. Mg) or deplete (e.g. Sr) trace element concentrations with increasing organic content (Schöne et al., 2010).

The common whelk, *Buccinum undatum* is a marine gastropod mollusc which has a shell comprised of 4 distinct layers which have all been shown to have an aragonitic composition with differences in organic matter and pigment content using Raman spectroscopy (Hollyman, 2017). Whilst the layers are all seemingly comprised of aragonite, significant differences in the relative abundances of Sr and Mg are seen between layers formed at similar times (Colvin, Hollyman & Chenery, unpublished data), suggesting some control on incorporation rates (such as organic content). Additionally, this species often suffers damage to the shell in its natural environment, which results in thicker and heavier shells. Colvin (2016) showed that shells which are artificially damaged can repair at a significantly faster rate than normal shell growth and also repair faster at warmer temperatures. The repaired sections of these shells go through a period of rapid expansion, during which, unexpected changes in elemental composition are seen (Colvin, Hollyman & Chenery, unpublished data, Figure 1). There is currently an experiment underway, where environmental and physiological factors are being controlled (two temperature treatments of 5 and 10°C and excess food supply). Quantifiable amounts of each shell are being removed following a suitable growth period to obtain baseline chemical and growth data. The shells are then being damaged and allowed to repair, enabling us to investigate the structural and chemical changes in shells, caused solely by periods of fast repair growth.

2. Experiment proposed - The proposed experiment will utilize fourteen of the experimental animals described above, 7 from the 5°C water treatment and 7 from the 10°C water treatment. Thin sections (~50 μm) will be made of pre-damage 'normal' growth shell and damage repaired 'fast' growth shell. These sections will be

adhered to Kapton tape and suspended over windows in custom microscope slides (following the sample preparation from rapid access proposal sp13616-1).

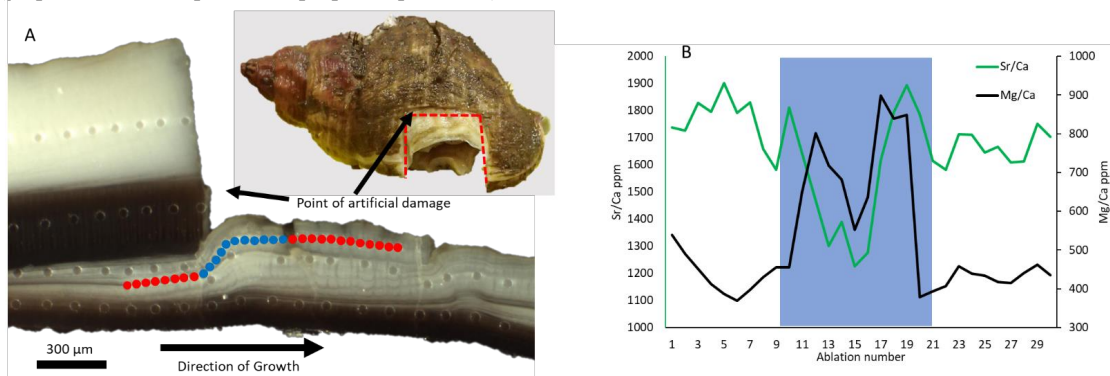


Figure 1. A, photomicrograph of a repair segment from an experimentally damaged *B. undatum*, highlighting a 25µm LA-ICP-MS sampling track (coloured dots) across the rapid expansion zone (blue dots). The inset image shows the point of artificial damage on an adult *B. undatum*. B, the resulting Sr/Ca and Mg/Ca data can be seen in the plot with reduced Sr and enriched Mg over the rapid expansion zone (blue box).

Firstly, differences in crystal structure between observable shell layers will be investigated using μ XRD to quantify structural heterogeneity over time between layers and between slow growing ‘normal’ shell and fast growing ‘repaired’ shell, using a track of 10 x 10µm beam spots over each area of interest (~ 2x2 mm²). Secondly, spatial changes in Sr incorporation during periods of rapid shell expansion during repair will be mapped using μ XRF at a 10 x 10µm resolution to produce spatial maps of Sr concentrations (~ 2x2 mm²). Lastly, to test whether spatial variations in Sr incorporation between layers and during repair are caused by differences in relative organic content, μ XANES will be used to map spatial changes in coordination states or lattice distortions of Sr across areas of interest (i.e. between layers and across damage repair areas). Areas with high organic content (and therefore more organically bound Sr) will have a different μ XANES profile to low organic content areas where the majority of Sr is intra-crystalline. Standards of organic and inorganic calcium carbonate (containing Sr) will be obtained and/or prepared prior to beamtime.

Synchrotron time is necessary for this project as it is the only way to spatially investigate crystallographic (μ XRD), elemental (μ XRF) and chemical (μ XANES) differences at the same resolution in the same samples, to answer our fundamental questions relating to controlling factors of trace element incorporation.

3. Results expected - We anticipate that the mineralogical structure of the fast and normal growth shell will differ to a degree measurable by XRD and XANES, which we could then correlate with concentration changes mapped by XRF. As all external environmental and physiological factors will have been controlled this must simply relate to biological growth. We also expect the differences in water temperature to have a marked effect on both the growth rate and concentration of Sr (with the 5°C treatment incorporating more). We believe this would be a first occasion of deconvolving internal and external controls on trace element concentrations. With an increased understanding of internal controls, we should be able to improve paleo-temperature records from wild shellfish

4. Publications

Hollyman, P.R., Chenery, S.R.N., EIMF, Konstantin Ignatyev, Laptikhovsky, V.V. & Richardson, C.A. (2017) Micro-scale geochemical and crystallographic analysis of *Buccinum undatum* statoliths reveals annual periodicity of visible growth rings. In Press, Chemical Geology, doi.org/10.1016/j.chemgeo.2017.09.034

Lloyd, N.S., Mosselmans, J.F.W., Parrish, R.R., Chenery, S.R.N., Hainsworth, S.V. and Kemp, S.J., “The morphologies and compositions of depleted uranium particles from an environmental case-study”, 2009, *Min. Mag.*, **73**, 495-510.

5. References

Gillikin DP, Lorrain A, Navez J, Taylor JW, André L, Keppens E, Baeyens W, Dehairs F (2005) Strong biological controls on Sr/Ca ratios in aragonitic marine bivalve shells. *Geochem Geophys Geosyst* 6:Q05009

- Schöne BR, Zhang Z, Jacob D, Gillikin DP, Tutken T, Garbe-Schoenberg D, McConnaughey T, Soldati A (2010) Effect of organic matrices on the determination of the trace element chemistry (Mg, Sr, Mg/Ca, Sr/Ca) of aragonitic bivalve shells (*Arctica islandica*)-Comparison of ICP-OES and LA-ICP-MS data. *Geochem J* 44:23-37
- Broecker WS, Peng TH (1982) Tracers in the sea. Lamont-Doherty Geological Observatory, Columbia University, New York
- Kastner M (1999) Oceanic minerals: Their origin, nature of their environment, and significance. *PNAS* 96:3380-3387
- Hollyman, P.R., Chenery, S.R.N., EIMF, Konstantin Ignatyev, Laptikhovsky, V.V. & Richardson, C.A. (2017) Micro-scale geochemical and crystallographic analysis of *Buccinum undatum* statoliths reveals annual periodicity of visible growth rings. In Press, *Chemical Geology*, doi.org/10.1016/j.chemgeo.2017.09.034
- Dietzel M, Gussone N, Eisenhauer A (2004) Co-precipitation of Sr²⁺ and Ba²⁺ with aragonite by membrane diffusion of CO₂ between 10 and 50°C. *Chem Geol* 203:139–151
- Galante-Oliveira S, Marçal R, Guimarães F, Soares J, Lopes JC, Machado J, Barroso CM (2014) Crystallinity and microchemistry of *Nassarius reticulatus* (Caenogastropoda) statoliths: towards their structure stability and homogeneity. *J Struct Biol* 186:292–301
- Weiner S, Traub W (1980) X-ray diffraction study of the insoluble organic matrix of mollusk shells. *FEBS Lett* 111:311–316
- Levi-Kalishman Y, Falini G, Addadi L, Weiner S (2001) Structure of the nacreous organic matrix of a bivalve mollusk shell examined in the hydrated state using cryo-TEM. *J Struct Biol* 135:8–17
- Kaplan D (1998) Mollusc shell structures: Novel design strategies for synthetic materials. *Curr Opin Solid State Mater Sci* 3:232-236
- Hollyman, P.R., 2017. Age, Growth and Reproductive Assessment of the Whelk, *Buccinum undatum*, in Coastal Shelf Seas. Unpublished PhD thesis. Bangor University (404 pp.).
- Colvin CN (2016) Timing of Shell Growth and Repair in the Whelk *Buccinum undatum* under Experimental Conditions. Master of Marine Biology thesis, Bangor University

Appendix 6 – Overview of analytical techniques

The following methods have all been used in the physiochemical analysis of the properties of *Buccinum undatum* shells. Techniques have been carried out at the British Geological Survey (BGS) and Diamond Light Source (DLS).

Raman Spectroscopy

Synchrotron analysis

Micro-X-ray Diffraction (μ XRD)

X-ray Absorption Spectroscopy (XAS) & Extended X-ray Absorption Fine Structure (EXAFS)

Micro-X-ray Fluorescence (μ XRF)

Laser Ablation-Inductively Coupled Plasma-Mass Spectrometry (LA-ICP-MS)

Raman Spectroscopy

Raman spectroscopy is a technique used to show the chemical and structural composition of a sample, to analyse materials based on scattered light and their vibrational state. Most materials, except for pure metals will produce a Raman spectrum. If the molecule can be polarised, Raman effects can be observed. Light can interact with matter in different ways and is affected by both the material and wavelength of light present. The Raman effect is very weak, with only about 1 in 10 million of the scattered light having a shifted colour, due to a changed frequency from interaction with molecular vibrations. This change is too weak to see with the naked eye and so we use a spectrometer.

The principle of Raman spectroscopy is to measure the inelastic scattering caused by a high intensity laser beam. Wavelengths in the visible-near infra-red spectrum are incident on the sample. Under normal conditions, molecules often occupy their ground-vibrational state, however the incident photons from the beam cause oscillation polarisation of the sample, exciting electrons to higher levels. Most incident photons are scattered from the molecule through elastic (Rayleigh) scattering, where the scattered wavelength is the same as the incident one. However, a small fraction (approximately 0.001%) is scattered with a different wavelength, resulting in inelastic (Raman) scattering. This can occur in two ways, as Stokes scattering, when the different frequency is lower, as energy is taken from the sample to excite electrons to a greater energetic level, or anti-Stokes as a result of higher energy photon scattering, whereby electrons are relaxed to a lower energetic level and this energy is transferred to the incident photons as they pass through (Figure A6.1) (Barhoum *et al.*, 2018¹¹; Renishaw, 2020¹²). It is this energy shift occurring within inelastic scattering that corresponds with characteristic frequencies, associated with vibrational states. A very high frequency vibration will show lighter atoms, held together with stronger bonds, resulting in a large energy change whereas a low frequency will indicate heavy atoms with weaker bonds. Wavenumbers can then be compared with a known compound (Renishaw, 2020¹²). The spectra are then

¹¹ Barhoum, A., García-Betancourt, M.L., Rahier, H., Van Assche, G., 2018. Physicochemical characterization of nanomaterials: Polymorph, composition, wettability, and thermal stability. In *Emerging applications of nanoparticles and architecture nanostructures*. pp. 255-278. Elsevier.

¹² <https://www.renishaw.com/en/raman-spectroscopy-explained--25801>

represented graphically, with intensity of scattered light plotted against the frequency of light (wavenumber = waves cm^{-1}).

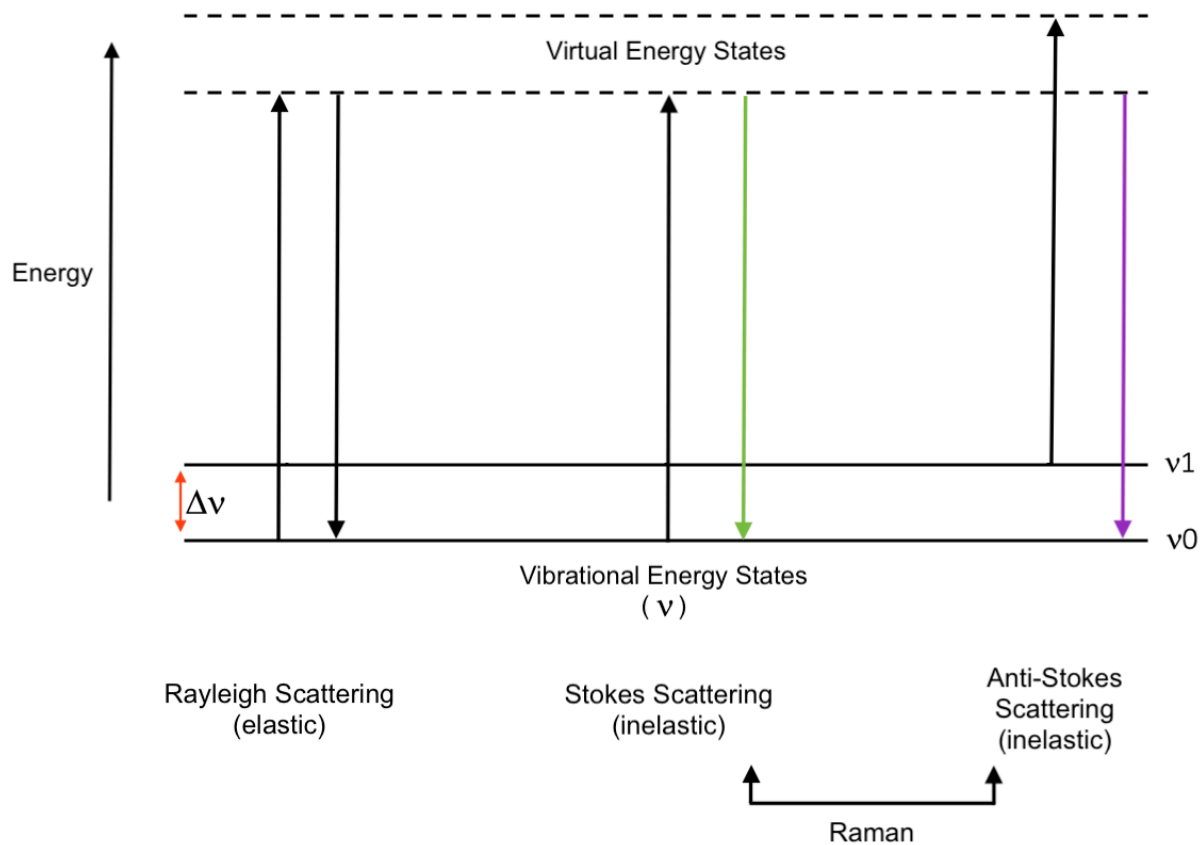


Figure A6. 1: Energy diagram, representing the different types of light scattering with inelastic (Raman) and elastic responses.

Synchrotron Analysis

A synchrotron (Figure A6.2) is a type of circular particle accelerator, providing a powerful source of X-rays. These X-rays are produced through the acceleration of charged particles (high energy electrons) through a sequence of magnets, circulating around the synchrotron. Accelerated towards the speed of light, the fast-moving electrons produce a bright light known as synchrotron light and is predominately in the X-ray region of the spectrum. The light is channelled down beamlines to experimental workstations where it is then used through a series of specialised equipment.

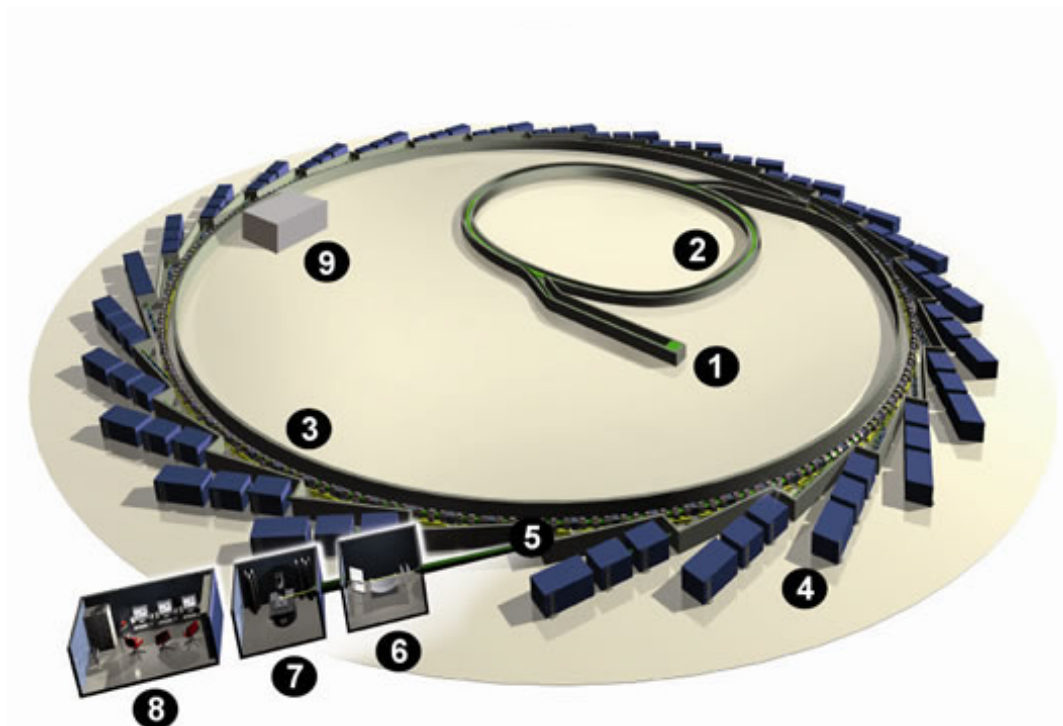


Figure A6. 2: Birds eye diagrammatic representation of the Diamond Light Source synchrotron Didcot, Oxford. 1) Injection system – electron gun and Linac, 2) Booster Synchrotron, 3) Storage Ring, 4) Beamline, 5) Front End, 6) Optics Hutch, 7) Experimental Hutch, 8) Control Cabin, 9) RF Cavities (Diamond Light Source, 2020).

There are several key components within the synchrotron used to produce and maintain these high energy beams. The electrons used to generate this ‘light’ are produced by an electron gun, which works through thermionic emission, whereby a high voltage cathode is heated under a vacuum giving electrons the energy to leave and escape from the surface. These electrons are then accelerated by earthed anodes, producing an energy stream of electrons of

90 keV, before being accelerated through the linear accelerator (linac) up to 100 MeV (0.1 GeV) using radio frequency (RF) cavities. The high energy electrons are injected from the linac through to the booster synchrotron, where they follow a track of two straight edges with curved ends. Dipole bending magnets are used here to allow the electrons to follow the curved track at each end, and a RF voltage accelerates them through the straight sections. The magnetic field is adjusted to maintain the course of the electrons as the energy rises to a final extraction level of 3 GeV. The storage ring is formed of 25 straight edge sections, combined to form a single closed loop. As before, large dipole bending magnets are used to curve the electron beam in the space between straight sections. This ring is maintained under a vacuum to minimise electron scattering because of air molecules and the 3 GeV electrons complete the 560m circuit in $2\mu\text{s}$. When the electrons are bent through a curve by magnets they emit radiation, primarily in the form of x-rays. From here the 'light' is extracted and is channelled into an individual beamline, through a shielded wall, where the X-rays can interact with the sample material and results are detected through specialised X-ray detectors. For this study, the I18 microfocuss spectroscopy beamline was used (Figure A6.3). This beamline uses a concentrated X-ray beam, operating within the range of 2.05-50.5 keV and has a spatial resolution of $2 \times 2\mu\text{m}$.

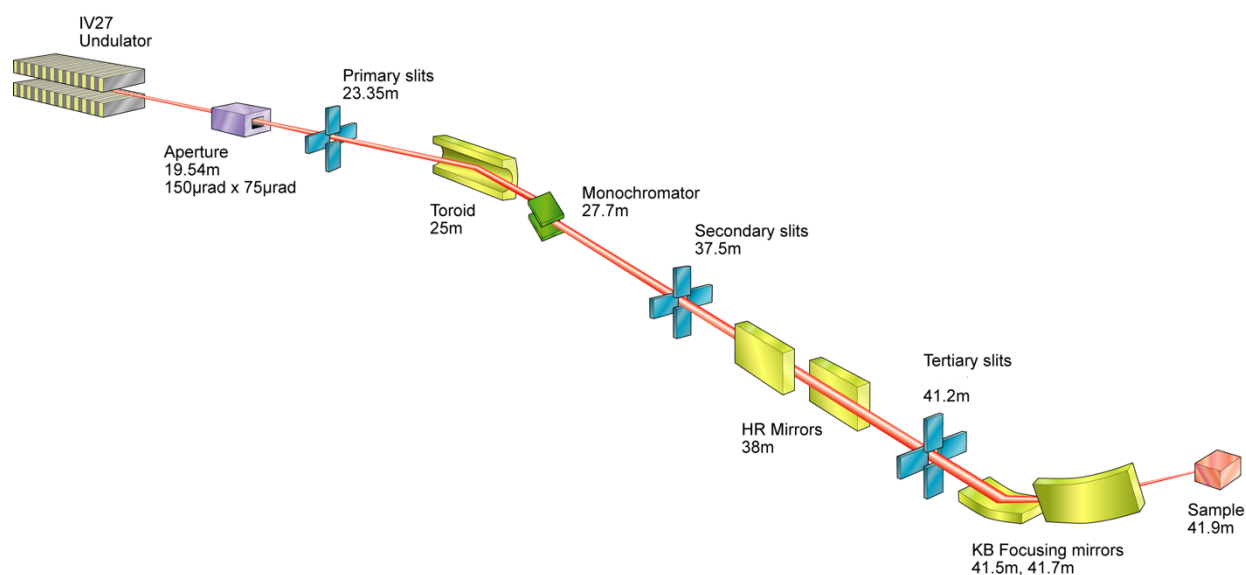


Figure A6. 3: Diamond Light Source I18 micro spectroscopy beamline schematic (Diamond Light Source 2020).

Micro-X-ray Diffraction μ XRD

To determine, the crystalline mineralogical phases of different materials, including crystal size and polymorphism XRD can be used. Due to the high intensity of synchrotron X-rays, the process of determining diffraction patterns is a much faster process, with higher sensitivity to changes within a smaller concentration of sample material than a conventional laboratory based XRD instrument with conventional 'cathode ray tube' where thermally produced x-rays from a cathode are simply accelerated onto a metal anode.

When an X-ray is used to irradiate a crystalline structure, a diffraction pattern is produced. This occurs because of X-ray scattering and relies upon the particle nature of the X-rays, to gain information about the crystalline structure. The diffraction pattern is made up of sharp peaks, known as Bragg diffraction peaks (Barhoum *et al.*, 2018¹³), and shows the variation in intensity of scattered X-rays because of interference from interaction with the regular and ordered crystalline structure. Conventionally XRD uses a powdered sample. Due to the random orientation of grains, the use of a powder will allow all possible reflections due to crystal orientation to be seen. X-ray patterns are collected and through computer software, a diffraction pattern is produced, comprising of peaks relating to specific crystalline structures and plane of orientation.

The intensities of diffracted waves correspond to the arrangement of atoms, while the wavelength compares spacing between atoms. These can then be compared using known samples through a database to determine composition. The process of μ XRD works in the same way as XRD, however a smaller beam size is used. Providing the beam can pass through the sample, through a thin even surface, the use of μ XRD will allow the sample to be analysed *in-situ*. The overall relationship of the wavelength from incident X-rays, angle of incidence and atomic spacing within the crystal lattice, is known as Bragg's, Law which forms the principle behind both XRD and μ XRD. This can be expressed as (Figure A6.4):

¹³ Barhoum, A., García-Betancourt, M.L., Rahier, H., Van Assche, G., 2018. Physicochemical characterization of nanomaterials: Polymorph, composition, wettability, and thermal stability. In *Emerging applications of nanoparticles and architecture nanostructures*. pp. 255-278. Elsevier.

$$n\lambda = 2d \sin\theta$$

n = An integer number representing the order of reflection

λ = Incident X-ray wavelength

d = Interplanar spacing within the crystal lattice

θ = Angle of incidence

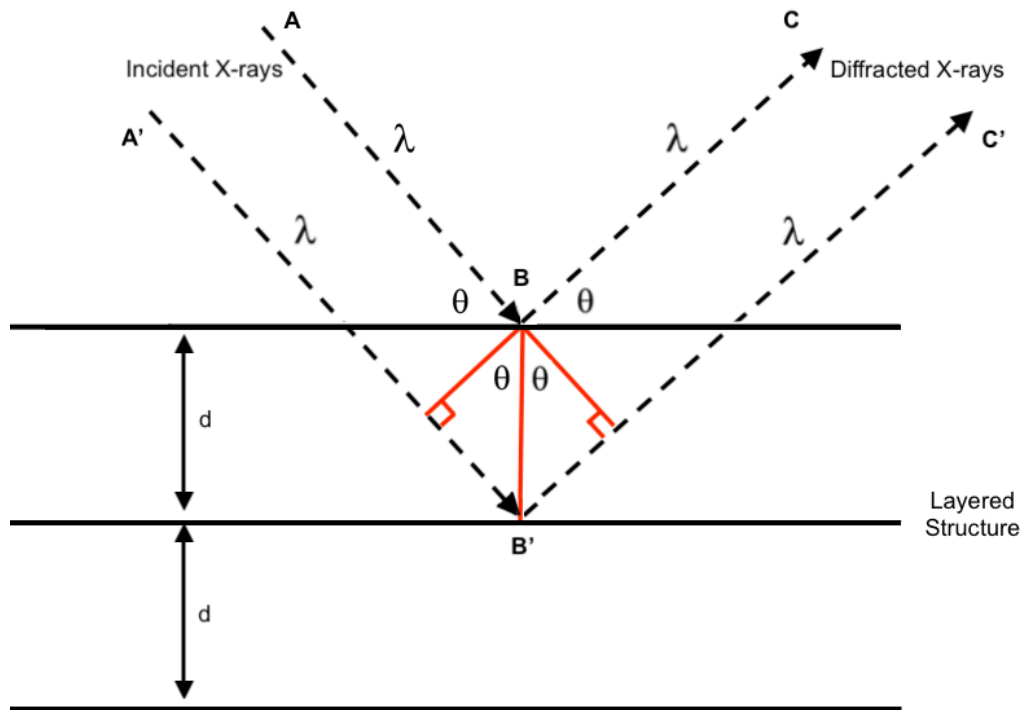


Figure A6. 4: Diagram depicting Bragg's Law. Diffracted X-rays from incident paths show constructive interference when the between distances of path ABC and A'B'C differs by the number of wavelengths (Image adapted from https://serc.carleton.edu/research_education/geochemsheets/BraggsLaw.html)

XAS – X-Ray Absorption Spectroscopy

XAS is the underlying process in which XANES and EXAFS work, through looking at the absorption of X-rays from core electrons of atoms within a sample. As an incident X-ray interacts with a sample, the electromagnetic radiation (EMR) is scattered or absorbed, consequently exciting the electrons, and the photoelectric effect occurs. This refers to the emission or ejection of electrons from a sample surface due to the EMR or light interference (Figure A6.5). Through using the X-ray region of the spectrum, the atoms dramatically absorb X-rays at certain wavelengths, which are known as absorption edges, and are characteristic of

a particular atom. Through using a specific energy of X-ray, we can account for the type of electron emitted (Diamond Light Source, 2020¹⁴).

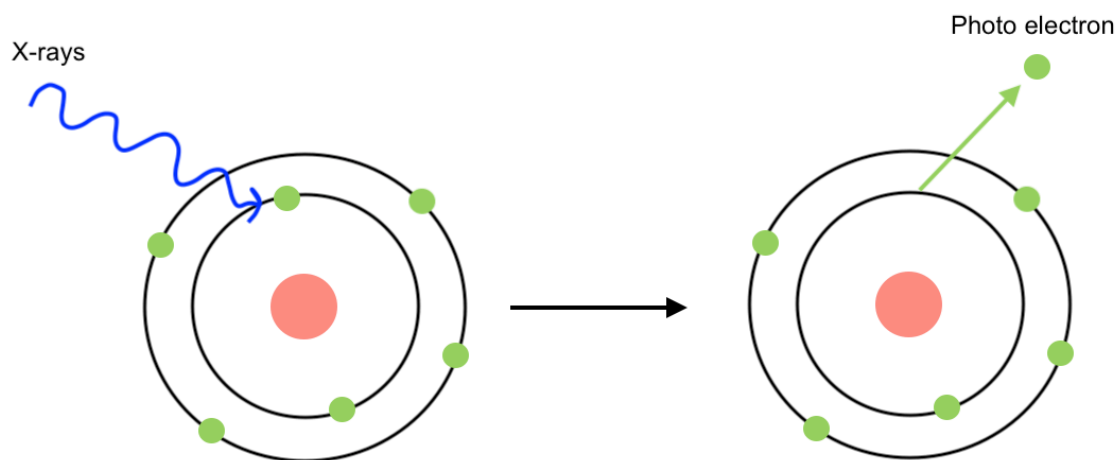


Figure A6. 5: Photoelectric emission. Image adapted from Diamond Light Source 2020.

There are different types of XAS techniques including X-ray Absorption Near Edge Structure (XANES), Near Edge X-ray Absorption Fine Structure (NEXAFS) and Extended X-ray Absorption Fine Structure (EXAFS) (Figure A6.6). XANES, is the absorption fine structure closest to the absorption edge (approximately 10 eV below and 20 eV above). This usually sees the largest variations in the X-ray absorption and usually has strong, narrow peaks, and gives information on the electronic structure of unoccupied levels and element geometry; it is commonly used to identify the valence state of atoms. Although XANES and NEXAFS are often interchangeable terms, today NEXAFS is more commonly used for soft X-ray absorption spectra (e.g., organics) and XANES for hard (e.g., coordination chemistry). EXAFS typically starts approximately 50 eV above the edge, this occurs from the scattering of the ejected photoelectron and is used to identify the local structure and surrounding elements of an element (Diamond Light Source, 2020¹⁴).

¹⁴ diamond.ac.uk/Instruments/Techniques/Spectroscopy/XAS.html

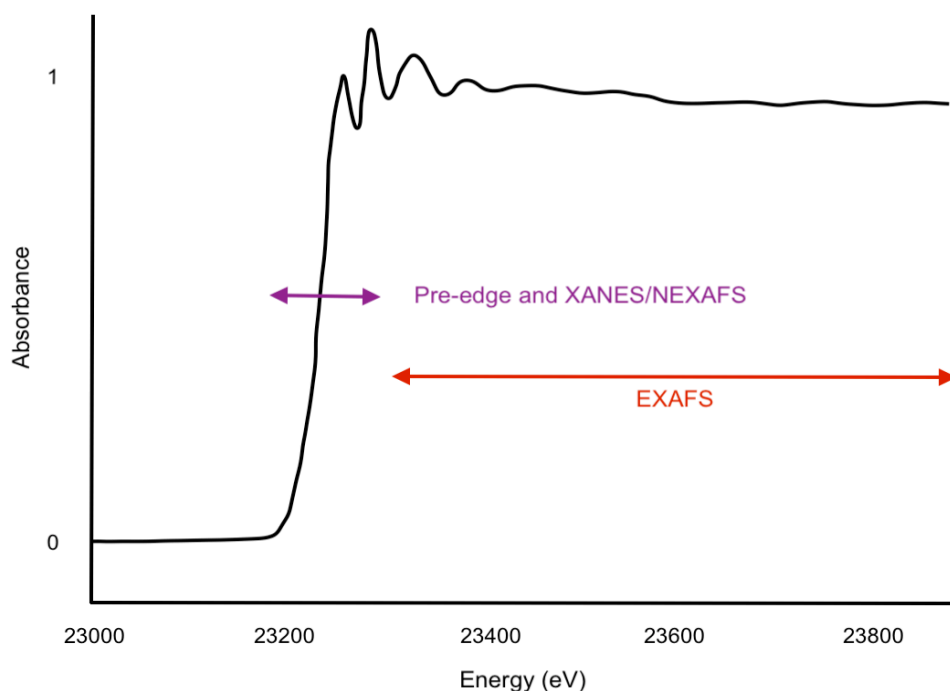


Figure A6. 6: X-ray absorption spectroscopy. Image adapted from Diamond Light Source 2020.

Extended X-ray Absorption Fine Structure EXAFS

EXAFS uses a similar reflective geometry to that of XRF and corresponds to the part of the spectrum to the right of the absorption edge, appearing as a sharp peak (starting approximately 50 eV to 1000 eV from the edge). Using EXAFS, information relating to the atom in question, including coordination number, disorder, and distance from and oxidation state of surrounding atoms can be attained. This X-ray spectroscopy involves an incident X-ray interacting with an atom. When the X-ray energy surpasses the ionisation energy of the shell an excited electron is ejected. This leaves a vacancy within the inner shell and resulting in the relaxation of an outer shell electron. EXAFS, data is taken based on the absorption coefficient; relationship between the incident X-ray and its intensity leaving after travelling a known distance within a sample. Within the spectrum, energy (eV) is plotted against absorbance and in a typical spectrum, sharp peaks will occur. The peaks or edges present vary by atom. Each peak corresponds to the ionisation of a core level, with K, L and M edges describing the excitation of the inner most and higher levels respectively. The downward oscillations occurring after the peaks (Figure A6.6) present the interaction of the wave between the photo electron and surrounding electrons in the atom. Peaks and troughs in the waves, correspond with constructive and destructive interference between waves, as they change direction because of

hitting neighbouring atoms. As these oscillations begin to decay, at approximately 30 eV past the edge the EXAFS fine structure region begins.

Micro-X-ray Fluorescence μ XRF

XRF is used to identify the concentration of particular elements within a sample. This elemental technique allows the examination of very small sample areas and can be used both qualitatively and quantitatively to identify material composition. Both XRF and μ XRF are similar, however μ XRF allows for smaller features to be analysed, due to the X-ray optics used. Here the excitation beam size is restricted or focussed onto a smaller spot on the sample. The techniques used in XRF are non-destructive and measure the characteristic fluorescence or secondary X-ray emitted from a sample.

The process of XRF works through the excitation of an inner electron. A primary X-ray source is used to irradiate a sample. When an atom is struck with sufficient energy, greater than the J or L shell binding energy, an electron from an inner shell is excited. As the X-ray is the electron is released up to a higher level. As stability is regained, an electron from an outer shell, relaxes and drops back down to fill the vacancy left in the inner shell. The return to the original energy level causes a lower energy X-ray to be emitted (Figure A6.7), which are also called secondary X-rays or fluorescence. The energy of these fluorescent X-rays is used to determine the elements within samples, with intensity at the characteristic energies proportional the abundance of element present. The detectors most commonly used in synchrotrons to quantify the X-rays are known as energy dispersive X-ray (EDX) analysers. These are semi-conductor devices that produce a voltage spike whose size is proportional to the energy of the X-ray and characteristic of the element. The number of voltage spikes of that particular size are proportional to the concentration of the element. This results in an energy spectrum, which when a significant number of elements are present in the sample may be quite complex. However, the reproducible nature of these fundamental physical processes has allowed software to 'deconvolve' these spectra.

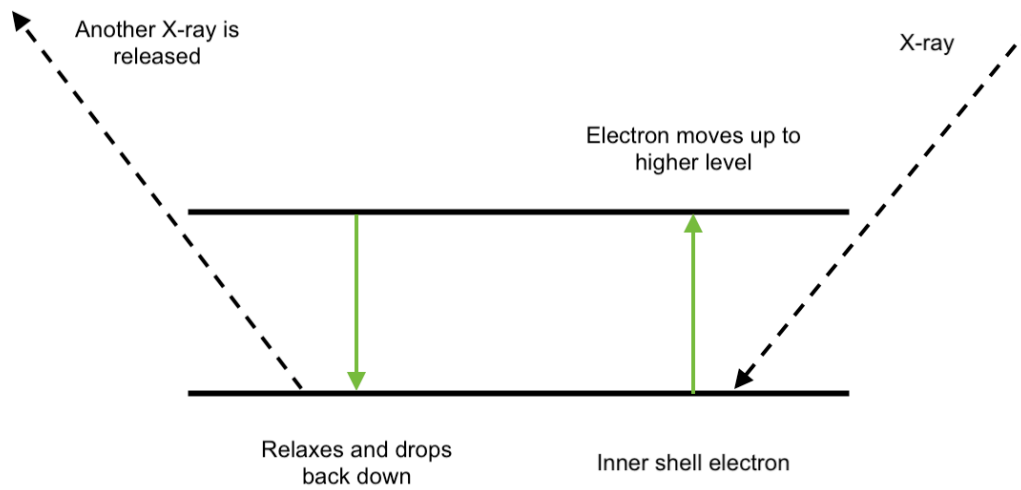


Figure A6. 7: Diagrammatic representation of the process of XRF. The inner shell electron is excited to a higher level before an electron relaxes and drops down to fill the gap. In this process a secondary X-ray/ fluorescence is emitted.

Laser Ablation-Inductively Coupled Plasma-Mass Spectrometry LA-ICP-MS

LA-ICP-MS is often the method of choice for quantitative trace element analysis; it provides access to more than 50 different elements and for a majority detection limit of below 1 ppm. This is combined with typical accuracy and precision below 10% RSD. The laser ablation system used at BGS consisted of the NewWave UP 193FX excimer (193nm) with an Agilent 7500 series ICP-MS. The NewWave UP 193FX excimer (193nm) laser ablation system is chiefly made up of four parts; the laser, optical beam delivery system, laser ablation cell and a computer system to control the system and allow the cell stage movement. It is important that the type of laser selected is carefully chosen based on energy density, laser wavelength and laser pulse length, to allow sufficient ablation of the sample material for ICP analysis. A shorter wavelength ensures good coupling, resulting in better craters and a greater degree of vaporisation (Chenery and Marriott 2022¹⁵) The sample is placed in the air-tight closed ablation chamber and flushed with helium as the carrier gas. Using the cell-in-cell design, samples are laid flat and raised to a defined height (Figure A6.8). The beam is then focussed onto each sample location specified by the computer, with the beam focussed through the cell window, using a specially adapted microscope and the cell is moved through an electro-mechanical drive through x-y directions.

¹⁵ Chenery, C., Marriott, A., 2022. Introduction to Laser Ablation – Inductively Coupled Plasma – Mass Spectrometry and Atomic Emission Spectrometry. *British Geological Survey*

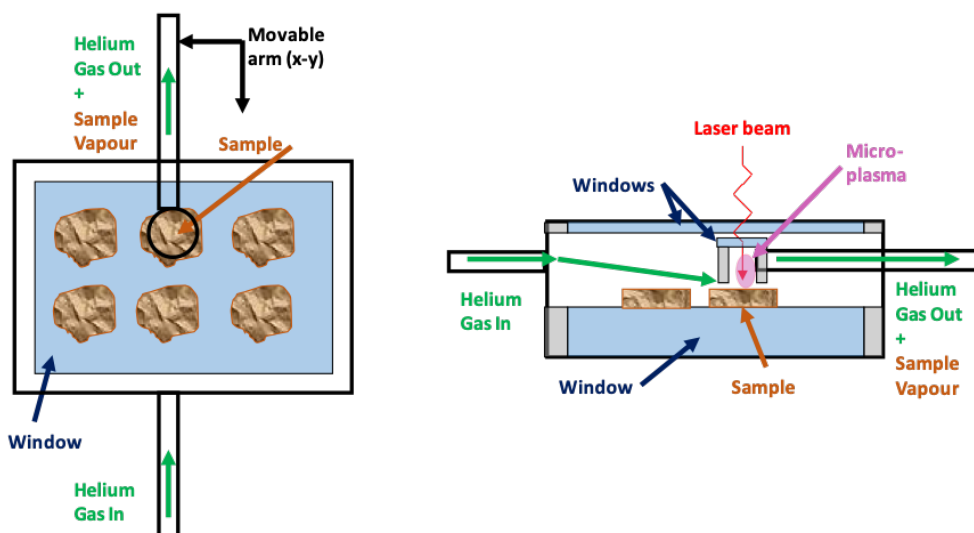


Figure A6. 8: Volume/ cell-in-cell laser ablation sampling cell. Left image shows top-down view, right side view. Image from Chenery and Marriott 2022⁵

On leaving the LA cell the He gas flow containing the aerosolised sample material is mixed with an argon (Ar) gas flow produced using an Aridus desolvating nebuliser. The nebuliser maybe used to provide a continuous dry aerosol from a solution elemental standard. This allows the ready tuning of the ICP-MS system.

The sample is then carried into a high temperature argon plasma (8,000-10,000 Kelvin). The argon plasma is a good source of singly charged positive ions which desolates and ionises the sample, producing positive ions. The ions are extracted from the plasma into a vacuum, containing a mass filter. This can quickly scan the range of masses and are sorted by mass-to-charge ratio (m/z) allowing for multi-element and isotopic analysis to be performed. An electron multiplier detector measures the response at a specific mass in counts per second, and this count rate can be compared using a calibration plot to provide a quantitative assessment for a particular element (Agilent Technologies, 2008). When producing the signal response for a series, spots on either the sample or a calibration standard the data was recorded in a time resolved fashion. This time resolved data stream were processed using the lolite™ software (version 2.5 initially and subsequently v 4). The software allowing both optimal selection of the ablation period, background correction and calibration.

Appendix 7 – Data processing; μ EXAFS - ATHENA

Data output from the Diamond synchrotron collected for μ EXAFS have been processed using the DEMETER package of software programs (ATHENA, ARTEMIS, HEPHAESTUS) (Ravel and Newville, 2005¹⁶).

For analysis, the first program used ATHENA, which is partly a graphical front-end for the programs IFEFFIT, AUTOBK and FEFFIT. The program allowed: (i) the transforming of raw data to give $\mu(E)$ spectra; (ii) background subtraction; (iii) Fourier transforms to change from energy (E) space to k-, R- or q- space required further processing in ARTEMIS; (iv) visualization of processed data as spectra. As part of these processes ATHENA also allows energy calibration, averaging and alignment of data from multiple spectra, use of reference spectra and the removal anomalous points.

ARTEMIS program first requires the sub-program ATOMS which converts the basic crystallographic data for our mineral phase (aragonite) to identify potential scattering paths in order of likely significance. The sub-program FEFF can generate a first estimate of the key parameters for each path and then optimize these terms based on the experimental spectra. Potential scattering paths can then be added to gradually improve the fit of the theoretical spectra to the experimental spectra. Avoiding an over-fit of data by adding unnecessary scattering shells was achieved by checking which scattering shells reproducibly produced good fits across multiple experimental spectra. Shells Sr-O1.2; Sr-Ca.3 and Sr-C.2 as defined in ATOMS and FEFF were found to give the best reproducible results. The output from the ARTEMIS program were best fit estimates of the Sr-C, Sr-O and Sr-Ca distances.

¹⁶ Ravel, B., Newville, M.A., 2005. ATHENA, ARTEMIS, HEPHAESTUS: data analysis for X-ray absorption spectroscopy using IFEFFIT. *Journal of synchrotron radiation*, 12(4), pp. 537-541.

Appendix 8 – Methods used for processing μ XRF maps

At the Diamond facility, the raw μ XRF energy dispersive X-ray (EDX) spectra with their associated spatial (x-y) coordinates were pre-processed using the Dawn™ software package. Within this software the XRF emission lines for the elements were defined and a background corrected response for each element was extracted. The combination of this elemental response and the x-y positioning allowed DAWN to produce a simple elemental map. However, to remove artifacts such as different emission efficiencies due to sample texture the trace element responses needed to be ratioed to the calcium (Ca) response; whilst differential elemental fluorescence around the sample edge required the masking of the edge. This was performed by post-processing in the following manner. Points 1-47 are notes made during my analysis to form a help guide.

1. Take TIFF formatted elemental image file from Dawn into ImageJ
2. File – save as – text image
3. Open Excel
4. Drag text file in
5. Save file as Excel worksheet
6. Can do this for lots of files in one individual Excel worksheet (new sheets) when you drop into Excel it will open in a new workbook, but you just need to copy it into a new sheet
 - Can right click on the sheet at the bottom – move or copy and move to the other document open with all of the sheets in
7. Each cell represents the intensity of the fluorescence at a point – each pixel
8. What we want to do is we want to set the black areas to 0 – decide on threshold at which point anything below this = 0
9. Make histogram of values – we should see a load of high ones – which are the sample and then a load of low ones. Decide at which point we set as 0 so anything below we set as 0 anything above we leave
10. Data analysis plug in
 - File
 - Options
 - Add ins
 - Analysis tool pack – will possibly be down as an inactive one.
11. Back on spreadsheet click data tab then data analysis – within this is histogram → click ok
 - Input range – select all of the data
 - Tick box for chart output
12. Will divide up in a strange way but can see where the high ones lie
13. Do this for both images within an overall shell pic i.e., if there is a main shell and new part image
14. Instead of clicking new worksheet can click output range – can select where you want to put the graph if you mark a cell – so you can put it with the other histogram made.
15. To be a bit more sophisticated - we can tell it our own bin range

- Select own range – can go up in thousands
 - Then re-create histogram as before – but with the bin range box – highlight our bin range type in (before we left it blank) and move output range – click random cell
 - Can look and get a more accurate value for where to cut it off as 0 values
16. Type in new cell cut off '18000 units' (value we are using for this e.g.) so we remember what to do!
 17. Save file
 18. Next, we want to actually apply this to our data file
 - To get rid of values less than 18000
 - This will set anything less as 0
 19. So, we get the right number of rows or columns that we are operating on if we move or copy and create a copy and then rename it as Masked
 20. Go to top left do if statement in masked file
 - =if(then go back to file were actually testing on
 - =if(click top left box to get reference to cell
 - =if(this<18000,0,(re-click original value
 - =if(this<18000,0,this)
 - If the value is less than 18000 it is 0 if it is not, then leave it as it is
 21. To apply this to all cells in the sheet – do multiple copy
 22. To do this:
 - Normal highlight cell and copy command shift up and right selects all to the right and command shift down highlights all down and then right click paste
 - So having copied the original file and done a new file with the same data (masked file) it clearly knows where to go and where the 0's are etc.
 23. So for the Sr we are going to apply this Ca mask we have just created
 - The Sr was much more energetic, and we got the ghosting at the edge at diamond so this way we can get rid of this effect by using the less energetic Ca – we know the true edge much better with the Ca.
 24. Make copies of the Sr sheets – again name masked
 25. Use if statement again but use a slightly different criterion
 - 1st cell in masked one
 - =If(go to masked Ca body masked sheet and click the top left cell
 - =If(this=0,0,Then click in Sr body sheet NOT masked one
 - =If(this=0,0,Sr top left cell for worksheet working on) then click enter
 - Then do the same copy click bit
 26. CHECK VALUES AT THE END – we found 18000 was too high – looking back it has cut bits off on the pic and in fact there are some patchy areas on the map – maybe more like 2 or 1000 can go back and lower the bins and edit the histogram to double check values
 27. As we changed the Ca to update with the new values – the Sr will automatically use these new values
 28. Save as worksheet
 29. Now we want to take these files into ImageJ
 30. To do this we need to save as csv or text files
 31. Using the masked sheets – file save as and click drop down to CSV file
 32. IN IMAGE J
 33. File - Import text image
 34. Select CSV file to import in

35. Make sure whatever colour scheme I use I apply the same to all images of the same shell as the values have all been the same
36. Image adjust – brightness and contrast B&C at the moment it auto does this but if you click set we can adjust this we want to make sure the maximum value is the same in both of them. Since the higher one in this e.g., is 24,000 something we can use 24,000 as our value to cover both then click apply so they both are on the same scale – set this for both.
37. Then go to image lookup tables – 16 colours for posters sake this looks cool
38. To save as a pic – file save as JPEG – seems to distort colour – have a play around with this to see effects
39. When adding in a calibration scale colour bar work on duplicated image as once the scale bar is in its in and it's in the way!
40. Normalising – accounting for differences in Ca across the shell
41. Ratio the Sr to the Ca
42. Can copy over one of the sheets as before so when doing the shift right and down it knows where to go
43. Top left cell
 - =Number in Sr Body top left NOT MASKED/Number in Ca body top left NOT MASKED
 - ENTER
 - Then copy this to all cells will give ratio values for each of the ones in the two sheets to replace what is in the sheet
 - Can x all numbers by 1000 to o make the numbers bigger so its clearer to see
44. Now we want to make a masked version of this
45. Copy this new spreadsheet to a new sheet and call masked
46. Top left
 - If(Original Ca body masked top left point=0,0,top left normalised Sr one)
 - Only using Ca as we are using the Ca as a mask – as we know the Sr doesn't give a true edge
47. So, we do this for both the body and the new growth

Appendix 9 – Process for data analysis of laser output

The following set of instructions are my methods used for translating the output from Agilent LA-ICP-MS software to a useable format in Excel using the Lolite v2.5 package. The resulting output file from Lolite will have 3 columns per data point (Mg, Sr, Fe etc).

- 1) Concentration ppm
- 2) 2 SE of concentration
- 3) Limit of detection - Is the concentration calculated above or below the detection?

Extracting the data

Most important step throughout is to make sure everything is saved!

Open IGOR, if already open go to file – new experiment

Import data → file type Agilent → Single/B --> Single

Select data + open, this will have an Excel logo .csv file

1. Data reduction scheme --> trace elements
2. Edit settings → index channel Ca42

Reference material → G_NIST610A

3. Index content in sample 0.085049
 - This value is for the GNIST612 glass

SAVE CHANGES

4. Primary channel Ca42
 - Secondary Al27

We use Al here as it is within the polishing powders. Because of this it gets in the cracks, so this checks for contamination from the polishing.

5. Active integration → Baseline
6. Put baseline points in
 - 3 at each end then 1 every few
 - Ctrl click, drag, and click again
 - To change size → shift and drag ends,
 - Can also delete with shift
 - Spline type = spline smooth auto

CRUNCH DATA → Check primary channel list → there should be a few more → SAVE CHANGES

7. Mark standards. When marking you need to go a bit away from left hand side and to end off cliff on right side
 - Active integration type G610A
 - Spline type linear fit

CRUNCH DATA → Check list → SAVE

8. Testing the unknown sample → treat as unknown
9. Active integration type --> Output 1
 - Mark points
 - Spline type → leave as automatic

CRUNCH (At this step it won't add to the list again unlike before) → SAVE

10. Export data – Right side of screen
 - File name → xxxSRM612 → Continue
 - Check save location
 - Drag and open in Excel

- xxxSRM612 All integrations
- Check values are as expected
- U 38/39
- Li 38/40

SAVE AS EXCEL WORKBOOK

11. To analyse actual sample now

Delete points on 612 glass → Shift click and delete

Edit settings - All the same but the index content in sample changes to 0.4004 (amount of Ca in CaCO₃ 40.04%)

- Can mark peaks manually OR use automatic integrations
 - Click
 - Drop down → detect from beam intensity --> continue
- New pop up will show all data at the start
 - Change channel to view to Ca42

On left hand side Ca42 > check scale on graph. If used bigger points on laser we will get a bigger signal

- Pick value → based on where values lie – on X axis what all of my data points are above and put into the box below 'is greater than'
- Select integration type → output
- Crop data – start at 2 seconds end 0 minimum duration 2 seconds
- LHS select all peaks

12. ADD INTEGRATIONS

- Pop up → YES delete all my previous selections
- Hopefully will get little boxes
- Close window → button above add integrations does this
- To see little boxes Active integration type to baseline then back to output 1
- Check boxes are in the right place in relation to the edge of the graphs can move as before with the shift key
 - Shift click and drag as before to change size of box → e.g., if can see Al spike below, to avoid its peak

SAVE → CRUNCH DATA → SAVE

13. Export data

- Change file name to sample as it's not the standard again
- Other boxes all ok
- Pop up → check save location and click ok

14. Drag file sample all integrations into excel – will have extra (3rd column) of data to right (repeats Li Li etc)

- Open new sheet and copy in all data
- In new sheet can now delete standard date from above
- Fit in each column 3 data to each data set

SAVE AS EXCEL WORKBOOK

Key points to do when in Excel.

- Sort decimal places, look at detection (column 3)
 - Based on the decimal places of the 3rd column so use 1-3 decimal places
- Uranium, where ppm numbers are smaller 2-3 decimal places as of the 0.00 etc
- For Strontium, where Column 3 was similar, as values are in 1000's, the decimal places make less difference, so this is not necessary

SAVE ALL CHANGES!

Appendix 10 – Paper manuscript

Author contributions: P.R. Hollyman, C.A. Richardson, S.R.N. Chenery and I.D. McCarthy provided comments on draft manuscripts and J.J. Waggitt manuscript advice and feedback. All research, data analysis and manuscript writing were led and carried out by C.N. Colvin.

<https://doi.org/10.1016/j.jembe.2022.151720>